Assessing the roles of contractility and polarity in the emergence of endothelial cell chirality

Ghina Badih

THÈSE

Pour obtenir le grade de

DOCTEUR DE L'UNIVERSITÉ GRENOBLE ALPES

École doctorale : CSV- Chimie et Sciences du Vivant
Spécialité : Biologie cellulaire
Unité de recherche : LPCV - Laboratoire de Physiologie Cellulaire Végétale

Evaluation du rôle de la contractilité et de la polarité dans l'expression de la chiralité cellulaire dans un modèle endothélial

Assessing the roles of contractility and polarity in the emergence of endothelial cell chirality

Présentée par :

Ghina BADIH

Direction de thèse :

Laetitia KURZAWA — Directrice de thèse
CEA

Rapporteurs :

Delphine DELACOUR
DIRECTRICE DE RECHERCHE, CNRS délégation Provence et Corse
Danijela MATIC VIGNJEVIC
DIRECTRICE DE RECHERCHE, INSERM Ile-de-France - Paris

Thèse soutenue publiquement le **5 juillet 2024**, devant le jury composé de :

Franz BRUCKERT, PROFESSEUR DES UNIVERSITES, Grenoble INP	Président
Laetitia KURZAWA, INGENIEURE DE RECHERCHE, CEA centre de Grenoble	Directrice de thèse
Delphine DELACOUR, DIRECTRICE DE RECHERCHE, CNRS délégation Provence et Corse	Rapporteure
Danijela MATIC VIGNJEVIC, DIRECTRICE DE RECHERCHE, INSERM Ile-de-France - Paris	Rapporteure
Virgile VIASNOFF, DIRECTEUR DE RECHERCHE, CNRS délégation Provence et Corse	Examinateur
Thomas BOUDOU, CHARGE DE RECHERCHE HDR, CNRS délégation Alpes	Examinateur

Assessing the roles of contractility and polarity in the emergence of endothelial cell chirality

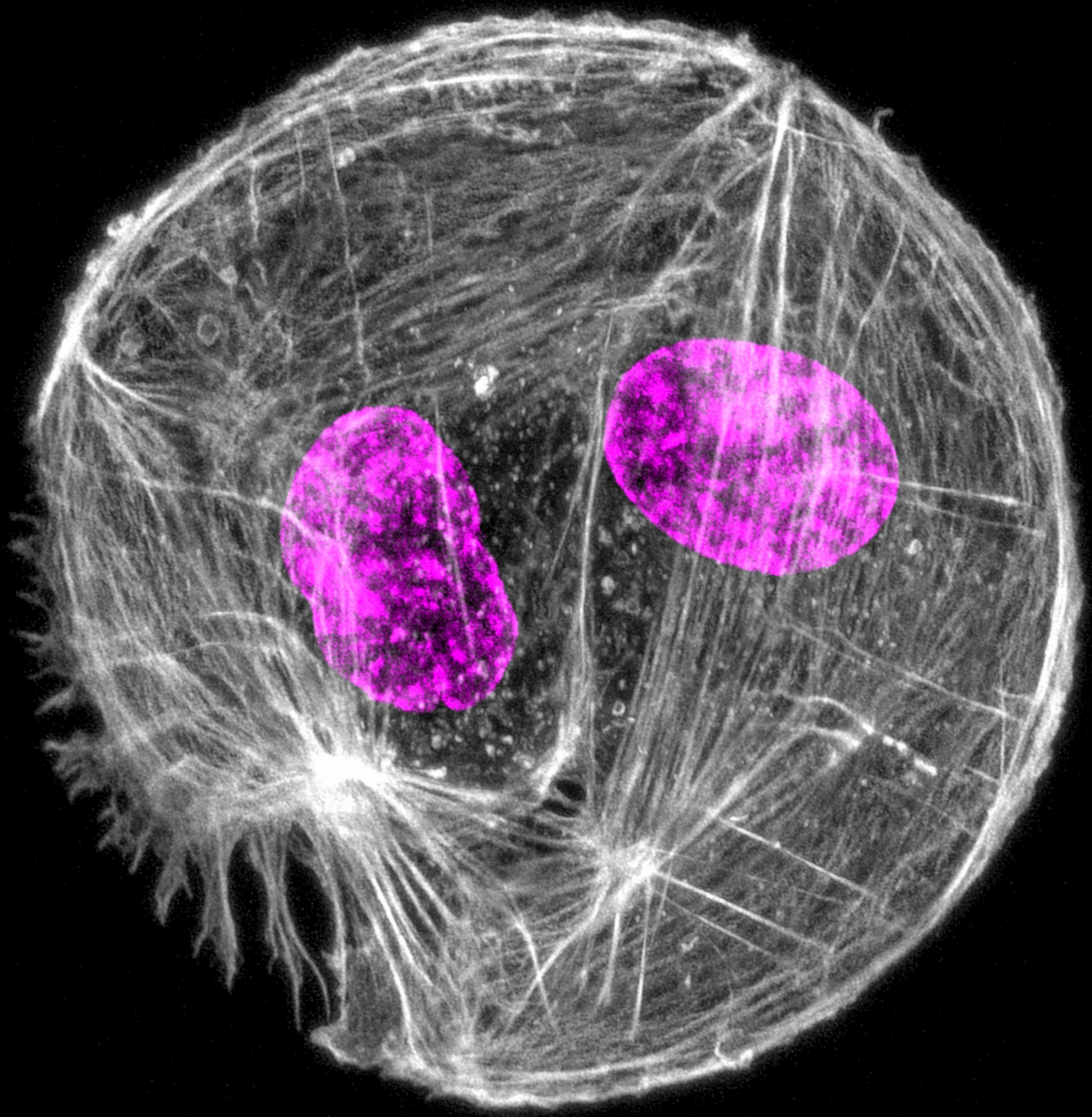

Ghina Badih

TABLE OF CONTENTS

I. ACKNOWLEDGMENTS

When writing this section, my journey during the last four years flashed before my eyes, with all its ups and downs, happy and sad moments, successes and failures, making it a particularly emotional moment.

This PhD was a very challenging, yet rewarding, intellectual and human experience, full of countless first hand encounters that shaped my personality and, more importantly, constant interactions with a lot of people, who guided and supported me all the way through. To those people, this section is for you…

Four years ago, I was lucky to become a part of the CytoMorpho Lab, which, in addition to having a solid foundation for groundbreaking scientific research, provided a friendly and caring atmosphere, suitable for developing personal bonds that extended far beyond the work environment.

The CytoMorpho is actually divided into two spatially separated realms, Grenoble and Paris, whose "steady state" is maintained by the "dynamic" interactions between two rulers, two enemy brothers: Laurent Blanchoin and Manuel Théry. I will always be grateful to you both for giving me the opportunity to join your team and work along your side. Thank you for all the time you dedicated for me over the past years.

Laurent, you were always there, whenever I needed help not only in my project but also in my personal life. You always saw in me what I could not see in myself. You made sure to congratulate me whenever I did a good job. Your constant encouragement and trust helped me overcome my fear and hesitation about experiments, pushed me to try new things, and boosted my self-confidence. Above all, thank you for genuinely caring about my well-being. I always knew that whenever I had a problem, I could count on you for help.

Manuel, I have always admired your passion and enthusiasm about science. Your curiosity and creativity have always been a source of inspiration for me. With you the sky is the limit, or maybe even not! I truly enjoyed our long discussions, which despite being mostly dedicated to making sense of my results, frequently opened the door to testing new hypotheses and performing new experiments. For this, and many other reasons, it was a great pleasure to work with you.

Laetitia, my supervisor, with whom I worked side-by-side on a daily basis for four years, I am glad to be your first official PhD student! Thank you for sharing the work on the bench with me, for teaching me all that you know, for pushing me to exceed my limits, for supporting me at all times, especially during the discussions with Laurent and Manuel, and for always being patient. With you, I never felt the conventional burden of a student-supervisor relationship. I was lucky to work along your side, and I sincerely thank you for all the help, guidance, and dedication you gave me during my PhD.

As a proud member of the Grenoble realm, I had the chance to work with some exceptional team members.

Ben, or as I like to call you, the savior because it suits very well! You moving to Grenoble was a blessing to me! I have no words that can express my gratitude for all the time you spent helping me troubleshoot experimental protocols, design experiments, analyze data, and discuss results. Your contribution to my project was of great and undeniable value, and I could not have done it without you. Above all, I would like to thank you and Anne Laure for welcoming me in your home, and even more, for trusting me to babysit your two adorable girls. I will always cherish the time I spent with you and your family.

Jérémie and Christophe, the famous Tic and Tac. You are the heart and soul of the CytoMorpho. I cannot imagine how my years in the lab would have been without you. You comforted me when I needed it most, made me laugh when I was down, looked after me at all times, and helped me with all my troubles. You two will always have a special place in my heart. Thank you for simply sharing this PhD experience with me!

Alexandra, you are one of the best examples I know for a successful woman in science. I have always admired your working spirit, your dedication for research, your ethical and scientific principles, and all your achievements so far, though I am quite sure that it is only the beginning! Despite your busy schedule, you always managed to find some time for me when I needed someone to talk to about science or life. You constantly reminded me that I was capable of overcoming all the problems that I might encounter. Thank you for believing in me!

Simona, my babysitter, my late evening companion, my all-time support system. Your comforting words and optimistic nature have avoided several of my stress-induced breakdowns. Despite joining the lab only a year ago, you already became the first person coming to my mind when I needed help of any sort. You always managed to cheer me up, whatever was on my mind, even if that required spending an entire Saturday binge-watching Star Wars Movies (we should plan part two soon by the way). I am so glad I met you, and I am extremely lucky to count you as one of my friends!

Clothilde, my partner in crime. Within a short period of time, you managed to become one of my favorite people, and not only because you always called me “little light”! We shared countless memorable laughs and moments, most of which might have included fries and cheddar. Thank you for helping me in all my conquests and, above all, thank you for putting up with some of my crazy quirks!

Anne Betty, thank you for your kindness, support, and, most importantly, your delicious vegan treats! I was happy I had the chance to share my humble experience in the “cell world” with you, even if briefly. You could not imagine how proud I was when you called me your “Yoda”. I wish you all the best for your future, which with no doubt will be bright!

Despite my unconditional and everlasting loyalty to Grenoble, my stay in the CytoMorpho comprised occasional visits to the Parisian realm, where I had the chance to interact with some wonderful Cytomorphers, whom I would like to thank more specifically here.

Tanguy, Alfredo, Yuhui, Bhagyanath, Louise, and Matthieu, you welcomed me whenever I visited and always dedicated a part of your day or weekend to catchup over drinks, meals, or climbing sessions (except you Tanguy!). With all of you around, I never felt like an

intruder, and I will always remember the great and fun moments we shared together in Paris.

Alexandre, your scientific intellect and unorthodox ways always intrigued me, as I am sure they did many other people. I never thought that your brief visit to Grenoble to teach us the microinjection ways could give rise to a friendship that would affect me on different levels. You always had more faith in my abilities than myself, and because of your constant help and support, I became a more confident and independent researcher. Thank you for the endless scientific discussions, the flawless experimental protocols, the codes that made my analysis possible, and, of course, your constructive criticism. Above all, I enjoyed being the test subject for some of your cooking recipes, although it did cost me some climbing sessions, of which I was not a big fan!

Overall, I would like to thank all the members of the CytoMorpho for sharing their scientific experience with me and for making my PhD journey an unforgettable experience!

I am also grateful to a group of special friends, whose company always feels like home! Lama, Lynn, Elie, Antoinette, Antonio, Rosy, Samuel, and Tala. You always managed to cheer me up at times when I thought it was simply impossible. We share many memories that I am particularly fond of, and I am happy and lucky to have met each one of you!

I owe a great deal of what I am today to my family; I would not have been the person that I am today without their endless support.

Mom, Dad, thank you for always believing in me, reminding me to be patient, and encouraging me to pursue my dreams no matter what!

My sisters, Jana and Naya, thank you for all the laughs that we shared over the phone every night. You both really helped me get through all the challenges of my daily life!

Finally, to my grandparents and my family members all over the world, thank you for always being one phone call away!

III. ABSTRACTS

1. English

Chirality, defined as the property of an object not being superimposable to its mirror image, is a conserved hallmark of biological systems with critical implications in various physiological processes, particularly tissue morphogenesis and embryonic development. Large-scale left-right asymmetries, including organismal body plans and directional tissue patterning, are believed to arise from the handedness of their constituting cells, commonly referred to as cellular chirality. It has been shown that in a geometrically confined environment, both individual cells and cell collectives spontaneously break symmetry and can exhibit distinctive chiral behaviors. Despite the lack of a clear molecular mechanism explaining the manifestation of this property at the cellular level, the primary chiral determinant in this phenomenon has always been linked to the actin cytoskeleton in interaction with its binding partners. In particular, several studies point at a key role for actomyosin network contractility in chiral cell alignment and rotation. However, the exact contribution of contractile forces to the emergence and maintenance of cellular chirality remains to be elucidated. Moreover, it has been reported that the expression of chirality in various models is closely associated with polarization, another type of symmetry breaking, which governs the organization of the cytoskeleton, biases the distribution of internal organelles, and plays an essential role in driving cellular motion. Despite the interdependence between these two symmetry-breaking phenomena, especially in terms of the implicated effectors, a clear understanding of the feedback existing between polarity and chirality is still lacking.

To begin with, our project addresses the role of contractility in establishing chirality in a minimalistic model of endothelial cell pairs. We show that cell doublets confined on disk-shaped micropatterns spontaneously display a persistent, rightward biased swirling that is strongly dependent on the contractile forces produced by the actin cytoskeleton. In particular, our experimental data demonstrates that varying cellular contractility levels not only affects the extent of rotation but also modulates the strength and the directionality of the chiral bias. Furthermore, a closer examination of the mechanics associated with the chiral rotation of doublets reveals the presence of a force asymmetry within the cell pair. Interestingly, our results indicate that the magnitude of forces in the more contractile cell is correlated with the speed and the direction of doublet rotation, suggesting that this cell would dominate the rotational behavior of the system and predict the bias of the doublet. Secondly, by adapting the geometry of the adhesive pattern, we identify the conditions required to trigger an equivalent chiral rotation among single endothelial cells. We use this system to challenge the intrinsic nature of cellular chirality and its relationship to polarity, while shedding light on a possible implication for motility in the emergence of a persistent chiral phenotype.

Taken together, our findings demonstrate that the balance of forces produced by the cells of a pair is actively involved in driving the expression of chirality in doublets. In addition, they provide preliminary insights into the mechanisms associated with the emergence of

chirality in cells, which would occur in response to their internal organelles symmetry-break and motility.

2. French

La chiralité, définie comme étant la propriété d'un objet de ne pas être superposable à son image miroir, est une caractéristique conservée des systèmes biologiques ayant des implications critiques dans divers processus physiologiques, comme la morphogenèse tissulaire et le développement embryonnaire. On pense que les asymétries gauches-droites rencontrées à grande échelle, au cœur de la programmation du développement des organes et du patterning des tissus, proviennent de l'asymétrie gauche-droite de leurs cellules constitutives, communément appelée chiralité cellulaire. Il a été démontré que dans un environnement à géométrie confinée, les cellules individuelles et les groupes de cellules brisent spontanément leur symétrie gauche-droite et présentent des comportements chiraux qui leurs sont propres. Malgré l'absence de mécanisme moléculaire clair expliquant la manifestation de cette propriété au niveau cellulaire, la plupart des études convergent vers un rôle essentiel du cytosquelette d'actine en interaction avec ses protéines partenaires. En particulier, plusieurs travaux indiquent que la contractilité du réseau d'actomyosine jouerait un rôle clé dans l'alignement et la rotation chirales des cellules. Cependant, la contribution exacte des forces contractiles à l'émergence et au maintien de la chiralité cellulaire reste à élucider. De plus, il a été rapporté que l'expression de la chiralité dans divers modèles coïncide avec une repolarisation des organelles de la cellule, un autre type de brisure de symétrie qui régit l'organisation du cytosquelette et joue un rôle essentiel dans la mise en place de mouvements cellulaires. Malgré l'observation de ce phénomène, une compréhension claire de la rétroaction existant entre polarisation des constituants cellulaire et expression du phénotype chiral fait encore défaut.

Dans ce contexte, notre projet aborde dans un premier temps le rôle de la contractilité dans l'établissement de la chiralité au sein d'un modèle minimal de paires de cellules endothéliales. Nous avons montré que des doublets de cellules confinés sur des micropatterns en forme de disque présentaient spontanément une rotation persistante et biaisée vers la droite qui dépend fortement des forces contractiles produites par le cytosquelette d'actine. En particulier, nos données expérimentales ont démontré que la variation du niveau de contractilité cellulaire n'affectait pas seulement le déclenchement de la rotation, mais modulait également la force et la direction du biais chiral. En outre, un examen plus approfondi du mécanisme associé à la rotation chirale des doublets a révélé la présence d'une asymétrie de force au sein de la paire de cellules. De manière intéressante, nos résultats ont montré que le niveau de contractilité de la cellule la plus contractile était corrélé avec la vitesse et la direction de la rotation des doublets, ce qui suggère que cette cellule hautement contractile dominerait le comportement chiral du système, prédisant ainsi le biais du doublet. Dans un deuxième temps, en adaptant la géométrie de nos micropatrons, nous avons réussi à identifier les conditions requises pour déclencher la rotation chirale de cellules endothéliales individuelles. Nous avons utilisé ce système pour questionner la nature intrinsèque de la chiralité cellulaire et sa relation avec la polarité, tout en mettant en lumière une implication possible de la motilité dans l'émergence d'un phénotype chiral persistant.

L'ensemble de ces résultats montrent que l'équilibre des forces produites par les cellules d'une paire serait activement impliqué dans l'expression de la chiralité dans les doublets. En outre, nos résultats préliminaires suggèrent que l'émergence de la chiralité cellulaire pourrait être liée avec la brisure de symétrie étant associée au processus de motilité cellulaire.

IV. LIST OF ABBREVIATIONS

Actin Associated Protein (AAP)

Actin Inner Center (AIC)

Actin Inner Zone (AIZ)

Actin related protein 2/3 (Arp 2/3)

Adenosine Triphosphate (ATP)

Adenosine Diphosphate (ADP)

Antigen presenting cell (APC)

Caenorhabditis elegans (C. Elegans)

Cell division Cycle 42 (Cdc 42)

Clockwise (CW)

Counter-clockwise (CCW)

Electron microscopy (EM)

Extracellular Matrix (ECM)

Filamentous actin (F-actin)

Focal adhesions (FA)

Geometrical center (GC)

Globular actin (G-actin)

Green Fluorescence protein (GFP)

Guanosine diphosphate (GDP)

Guanosine triphosphate (GTP)

Hexamethyldisilazane (HMDS)

Human Umbilical Vein Endothelial Cells (HUVEC)

Immune synapse (IS)

Madin-Darby Canine Kidney Cells (MDCK)

Microtubule Associated Protein (MAP)

Microtubule organizing centers (MTOC)

Mouse Embryonic Fibroblast (MEF)

Myosin ID (MyoID)

Myosin IC (MyoIC)

Non-muscle Myosin II (MyoII)

Non-rotating (NR)

Partition defective 3 (PAR3)

Partition defective 6 (PAR6)

Phospho-myosin (p-MLC)

Polyacrylamide (PAA)

Polyethylene glycol (PEG) Poly-L-lysine (PLL)

Post translational modification (PTM)

Protein kinase C (PKC)

Protofilaments (PF)

Ras homolog family member A (Rho-A)

Ras homologous protein (RHO)

Ras related C3 botulinum toxin (RAC)

Reverting (REV)

Rho associated protein kinase (ROCK)

Rotating (R)

Traction Force Microscopy (TFM)

Traction Forces (TFs)

Traction Force Imbalance Method (TFIM)

V. INTRODUCTION

V.1. Asymmetry in living organisms originates from the cytoskeleton

The development of all organisms is based on complex morphogenetic processes in which symmetry is repeatedly broken to enable the generation of a greater degree of diversity coupled to higher morphological and functional specialization. Such processes are characterized by two major symmetry-breaking events occurring at different scales that extend all the way to individual cells.

During the early stages of development, the main axis connecting the anterior and the posterior poles of the organism is first established. At the cellular level, the definition of this primary axis is associated with the phenomenon of polarization, in which the intracellular organization of cells is biased, resulting in a functional asymmetry that can support a wide range of cellular functions during development, including migration and division. *(Pohl, 2015, Symmetry; Zagórska-Marek, 2021, Current Topics in Chirality—From Chemistry to Biology; Ierushalmi & Keren, 2021, Current Opinion in Cell Biology)*

The subsequent deviation of certain structures to the left or right of the predefined axis gives rise to Left-Right (LR) asymmetry, a striking characteristic that is indispensable for normal embryonic morphogenesis. Aberrant LR symmetry breaking events can be associated with severe malformations and developmental disorders, such as congenital heart diseases or heterotaxia in humans and, less frequently, with full structural inversions and no functional perturbation – situs inversus. LR asymmetry is ubiquitously present in biological systems of varying complexity, as manifested by the helical or spiral organization of leaves and petals in plants, the growth of twinning vines, the spiral coiling of snail shells, the biased positioning of body organs, and, of course, our left and right hands. LR asymmetry extends to the level of individual cells and multicellular entities, whose behaviors demonstrate inherent handedness, commonly referred to as cellular chirality. The conserved nature of LR asymmetry at multiple scales and across diverse species raises interesting questions regarding its importance in physiological processes as well as the existence of a common molecular mechanism underlying the initial symmetry breaking and its propagation. *(Pohl, 2015, Symmetry; Ierushalmi & Keren, 2021, Current Opinion in Cell Biology; Zagórska-Marek, 2021, Current Topics in Chirality—From Chemistry to Biology; Levin, 2005, Mechanisms of Development; Balan et al., 2012, Journal of Cardiovascular Computed Tomography; Brueckner, 2007, Circulation)*

Intriguingly, key to all symmetry breaking phenomena is the polarized and chiral self-organization of the cytoskeleton, a complex network of filamentous proteins that span the entire cell volume to preserve cellular integrity and generate the forces necessary to carry out diverse functions. Out of the three classes of cytoskeletal filaments, two possess inherent abilities to drive spontaneous symmetry breaking: actin, described as being a

viscoelastic gel across the cytoplasm, and microtubules, which classically form a cytoplasmic, astral network of elastic bundles.

In the following section, we will briefly describe how the intrinsic characteristics of these two cytoskeletal polymers, as well as their interactions with certain binding partners can support their inherent symmetry-breaking abilities.

V.2. The cytoskeleton: a backbone based on polar, chiral building blocks and interactions

1. The microtubule network

1.1. Microtubules

Microtubules (Figure 1A) are the major cellular structures responsible for proper organelle positioning and active vesicular transport. They are dynamic polymers consisting of thirteen protofilaments arranged in the form of a tube. Each protofilament is made up by the longitudinal stacking of tubulin heterodimers (100kDa) that individually comprise an α-tubulin and a β-tubulin molecules *(Alberts, 2017; Thomas Dean Pollard & Goldman, 2017)*. The homogeneous head-to-tail organization of tubulin heterodimers renders microtubules intrinsically polar with two asymmetrically dynamic extremities: a fast growing and highly dynamic plus (+) end, terminating in β-tubulin and a less dynamic minus (-) one, ending in α-tubulin that is usually captured and stabilized by certain proteins (Figure 1A-B).

A key feature of microtubules is their dynamic instability. Unlike other polymers, microtubules randomly switch from polymerization to depolymerization states *(Mitchison & Kirschner, 1984a, Nature; 1984b, Nature)*. Whereas both α- and β-tubulin can bind GTP, only the latter can hydrolyze the bound GTP molecule into GDP, inducing a conformational change in the tubulin dimer that destabilizes the lattice and favors microtubule depolymerization. Interestingly, GTP hydrolysis by β-tubulin is required only for microtubule destabilization and is highly accelerated upon the incorporation of the dimers into microtubules. Microtubule stability at the (+) end depends on the presence of a GTP-tubulin cap, whose length is determined by the speed at which new dimers are incorporated, as well as the rate at which GTP is hydrolyzed to GDP *(Kirschner & Mitchison, 1986, Cell)*. In response to a sudden drop in free GTP-tubulin, the speed of dimer incorporation at the tip slows down, causing the gradual decrease in the size of the GTP-cap and, eventually, its complete loss. The resulting instability causes the GDP lattice to break apart, and the microtubule to depolymerize, an event commonly referred to as catastrophe *(Padinhateeri et al., 2012, Biophys J)*. Interestingly, rescue events, in which depolymerizing microtubules revert to a polymerization state, are also described, although the underlying mechanism remains unclear *(Gardner et al., 2013, Curr Opin Cell Biol)*. However, it has been recently demonstrated that due to the presence of defects within their lattice, microtubules can also incorporate new GTP-tubulin all along their length, which can further stabilize them and favor their rescue *(Aumeier et al., 2016, Nat Cell Biol; Théry & Blanchoin, 2021, Current Opinion in Cell Biology)*. This suggests that microtubule dynamics are not limited to their extremities (Figure 1B).

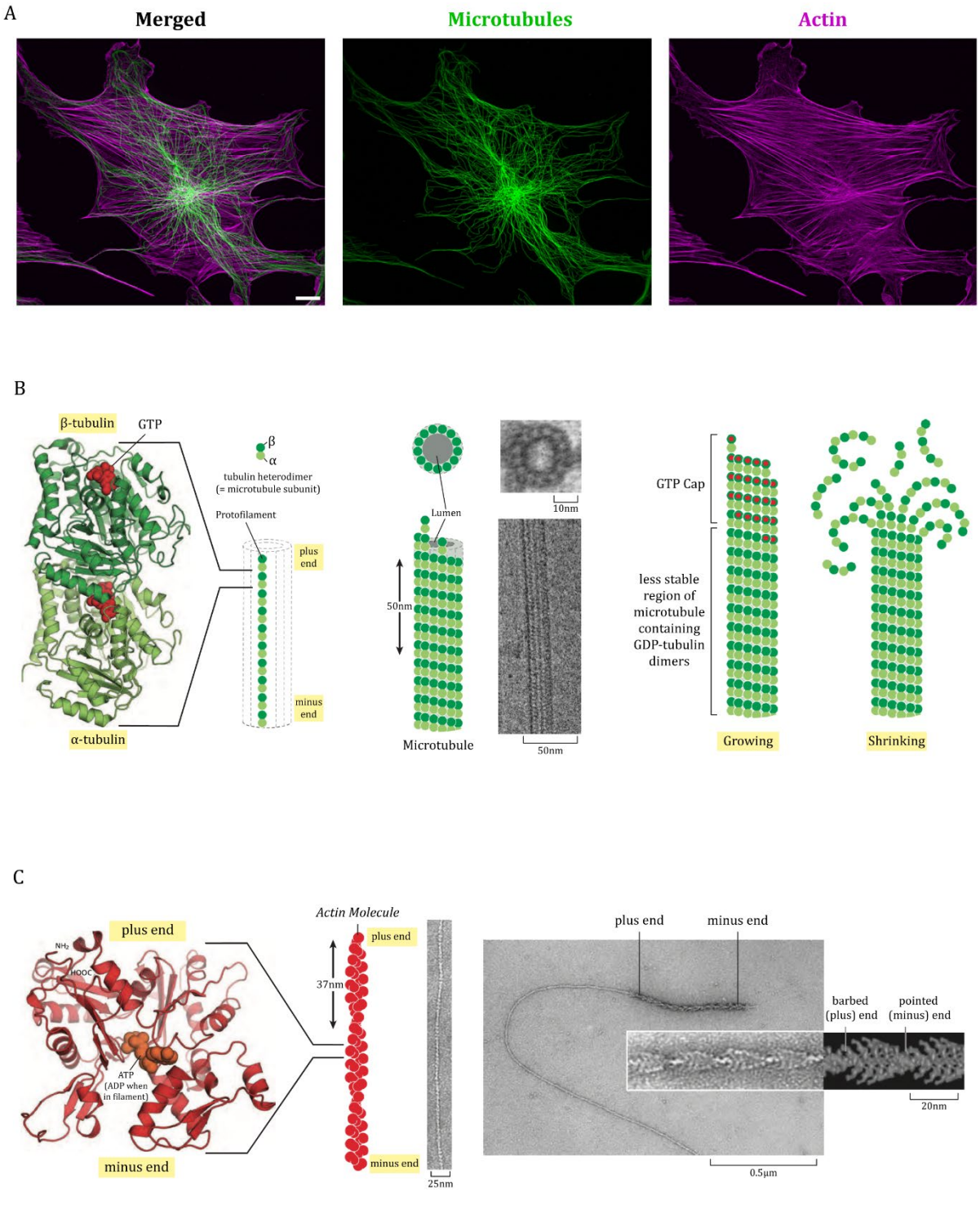

Figure1: The cytoskeleton is a polar and chiral backbone.
Adapted from *(Schaeffer, 2023)*.
A: Representative images of the microtubule and actin networks in a Mouse Embryonic Fibroblast (MEF). Microtubules in green and actin in magenta (Scale Bar = 10µm). Images were adapted from *Alexandre Schaeffer*.
B: The structure of a microtubule and its subunit adapted from *(Alberts, 2017)*.
From left to right: the structure of the αβ tubulin heterodimer; schematic representation of the organization of the αβ tubulin heterodimers along a protofilament; transverse and

side views of a schematic representation of a microtubule; electron microscopy (EM) image of a microtubule; schematic representation of a growing microtubule with a GTP-cap; schematic representation of a depolymerizing microtubule without its cap.
C: The structure of an actin filament and its subunit adapted from *(Alberts, 2017)*.
From left to right: the structure of the actin monomer; schematic representation of the organization of the actin monomer along an actin filament with the corresponding EM image; EM image of an actin filament; 3D reconstruction of an actin filament illustrating its barbed and pointed ends.

Overall, microtubules are polar filaments with asymmetric dynamics at their (+) and (-) ends and, therefore, represent attractive models for the study of symmetry breaking events.

Microtubules interact with a wide array of proteins, called microtubule-associated proteins (MAPs) that can specifically drive their stabilization, capping, bundling, polymerization, depolymerization, branching, or severing. Molecular motors constitute a particularly interesting family of MAPs because they provide insights into the ability of the microtubule network to break its own symmetry.

1.2. Molecular motors govern microtubule organization

Molecular motors use microtubules as railroads to mediate the intracellular transport of vesicles and organelles. They have the ability to read the structural polarity of the underlying microtubules and consequently hydrolyze ATP to drive processive motions in accordance with that polarity. There are two superfamilies of microtubule-associated molecular motors. The kinesin superfamily comprises 45 individuals that all possess true motor activity and mostly move toward the microtubule (+) end. Distinct kinesins are associated with the motion of different organelles or vesicles along particular subpopulations of microtubules. On the other hand, members of the dynein superfamily are all (-) end-directed motors that belong to either the family of axonemal dyneins (specific to cilia and flagella) or that of cytoplasmic dyneins, which are characterized by different cargos. Because the joint activity of kinesin and dynein on the polarized microtubule network results in the positioning of certain cargoes at the (+) end and others at the (-) end, they can be key effectors in the translation of structural polarity into a functional one *(Alberts, 2017; Thomas Dean Pollard & Goldman, 2017; Schliwa & Woehlke, 2001, Nature)*.

Motor-associated forces can drive the motion of the microtubules themselves and, consequently, reshape the network. For example, the formation of the mitotic spindle encompasses motor-induced microtubule sliding and bundling *(Pavin & Tolić, 2016, Annu Rev Biophys; Petry, 2016, Annu Rev Biochem)*. At the spindle poles, dyneins mediate a strong clustering of the microtubule (-) ends, whereas kinesins produce pushing forces to allow their separation. In addition, the repositioning of the centrosome accompanying polarization events, like immune synapse formation or asymmetric division, is mediated by dynein pulling forces *(R. Li & Gundersen, 2008, Nat Rev Mol Cell Biol; O. J. Gros et al., 2021, MBoC)*. Moreover, due to their helical motions along the microtubules, both kinesins

and dyneins have the ability to generate molecular torques that can be implicated in LR symmetry breaking processes *(Can et al., 2014, ELife; Mitra et al., 2020, Nat Commun)*.

2. The actin cytoskeleton

2.1. Actin

The actin cytoskeleton (Figure 1A) is key to maintaining cellular integrity as well as sensing the properties of the surrounding environment and integrating the appropriate cellular response *(Alberts, 2017; Thomas Dean Pollard & Goldman, 2017; Blanchoin et al., 2014, Physiological Reviews)*. Filamentous actin (F-actin) refers to actin filaments composed of two strands intertwined into a right-handed helix with a final diameter of 8nm (Figure 1C). The polymerization of F-actin from globular actin (G-actin) monomers (42kDa) requires the presence of ATP, ADP, and divalent magnesium cations and occurs in two steps *(Holmes et al., 1990, Nature; Kabsch et al., 1990, Nature; Blanchoin & Pollard, 2002, Biochemistry; Melki et al., 1996, Biochemistry)*. First, an unfavorable nucleation event results in the formation of unstable oligomers made up of two to three actin monomers *(Sept et al., 1999, Journal of Molecular Biology)*. After that, the incorporation of a fourth monomer stabilizes the previously formed oligomers, which then readily elongate into actin filaments *(Wegner & Engel, 1975, Biophysical Chemistry)*. During polymerization, the homogeneous stacking of G-actin monomers, which have two functional poles, results in intrinsically polar actin filaments having two distinct extremities (Figure 1C): a highly dynamic barbed end, with a 0.12μM critical concentration to ATP-actin, and a less dynamic pointed end, with a five times higher critical concentration for ATP monomers *(T D Pollard, 1986, Journal of Cell Biology)*. As the rate of ATP hydrolysis increases with the incorporation of new actin monomers, the actin filament becomes increasingly enriched with ADP-actin along its length. Knowing that the dissociation of ADP-actin from the filament end is much faster than that of ATP-actin, distinct critical concentrations for the latter at the two extremities give rise to a phenomenon called filament treadmilling, which allows the amount of polymerizable actin monomers to remain constant *(Thomas D Pollard & Borisy, 2003, Cell)*. Within a certain range of concentrations of available ATP-actin, monomer incorporation at the barbed end is fast enough to maintain actin filament stability and is slower than ATP hydrolysis at the pointed end. Consequently, F-actin filaments will be allowed to grow from their barbed end and depolymerize from their pointed end.

In addition to being intrinsically polar with asymmetric dynamics at their opposing barbed and pointed ends, F-actin filaments are chiral biomolecules that have distinctive helical structures *(Jegou & Romet-Lemonne, 2020, Seminars in Cell & Developmental Biology)*. X-ray diffraction and electron microscopy studies reveal that a single actin filament is characterized by a right-handed double helix with a crossover distance of 36nm; a full helical turn along the filament occurs every 72nm (Figure 2) *(Oda et al., 2009, Nature; Fujii et al., 2010, Nature; Chou & Pollard, 2019, Proceedings of the National Academy of Sciences; Jegou & Romet-Lemonne, 2020, Seminars in Cell & Developmental*

Biology). The resulting inherent periodicity supports the packing of filaments into tight bundles by imposing sufficient geometrical constraints. Moreover, the helical structure of

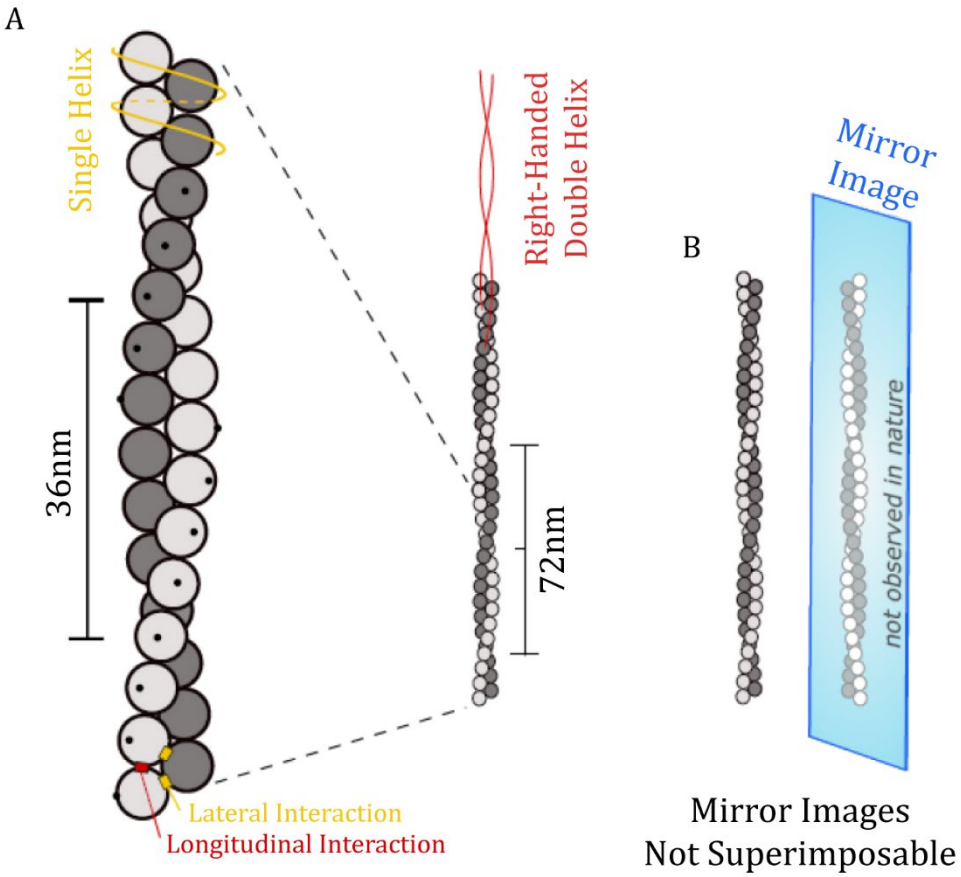

Figure 2: Sc**hematic representation of an actin filament.**
Adapted from *(Jegou & Romet-Lemonne, 2020, Seminars in Cell & Developmental Biology)*.
A: Actin monomers represented as spheres. The two strands are indicated in different shades of gray. The black dots specify the orientation of the monomers. The pitch of the double helix is 72nm. The actin filament is a right-handed, two-start, long-pitch helix (indicated by the red lines), but it can also be described as a left-handed, one-start, short-pitch helix (indicated by the orange line).
B: Actin filaments are chiral: they do not superimpose on their mirror image.

actin filaments facilitates the generation of mechanical torques upon the interaction with certain proteins, which, unlike the nucleotide state of actin monomers, pH, or ionic strength, can significantly modify the helical properties of the filaments *(Crevenna et al., 2013, Journal of Biological Chemistry; Merino et al., 2018, Nat Struct Mol Biol; Chou & Pollard, 2019, Proceedings of the National Academy of Sciences)*.

Actin filaments can interact with a variety of proteins collectively referred to as actin-binding proteins (ABPs), which associate with them to mediate their nucleation, elongation, stability, reorganization, and disassembly. Interestingly, the activity of these proteins not only modifies the helicity of the actin filaments but is also affected by it (described in more details in the sections to follow).

Overall, actin filaments are polar polymers that are characterized by asymmetric dynamics at their barbed and pointed ends as well as distinctive chiral, helical structures.

V.3. Breaking Symmetry

The development of living organisms and their proper functioning rely on certain key instances where symmetry is broken to support the emergence of specialized structures that are adapted for particular functions and processes. In this section, we will discuss the two major cytoskeleton-based symmetry-breaking events that can occur in cells, highlighting several examples for each and briefly recapitulating some of the mechanisms involved.

1. Axial Symmetry Breaking: emergence and maintenance of polarity

Cellular polarity is marked by the definition of a vectorial axis that biases the organization of the cell. Despite its existence in almost all living organisms of various complexities, cell polarity always depends on two fundamental parameters: the establishment of structural polarity through the biased orientation of inherently polar cytoskeletal filaments, as well as the interpretation of this structural polarity and its translation into a functional asymmetry by the reorganization of key intracellular components at the opposing cellular poles. Due to its essential roles in diverse cellular processes and functions, polarity has been the subject of extensive research that aimed at properly characterizing the associated events and uncovering the underlying mechanisms in different contexts.

1.1. The intrinsic polarity and interactions of cytoskeletal components are sufficient to break symmetry in reconstituted systems

Cellular symmetry breaking events have been reconstituted in a variety of simplified systems in vitro. By providing more controllable experimental setups, these approaches have identified the necessary players involved in symmetry breaking and, thus, have greatly contributed to the understanding of the underlying mechanisms. A few of these reconstituted systems will be briefly presented here.

It has been demonstrated that molecular motors associated with microtubules can drive symmetry breaking in vitro. For example, the confinement of microtubules and kinesins to the surface of an emulsion droplet resulted in its random movement by the motor-driven microtubule flow generated within the droplets (Figure 3A-1) *(Sanchez et al., 2012, Nature)*. Moreover, it was shown that the interaction of microtubules with motors of opposing polarities bound to a fluid membrane could result in the formation of distinctive patterns, in which the differential segregation of motors at the level of individual microtubules translated into a large-scale polarized microtubule orientation (Figure 3A-2). Maintained at steady state by the balance of forces the two motors apply on the

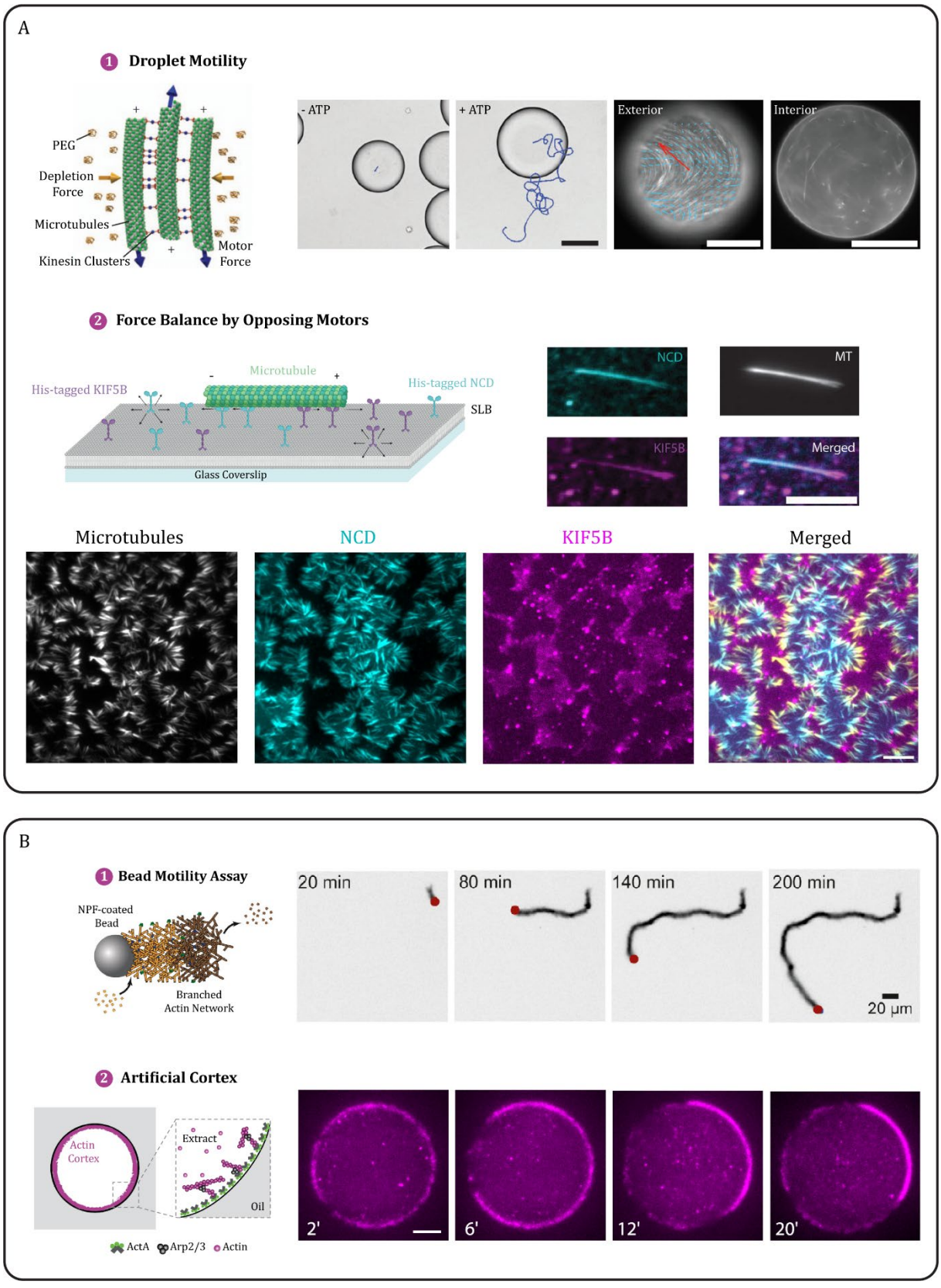

Figure 3: The polar nature of microtubules and actin drives diverse symmetry breaking phenomena in vitro.

A: In vitro microtubule-based symmetry breaking phenomena

(1) Droplet Motility: To the left, schematic illustration of an extensile microtubule-kinesin bundle. Kinesin clusters exert inter-filament sliding forces. To the right, trajectories of droplets containing extensile microtubule bundles in the absence and presence of ATP (Scale Bar = 80mm); fluorescence image of active microtubule bundles at the oil-water interface; streaming flows are indicated by blue arrows; the direction of instantaneous droplet velocity is indicated by the red arrow; microtubule bundles are largely excluded from droplet interior (Scale Bar = 100μm). Adapted from *(Sanchez et al., 2012, Nature)*.

(2) Force Balance by Opposing Motors: On top, to the left, schematic representation of a microtubule under the action of plus-end directed KIF5B and minus-end directed NCD attached to a supported lipid bilayer. To the right, motors accumulate under individual microtubules and are sorted to their respective ends (Scale Bar = 10μm). On the bottom, microtubules, KIF5B, and NCD form domains that result in pattern formation within 60mins of gliding (Scale Bar = 20μm). Adapted from *(Utzschneider et al., 2024., Under Revision)*.

B: In vitro actin-based symmetry breaking phenomena

(1) Bead Motility Assay: To the left, scheme of a bead coated with nucleation-promoting factors (NPF) of Arp2/3 complex able to generate a branched actin comet. In orange is the freshly assembled ATP or ADP-Pi actin network; in brown is the ADP-actin network. To the right, snapshots of the growth of one actin comet from a bead (red dot) in a flow chamber. Scale Bar = 20μm. Adapted from *(Colin et al., 2023, EMBO J)*.

(2) Artificial Cortex: To the left, a scheme of an actin cortex formed at the inner interface of a water-in-oil emulsion. To the right, images showing the development of a polar actin cap in the emulsion. Adapted from *(Abu Shah & Keren, 2014, ELife)*.

---

microtubules, this system was characterized by being dynamic and readily able to reorganize in response to external cues *(Utzschneider et al., 2024., Under Revision)*.

An example of actin-based symmetry breaking in vitro was described by the emergence of directional comet tail motility from symmetric actin filaments clouds surrounding a spherical bead, homogeneously coated with proteins driving actin polymerization (Figure 3B-1). In this case, the symmetry-breaking event was associated with tension buildup inside the actin gel *(van der Gucht et al., 2005, Proceedings of the National Academy of Sciences; van Oudenaarden & Theriot, 1999, Nat Cell Biol; Colin et al., 2023, EMBO J)*. Upon reaching a certain threshold, actin filaments break, leading to the polarization of the gel and the initiation of directional bead motility. In another example, a reconstituted contractile cortex encapsulated within a droplet was shown to break symmetry in a way that could recapitulate the initial polarization event in certain cells (Figure 3B-2). Increased contraction induced the spontaneous transition of a uniform cortical layer into an asymmetric organization with a polar apical cap through contractile actomyosin flows *(Abu Shah & Keren, 2014, ELife)*.

1.2. The polarization event in cells

The process of cell polarization occurs in two steps. First, the actin network breaks the initial symmetry of the system. Then, guided by actin reorganization, the polarization of

the microtubules and the repositioning of the centrosome follow to stabilize the emergent asymmetry and maintain cell polarity. In the following sections, we will recapitulate some of the polarization phenomena that have been implicated in particular cellular processes or functions.

1.2.1. The immune synapse formed by T-lymphocytes

The immune synapse is an important physiological structure, whose formation during specific immune responses is crucial for the effective elimination of target pathological agents as well as for the coordination between immune cells. The interaction between an antigen-presenting cell (APC) and a T-lymphocyte initiates a symmetry-breaking event that is independent of microtubules (Figure 4A). A large-scale polarization of the actin cytoskeleton occurs in response to the first contact with an APC. The resulting actin organization biases the distribution of cortical dynein motors, which pull on microtubules to reposition the centrosome in close proximity of the immune synapse and globally polarize the entire microtubule network *(R. Li & Gundersen, 2008, Nat Rev Mol Cell Biol; X. Liu et al., 2013, Proceedings of the National Academy of Sciences; O. J. Gros et al., 2021, MBoC)*. The subsequent biased recruitment of the vesicular system components facilitates the directed delivery of secretions into the APC *(Ritter et al., 2015, Immunity)*. Thus, following the initial symmetry break by actin, the correct polarization of the microtubule network is required to reinforce the stability of the immune synapse and ensure its proper functioning.

1.2.2. Ciliogenesis in adherent cells

Upon exiting the cell cycle, cells enter into a quiescent state marked by the formation of a primary cilium originating from a plasma membrane-docked centrosome (Figure 4B). Therefore, this process necessitates the off-centering of the centrosome from its classical position in close proximity of the cell's geometrical center near the ventral surface so that it contacts the plasma membrane. In 2D patterned cells, such a symmetry-breaking event is associated with the global organization of the actin cytoskeleton. The interplay between asymmetric local contractility levels and differential enrichment of particular proteins at the ventral and dorsal domains biases the subsequent repositioning of key cellular components, like dynein molecular motors. This favors the recruitment of the centrosome to the dorsal surface of the plasma membrane, where it can initiate the generation of a primary cilium. *(Pitaval et al., 2010, Journal of Cell Biology; 2017, Journal of Cell Biology)*

1.2.3. Asymmetric cell division of the Caenorhabditis elegans (C. elegans) zygote

Cell fate diversification during development is mediated by asymmetric cell division, which is largely dependent on polarity *(Gönczy, 2008, Nat Rev Mol Cell Biol)*. One extensively studied example is the first division of the C. elegans zygote that relies on the establishment of an anteroposterior (AP) polarity axis shortly after fertilization (Figure 4C) *(Cowan & Hyman, 2004, Annu Rev Cell Dev Biol)*. Sperm entry provides the initial cue for symmetry breaking as it locally weakens the actin cortex at the prospective posterior pole, and, through the activation of the Rho pathway, initiates myosinII (MyoII)-driven

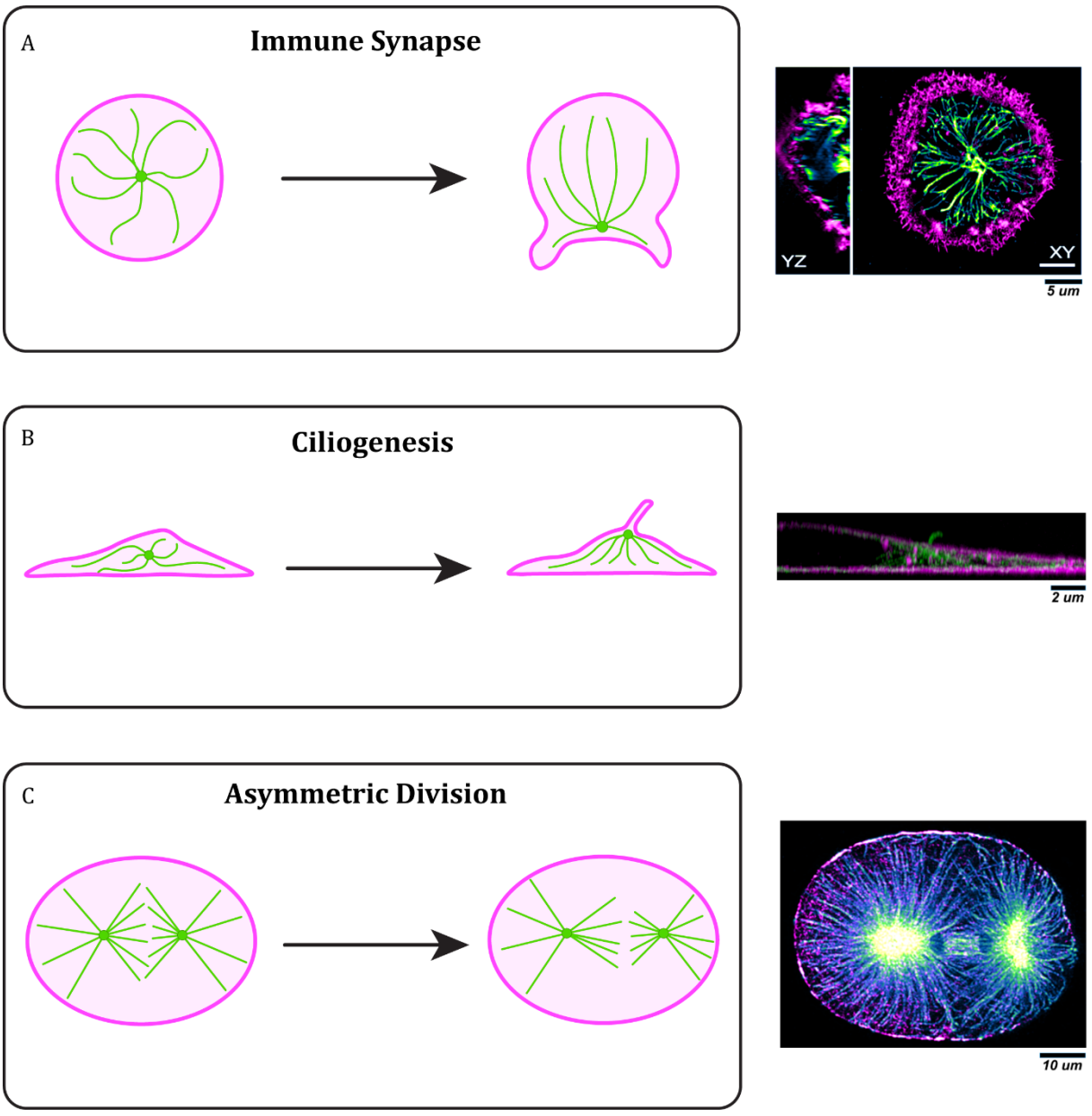

Figure 4: Examples of cellular symmetry breaking events.
Adapted from *(Schaeffer, 2023)*.
A: To the left, schematic representation of the transition of a lymphocyte from a non-polarized to a polarized state after forming an immune synapse. To the right, representative images of a polarized lymphocyte: reconstruction of the lymphocyte along its height showing the recruitment of the centrosome to the plane of the synapse; the organization of the actin and microtubule networks at the focal plane of the immune synapse. Adapted from *(Ritter et al., 2015, Immunity)*.
B: To the left, schematic representation of the polarization of an adherent cell during ciliogenesis. To the right, Expansion microscopy (4.5X) image of a ciliated epithelial cell; image reconstruction of the cell along its height shows the primary cilia located at the apical plasma membrane with microtubules in green and actin in magenta.
C: To the left, schematic representation of the transition of the mitotic spindle from a symmetric to an asymmetric position. To the right, representative image of an asymmetrically positioned mitotic in the C. Elegans zygote with microtubules in green and actin in magenta. Adapted from *Bruce A Bowerman's website*.

contraction of the network toward the anterior pole *(Jenkins et al., 2006, Science; Motegi & Sugimoto, 2006, Nat Cell Biol)*. Certain polarity markers are selectively transported by the directional network contraction toward the anterior pole, thereby leading to the specific enrichment of the posterior pole with other markers *(Hao et al., 2006, Developmental Cell, p. 2; Watts et al., 1996, Development, p.)*. The antagonistic effects of the opposing polarity markers on the contractility of the system help amplify the small force asymmetry triggered by initial sperm entry, thereby reinforcing the established contractility gradient and translating it into a stable segregation of proteins and a well-defined cell polarity *(Cuenca et al., 2003, Development; Severson & Bowerman, 2003, Journal of Cell Biology; Munro et al., 2004, Developmental Cell)*. The resulting composition of the posterior cortex mediates the anchorage of more dynein motors, which pull strongly on the mitotic spindle, causing its displacement toward the posterior pole *(Cowan & Hyman, 2004, Annu Rev Cell Dev Biol; Gönczy, 2008, Nat Rev Mol Cell Biol; R. Li & Gundersen, 2008, Nat Rev Mol Cell Biol)*. This biased spindle-positioning causes the deviation of the cleavage plane from the middle of the embryo, giving rise to two daughter cells of different sizes and fates (a larger anterior blastomere AB, and a smaller posterior blastomere P).

1.2.4. Directional mesenchymal cell migration

1.2.4.1. In single cells

The initiation of directional cell migration is largely dependent on the establishment and the maintenance of cell polarity. Most cells exhibit a bi-stable behavior, switching from a symmetric, stationary state to a polarized, motile one under certain conditions (Figure 5A). Such a transition occurs through a symmetry-breaking event that can be either spontaneous or triggered by external cues. Initial symmetry breaking involves the polarization of the actin cytoskeleton, resulting in the formation a protrusive, leading edge maintained by Arp2/3-mediated actin polymerization continuously pushing the membrane forward, and a contractile trailing edge, where MyoII-driven contraction detaches the cell rear and powers the effective translocation of the cell body *(R. Li & Gundersen, 2008, Nat Rev Mol Cell Biol; Blanchoin et al., 2014, Physiological Reviews)*.

Early events preceding symmetry break often involve actomyosin fluctuations that lead to a local increase in contractility associated with a polarized recruitment of MyoII at the prospective rear. This gives rise to an anisotropic cytoskeletal organization that drives cell translocation. The latter reinforces the existing actomyosin asymmetry, further supporting directional migration. Such is the case for keratocyte cells and fragments, which, upon a global or local increase in contractility, transition from their circular, stationary state, characterized by a symmetric actin organization and a centripetal flow, into a fully polarized, motile state, with predominant actin polymerization at the front and localized MyoII contraction at the rear (Figure 5B) *(Verkhovsky et al., 1999, Current Biology; Yam et al., 2007, Journal of Cell Biology)*. On the other hand, decreasing

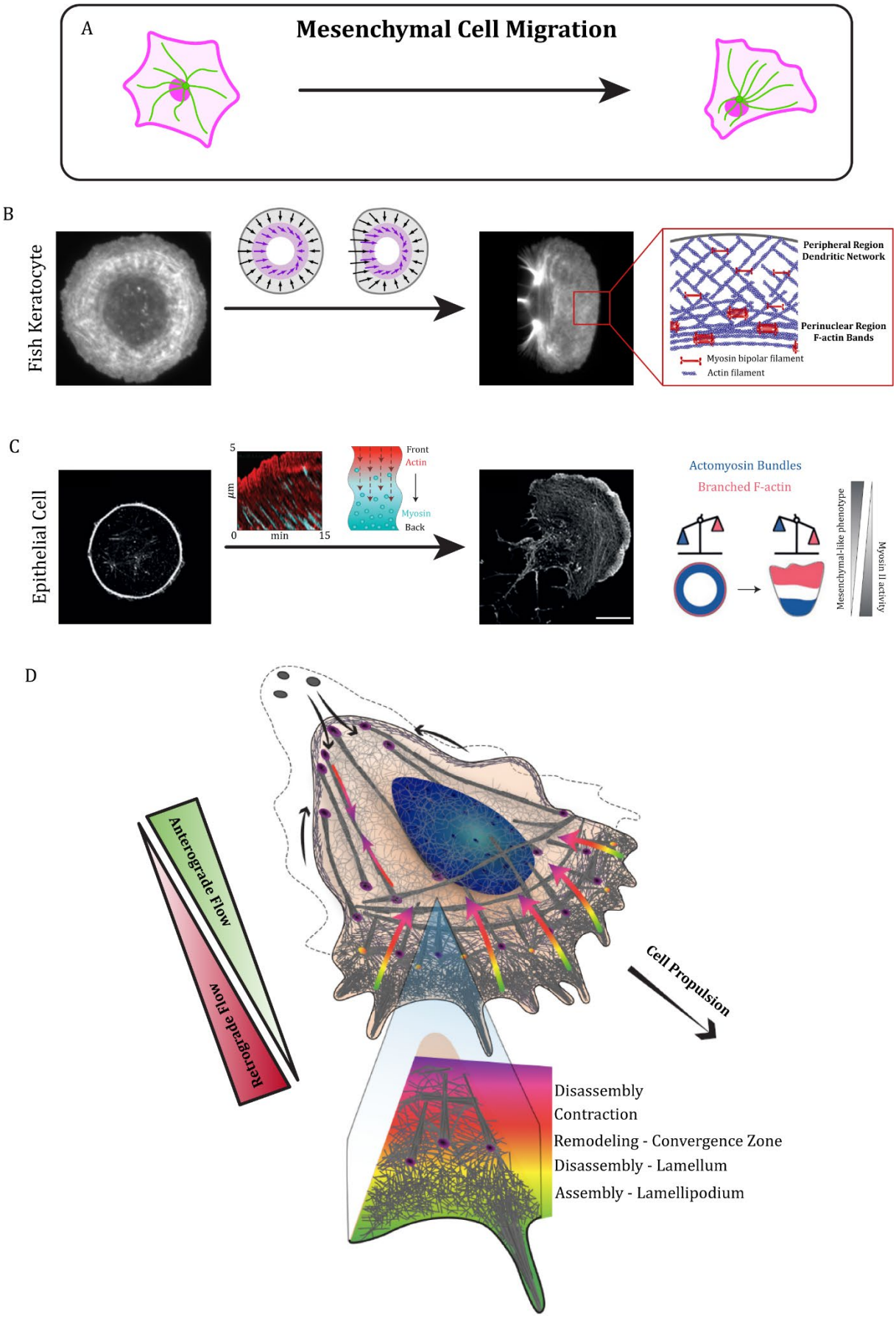
A
Mesenchymal Cell Migration
B
Fish Keratocyte
Peripheral Region
Dendritic Network
Perinuclear Region
F-actin Bands
Myosin bipolar filament
Actin filament
C
Epithelial Cell
5
μm
0
min
15
Front
Actin
Myosin
Back
Actomyosin Bundles
Branched F-actin
Mesenchymal-like phenotype
Myosin II activity
D
Anterograde Flow
Retrograde Flow
Cell Propulsion
Disassembly
Contraction
Remodeling - Convergence Zone
Disassembly - Lamellum
Assembly - Lamellipodium

Figure 5: The polarization events underlying single cell directional cell migration.
A: Schematic representation of the polarized state acquired by an adherent cell upon the initiation of migration. Adapted from *(Schaeffer, 2023)*.
B: To the left, representative images of fish keratocytes highlighting the changes in F-actin organization upon the initiation of directional migration: transition from a stationary state with radially symmetric centripetal actin flow to polarized, motile state with decreased actin flow speed at the cell front. To the right, model of actomyosin organization in keratocytes at the time of symmetry break. At the periphery of the lamellipodium, myosin bipolar filaments cross-link a dendritic F-actin network without contraction. Toward the cell body, the activity of large myosin II clusters contracts and reorganizes the dendritic network to form F-actin bands and bundles. Adapted from *(Yam et al., 2007, Journal of Cell Biology)*.
C: To the left, representative images highlighting the changes in F-actin organization in an epithelial cell upon the initiation of directional migration mediated by the accumulation of MyoII at the back of the cell by means of actin–myosin retrograde flows. Scale Bar = 10μm. To the right, a simplified model depicting that a stationary epithelial cell can be transformed into mesenchymal-like cells after lowering levels of actomyosin contractility and shifting the balance between Arp2/3- and myosin-dependent actin networks. Adapted from *(Lomakin et al., 2015, Nat Cell Biol)*.
D: Dynamics of actin structures during motility. The specialized actin organizations are involved in assembly and protrusive force production at the cell front and in contraction and disassembly at the center and at the trailing edge of motile cells. The tight spatiotemporal coordination of actin turnover and dynamics gives rise to two competing actin flows that reinforce the initial symmetry break: a treadmilling-mediated retrograde flow and a MyoII contraction-driven anterograde flow. The color code in the zoom region highlights the different mechanisms controlling actin dynamics (assembly, fragmentation, disassembly, remodeling, contraction, and disassembly) and is used in large arrows in the cell to illustrate where these different mechanisms occur during cell motility. Adapted from *(Blanchoin et al., 2014, Physiological Reviews)*.

contractility among strictly immotile, discoidal epithelial cells triggers their front-rear polarization and migration initiation (Figure 5C) *(Lomakin et al., 2015, Nat Cell Biol)*. This effect is attributed to the generation of actin retrograde flow driven by branched actin polymerization, which is enhanced due to increased availability of free actin monomers previously engaged in rather stable contractile structures.

In migrating cells, the anisotropy in contractility resulting from the initial symmetry-breaking event is reinforced by the emergence of two opposing flows (Figure 5D) *(Levayer & Lecuit, 2012, Trends in Cell Biology)*. At the leading edge, a treadmilling-mediated retrograde flow governed by actin turnover transports actin and MyoII backward. Initiating from the lamellum is a MyoII contraction-driven anterograde flow that brings actin filaments to the front *(Ponti et al., 2004, Science; Vallotton et al., 2004, Proceedings of the National Academy of Sciences; Vicente-Manzanares et al., 2009, Nat Rev Mol Cell Biol)*. These two distinct flows are essential for cell migration. While polymerization at the front, sustained by the large pool of monomeric actin provided by the convergence of the retro- and anterograde flows, induces forward membrane movement, leading to the emergence

of protrusions that explore the surrounding environment, the coordinated contraction and substrate attachment at the lamellum and the cell rear drive the displacement of the cell body.

However, asymmetry and motility established by actin-mediated symmetry break require the subsequent polarization of the microtubule network to further stabilize cell polarity and ensure persistent migration (Figure 5A). Following protrusion formation, microtubules growing toward the leading edge become increasingly enriched in certain post-translational modifications (PTMs) that confer additional stability. This selective stabilization of a subset of microtubules induces the polarization of the entire network, subsequently leading to a biased orientation of the secretory machinery toward the cell front, marked by the reorientation of the Nucleus – Centrosome – Golgi in the direction of migration *(Gundersen & Bulinski, 1988, Proceedings of the National Academy of Sciences; Palazzo et al., 2001, Nat Cell Biol; Wittmann & Waterman-Storer, 2001, Journal of Cell Science; R. Li & Gundersen, 2008, Nat Rev Mol Cell Biol)*. Interestingly however, in certain cell types, such as T-lymphocytes and leader cells of the Zebrafish lateral line, directional migration is marked by a rear localization of the centrosome. Additionally, it has been demonstrated that in response to the confinement of individual cells on 1D lines, the centrosome, together with the Golgi, predominantly localize to the cell rear after symmetry break to support persistent migration *(Pouthas et al., 2008, Journal of Cell Science; J. Zhang et al., 2014, Proceedings of the National Academy of Sciences; J. Zhang & Wang, 2017, MBoC)*. Hence, despite always being a pre-requisite for maintaining directional migration, the off-centering of the centrosome and the closely related Golgi, as well as its correlation with the direction of migration, highly depend on the cellular context and the existing geometrical constraints. By acquiring an off-centered position, the centrosome can polarize the microtubule network even further.

Interestingly, the speed at which the cells move following symmetry break and migration initiation is tightly dependent on their contractility levels. In fact, a biphasic relationship has been reported to exist between migration velocity and contractility based on the strength of focal adhesions (FAs) and the actomyosin retrograde flow. This suggests that the highest migration speed is associated with an optimum of contractility, defined by an intermediate adhesion strength accompanied by a relatively low retrograde flow *(Jurado et al., 2005, MBoC; Gupton & Waterman-Storer, 2006, Cell; Barnhart et al., 2011, PLOS Biology).*

1.2.4.2. In cell collectives

The same mechanism of cell polarization described above is employed by leader cells to initiate directional migration of cell collectives. These coordinated, large-scale motions have been extensively studied using approaches, like wound healing assays and micropatterning techniques, to better understand the principles underlying the emergence and the maintenance of collective behaviors.

When exposed to a free edge, an epithelial monolayer forms finger-like protruding structures that are several tens of cells in diameter (Figure 6A) *(Poujade et al., 2007, Proceedings of the National Academy of Sciences)*. Cells at the very tip of these structures

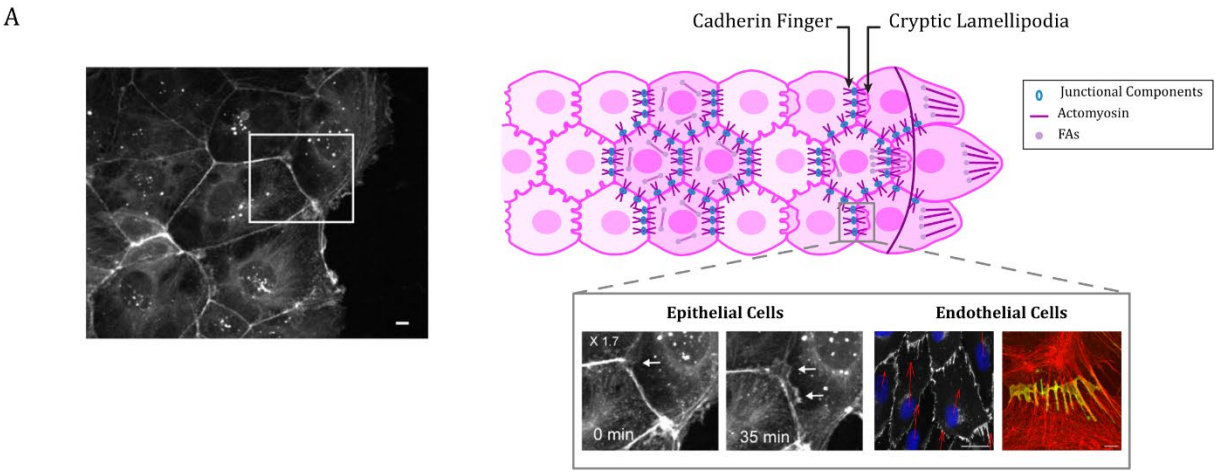
A
Cadherin Finger
Cryptic Lamellipodia
Junctional Components
Actomyosin
FAs
Epithelial Cells
Endothelial Cells
X 1.7
0 min
35 min

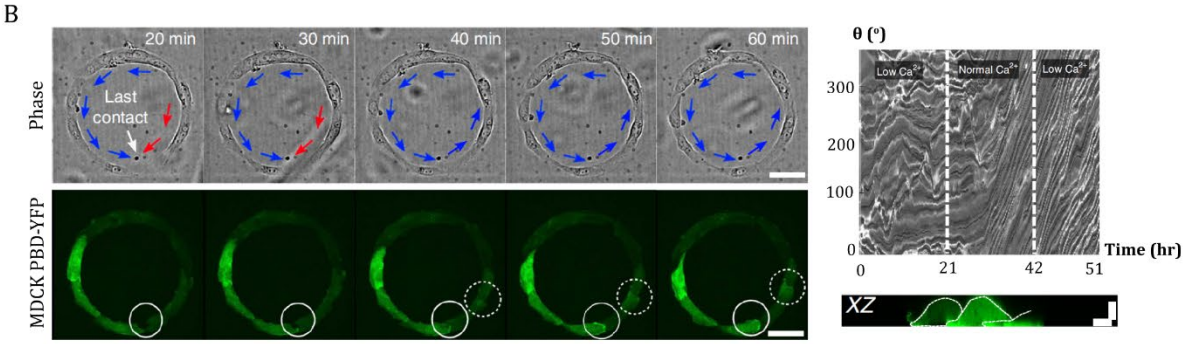
B
20 min
30 min
40 min
50 min
60 min
Phase
Last contact
MDCK PBD-YFP
θ (°)
Low Ca2+
Normal Ca2+
Low Ca2+
300
200
100
0
Time (hr)
0
21
42
51
XZ

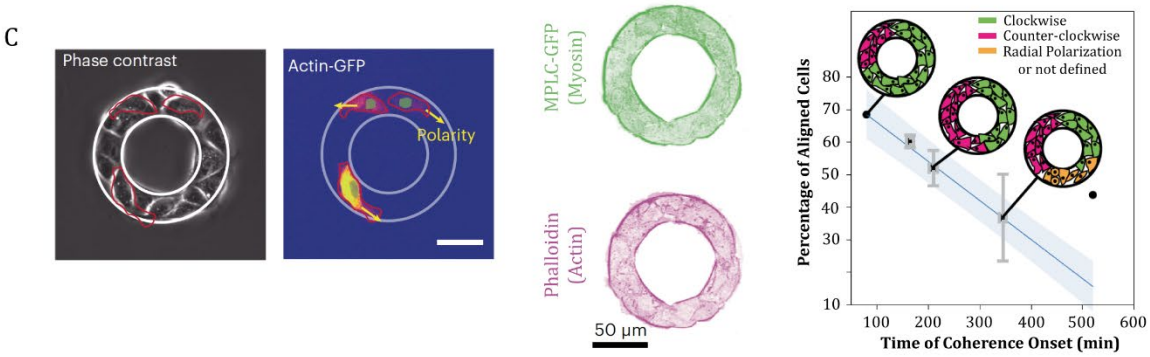
C
Phase contrast
Actin-GFP
Polarity
MPLC-GFP (Myosin)
Phalloidin (Actin)
50 μm
Clockwise
Counter-clockwise
Radial Polarization or not defined
Percentage of Aligned Cells
80
70
60
50
40
30
10
100
200
300
400
500
600
Time of Coherence Onset (min)

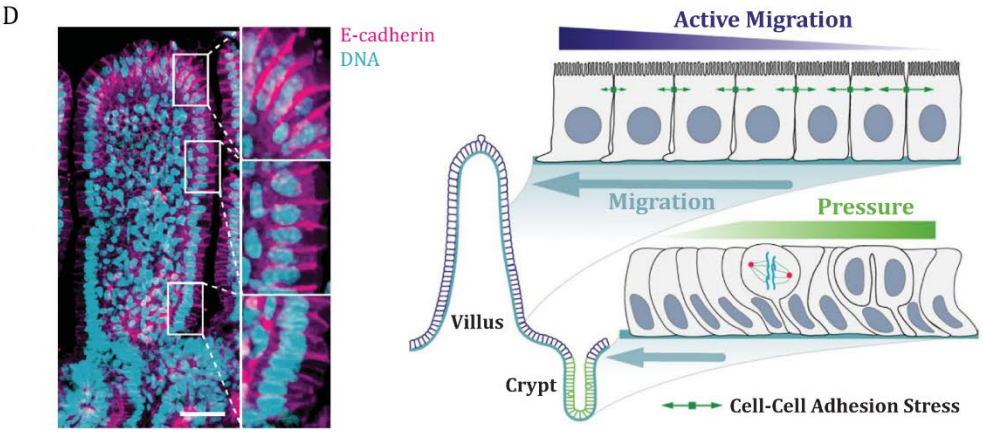
D
E-cadherin
DNA
Active Migration
Migration
Pressure
Villus
Crypt
Cell-Cell Adhesion Stress

Figure 6: Examples of collective migration phenomena.
A: To the left, representative image of actin organization in epithelial cell collective engaging in wound-healing movement. Scale Bar = 10μm. To the right on top, schematic illustration of the topologies of intercellular junctions, focal adhesions, contractile actin fibers, and protrusive lamellipodia in migrating epithelium and endothelium monolayers. On the bottom, magnified images showing the specialized structures forming at cell-cell contacts: cryptic lamellipodia or protrusions that crawl under the cells (white arrows) in epithelial monolayers (Scale Bar = 10μm) in addition to the polarized cadherin fingers of endothelia that extend in the direction of motion (Scale Bar = 20μm) and are extensively embedded within the actin cytoskeleton (3D SIM; Scale Bar = 2μm). Adapted from *(Hayer et al., 2016, Nat Cell Biol; Ladoux & Mège, 2017, Nat Rev Mol Cell Biol; Ozawa et al., 2020, Journal of Cell Biology)*.
B: To the left, confocal microscopy images (basal plane) of MDCK PBD–YFP (yellow fluorescent protein) cells just before and after the establishment of last contact (white circle) between two oppositely migrating cell trains showing the change in intensity of PBD–YFP biosensor signal in the cell reversing its direction of migration (dashed circle). Arrows indicate the direction of motion of the cell trains (Scale Bar = 50μm). To the right on top, XZ plane of a confocal microscopy image showing the establishment of Rac1-rich cryptic lamellipodia in MDCK cells (Scale Bar = 4μm). On the bottom, Representative spatiotemporal displacement kymograph of cell trains on a 20μm ring depicting the changes in the collective rotational behavior in the absence or presence of EGTA at different time points. Adapted from *(Jain et al., 2020, Nat. Phys.)*.
C: To the left, a phase contrast image of MDCK cells on an 80μm ring with actin-GFP signal visualized. Arrows indicate the cell polarity based on the direction/orientation of cell lamellipodium (Scale bar 50μm). Immunostaining of an 80μm ring, showing myosin and actin organization in green and purple, respectively. To the right, percentage of aligned cells (based on their polarity) with respect to the time of coherence onset. For each data point, a schematic view of cell polarity within the ring is presented. Adapted from *(Lo Vecchio et al., 2024, Nat. Phys.)*.
D: To the left, representative image of an intestinal villus (longitudinal section – E-cadherin in hot pink and DNA in blue). Regions in boxes are magnified (Scale Bar = 40μm). To the right, mechanical model for epithelial cell migration in the different regions of the small intestine. Adapted from *(Krndija et al., 2019, Science)*.

are defined as leader cells, which acquire notable migratory capacities, marked by large lamellipodia, and maintain strong cadherin-based contacts with the follower cells, thereby enabling them to drive directional collective motion *(Reffay et al., 2011, Biophysical Journal)*. In addition, leader cells exert significantly high traction forces that are associated with the formation of large FAs. However, certain sites with considerable magnitude of forces can still be identified further away from the leading edge *(du Roure et al., 2005, Proceedings of the National Academy of Sciences; Poujade et al., 2007, Proceedings of the National Academy of Sciences; Trepat et al., 2009, Nature Phys; Reffay et al., 2014, Nat Cell Biol)*. The transmission of forces within a cell monolayer relies on the interaction of cells with the ECM through FAs as well as with the neighboring cells through adherens junctions *(Ladoux & Mège, 2017, Nat Rev Mol Cell Biol)*. Although signals from

the substrate favor the migration of the cells away from each other, higher tension at the cell-cell contacts maintains collective coherence. This suggests that the coordination between cells in a monolayer is driven by the transmission of forces across intercellular junctions *(Mertz et al., 2013, Proceedings of the National Academy of Sciences; Bazellières et al., 2015, Nat Cell Biol)*. Despite exerting strong traction forces that can destabilize cell-cell adhesions, leader cells are capable of maintaining cadherin-based contacts with follower cells *(Poujade et al., 2007, Proceedings of the National Academy of Sciences)*. This can be in part attributed to the formation of contractile actin cables spanning multiple cells at the leading edge *(Ladoux & Mège, 2017, Nat Rev Mol Cell Biol)*. These structures generate inward-directed stresses that help preserve the integrity of the finger-like collectives.

To ensure coherent collective motion, cell polarization established by single cells at the leading edge must be propagated across the monolayer. This raises important considerations about the role of cell-cell adhesions and their associated force transmission in cell polarization *(Begnaud et al., 2016, Current Opinion in Cell Biology)*. The exposure to a free surface and the subsequent engagement of integrins result in the polarization of leader cells; the establishment of opposing gradients of RhoA and Rac lead to the emergence of front-rear polarization: a protruding leading edge, dominated by Rac and a contractile trailing edge, dominated by RhoA *(Lawson & Burridge, 2014, Small GTPases; Mayor & Etienne-Manneville, 2016, Nat Rev Mol Cell Biol)*. At adherens junctions, the engagement of cadherin activates RhoA, indicating that intercellular junctions provide additional cues to maintain a stable front-rear polarization of the leader cells at the front row of a migrating monolayer *(Desai et al., 2009, Journal of Cell Science; Ouyang et al., 2013, Nat Commun; Lecuit & Yap, 2015, Nat Cell Biol; Mayor & Etienne-Manneville, 2016, Nat Rev Mol Cell Biol)*. In addition, cell-cell contacts are also involved in the propagation of the polarized RhoA-Rac gradients to the multicellular level through mechanisms that often involve the extension of cryptic lamellipodia in the direction of migration as well as polarized cadherin fingers by cells behind the leading edge *(Farooqui & Fenteany, 2005, Journal of Cell Science; Ng et al., 2012, Journal of Cell Biology; Reffay et al., 2014, Nat Cell Biol; Cai et al., 2014, Cell; Hayer et al., 2016, Nat Cell Biol)*. These polarized structures provide guiding signals that help maintain the persistent and coherent directional migration of the cell collective (Figure 6A).

During development, certain tissue monolayers lacking a free front edge break symmetry and initiate collective migratory behaviors that can drive tissue morphogenesis. Reproducing these motions using micropatterns with particular curvatures has provided valuable insights into the possible implicated mechanisms. For example, at confluence, epithelial cells confined on one-dimensional rings engage in a persistent directional rotation (Figure 6B). While the transmission of forces through cell-cell adhesions seems essential for rotation onset, the coherence of this collective directional motion is mostly mediated by the stable establishment of front-rear polarities (opposing Rac and RhoA gradients) at the level of individual cells that are coordinated by cryptic lamellipodial structures. The disruption of this polarity gradient results in the complete arrest of the collective rotation *(Jain et al., 2020, Nat. Phys.)*. Early events preceding rotation initiation of epithelial cell clusters are characterized by a tug-of-war imposed by the opposing polarities of the constituting cells (Figure 6C). The time necessary to resolve this polarity

competition is dependent on the distribution of single cell polarities. The propagation of polarity signals mediated by supra-cellular actomyosin structures (actomyosin cables) results in coordinated reorientation of the cells across the collective and, subsequently, the emergence of coherent rotation *(Lo Vecchio et al., 2024, Nat. Phys.)*.

The gut epithelium provides another interesting example of a coordinated collective behavior, in which polarized, columnar cells continuously migrate between two spatially separated functional compartments (crypts and the villi) to ensure rapid gut epithelial renewal (Figure 6D) *(van der Flier & Clevers, 2009, Annu Rev Physiol)*. In addition to their classical apicobasal polarity, epithelial cells migrating along the villi are characterized by a distinctive front-rear polarization, marked by Arp2/3-mediated extension of actin-based lamellipodia that, together with traction forces accumulated at the bottom of the villus, drive their active migration toward the top. Moreover, cell-cell adhesions maintain the coherence of the collective movement by minimizing the dispersion between the enterocytes, whose migration velocity is accelerated as they approach the villus tip *(Kaur & Potten, 1986, Cell Tissue Kinet; Krndija et al., 2019, Science)*. This suggests that the collective motion of these epithelial cells is driven by an active migration mechanism and not simply by the pushing forces resulting from cell division – mitotic pressure *(Cheng & Leblond, 1974, Am J Anat; Parker et al., 2017, FASEB J)*.

2. LR Symmetry Breaking: emergence and maintenance of chirality

LR symmetry breaking is a hallmark event during the early development of organisms that is crucial for their normal morphogenesis and proper functioning. Indeed aberrant LR asymmetries can result in structurally inverted, fully functional organisms (as in the case of situs inversus), but they often lead to severe physiological malformations associated with developmental disorders (like congenital heart diseases, or heterotaxia in humans) and even death *(Brueckner, 2007, Circulation; Levin, 2005, Mechanisms of Development)*. Interestingly, LR asymmetry consistently emerges in diverse species of varying complexity with different manifestations, including organ positioning in humans, shell coiling in snails, spiral arrangement of leaves in plants, to serve developmentally conserved functions *(Azpeitia et al., 2021, Science; Levin, 2005, Mechanisms of Development)*. The conserved nature of LR asymmetry raises a series of fascinating biological questions. What selective advantage does this asymmetry provide? What type of cue does asymmetry represent in development and function? How early in development is asymmetry initiated?

Other interesting questions that come to one's mind are if and how the different forms of asymmetries across species are connected. The key to answering these questions lies in the fact that all biological systems are fundamentally assembled from common homochiral molecular components. However, whether the macroscopic LR asymmetries observed in living organisms are directly emanating from the molecular chirality of their constituents remains an open question.

In the following sections, we will present various examples of LR asymmetry described at different scales of complexity while discussing the current hypotheses on the potential origin of chirality.

2.1. Molecular chirality originating from the cytoskeleton

Owing to their intrinsically chiral nature, actin and microtubules can demonstrate chiral behaviors upon interacting with their associated proteins, particularly those that are capable of generating molecular torques. This results in their helical rotation that has been characterized in a wide variety of reconstituted in vitro assays, in which the interacting protein dictates the bias of the reported motion.

Kinesin motors can produce molecular torques that are large enough to induce microtubule coiling and twisting. In particular, kinesin-14 and kinesin-5 can drive a biased helical rotation of crosslinked, antiparallel microtubules in vitro (Figure 7A-1). Interestingly, the simultaneous action of the two opposing motors on the same microtubule suppresses the helical motion and induces its chiral twisting instead *(Mitra et al., 2020, Nat Commun)*. This function described for crosslinking kinesins can play a key role in the proper organization of the mitotic spindle, thereby contributing to its intrinsic left-handed chirality reported in vivo (Figure 7A-2) *(Trupinić et al., 2022, Current Biology)*.

Similarly, actin-binding proteins (ABPs) capable of modulating the helicity of the actin filaments with which they bind and interact are associated with particular chiral behaviors that can contribute to LR symmetry breaking across scales.

2.1.1. Formins

Formins constitute a family of actin nucleators actively involved in the elongation of unbranched, parallel and anti-parallel actin bundles *(Rottner et al., 2017, Journal of Cell Science)*. Formins are homodimers, composed of an FH1 domain that captures and routes profilin-actin, and an FH2 domain, which interacts with actin filaments barbed ends *(Moseley et al., 2004, MBoC; Oosterheert et al., 2024, Science)*. A distinctive feature of formins is their mechanosensitive nature, which enables them to sense myosin-pulling forces and accordingly adjust their actin polymerization activity *(Jégou et al., 2013, Nat Commun; Yu et al., 2017, Nat Commun; Vavylonis & Horan, 2017, Curr Biol; Zimmermann & Kovar, 2019, Current Opinion in Cell Biology; Alieva et al., 2019, Nat Commun)*. The fact that formins can remain proccessively bound to the barbed end of F-actin suggests that they tend to rotate during elongation in order to follow the filament helix *(Higashida et al., 2004, Science; Kovar & Pollard, 2004, Proceedings of the National Academy of Sciences; Romero et al., 2004, Cell; Shemesh et al., 2005, Journal of Cell Biology)*. However, in cells, formin rotation is hindered by their anchorage to the membrane, as well as by the interconnection of the filaments they elongate. Due to F-actin helicity, these rotationary-constrained formins can apply molecular torques while elongating actin filaments, causing their under-twisting (Figure 7B-1) *(Mizuno et al., 2011, Science; 2018, Proceedings of the National Academy of Sciences)*. Indeed, Mizuno et al. showed that mDia1 formins immobilized on glass substrates generated a right-handed helical rotation of polymerizing actin filaments. In addition to its implication in the development of chirality across scales, this helical rotation could contribute to the stability of the elongating actin filaments by increasing their resistance to cofilin-mediated severing *(Mizuno et al., 2011, Science; 2018, Proceedings of the National Academy of Sciences)*. Interestingly, the generated torques could influence formin functioning by increasing the efficiency of actin

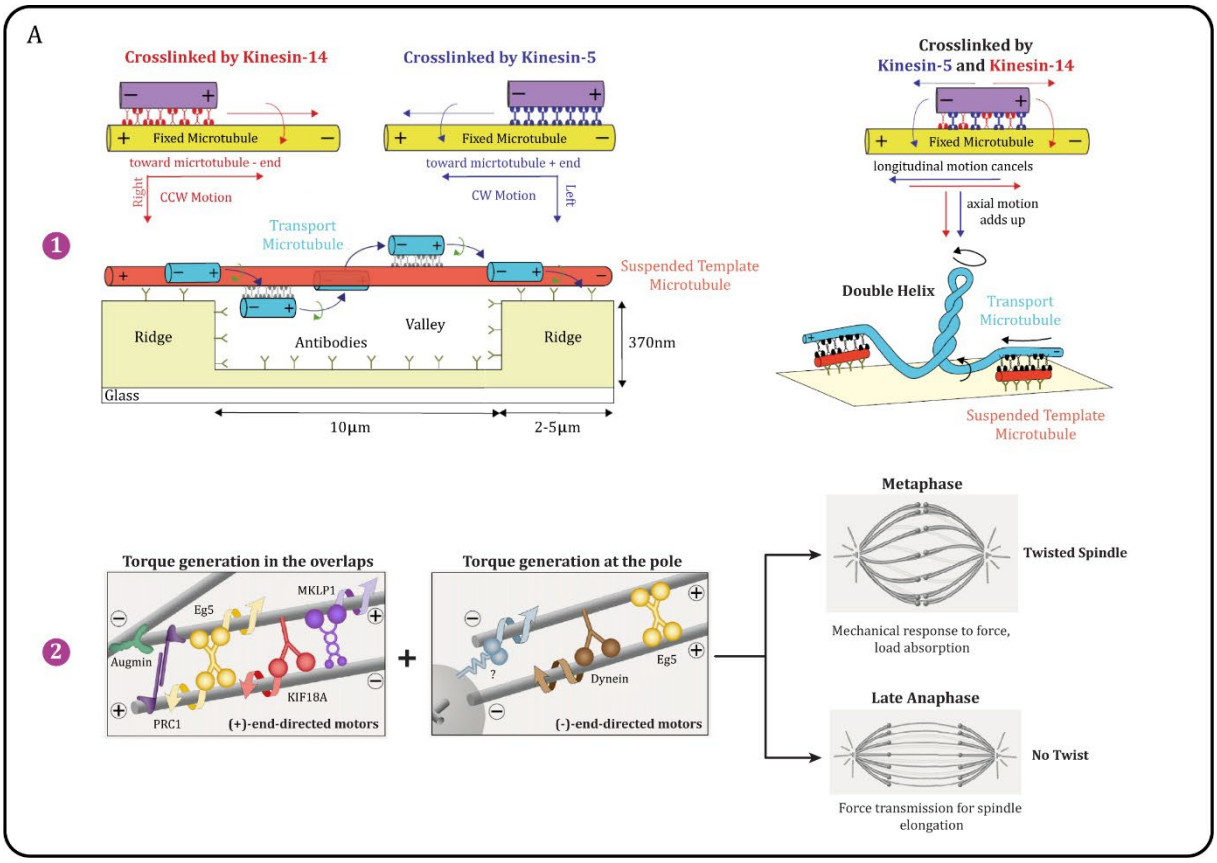
A
Crosslinked by Kinesin-14
Crosslinked by Kinesin-5
Fixed Microtubule
toward micrtotubule - end
Right
CCW Motion
toward micrtotubule + end
CW Motion
Left
Crosslinked by
Kinesin-5 and Kinesin-14
longitudinal motion cancels
axial motion
adds up
1
Transport
Microtubule
Suspended Template
Microtubule
Ridge
Antibodies
Valley
Ridge
370nm
Glass
10µm
2-5µm
Double Helix
Transport
Microtubule
Suspended Template
Microtubule
Metaphase
Twisted Spindle
Mechanical response to force,
load absorption
2
Torque generation in the overlaps
Torque generation at the pole
MKLP1
Eg5
Augmin
KIF18A
PRC1
(+)-end-directed motors
?
Dynein
Eg5
(-)-end-directed motors
Late Anaphase
No Twist
Force transmission for spindle
elongation

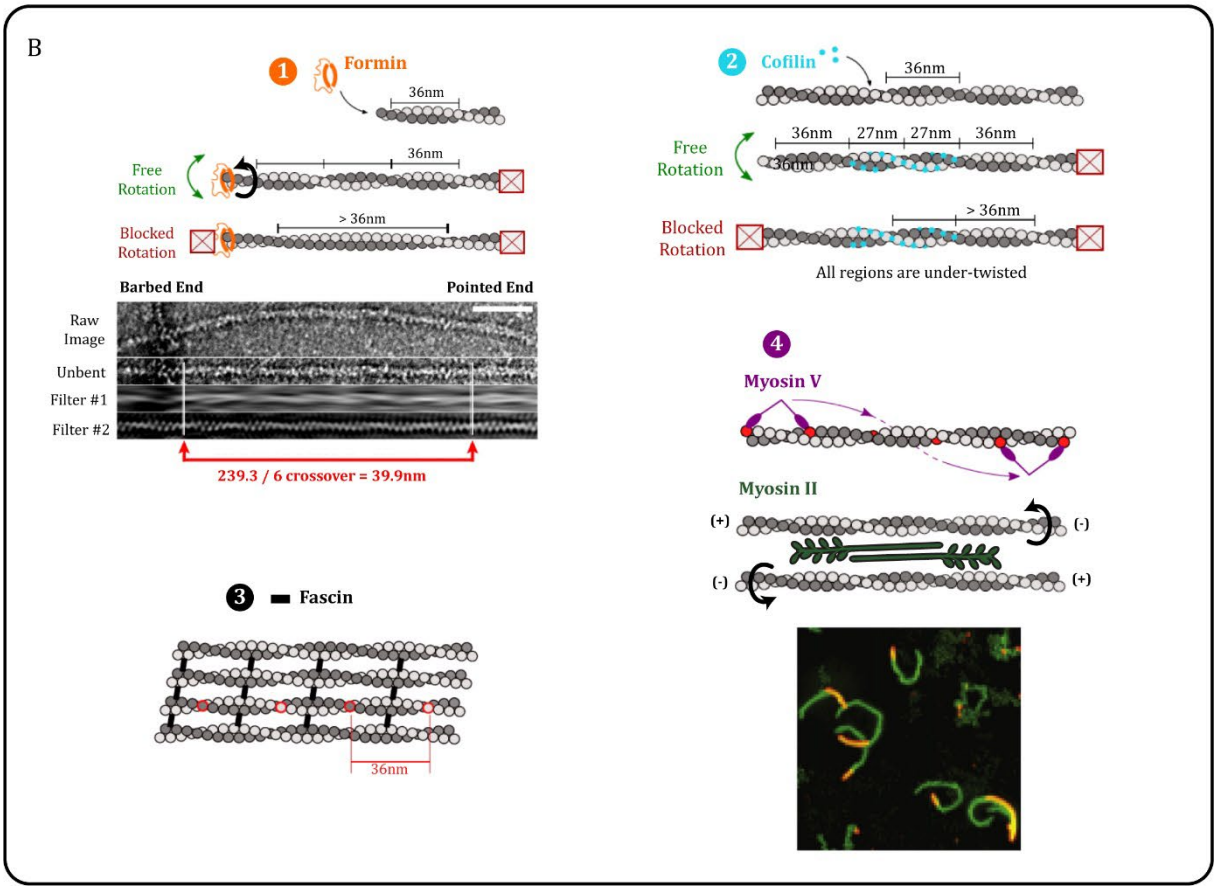
B
1
Formin
36nm
Free
Rotation
36nm
Blocked
Rotation
> 36nm
Barbed End
Pointed End
Raw
Image
Unbent
Filter #1
Filter #2
239.3 / 6 crossover = 39.9nm
2
Cofilin
36nm
Free
Rotation
36nm
27nm
27nm
36nm
36nm
Blocked
Rotation
> 36nm
All regions are under-twisted
4
Myosin V
Myosin II
(+)
(-)
(-)
(+)
3
Fascin
36nm

Figure 7: The molecular origin of LR asymmetry.
A: Microtubule chirality demonstrations
(1) Illustrations to visualize the motion of antiparallel microtubules cross-linked by Ncd. To the left, on a suspended template microtubule, kinesin-14 motors drive the helical motion of transport microtubules towards the minus-end of the template microtubule in a right-handed manner (clockwise motion), while kinesin-5 motors drive the helical motion of transport microtubules towards the plus-end of the template microtubule in a left-handed manner (counter-clockwise motion). To the right, the simultaneous action of kinesin-5 and kinesin-14 results in microtubule overlap, in which the motion in the longitudinal direction cancels out while the motion in the axial direction adds up. Adapted from *(Mitra et al., 2020, Nat Commun)*.
(2) To the left, opposing motors apply differential torques in different regions of the mitotic spindle that generate a global spindle twist. To the right on top, during metaphase, spindle twist absorbs the load and provides mechanical support against external forces. On the bottom, in late anaphase, the absence of the twist promotes force transmission for spindle elongation and chromosome separation. Adapted from *(Trupinić et al., 2022, Current Biology)*.
B: Actin chirality demonstrations
(1) On top, a formin tracking the elongating barbed end of an anchored actin filament must be free to rotate in order to follow the helical pitch. If the formin cannot rotate, the filament cannot incorporate new turns and becomes under-twisted. On the bottom, electron micrographs of F-actin elongated from immobilized mDia1 aggregates (Scale bar = 50nm). Adapted from *(Jegou & Romet-Lemonne, 2020, Seminars in Cell & Developmental Biology; Mizuno et al., 2018, Proceedings of the National Academy of Sciences)*.
(2) Cofilin forms domains as it binds to the sides of an actin filament. If the filament is free to rotate, both bare filament and cofilin-decorated regions adopt their natural helicity. If the filament cannot rotate, new turns cannot be added, and both regions become under-twisted. Adapted from *(Jegou & Romet-Lemonne, 2020, Seminars in Cell & Developmental Biology)*.
(3) Actin filaments bundled by fascin adopt a regular geometrical packing that can give rise to torques at the level of both individual filaments and bundles. Adapted from *(Jegou & Romet-Lemonne, 2020, Seminars in Cell & Developmental Biology)*.
(4) Myosin V follows a left-handed helix as it moves along the filament, taking steps that are shorter than the half-pitch of the actin double helix. While pulling on anti-parallel actin filaments, Myosin II generates both contractile forces and molecular torques. On the bottom, maximum projection from a 10min time series of actin motility powered by MyoIC bound to a supported lipid bilayer. The whole track of actin filaments is colored in green, while the actin filament at t = 0secs is colored in orange (Scale Bar = 5μm). Adapted from *(Jegou & Romet-Lemonne, 2020, Seminars in Cell & Developmental Biology; Pyrpassopoulos et al., 2012, Current Biology)*.

elongation and supporting the production of filaments having natural helicities *(Yu et al., 2017, Nat Commun; 2018, Nano Lett.; Suzuki et al., 2020, Nano Lett.)*.

2.1.2. Cofilin

Members of the cofilin family are the key players of actin filament disassembly *(Bamburg et al., 1980, FEBS Letters; Bernstein & Bamburg, 2010, Trends in Cell Biology; Reymann et al., 2011, MBoC; Ingerman et al., 2013, Journal of Cell Biology)*. The binding of cofilin to F-actin results in the formation of cofilin-decorated domains (cofilactin) that adopt a special conformation, in which the filament helical properties are significantly altered; the helical pitch of cofilactin is shorter compared to that of bare F-actin *(McGough et al., 1997, Journal of Cell Biology; Galkin et al., 2011, Proceedings of the National Academy of Sciences; Tanaka et al., 2018, Nat Commun)*. Consequently, while decorating rotationary-hindered actin filaments, cofilin can also generate mechanical torques (Figure 7B-2). While the applied torques do not affect the binding of cofilin, they greatly increase its activity, as severing rates are accelerated in regions near cofilactin domains *(Wioland et al., 2019, Proceedings of the National Academy of Sciences)*.

2.1.3. Crosslinkers

Certain ABPs, including α-actinin, fascin, filamin, and fimbrin, can connect filaments together, thereby shaping actin networks inside the cells. Doing that, they not only influence the mechanical properties of the networks, but also govern the polarity of their constituting filaments *(J. H. Shin et al., 2004, Proceedings of the National Academy of Sciences; Laporte et al., 2012, MBoC; Blanchoin et al., 2014, Physiological Reviews; Jegou & Romet-Lemonne, 2020, Seminars in Cell & Developmental Biology)*.

The activity of crosslinkers results in a significant geometrical packing of actin filaments, which, depending on the elasticity of the protein involved, can trigger changes in F-actin helicity *(Claessens et al., 2008, Proceedings of the National Academy of Sciences; H. Shin et al., 2009, Phys. Rev. Lett.)*. Moreover, crosslinkers can produce torques at the level of both individual filaments and whole bundles *(Heussinger & Grason, 2011, The Journal of Chemical Physics)*. Consequently, bundle assembly is coupled to spontaneous twisting arising from the additional geometrical constraints, which are imposed by the helicity of actin filaments (Figure 7B-3).

2.1.4. Myosins

The myosin super family comprises a variety of conventional and unconventional members that play central roles in diverse cellular processes, such as vesicular transport, network contraction, membrane deformation, and motility *(Hartman & Spudich, 2012, Journal of Cell Science)*. Myosin motors are essentially composed of two domains: a quite conserved motor domain, harboring the ATP- and actin-binding sites, and a highly divergent tail domain that determines the localization and the motor function of the different myosin family members *(Howard, 1997, Nature; Thompson & Langford, 2002, The Anatomical Record)*. The movement of myosins along actin filaments is powered by its ATPase activity; ATP hydrolysis induces a conformational change and subsequent movement (powerstroke), whereas the replacement of ADP by ATP causes myosin detachment *(Howard, 1997, Nature)*. Consequently, individual unipolar myosins are not processive, but their tail-to-tail assembly generates bipolar, highly processive minifilaments. Almost all myosin motors, except myosin VI, move toward actin filament barbed end *(Niederman & Pollard, 1975, Journal of Cell Biology; Finer et al., 1994, Nature)*.

Members of the non-muscle Myosin Class II (MyoII) are the principle myosin isoforms underlying cellular contractility.

Myosin rotation is hindered along parallel actin filaments, whose tight bundling imposes additional rotational constraints. By contrast, myosin motors pull on anti-parallel actin filaments, causing them to slide relative to each other, thereby producing contractile forces *(Levayer & Lecuit, 2012, Trends in Cell Biology; Blanchoin et al., 2014, Physiological Reviews; Jegou & Romet-Lemonne, 2020, Seminars in Cell & Developmental Biology)*. In the latter case, due to their helical nature, the interaction of actin filaments with myosin motors is characterized by a small angular component that leads to the simultaneous generation of a molecular torque in addition to the classical force production (Figure 7B-4). Myosin-induced torques can also alter the helical properties of actin filaments, thereby modulating their interactions with other ABPs *(Uyeda et al., 2011, PLOS ONE)*. In vitro, this torque component is reflected by the ability of myosin members to twist, rotate, or supercoil actin filaments in a direction that is specific to the motor implicated: muscle myosin is reported to be a CW motor; myosin V is shown to be a CCW spiral motor; myosin X is found to be a CCW helical motor *(Nishizaka et al., 1993, Nature; Cheney et al., 1993, Cell; Ali et al., 2002, Nat Struct Mol Biol; Vilfan, 2009, Biophysical Journal; Sun et al., 2010, Nat Struct Mol Biol).* Interestingly, certain MyoI isoforms (MyoID and MyoIC), driving a biased rotational motion of gliding actin filaments in vitro, are involved in the regulation of LR symmetry breaking at the level of organisms; in Drosophila, the antagonistic effects of MyoID and MyoIC determine the headedness of organs during development *(Pyrpassopoulos et al., 2012, Current Biology; Lebreton et al., 2018, Science; Y. Sato et al., 2023, Sci Rep)*.

The critical implications of both formins and myosin isoforms in the expression of chirality at the level of organisms question the existence of a relationship between these two multi-scale asymmetries.

2.2. LR symmetry breaking in vivo – Organisms

To provide some insights into the mechanisms leading to the emergence of chirality in living systems, the following section will focus on some of the most common examples of LR asymmetry in both invertebrates and vertebrates, as well as the mechanisms associated with chirality establishment in these systems.

2.2.1. Among Invertebrates

2.2.1.1. The nematode Caenorhabditis elegans (C. elegans)

One of the most studied examples of organismal LR symmetry breaking occurs during the development of the C. elegans embryo, which displays chirality as early as the single-celled zygote (Figure 8A). Shortly after the establishment of the anteroposterior (AP) axis through a MyoII-dependent contractility gradient triggered by sperm entry (described previously), the actomyosin cortex exhibits chiral counter-rotations: the anterior half rotates CW, whereas the posterior half rotates CCW. Using a thin film active chiral fluid theory, Grill and coworkers propose that these opposing cortical rotations are driven by a chiral flow generated by a gradient of active torques along the AP axis. Originally, this has been attributed to MyoII motors, whose activity on actin filaments can produce not

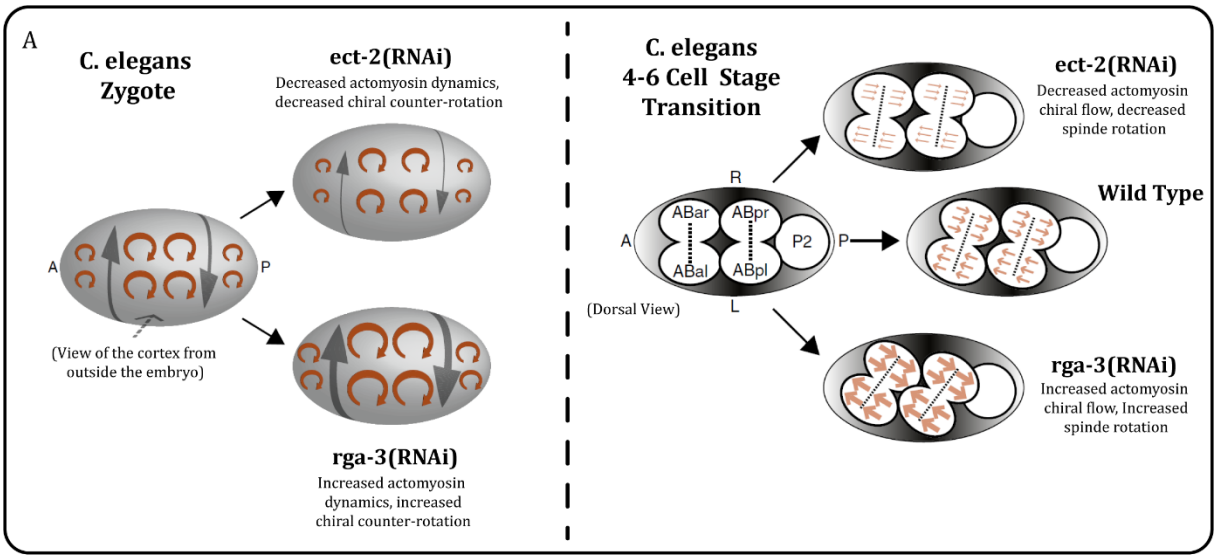
A
C. elegans
Zygote
ect-2(RNAi)
Decreased actomyosin dynamics, decreased chiral counter-rotation
A
P
(View of the cortex from outside the embryo)
rga-3(RNAi)
Increased actomyosin dynamics, increased chiral counter-rotation
C. elegans
4-6 Cell Stage
Transition
R
A
ABar
ABpr
P2
P
ABal
ABpl
L
(Dorsal View)
ect-2(RNAi)
Decreased actomyosin chiral flow, decreased spinde rotation
Wild Type
rga-3(RNAi)
Increased actomyosin chiral flow, Increased spinde rotation

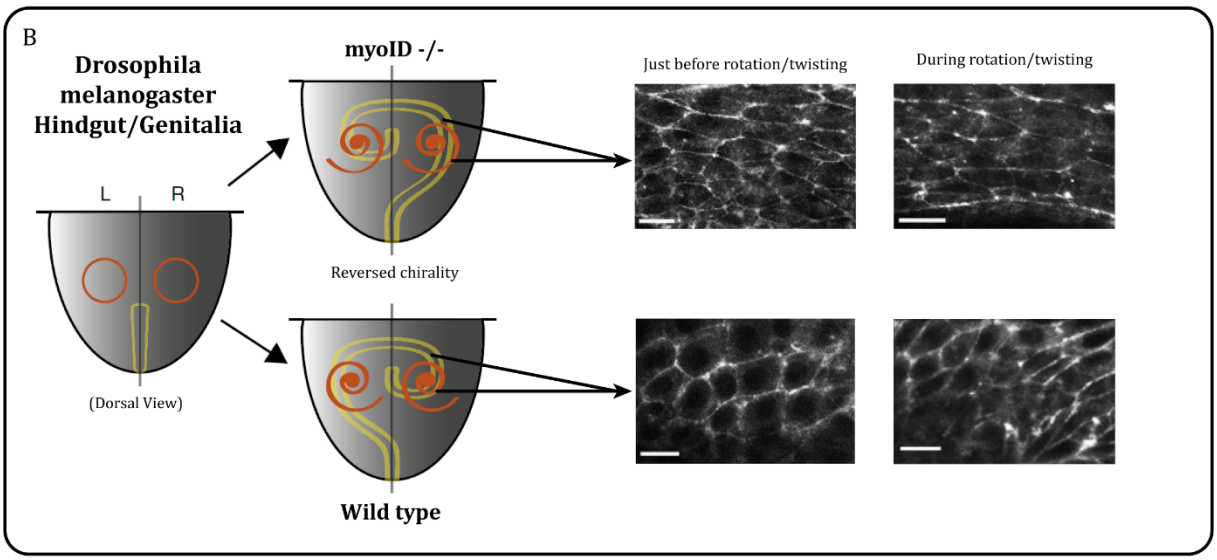
B
Drosophila
melanogaster
Hindgut/Genitalia
L
R
(Dorsal View)
myoID -/-
Reversed chirality
Wild type
Just before rotation/twisting
During rotation/twisting

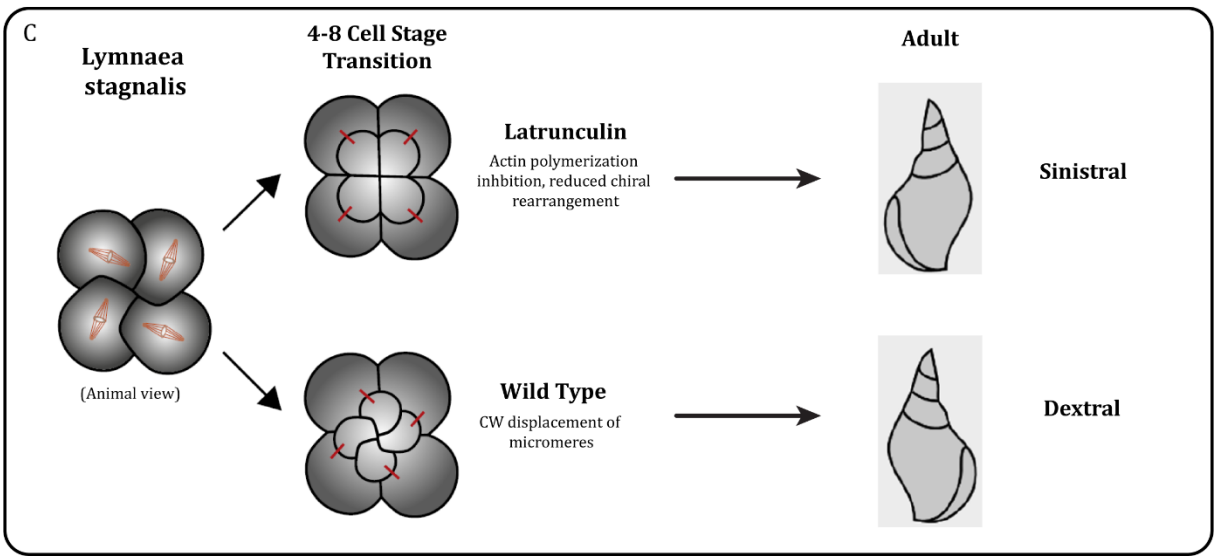
C
Lymnaea
stagnalis
(Animal view)
4-8 Cell Stage
Transition
Latrunculin
Actin polymerization inhbition, reduced chiral rearrangement
Wild Type
CW displacement of micromeres
Adult
Sinistral
Dextral

Figure 8: Illustrations of LR asymmetries at the level of organisms.
A: C. elegans. To the left, in the zygote, the actomyosin cortex exhibits clockwise rotations (beige arrows). A gradient in myosin activity leads to counter-rotating cortical flows (black arrows) breaking chiral symmetries. Size/width of the arrows represents the magnitude of torques/flow velocities. To the right, at the 4-cell stage, the two cells dividing into ABar-ABal and ABpr-ABpl exhibit a clockwise spindle skew driven by counter-rotating cortical flows (beige arrows), the magnitude of which is controlled by the Rho signaling pathway, with ect-2 and rga-3 (RNAi) leading to Rho inactivation and activation, respectively. Adapted from *(Naganathan et al., 2016, Current Opinion in Cell Biology)*.
B: Drosophila melanogaster. Chiral asymmetries of organs that are controlled by the actomyosin cytoskeleton. Hindgut in yellow, testes in beige. Mutating myosin 1D reverses wildtype chirality. To the right, representative images showing the Myo-II signal in the cells constituting the tissues in control and MyoID knockout flies right before and at the time of organ twisting (Scale Bar = 10μm). Adapted from *(Naganathan et al., 2016, Current Opinion in Cell Biology; K. Sato et al., 2015, Phys. Rev. Lett.)*.
C: Lymnaea stagnalis. At the 4-to-8 cell stage transition, dextral species exhibits a clockwise displacement of emerging micromeres (red lines indicate corresponding macromeres) driven by the actin cytoskeleton. Spindles in beige are also arranged in a clockwise fashion. Adapted from *(Naganathan et al., 2016, Current Opinion in Cell Biology)*.

only tension, but also torque that twists actin filaments, subsequently generating a global rotational flow based on two parameters. First, active torques must be heterogeneously distributed across the entire cortex to allow a net twist deformation. This is ensured by the pre-established contractile flow and the associated MyoII gradient along the AP axis. Second, the torque generators (F-actin and MyoII torque dipoles) must be differentially aligned to allow the emergence of large-scale chiral flows across the entire zygote/embryo. This can be achieved by an inherent difference in frictional forces at the two sides of the cortical layer (membrane and the cytosol). However, subsequent experiments have revealed that the strength of the chiral flow and the cortical counter-rotations is significantly affected when modulating the activity of RhoA but not MyoII directly. *(Naganathan et al., 2014, ELife; 2016, Current Opinion in Cell Biology)*

A later study by the Grill group demonstrates that cortical CYK-1/Formin, whose activity is regulated by RhoA signaling, promotes active torque generation by counter-twisting actin filaments elongating in opposite directions, which eventually leads to the emergence of the cortical counter-rotations. Interestingly, the activity of CYK-1/Formin on its own is not sufficient to drive chiral counter-rotatory flows. This suggests mechanistically distinct roles for MyoII and CYK-1/Formin in the development of chirality in this system: MyoII is essential for driving the cortical actomyosin flows and their associated contractility gradients, whereas the activity of CYK1-Formin is believed to trigger the chiral symmetry breaking of the flows. *(Middelkoop et al., 2021, Proceedings of the National Academy of Sciences)*

By following the first nine divisions in the C. elegans embryo, an equivalent LR asymmetric phenomenon in the cells belonging to the AB lineage has been identified; cortical counter-rotations emerge through the same mechanism described above. These chiral flows are involved in triggering a chiral skew in the mitotic spindle, causing it to deviate rightward from its original orientation along the LR axis. Accordingly, this results in the reorientation of the future daughter cells, which in turn ensures the correct positioning of the cells in the AB lineage. Cells belonging to the P lineage do not experience cortical counter-rotatory flows and, consequently, do not exhibit chiral spindle skews during their division cycles. *(Pimpale et al., 2020, ELife)*

2.2.1.2. The fruit fly Drosophila melanogaster

LR patterning is extensively studied in Drosophila because its embryonic development comprises directional rotation of certain organs (hindgut and male genitalia) that ensures their proper positioning in the adults (Figure 8B). Two isoforms MyoID and MyoIC have competing effects on LR asymmetry during Drosophila development. MyoID induces dextral rotation; decreasing the levels of active MyoID as well as the overexpression of MyoIC result in a leftward-biased rotation. Although both are expressed under normal conditions, the activity of MyoID predominates and foresees the emergence of LR asymmetry. Targeting certain effectors in actin organization (RhoA, Rac) or cell-cell adhesion (De-Cadherin) results in LR asymmetry defects, suggesting that the actin cytoskeleton and intercellular junctions are essential for the establishment of chirality in Drosophila. *(Hozumi et al., 2006, Nature; Taniguchi et al., 2011, Science; Petzoldt et al., 2012, Development; Hatori et al., 2014, Mechanisms of Development)*

The onset of rotation in both the hindgut and the genitalia is preceded by a biased polarization of the tissue arising from individual cells adopting a planar cell chirality (PCC) through their biased alignment relative to the long axis of the tissue in question. An asymmetric distribution of MyoID, MyoII, and De-cadherin has been observed in these tissues, where junctional planes parallel to the biased cell and tissue alignment demonstrate the strongest protein deposition. Interestingly, knockdown of MyoID reverses the polarized accumulation of MyoII, suggesting that MyoID acts upstream MyoII in this system and regulates its function. In addition, the absence of functional MyoII abolishes both biased tissue alignment and organ rotation. Using a vertex model, in which the cells were simulated as interconnected polygons, Sato et al. showed that oriented junctional planes, characterized by stronger actomyosin and junctional protein deposition, demonstrated high tension that was sufficient to drive the biased alignment of cells and their unidirectional rotation. They also proposed that such an asymmetry in tension could give rise to a polarized MyoII contractile flow that in turn could reinforce the asymmetric deposition of MyoII, thereby contributing to the emergence of chiral cell alignment. *(Taniguchi et al., 2011, Science; Hatori et al., 2014, Mechanisms of Development; K. Sato et al., 2015a, Nat Commun)*

In an attempt to investigate further the role of MyoID in Drosophila laterality, Lebreton et al. showed that the ectopic expression of MyoID induced dextral twisting in organs that were symmetric in nature (trachea), as well as in naïve tissues, thereby highlighting the ability of MyoID to generate de novo asymmetries. Moreover, they demonstrated that this particular function of MyoID required its capability to bind actin and hydrolyze ATP and

was mediated by its motor domain, which they described as the chirality-determining factor. In a later study, genetic screening in Drosophila revealed that certain proteins involved in actin polymerization and organization (particularly DAAM formin), cell-ECM adhesions, and intercellular junctions were key to the emergence of chirality. The authors proposed that together with MyoID, these proteins would generate a chiral actomyosin cytoskeleton supported by biased cell-ECM and cell-cell adhesion that could drive the emergence of LR asymmetry in individual cells and its propagation to the scale of tissues and organs. *(Lebreton et al., 2018, Science; Chougule et al., 2020, PLOS Genetics)*

2.2.1.3. The snail Lymnaea stagnalis

Another interesting chiral pattern identified among animals is the spiral coiling of shells in pond snails (Figure 8C). An early study has shown that two events occurring at the 4-8 cell stage transition determine the shell coiling direction: biased helical spindle inclination (SI) and spiral blastomere deformation (SD). The prevalent direction of shell coiling is species-dependent. In the snail *Lymnaea stagnalis*, dextral shell coiling predominates and is associated with a CW spindle twisting (SI) and a rightward deformation of blastomeres (SD) occurring precisely during metaphase/anaphase at the 4-8 cell stage transition. On the other hand, sinistral individuals do not display spindle twisting during cleavage; instead chirality emerges later through a leftward blastomere deformation during telophase or furrow ingression. Modulating actin but not microtubule dynamics abolishes SI and SD in dextral snails and leads to sinistral shell development. *(Shibazaki et al., 2004, Current Biology)*

Later genetic analysis identified actin-related diaphanous gene Lsdia1 as a chirality-determining factor since its presence drove rightward spindle twisting and the subsequent emergence of the dextral phenotype. Interestingly, inhibiting Lsdia1 activity (using SMIFH2 or genetic engineering) in dextral snail embryos at early cleavage stages abolished rightward spindle inclination and blastomere deformation at metaphase/anaphase, giving rise to sinistral adults. A recent study by Abe and Kuroda has revealed that chiral SI and SD occur during the first cleavage, where they are also regulated by the presence of Lsdia1, suggesting that the LR symmetry breaking event takes place at earlier stages of development. *(Kuroda et al., 2016, Sci Rep; Davison et al., 2016, Current Biology; Abe & Kuroda, 2019, Development)*

2.2.2. Among Vertebrates

The establishment of the LR asymmetric body plans of vertebrates is often mediated by the node, a transient structure that forms at the anterior end of the primitive streak in a gastrulating embryo. In particular, the CW rotation or beating of nodal monocilia generates a leftward flow that activates LR asymmetric gene expression; dysfunctional cilia giving rise to a rightward flow often lead to situs inversus totalis, an asymptomatic condition associated with the reversal of all body asymmetries. The fact that cilia are microtubule-based structures originating from basal bodies, whose position and orientation are determined by the actin network, suggests the implication of cytoskeletal components in the emergence of LR asymmetry among vertebrates. *(Pohl, 2015, Symmetry; Brücker et al., 2020, The International Journal of Biochemistry & Cell Biology)*

Although the Nodal pathway plays a key role in LR patterning, increasing evidence indicates that organismal LR asymmetry can originate from actomyosin-based cell or tissue chirality that can either affect the asymmetry of the node itself or drive Nodal-independent symmetry breaking. For instance, interfering with the actin cytoskeleton dynamics by modulating the activity of formin and Arp2/3 in Xenopus embryos disrupts LR asymmetry, giving rise to heterotaxia. In addition, cleaving Xenopus embryos often exhibit a large-scale cortical actin reorganization, resulting in an exclusively CCW torsion of the actomyosin cortex *(Pohl, 2015, Symmetry; Qiu et al., 2005, Developmental Dynamics; Danilchik et al., 2006, Development; Davison et al., 2016, Current Biology)*. Similarly, it has been shown that the heart looping in the Zebrafish embryo is abolished upon inhibiting actin polymerization and MyoII-dependent contractility. This suggests that the LR asymmetric heart looping in Zebrafish involves morphogenetic tissue remodeling, driven by collective directional cell migration, which originates from asymmetric cellular actomyosin contractility *(Noël et al., 2013, Nat Commun; Pohl, 2015, Symmetry)*.

On the other hand, it has been established that chick embryos lack cilia, and yet they have chiral nodes that are crucial for LR asymmetric gene expression. According to Gros et al., this can be mediated by a morphogenetic mechanism driven by asymmetric Myo-II-dependent contractility, which selectively induces the directional collective migration of cells expressing particular genes *(J. Gros et al., 2009, Science)*. Furthermore, it has been demonstrated that the CW looping of the chick heart is preceded by a rightward collective cell alignment originating from individual cell PCC. In a mechanism similar to that occurring in Drosophila (described above), the biased accumulation of MyoII and junctional N-cadherin at the right-oriented cell boundaries results in an asymmetry in tension that can drive biased cell alignment and subsequent directional organ rotation or looping *(Ray et al., 2018, Proceedings of the National Academy of Sciences)*.

Overall, these findings support the existence of an actomyosin-based LR asymmetry prior to the Nodal flow and suggest that the latter may serve as a secondary mechanism for the amplification of the existing LR asymmetric information.

Taken together, all of the examples described above suggest that the emergence of LR asymmetry in complex systems relies on the propagation of the chirality originating at the molecular level. However, assuming that the asymmetry of organisms arises from the chirality of their constituents, how can a molecular scale chirality be translated into multicellular and organismal chirality? Brown and Wolpert hypothesize that this can be mediated by a process known as “conversion”, in which putative, intrinsically chiral F-molecules, align themselves in reference to the anteroposterior (AP) and dorsoventral (DV) axes, established earlier during development *(Brown & Wolpert, 1990, Development)*. Subsequently, oriented actions triggered by the asymmetric structure of the F-molecule bias the system along the LR axis (Figure 9A). The intrinsic chiral nature and handed dynamics of cytoskeletal components makes them candidates of choice for the F-molecules. Interestingly, it is has been proposed that, by driving asymmetric morphogenesis, intracellular chirality can give rise to the chiral tissue and organ patterns of invertebrates and generate the LR biased embryonic node of vertebrates, which in turn triggers asymmetric gene expression (Figure 9B) *(Brown & Wolpert, 1990, Development; Pohl, 2015, Symmetry; Naganathan et al., 2016, Current Opinion in Cell Biology)*.

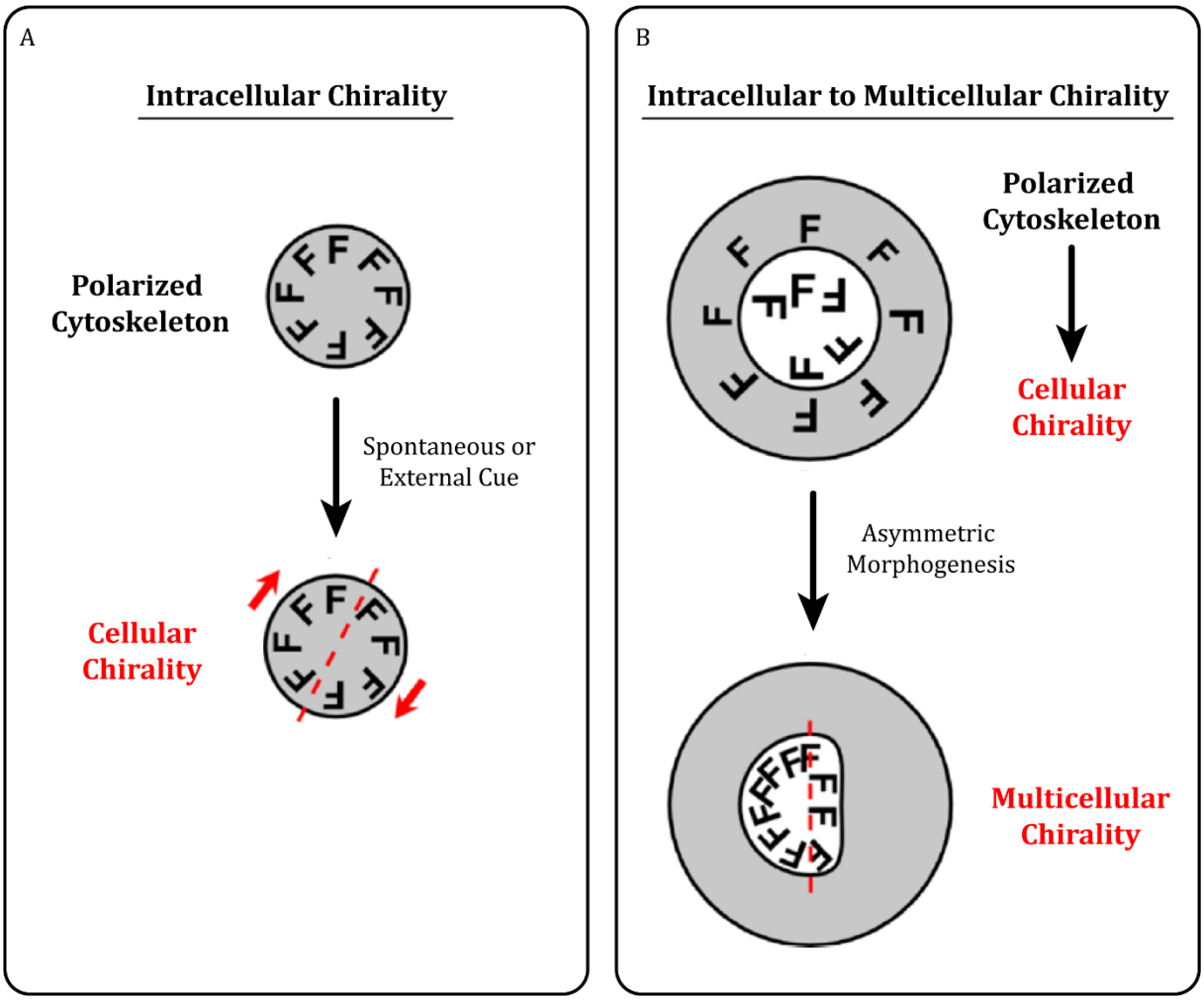

Figure 9: Model for the origin of chiral symmetry breaking in organisms.
Adapted from *(Pohl, 2015, Symmetry)*.
A: Cellular chirality emerges due to the asymmetric organization of putative, intrinsically chiral F-molecules that occurs either spontaneously or in response to an external cue
B: Cellular chirality is then used to generate chiral tissue/organ patterns or global organism chirality by driving asymmetric morphogenesis.

As such, investigating the emergence of chirality at the intermediate and less complex cellular level, along with the actomyosin-based mechanisms underlying its origin and propagation would help bridge the existing gap between molecular and organismal scale chirality.

2.3. LR Symmetry Breaking in Tissues and Cell Collectives

During the development of organisms, LR symmetry breaking involves large-scale chiral morphogenesis that is mediated by directional collective cell migration and biased tissue reorganization. The latter rely on both the intrinsic chirality of the cells belonging to the tissue as well as the physical boundary conditions imposed by the surrounding

environment: the extracellular matrix in addition to the neighboring cells and tissues. Given the complexity of organisms, the use of innovative micropatterning techniques, which can reproduce the conditions of geometrical confinement of the tissues existing in vivo, has facilitated the recapitulation of these phenomena in vitro using systems of cell collectives. This has contributed great insights into the mechanisms of collective cell behaviors and paved the way toward a better understanding of the processes of chiral tissue morphogenesis, particularly regarding the key players and parameters involved in their emergence, regulation, and maintenance *(Théry, 2010, Journal of Cell Science)*.

Collective cell chirality has been shown to manifest in two main biased behaviors, alignment and rotation. In the following section, we will present some examples of collective systems, displaying either of the two chiral behaviors, while discussing the implication of certain identified effectors, as well as the proposed mechanisms underlying these phenomena.

2.3.1. Chiral Collective Alignment

Biased collective alignment appears when cells are confined on geometries with oppositional boundaries, like donut-shaped micropatterns, alternating adhesive and non-adhesive stripes, and lines. Shortly after seeding, the cells are initially randomly oriented. Once they reach a certain confluence, some cells sense opposing boundaries, polarize accordingly, and initiate migration in opposite directions, thereby generating a global flow, which simultaneously aligns the cells at the interior. This suggests that the emergence of collective alignment requires motion triggered by the oppositional boundaries to reorient the cells, a certain degree of confluence (≥75%) to inhibit cell random walk, and sufficient time to establish coherent motion (≥15hrs) *(Wan et al., 2011, PNAS)*. The resulting alignment is defined by the orientation of individual cells and their velocity vectors, cell-cell junctions, intracellular actin stress fibers, or nuclei, which can all be used as parameters for quantification.

Using donut-shaped adhesive patterns, Wan et al. have shown that different cell types demonstrate distinct biased alignment, which depends on the actin cytoskeleton, as interfering with actin dynamics alters the chiral phenotype (Figure 10A). The biased alignment is reversed in cancerous cells, compared to their normal counterparts, suggesting that the expression of chirality is related to the disease state. Interestingly, the same treatments applied to collectives of different cell types did not generate the same effects on chiral alignment. For example, LatA reversed the bias of C2C12 from CCW to CW, but it did not necessarily have the same effect on all the other cell types tested. This implies that inherent cellular actin levels may be implicated in the emergence of cell-specific collective biased alignment, as well as in its response to perturbations. As such, the authors suggest that chirality is an intrinsic cellular characteristic that depends on the organization and the functionality of the actin cytoskeleton. *(Wan et al., 2011, PNAS)*

Using endothelial cells in the same system, Fan et al. demonstrated that the chirality of the individual cells in a collective could itself influence the integrity of the intercellular junctions and, consequently, alter the permeability of the endothelial monolayer (Figure 10B). By defining a new chirality parameter based on the positioning of the cell centroid relative to the Nucleus – Centrosome axis, the authors showed that individual cells

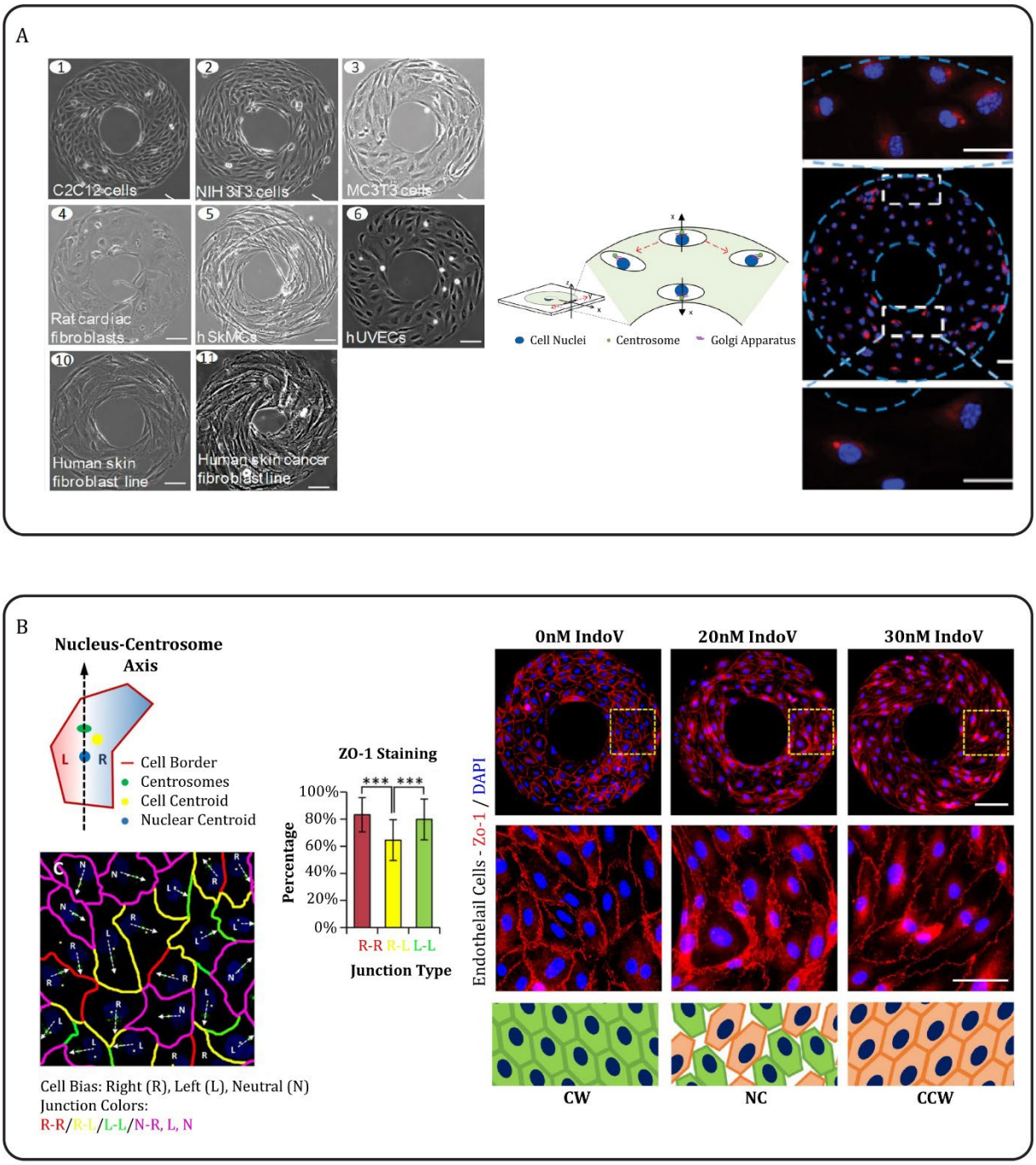

Figure 10: Chirality is an intrinsic cellular characteristic.
A: To the right, phase contrast images of various cell types on patterned substrates (Scale Bars = 100μm). To the left, schematic representation for the emergence of the cellular chiral bias resulting from the boundary conditions that influence cell alignment and polarity: cells on a donut sense the z-axis through attachment to the substrate and the x-axis through the ring boundaries; the cell alignment bias of the y-axis (dash red lines) creates the observed cellular chiral behavior. Example of a donut composed of aligned HUVECs: the Golgi apparatus (in red) is positioned closer to ring boundaries than nuclei (in blue) (Scale Bar = 50μm). Adapted from *(Wan et al., 2011, PNAS)*.
B: To the left on top, schematic illustration of the determination of the left (L) or right (R) cell bias based on the biased positioning of the cell centroid relative to the nucleus-

centrosome axis. On the bottom, representative image showing the segmented cell nuclei (in blue), centrosomes (in green), and junctions classified as "R-R", "R-L", and "L-L" based on the LR biases of two adjacent cells (Scale Bar = 50μm). Percentage of ZO-1 staining along the R-R, R-L, and L-L junctions. To the right, top row: immunofluorescence images of HUVECs on the donut-shaped micropatterns labeled for ZO-1 (in red) and nuclei (in blue) (Scale Bar = 100μm); middle row: magnified images of the yellow boxed areas (Scale Bar = 50μm); bottom row: schematics of the CW, CCW, and NC cell alignment on micropatterns. Adapted from *(Fan et al., 2018, Science Advances)*.

---

exhibited an intracellular chirality reflected by the LR biased orientation of their centroids, which contributed to the emergence of the global rightward-biased alignment in collectives on donut-shaped micropatterns. Junctions between cells displaying the same chirality were characterized by the highest intensity of junctional protein and fewer gaps. In addition, treating the biased cell collectives with increasing concentrations of Protein Kinase C (PKC) activator (Indolactam V – IndoV) led to the gradual reversal of the chiral alignment (Rightward – No bias – Leftward). Interestingly, these chirality variations were accompanied by altered junction permeability; IndoV concentrations associated with a prominent chiral bias had high junctional protein and low permeability, whereas those at which the cells displayed no bias were characterized by the lowest junctional protein and highest values of permeability. The authors attributed the chirality reversal upon the over activation of PKC to its functions in PI3K/AKT stimulation and actin network regulation. A later study performed on fibroblast collectives in the same context indicated that chirality reversal achieved through the modulation of PKC involved the activity of the actin crosslinker fascin. *(Fan et al., 2018, Science Advances; H. Zhang et al., 2023., Advanced Biology)*

Chen at al. reported an equivalent rightward biased alignment upon seeding vascular mesenchymal cells on alternating adhesive and non-adhesive stripes (Figure 11A). This alignment was accompanied by the selective accumulation of stress fibers at the adhesive-to-non-adhesive boundaries, as well as by a biased orientation of the Nucleus – Centrosome axis, reflecting a possible implication of cell polarity in biased alignment. Moreover, suppressing stress fiber accumulation by treating the cells with Rho or MyoII inhibitors or removing the interface disrupted LR asymmetric alignment, which implied that actomyosin contractility is crucial for the emergence of LR asymmetry in collectives. To investigate further the development of unidirectional, chiral cell clusters, the authors used a combined reaction-diffusion and chemotaxis model. The latter was based on a slowly diffusing activator (BMP-2) and a faster propagating inhibitor (MGP) as well as an anisotropic cell migration biased toward the areas with higher amounts of activator. The simulated cellular aggregates generated parallel, aligned ridges, similar to the ones obtained experimentally. This suggested that the development of LR biased alignment in cell collectives could be attributed to a coordinated combination of reaction-diffusion and anisotropic migration guided by coherent, polarized orientation. *(T.-H. Chen et al., 2012, Circulation Research)*

Later, Zhu et al. used the same system to study the mechanics underlying this chiral behavior (Figure 11B). They showed that, compared to the ones on rigid substrates,

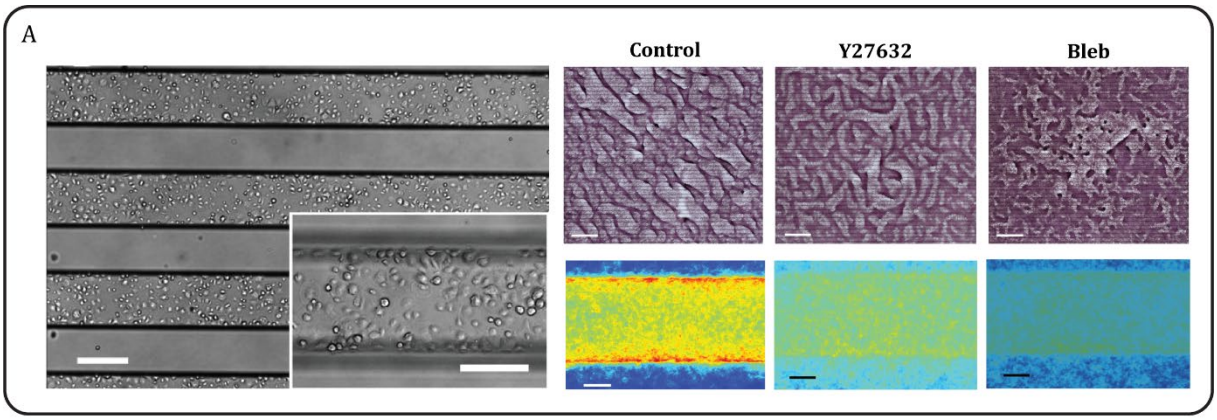
A
Control
Y27632
Bleb

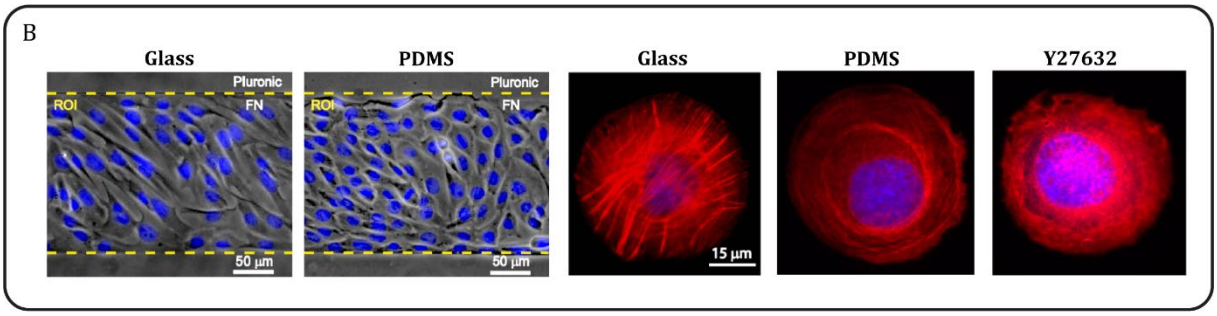
B
Glass
PDMS
Pluronic
ROI
FN
50 µm
Glass
PDMS
Y27632
15 µm

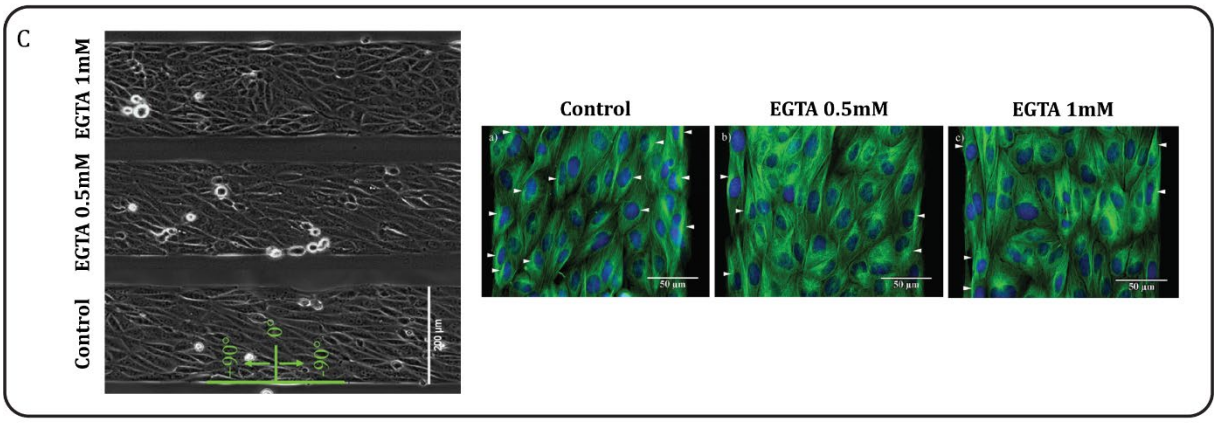
C
EGTA 1mM
EGTA 0.5mM
Control
Control
EGTA 0.5mM
EGTA 1mM
50 µm

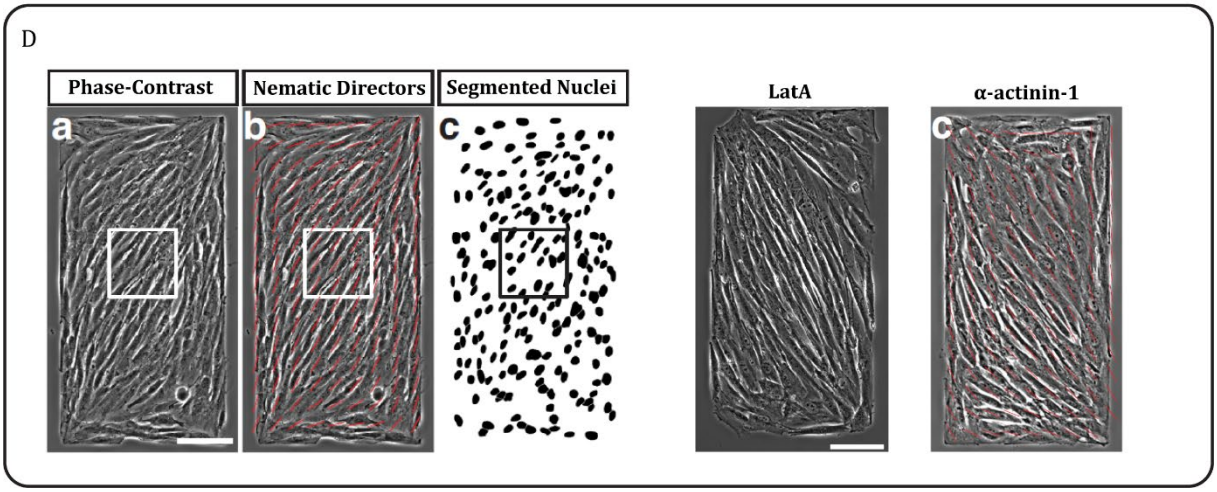
D
Phase-Contrast
Nematic Directors
Segmented Nuclei
a
b
c
LatA
α-actinin-1

Figure 11: Chirality in cell collectives is demonstrated by a biased alignment.
A: To the left, phase contrast images of mesenchymal cells on FN/PEG substrates showing preferential attachment of cells to FN-coated surfaces (Scale Bar = 2mm). Insets: higher magnification images of multicellular aggregates (300μm). To the left, on top, representative images in bright field showing a biased pattern along principal diagonal axis that is abrogated upon treatment with Y27632 or Blebbistatin. On the bottom, stacked images of immunofluorescence microscopy of non-muscle myosin-IIA in mesenchymal cells on FN/PEG substrate depicting an accumulation of stress fibers at the boundaries in control conditions, which is inhibited upon treatment with Y27632 or Blebbistatin. (Scale Bar = 100μm). Adapted from *(T.-H. Chen et al., 2012, Circulation Research)*.
B: To the left, phase contrast microscopy images showing the orientation of C2C12 cells with nuclei staining (in blue) grown on micropatterned FN stripes of a rigid (glass) and soft (PDMS; no alignment) substrates (Scale Bar = 50μm). To the right, immunofluorescence images of actin filaments (in red) and nuclei (in blue) in untreated C2C12 myoblasts on circular micropatterns on glass or PDMS substrate as well as those treated with Y27632. Adapted from *(Zhu et al., 2017a, Micromachines (Basel))*.
C: To the left, phase contrast images of MDCK cells on 200μm width micropterned lines under control as well as 0.5mM and 1mM EGTA treatments (Scale Bar = 200μm). To the right, immunofluorescence images of microtubules (in green) and nuclei (in blue) showing the polarity and alignment of MDCK cells under control as well as 0.5mM and 1mM EGTA treatments; white arrowheads indicate the positions of the centrosomes (Scale Bar = 50μm). Adapted from *(Worley et al., 2015, Integrative Biology)*.
D: To the left, phase-contrast images of fibroblasts 48hrs following plating on rectangular adhesive pattern (300 × 600μm); red lines represent average local orientation of cells (nematic directors); the orientation of segmented nuclei of the cells is also represented. To the right, phase-contrast images showing the reversed alignment of fibroblasts upon LatA treatment or α-actinin overexpression (Scale Bar = 50μm). Adapted from *(Tee et al., 2023, Nat Commun)*.

muscle cell clusters seeded on soft substrates displayed no apparent biased directional alignment. This effect was reproduced when actomyosin contractility of the cells aligned on glass was reduced by inhibiting the Rho pathway. The authors proposed that, in these conditions, the absence of stress fibers, that usually aligned along the boundaries to aid cell orientation, could account for the observed effect. Overall, these results suggest that chirality can be a mechanosensitive cellular property that relies on the actomyosin cytoskeleton. *(Zhu et al., 2017b, Micromachines (Basel))*

By assessing the behavior of epithelial cell collectives on adhesive lines, Worley et al. identified another key factor involved in biased collective cell alignment: the intercellular junction (Figure 11C). Opposite to control conditions, cell clusters with inhibited cell-cell junctions (through EGTA treatment) demonstrated random orientation with no clear bias. Thus, cell-cell adhesions may be involved in the transmission of polarizing boundary and chiral signals, which ensure the coordination and coherence between the cells, leading to their collective biased alignment. *(Worley et al., 2015, Integrative Biology)*

In a recent study, Tee et al. showed that clusters of fibroblasts seeded on relatively large rectangles displayed a leftward-biased alignment that was largely dependent on the dynamics and the reorganization of the actin cytoskeleton: mDia1 knockdown abolished the chiral alignment; by contrast, α-actinin overexpression and LatA treatment reversed the observed bias (Figure 11D). Moreover, by simultaneously applying the same manipulations (knockdown, overexpression, and chemical drug treatment) on cell collectives and single cells confined on disks (described in 2.4), the authors suggested that the same mechanism could drive the emergence of chirality in the two systems, although some proteins were found to have different or opposite effects on the chiral bias. *(Tee et al., 2023, Nat Commun)*

2.3.2. Chiral Collective Rotation

Upon confinement on some micropattern geometries, including homogeneous disks and rings of certain widths, LR symmetry break gives rise to a coherent, directional migration that persists over extended periods of time. Investigating the mechanisms underlying the emergence and the maintenance of such collective behaviors is particularly interesting because it can help understand the dynamics of similar swirling motions occurring within tissues in vivo or driving morphogenesis during development. However, unlike the collective alignment described above, where cell orientation is always biased, the chiral bias in systems exhibiting directional rotation remains controversial. Certain studies demonstrate that collective rotational behaviors are random, with equal probabilities of clockwise (CW) and counterclockwise (CCW) rotation; others only report a chiral bias while focusing on the mechanics of the collective motion itself.

For example, persistently rotating epithelial cells confined on 1D rings (described in 1.2.4.2), did not display a directional bias following symmetry break and rotation initiation (Figure 12A) *(Jain et al., 2020, Nat. Phys.)*. Similarly, despite identifying a CW bias among rotating epithelial cell clusters with "flexible" confinement (described in 1.2.4.2), Lo Vecchio et al. did not explore further the mechanisms implicated in the emergence of the chiral bias in this system (Figure 12B) *(Lo Vecchio et al., 2024, Nat. Phys.)*. However, both of these studies reveal that the initial symmetry-breaking event and the emergence of a persistent and coherent collective motion is tightly associated with the coordination of polarity at the level of the constituting single cells.

Interestingly, a combined experimental and theoretical approach by Segerer et al. demonstrated that directional and coherent rotations with no apparent chiral bias could even occur in confined clusters composed of only two to eight cells (Figure 12C). The authors suggested that the transition from a disordered state to a coherent rotational one was mediated by the interplay between the geometrical arrangement of neighboring cells and their internal polarization, which was influenced by the guidance cues a cell received from its neighbors through cell-cell adhesions *(Segerer et al., 2015, Phys. Rev. Lett.)*. Accordingly, they showed that the persistence of rotation increased with cell density for small clusters containing less than five cells; larger cell clusters exhibited a drop in coherence. This was attributed to the reorganization of these clusters into a configuration having a central cell, which failed to establish a stable internal polarization due to confounding cues from the surrounding cells. In a later study, Wang & Xu simulated similar cell clusters using a biomechanical model to investigate the relationship between

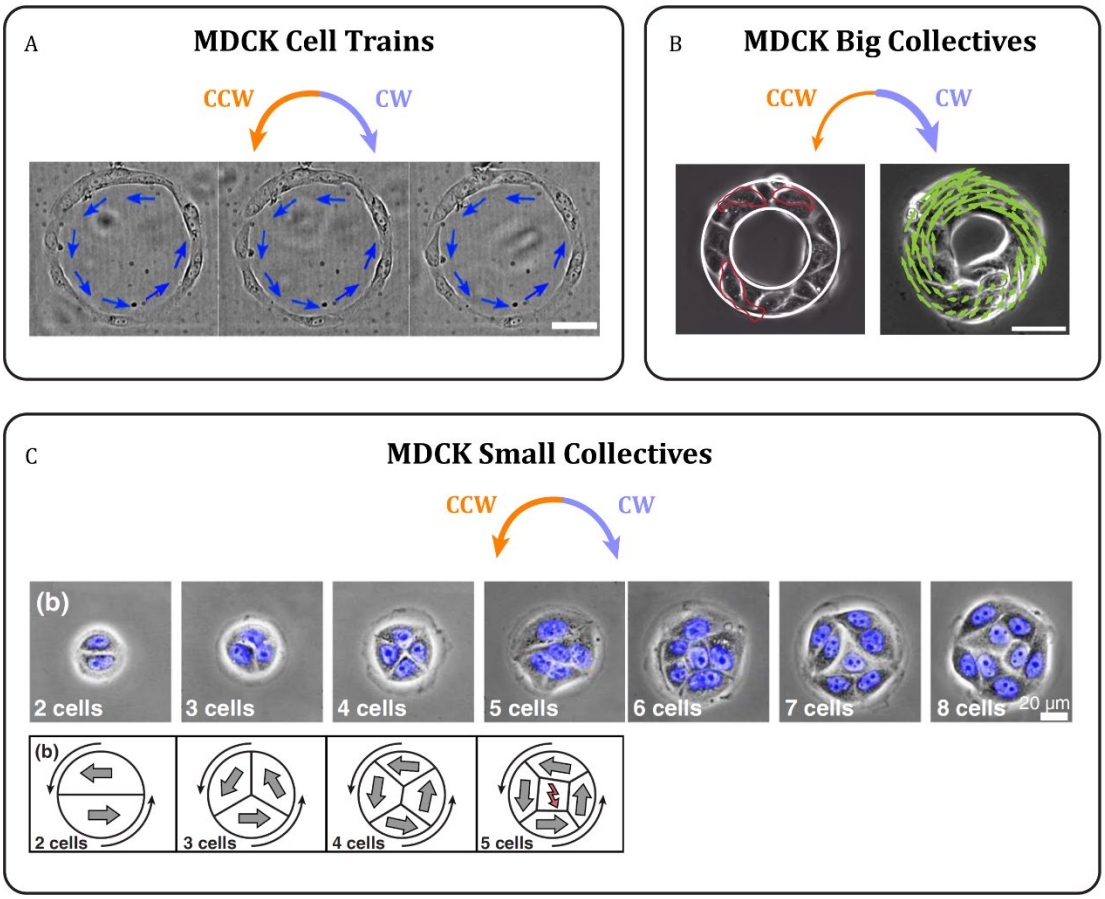

Figure 12: Collectives of the same cell type display distinct chiral bias under different conditions.
Arrows in purple indicate CW rotation; those in orange indicate CCW rotation. The thickness of the arrows depicts the presence or absence of a chiral bias under a given condition.
A: Confocal microscopy images of coherently rotating MDCK cell trains. Arrows indicate the direction of motion (Scale Bar = 50μm). Adapted from *(Jain et al., 2020, Nat. Phys.)*.
B: Phase contrast image of MDCK cells on an 80μm ring with the corresponding velocity field (Scale Bar = 50μm). Adapted from *(Lo Vecchio et al., 2024, Nat. Phys.)*.
C: On top, phase contrast images of two to eight MDCK cells occupying circular micropatterns with the nuclei labeled in blue; disk size increases such that the average area per cell is constant at approximately 830μm² (Scale Bar = 20μm). On the bottom, schematic illustrations of possible polarization alignments during coherent motion for different cell numbers. Arrows indicate the direction of motion. Adapted from *(Segerer et al., 2015, Phys. Rev. Lett.)*.

the rotation direction of the cluster and the chiral cytoskeletal organization of the constituting cells *(B.-C. Wang & Xu, 2022, Biophysical Journal)*. In these simulations, all cells in a small cluster adopted a chiral cytoskeletal pattern that was inversely related to the direction of their persistent rotation. On the other hand, clusters composed of more than five cells rearranged into the configuration with symmetric peripheral rotating cells and a constrained central cell displaying a chiral pattern that was not correlated with

cluster rotation direction. Once again, here, a chiral bias was not reported. Overall, these findings indicate that the geometric arrangement of a collective and the resulting positioning of cell-cell contacts regulate the establishment of polarity and chirality in individual cells, thereby effecting the properties of their emergent collective motion.

Taken together, these studies, among others, demonstrate that the behavior and motion of cell collectives is influenced by factors including cell-ECM traction forces, cell-cell adhesions, polarization, and the properties of the surrounding environment *(Ladoux & Mège, 2017, Nat Rev Mol Cell Biol)*. However, it remains unclear and understudied whether and to what extent these factors are implicated in chiral tissue demonstrations. In particular, the complexity associated with the described collective cellular systems tend to mask the implication of certain key parameters in driving the chiral swirling and the emergence of a directional bias, which renders the formulation of conclusions about chiral rotation much more challenging.

Finally, it is worth mentioning here that despite using the same cellular model consisting of kidney epithelial cells, MDCKs, the studies discussed above report different results concerning the existence of a chiral bias (Figure 12). This suggests that the same cell type can modulate its bias depending on the surrounding extracellular environment – geometrical confinement, substrate rigidity, and cell density. Indeed, it was shown that varying the width of the micropatterned stripes could significantly influence the biased collective alignment of epithelial and endothelial cell collectives by either enhancing or abolishing it *(Worley et al., 2015, Integrative Biology; Hernández et al., 2022, RSC Adv.)*. Similarly, increasing the diameter of the used adhesive disks increased the proportion of fibroblasts demonstrating chirality *(Jalal et al., 2019a, Journal of Cell Science)*. Moreover, as previously described, the collective chiral bias of muscle cells was strongly dependent on the rigidity of the underlying substrate *(Zhu et al., 2017b, Micromachines (Basel))*.

2.3.3. Collective Chiral Behaviors in 3D environments

Despite all the advances in understanding cell chirality that have been achieved on 2D substrates, the latter cannot fully recapitulate the behavior of cells within the 3D environment of native tissues, which are characterized by reduced integrin use, co-localized adhesion proteins, and enhanced motile capacities. Therefore, several recent attempts have focused on using 3D cell culture techniques to investigate the existence of biased, chiral cellular demonstrations and to question the conservation of the implicated mechanisms previously identified in 2D systems.

It was shown that kidney epithelial (Madin-Darby canine kidney cells – MDCKs) microspheroids embedded in two Matrigel layers displayed a CCW-biased rotation driven by actomyosin contractility (Figure 13A). By modulating the actin cytoskeleton through either small doses of LatA or α-actinin overexpression, the rotational bias of both microspheroids and doublets was reversed to CW. This suggested that chiral rotation in 3D environments might be mediated by the same actomyosin-based mechanism, previously described for collective behaviors in 2D, which could be propagated across increasing levels of complexity. *(Chin et al., 2018, Proc. Natl. Acad. Sci. U.S.A.)*

Lu et al. employed the same system described above to investigate the polarity-based mechanisms underlying the initiation and the maintenance of directional doublet

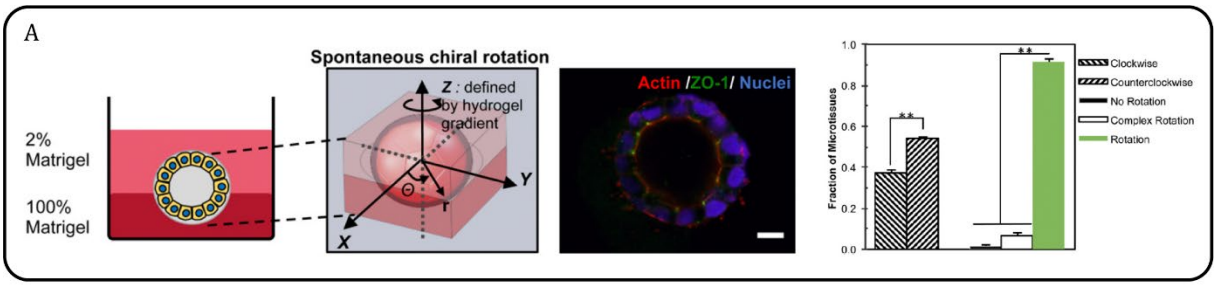
A
Spontaneous chiral rotation
2%
Matrigel
100%
Matrigel
Z : defined
by hydrogel
gradient
Y
X
Actin /ZO-1/ Nuclei
Fraction of Microtissues
Clockwise
Counterclockwise
No Rotation
Complex Rotation
Rotation

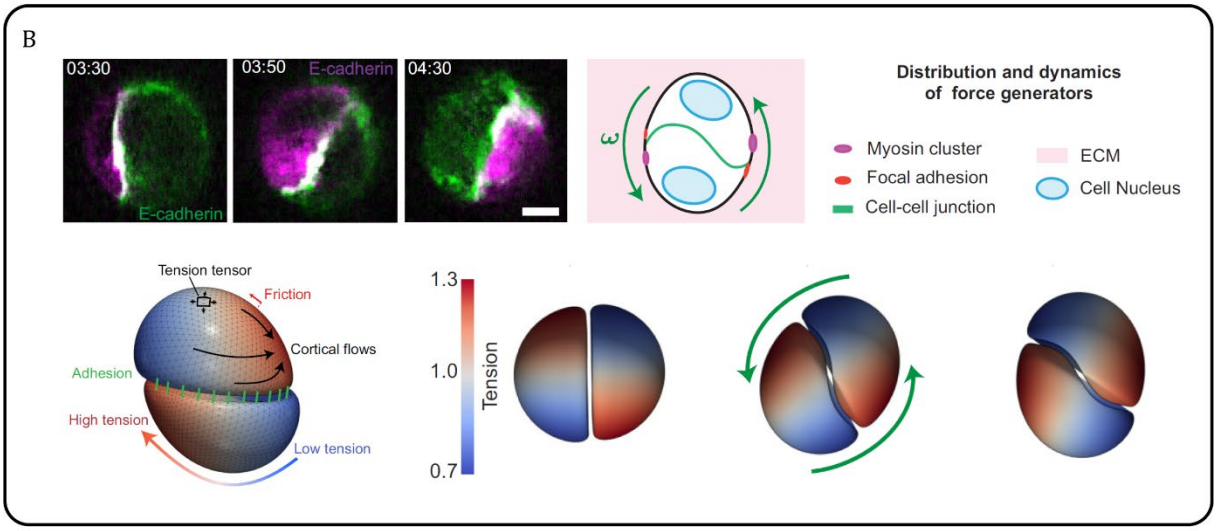
B
03:30
03:50
E-cadherin
04:30
E-cadherin
Distribution and dynamics
of force generators
Myosin cluster
Focal adhesion
Cell-cell junction
ECM
Cell Nucleus
Tension tensor
Friction
Cortical flows
Adhesion
High tension
Low tension
1.3
1.0
0.7
Tension

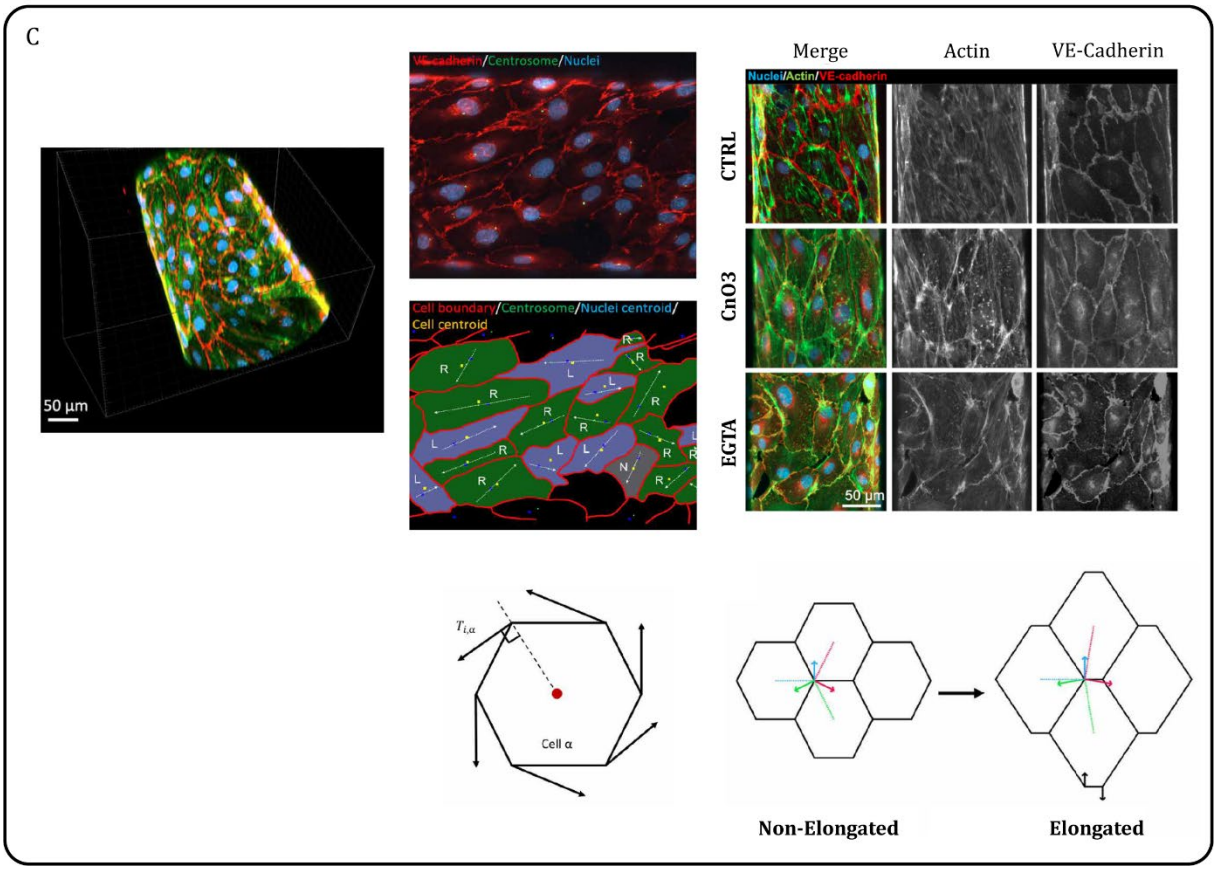
C
50 µm
VE-cadherin/Centrosome/Nuclei
Cell boundary/Centrosome/Nuclei centroid/
Cell centroid
Merge
Actin
VE-Cadherin
Nuclei/Actin/VE-cadherin
CTRL
CnO3
EGTA
50 µm
Cell α
Non-Elongated
Elongated

Figure 13: The different demonstrations of chirality in 3D.
A: To the left, schematic representation of the 3D cell chirality assay for epithelial microspheroids. Individual epithelial cells, embedded between a 100% Matrigel base layer and a 2% Matrigel top layer, are allowed to proliferate and form microspheroids containing a lumen. A confocal cross-section through an immunofluorescence of a microspheroid shows a hollow lumen surrounded by cells; actin in red, ZO-1 in green, and nuclei in blue (Scale Bar = 10μm). The microspheroids undergo spontaneous in-plane (x-y) rotation, with a CCW bias. Adapted from *(Chin et al., 2018, Proc. Natl. Acad. Sci. U.S.A.)*.
B: On top, to the left, representative images of a rotating doublet with two cells expressing E-cadherin of different color labels (green and red) (Scale Bars = 5μm). To the right, schematic illustration of the distribution of force-generating and adhesion proteins in the rotating doublet. On the bottom, schematic representation of the model simulation of a rotating doublet. Green arrows indicate the direction of motion. Adapted from *(Lu et al., 2022)*.
C: To the left, 3D reconstruction an in vitro vessel using a confocal microscope. The vessel is stained for actin (in green), VE-cadherin (in red), and nuclei (in blue) (Scale Bar = 50μm). Projection image of the vessels and the corresponding processing to identify the chirality based on cell alignment: rightward biased cells (R, green), leftward biased cells (L, purple), non-biased cells (N, gray). On the bottom, schematic illustration of the used cell vertex model: hexagonal tissue showing the chiral forces acting on all associated vertices. To the right, two-dimensional projections vessels treated with CN03 or EGTA. The vessels were stained for actin (in green), VE-cadherin (in red), and nuclei (in blue) (Scale Bar = 50μm). Adapted from *(H. Zhang et al., 2024, Science Advances)*.

rotation; whether or not this rotation was biased was unclear (Figure 13B). Despite identifying several modes of junction deformation following symmetry break, only the orientation of the Yin-Yang mode was found to be correlated with the direction of doublet rotation. The symmetry-breaking event involved the polarization of key cytoskeletal components: F-actin and E-cadherin, were enriched at the cell-cell interface, whereas p-MLC and FAs, accumulated into cortical clusters that were positioned on opposite sides of the intercellular junction. The emergent cortical myosin polarity axis was correlated with doublet rotation and the direction of the Yin-Yang junction deformation. Using a physical theory, in which cells of the doublet were modelled as two interacting surfaces, the authors showed that gradients of active tension, generated by myosin polarization across the doublets, drove the directional rotation. The suppression of active tension gradients among simulated doublets flattened the junctional interface and arrested rotation. Lu et al. validated the predictions of the model through experimental approaches that inhibited tension gradients by disrupting the established polarity: global contractility reduction, laser ablation of the two myosin clusters, or induction of new myosin clusters by optogenetics. Overall, these findings strongly suggest that the cell polarity established and regulated by gradients of actomyosin is essential for driving the emergence of doublet chiral rotation and ensuring its maintenance. *(Lu et al., 2022)*

In a recent study, Zhang et al revealed that endothelial cells cultured in microfluidic devices form 3D vessels that displayed a rightward biased helical alignment, whose

directionality was independent of flow profiles or even the presence of a flow (Figure 13C). The simultaneous application of increasing IndoV concentrations on the 2D and 3D systems gradually reversed the chirality of endothelial cells in both systems: rightward bias under control conditions – no bias at intermediate IndoV concentrations – leftward bias at higher IndoV concentrations. To identify additional parameters regulating this 3D chiral behavior, the authors simulated their system using a chiral torque vertex model, in which cells were defined as polygons interconnected through edges that represented cell-cell junctions. Active chiral forces applied at the vertices of each cell generated a net chiral torque that induced cell rotation. The model predicted that under a gradient of chiral torque strength, the cells could directionally migrate or rotate, thereby driving collective LR asymmetric migration or alignment. In addition, it indicated that tissues with more fluid-like properties experienced a greater degree of migration, elongation, and alignment, suggesting that chiral morphogenesis could be regulated by cortical tension and cell-cell adhesion. To verify these model findings, Zhang et al. modulated the fluidity of the tissue by increasing cell contractility or reducing cell-cell adhesions. Consequently, treated vessels exhibited attenuated or non-biased morphologies when compared to the control, indicating that vessel fluidity affected cell chirality, which in turn could influence certain vascular functions. Finally, by reporting a right-handed helical alignment of cells in microvessels of mouse retinal tissues, the authors confirmed that asymmetric helical endothelial morphogenesis occurred in vivo and, thus, was physiologically relevant. *(H. Zhang et al., 2024, Science Advances; Rahman et al., 2024, Mechanobiology in Medicine)*

2.4. LR Symmetry Breaking in Single Cells

The ensemble of findings in organisms and tissues imply that individual cells, the basic units of life, would also possess chiral properties that can be attributed to their inherently chiral cytoskeletal components and interactions. Investigating the existence of chirality in single cells as well as the mechanism underlying their LR symmetry break may be the key to understand how molecular chirality is propagated to higher levels, which will facilitate bridging all the chiral phenomena identified across scales. Consequently, several studies addressing this question have revealed that, depending on the extracellular environment, the chirality of individual cells can manifest in two major forms: motile and static.

In the first case (motile), single cells display a biased directional motion, similar to the one previously described in cell collectives. Such a chiral behavior was identified among isolated neutrophils, which, in the absence of an external cue, adopted a resting, non-polarized configuration. Upon their stimulation by a chemoattractant, these neutrophils rapidly transition into a polarized state and initiate directional migration (Figure 14A). The emerging polarization, characterized by the reorientation of the Nucleus – Centrosome axis relative to its original configuration in the resting state, was reported to be biased toward the left. Depolymerization of microtubules or the interference with key polarity factors, such as Cdc42 or the Par3/Par6/aPKC complex, led to the loss of this directional bias. Thus, unlike the different chiral manifestations described above, microtubules seem to be involved in the biased migration of neutrophils, although the role of actin dynamics has not been assessed in this study. The differences in the contributions of actin and microtubules identified here can be attributed to chiral phenotype itself. The

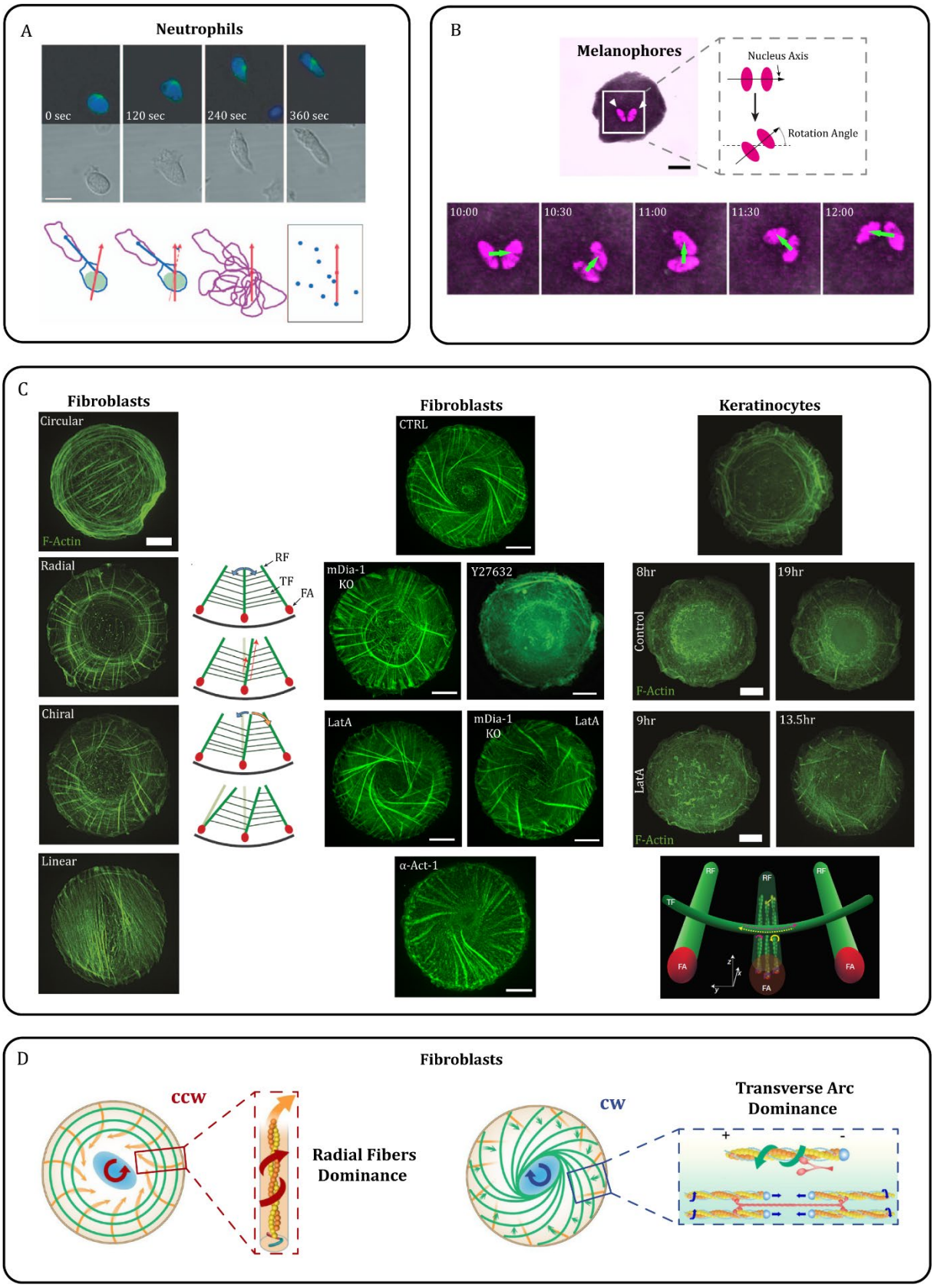

Figure 14: Single cells can also display chirality in different ways.
A: On top, representative images from a time-lapse following the behavior of a uniformly stimulated dHL-60 (bright filed and fluorescence signals of the centrosome and the

nucleus). On the bottom, to the left, image processing to correct the detected outlines of all the cells at 180secs (in purple) so that their red arrows, drawn through the nucleus centroid, point in the same direction (upward). To the right, graph showing the locations of centrosomes (blue dots) at 180secs (Scale Bar = 10μm). Adapted from *(Xu et al., 2007, PNAS)*.
B: On top, to the left, representative image of a Zebrafish melanophore with white arrows heads pointing at the nuclei (Scale Bar = 20μm). To the right, schematic representation for the definition of the nuclear axis (passing through the centroids of the two nuclei) and the rotational angle. On the bottom, magnified images of the rectangular region showing the counterclockwise rotation of the nuclei. Adapted from *(Yamanaka & Kondo, 2015, Genes to Cells)*.
C: To the left, representative images of fibroblasts fixed 6hrs after seeding on fibronectin-coated islands of 1800μm^2 showing the evolution of F-actin distribution that accompany the transition from a circular to chiral pattern (Scale Bar = 10μm), along with schematic illustrations of the described physical model underlying this transition. In the middle, representative images of fibroblasts depicting the changes occurring at the level of the chiral F-actin pattern in response to various interventions (Scale Bar = 10μm). To the right, on top, representative images of keratinocytes illustrating the transition to chiral pattern in response to LatA treatment (Scale Bar = 10μm). On the bottom, model suggested to explain how individual actin filament rotation determines the direction of cytoskeleton swirling. Adapted from *(Tee et al., 2015a, Nat Cell Biol; 2023, Nat Commun; Jalal et al., 2019a, Journal of Cell Science)*.
D: To the left, schematic representation of cell chirality when the radial fibers are dominant, causing a right-screw motion tilt rightward that drives an overall CCW rotation of the entire cytoskeleton around the cell nucleus. To the right, schematic representation of cell chirality when the transverse arcs are dominant, which swirl CW as they approach during retrograde flow, giving rise to a CW pattern around the nucleus. Adapted from *(Kwong et al., 2023, ELife)*.

---

established chirality in neutrophils involves actual cell motion in the form of amoeboid migration, in which the events associated with actin and microtubule polarization differ from those described for mesenchymal cell migration in the previous sections. *(Xu et al., 2007, PNAS)*

On the other hand, the second chiral phenotype (static) arises in predominantly immotile cells, confined on micropatterns or not, and manifests as a transient, biased actin cytoskeletal swirling, coupled to nucleus rotation. For example, isolated Zebrafish binucleated melanophores exhibited a CCW-biased rotation of the nuclei that was arrested upon the treatment with the actin polymerization inhibitor Cytochalasin D, suggesting the implication of the actin cytoskeleton dynamics in this phenomenon (Figure 14B) *(Yamanaka & Kondo, 2015, Genes to Cells)*. A similar CW-biased nuclear rotation was demonstrated among epithelial cells, in which the activities of both actin and MyoII were involved in the generation of a unidirectional cytoplasmic flow *(Yamamoto et al., 2023, BioRxiv)*.

A pioneer study performed by Tee el al. revealed that upon confinement on circular adhesive areas, the organization of the actin cytoskeleton in fibroblasts transitioned from

an isotropic radial arrangement into a chiral pattern (Figure 14C). This transformation was mediated by the CCW-tilting of radial fibers, which gave rise to a transient biased cytoskeletal swirling accompanied by nucleus rotation that resolved after a certain duration of time. The physical model proposed by the authors to explain this symmetry-breaking event is based on the dynamics of actin fibers. Non-contractile radial fibers originating from FAs at the cell periphery are polymerized toward the center. As they grow, elongating actin filaments within the radial fibers are rotated by immobilized formins. Frictional forces transmitted from the centripetally swirling, contractile transverse arcs to the radial fibers generate a net torque that drives the CCW-tilting of the latter and the subsequent establishment of the chiral organization. Whereas the selective knockdown of mDia-1 suppressed radial-to-chiral pattern transition due to the absence of radial fiber tilting, inhibiting contractility entirely abolished the self-organization of the actin cytoskeleton. On the other hand, overexpressing the actin crosslinker α-actinin in these cells reversed the swirling direction to CW, potentially because the free rotation of polymerizing actin filaments was hindered by the additional crosslinks, leading to the gradual buildup of torsional strain, which could be relaxed by periodic rotation in the opposite direction. As most of the interventions effecting the radial fibers tilting in single cells also modulated the biased collective alignment in a similar fashion, the authors suggested that the same effectors were involved in the emergence of the two chiral phenotypes, thereby implying that actomyosin-based cell chirality was at the origin of LR asymmetry in collectives. However, it was shown, in the same study, that the knockdown of certain ABPs was associated with different or even opposing effects on the chirality of the two systems. For example, the knockdown of MyoIC enhanced the biased alignment of cell collectives but had no effect on the chiral swirling of individual cells. Such inconsistencies challenge the conservation of the mechanism driving LR symmetry breaking across scales and suggest the implication of other, yet to be identified factors in this phenomenon. *(Tee et al., 2015a, Nat Cell Biol; 2023, Nat Commun)*

In a follow-up study, the authors showed that bias reversion induced under certain conditions, such as low-dose LatA treatment, required the activity of α-actinin but not that of formins. Interestingly, confined keratinocytes, which were normally stuck at the radial actin organization, could adopt a similar chiral pattern in response to low doses of latrunculin A (LatA), which interfered with actin dynamics (Figure 14C). The reversed swirling direction (CW versus CCW in fibroblasts) was attributed to a potentially excessive activation of formins due to the increased availability of free G-actin monomers. (Jalal et al., 2019a, *Journal of Cell Science*)

Using the experimental model described above, Kwong et al. showed that bias reversal, induced mechanically by the modulation of the cell-projected area or biochemically by altering the function of certain components associated with the actin cytoskeleton, could be explained by an imbalance between two classes of actin fibers, radial fibers and transverse arcs (Figure 14D). They suggested that actin swirling in opposite directions could be associated with two distinct phenomena: actin polymerization primarily occurring in the radial fibers underlied CCW-swirling, whereas predominant MyoII

contraction in the transverse arcs drove swirling in the CW direction *(Kwong et al., 2023, ELife)*. Moreover, it was shown that mesenchymal cells displayed an equivalent chiral phenotype that could be modulated by varying the levels of actin polymerization or crosslinking, which would subsequently influence their lineage differentiation. The authors demonstrated that reducing F-actin polymerization induced a CW bias among mesenchymal cells, which favored their adipogenic differentiation. By contrast, increased levels of actin crosslinking characterized a CCW-biased cell population with a future osteogenic commitment. *(Bao et al., 2020, Advanced Biosystems)*

2.5. Puzzles remaining in cell chirality research

The biased cellular behaviors described above point at the existence of an inherent cellular chiral feature. However, given its subtle and transient nature, can this intracellular chirality by itself be at the origin of the directional tissue rearrangements and motions, which underlie the LR asymmetric development of organisms essential for their proper functioning?

Regardless of its role in organismal development, the emergence of cellular LR asymmetry seems to be always dependent on the conserved chirality of the actin cytoskeleton. This raises a series of important mechanistic questions. How does the intrinsic chirality residing in the helical nature of actin filaments propagate to cytoskeletal arrays, cells, and tissues? Moreover, how can different cell types generate distinct biased phenotypes at the cellular and multicellular levels using the same intrinsically chiral molecules? Even more striking is the fact that chirality is not uniform within cell populations: cells from the same tissue have the ability to break symmetry in both directions or to shift their chirality under certain conditions *(Wan et al., 2011, PNAS)*. Although it has been suggested that the emergent non-absolute intracellular chirality is sufficient to drive biased tissue-level behaviors, how can one explain this non-binary (zero/one) nature of chirality?

2.5.1. One master regulator for actin-based LR symmetry breaking?

The key to answering these questions may reside within the interactions of actin filaments with certain ABPs through different mechanical processes that can influence their helical properties, eventually giving rise to distinct actin network organizations. As previously described, two major actin-ABP interactions have been identified as starting points for cytoskeletal chirality emergence. In one, a constrained formin applies a torque on an elongating actin filament causing it to rotate around its axis during polymerization. In the other, while pulling on actin filaments, myosin molecular motors move helically, thereby producing a torque that rotates the associated actin filaments *(Jegou & Romet-Lemonne, 2020, Seminars in Cell & Developmental Biology; Maxian & Mogilner, 2024, European Journal of Cell Biology)*. As such, can the actions of formins and myosins on actin filaments be associated with distinct directional bias? In other words, can formin and myosins serve as the ultimate chirality denominators?

One theoretical model simulating a cross-linked filopodial actin bundles under the action of both formin and myosin shows that there is no preferential direction for filament twisting by either of the two effectors. In addition, formins must synergize with the

myosin motors to generate efficient bundle compaction and coiling in the direction of the motor activity *(Maxian & Mogilner, 2024, European Journal of Cell Biology)*. On the other hand, Tee et al. has demonstrated that CW actin bundle rotation by the formin mDia1 is translated into CCW actin swirling in individual confined fibroblasts and CCW alignment in cell collectives, which are abolished in the absence of myosin activity. Surprisingly, mDia1 appears to be dispensable for CW actin swirling and collective alignment *(Tee et al., 2015b, Nat Cell Biol; 2023, Nat Commun)*. This indicates that the activity of formin mDia1 alone cannot account for symmetry break in the opposite direction. Interestingly, while their model postulates that formin activity strictly rotates actin filaments in the CW direction, another model simulating the emergence of chirality in individual cells shows that actin filaments elongated by formins can rotate in either direction with equal probabilities *(X. Li & Chen, 2022, Biophysical Journal)*.

Early LR asymmetry establishment in C. elegans requires CYK-1/Formin, which functions in parallel to MyoII activity for the generation of cortical counter-rotations, responsible for driving chiral skews in mitotic spindles that properly position daughter cells in the zygote and embryo *(Middelkoop et al., 2021, Proceedings of the National Academy of Sciences)*. Moreover, in Drosophila, chirality emergence requires the activity of formin DAAM, which together with E-cadherin and FAs, generates a specific, polarized actin network that serves as a substrate for the LR asymmetry determinant MyoID *(Chougule et al., 2020, PLOS Genetics)*.

As such, intracellular chirality cannot be attributed to the activity of a single master regulator. Instead, LR symmetry breaking appears to be mediated by a group of conserved proteins, whose contributions to and chiral interactions with the polarized actin network are essential for the emergence and the maintenance of chirality.

2.5.2. LR symmetry breaking requires a polarized background

The fundamental feature of LR symmetry break is essentially to distinguish left and right by a certain mechanism. How difficult could that be? In fact, this process is not that straightforward, primarily because the LR axis is not independent; it is always oriented relative to the two other existing axes: AP and DV. This poses a problem, especially regarding the stability of LR asymmetry, because if either of the two axes is inverted, the left and right properties will be swapped. Thus, how is it possible to specify left and right? Brown and Wolpert argue that one way to overcome this problem is through a conversion mechanism in which a handed molecule, F, aligns itself in reference to the AP and DV axes, so that its handedness is converted to define left and right. They suggest that this may be the mechanism by which molecular asymmetry can be manifested at the cellular and multicellular levels *(Brown & Wolpert, 1990, Development).* Therefore, the emergence of LR asymmetry appears to be second-order symmetry breaking event, occurring in a system with pre-established AV and DV polarities.

Such an interplay between chirality and polarity can been seen in the development of Drosophila male genitalia. The pre-established polarized MyoII flow causes a greater deposition of MyoII on junction plates to the right of the AP axis. The resulting asymmetry in contraction induces diagonal cell intercalation and, subsequently, anisotropic cell

shape (PCC), which eventually leads to the dextral rotation of the genitalia *(K. Sato et al., 2015b, Nat Commun)*. Similarly, during the development of the C. elegans, the polarization of the zygote along the AP axis is accompanied by the generation of a polarized, MyoII-dependent cortical AP flow. The latter is essential for the emergence of chiral cortical counter-rotations, which are critical for the establishment of LR asymmetry in the zygote and the embryo *(R. Li & Gundersen, 2008, Nat Rev Mol Cell Biol; Naganathan et al., 2014, ELife; Pimpale et al., 2020, ELife)*. Taken together, chirality emergence seems to be associated with a secondary symmetry-breaking event, essentially requiring a pre-polarized system to manifest.

Overall, it appears that the same cytoskeletal components actively participate in the development of both polarity and chirality. This, in addition to the use of cell polarity as a readout for intrinsic chirality under certain conditions, suggests that the two phenomena could be interconnected, which in turn raises some interesting questions. What feedback mechanisms exist between the events underlying the two types of symmetry breaking described in the previous sections? Does the establishment of cell polarity influence the emergence of chirality?

VI. CONTEXT AND OBJECTIVES

As seen throughout the previous sections, chirality is an emergent characteristic of cellular systems that can manifest in diverse forms. In particular, cell collectives, when grown in a confined environment, display persistent chiral rotation, which leads to the emergence of a characteristic cell alignment that varies with the cell type and disease state *(Wan et al., 2011, PNAS)*. Previous studies have targeted the resultant static phenotype to identify key parameters involved in the expression of chirality in cell collectives, overlooking the contribution of the mobile phase, which seems to be critical for the emergence and maintenance of chirality at this level *(Fan et al., 2018, Science Advances; Tee et al., 2023, Nat Commun)*. On the other hand, rotation has been investigated in the context of collective cell migration, where the major players identified include cell polarity, contractility, and intercellular junctions *(Lo Vecchio et al., 2024, Nat. Phys.; Jain et al., 2020, Nat. Phys.)*. However, the existence of a chiral bias in these models remains controversial.

One factor limiting the investigation of chirality-related mechanisms in cell collectives is the complexity of these systems. The chirality of a tissue or collective originates from the chirality of its constituting cells, which, as mentioned previously, is directly sensitive to their environment. Moreover, in the big collectives utilized by previous studies, rotation is restricted to the individual cells at the boundaries and is significantly influenced or even interrupted by the dynamics of the cells in the interior: random motion or swirling, extrusion, and division that frequently breaks the coherence of the motion. All of these confounding factors impose important challenges to the characterization and the interpretation of the emergent chiral behavior, as well as the identification of an existent directional bias. Key to addressing these limitations is the use of small cell clusters displaying coherent chiral motions, of which the most convenient is a system comprising the bare minimum for a cell collective: two cells and a single junctional interface – a cell doublet.

Several studies have pointed at a critical role for contractility, the major force driving cell motility, in LR symmetry-breaking events and the subsequent emergence of biased cytoskeletal swirling in individual cells and biased alignment in cell collectives. Yet, its contribution to the establishment and maintenance of a dynamic, biased chiral phenotype is still unclear. In addition, the different chiral models described so far suggest that LR asymmetry is tightly associated with the symmetry-breaking event underlying polarity emergence, which, interestingly, is largely dependent on variations in contractility. However, understanding how and to what extent these two co-existing asymmetries influence each other requires further investigation.

To this end, the goals of our study fall into two main categories:

1. Using a system of cell doublets, we attempt to address the existence of a biased persistent, chiral behavior in minimal cell collectives, as well as the exact contribution of cellular contractile forces to the emergence of this phenotype.
2. By triggering a dynamic chiral rotation among individual cells, we try to challenge the intrinsic nature of cell chirality as well as its relationship to polarity.

VII. RESULTS

VII.1. Chirality in minimal tissues: Cell Doublets

Previous experimental and theoretical studies have reported the ability of cell doublets to break symmetry and initiate rotation upon geometrical confinement in a 2D or 3D environment *(Huang et al., 2005, Cell Motil. Cytoskeleton; Tseng et al., 2012, Proc. Natl. Acad. Sci. U.S.A.; Leong, 2013, Biophysical Journal; Camley et al., 2014, Proceedings of the National Academy of Sciences; Lu et al., 2022)*. Therefore, we wondered about the existence of a chiral bias in this system, as well as the possible implication of contractility in driving such a dynamic and persistent motile phenotype.

1. Cell doublets are minimal collective systems that display a chiral bias

To explore the phenomenon of chiral rotation among doublets, we started by testing different cell types, which were characterized by distinct migratory capacities: Human Umbilical Vein Endothelial Cells (HUVECs), Madin-Darby Canine Kidney Cells (MDCKs), Mouse Embryonic Fibroblasts (MEFs), and HeLa Cells. In previous studies, these cell lines (endothelial, epithelial, fibroblasts, cancerous) presented different migration speeds on plane surfaces, which could be attributed, in part, to variations in the magnitude of their contractile forces *(Fernández-Muñoz et al., 2011, The International Journal of Biochemistry & Cell Biology; Tsai et al., 2014, Nat Cell Biol; Yamahira et al., 2014, Macromolecular Bioscience; Zhong et al., 2012, PLOS ONE)*.

It was shown that the ability of doublets to migrate was largely dependent on the geometry of the extracellular matrix (ECM), which directly influenced the stability of the intercellular junction by modulating their relative positioning *(Tseng et al., 2012, Proc. Natl. Acad. Sci. U.S.A.)*. The absence of ECM triggered the stabilization of the intercellular junctions, which inhibited their dynamic displacement and, consequently, suppressed doublet migration. As a result, to promote doublet rotation, we decided to use homogenous, disk-shaped adhesive micropatterns, which additionally offered a way to standardize cells in an initially symmetrical organization.

By assessing the cell area in a representative cell line (HUVECs), we identified the average population size to be around 1800μm^2 (Figure 15). This prompted the use of 60μm diameter adhesive disks for HUVECs, MEFs, and HeLa cells that had comparable sizes. MDCKs, on the other hand required smaller disks (40μm diameter) to be able to fully spread and rotate as doublets.

Seeding the cells on micropatterns and imaging them for 15hrs (Figure 16A), we first noticed that most cell doublets rotated, which confirmed the absence of junction stabilization and, thus, the choice of the micropattern geometry (Figure 16B). However, we detected differences in the amount of doublet rotation between the tested cell lines; HUVECs were characterized with the highest rotation percentage, whereas HeLa cells displayed the lowest rotation (Figure 16C). The initiation of persistent rotation was

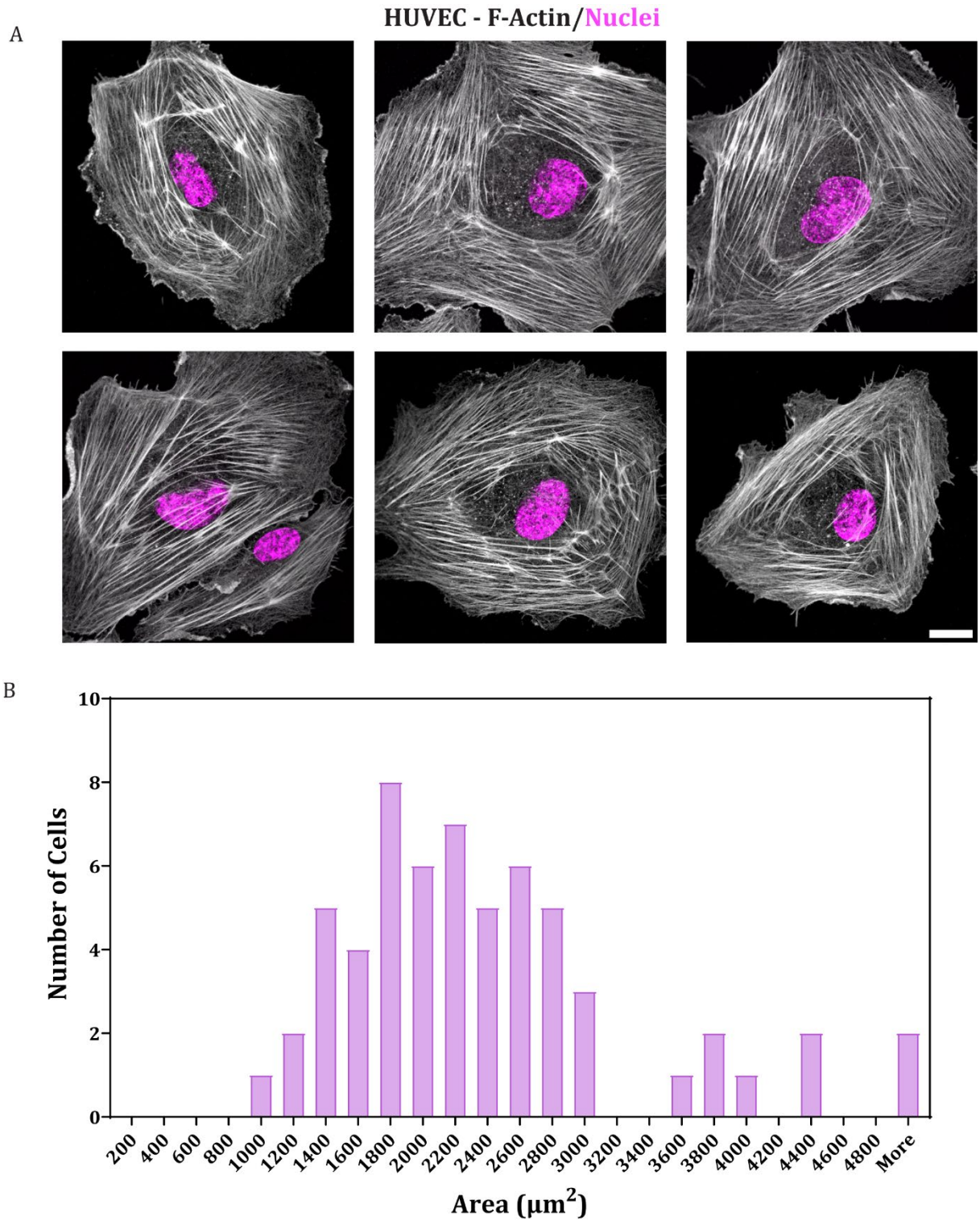

Figure 15: HUVECs display an average population size of 1800µm².
A: Examples of HUVECs plated on FN surfaces fixed and stained for F-actin and Nuclei. Scale Bar = 15µm
B: Bar graph representing the area (µm²) distribution in a population of HUVEC cells.

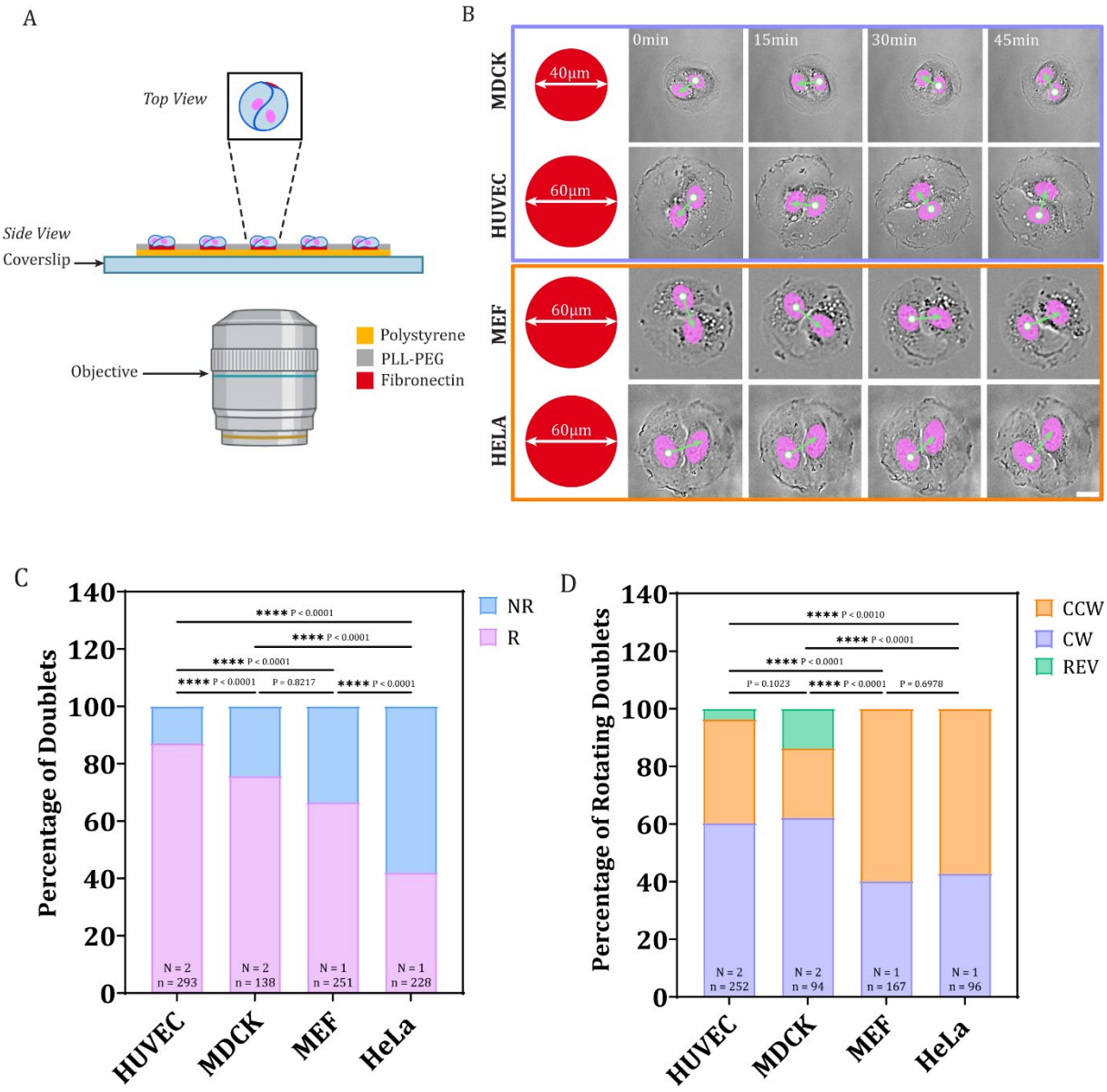

Figure 16: Cell doublets are minimal collective systems that display a chiral bias.
A: Schematic representation of the experimental setup from the side and top views.
B: Montage of rotating doublets of different cell types on FN-coated, disk shaped micropatterns; the size of the micropattern used for each cell type is represented to the left of the montage of the respective cell type. The green arrows follow the direction of the nuclei displacement. Doublets within the purple rectangle have a CW bias; those in an orange rectangle have a CCW bias. Scale Bar = 15µm
C: Bar graph representing the quantification of the percentage of rotating and non-rotating doublets in the different cell types tested.
D: Bar graph representing the quantification of the percentage of CW, CCW, and reverting (REV) doublets in the different cell types tested.
N is the number of independent experiments performed; *n* is the total number of doublets analyzed. Statistical significance was assessed using Chi-square (Fischer's exact) test.

preceded by a symmetry-breaking event, in which the cells of a pair established a stable front-rear polarization that was accompanied by a deflection in the junction so that the latter adopted the characteristic shape of a Yin-Yang. Therefore, the identified differences in doublet rotation might be associated with the intrinsic ability of the constituting cells to polarize and initiate migration. This could be greatly influenced by cellular contractility levels, which, interestingly, were also shown to modulate the strength of the intercellular junctions and, consequently, their deformability and shape *(Huang et al., 2005, Cell Motil. Cytoskeleton; Leong, 2013, Biophysical Journal; Camley et al., 2014, Proceedings of the National Academy of Sciences; Lu et al., 2022; B.-C. Wang & Xu, 2022, Biophysical Journal)*.

We then quantified the directionality of rotating doublets. Intriguingly, doublets of all the cell types tested were biased but not in the same direction: HUVECs and MDCKs displayed a rightward, clockwise (CW) bias, while MEFs and HeLa cells demonstrated a leftward, counter-clockwise (CCW) bias (Figure 16D). These results were consistent with the previously reported chiral bias in big collectives of the respective cell types, which further confirmed the validity of our minimal collective system *(Wan et al., 2011, PNAS; Lo Vecchio et al., 2024, Nat. Phys.)*. In addition to the doublets undergoing persistent directional rotation, we identified a subpopulation of reverting doublets (REV), which changed the direction of rotation over the course of the recorded movie. Despite being negligible among HUVEC doublets, REV cells represented about 20% of rotating MDCK doublets. This increase in the proportion of REV doublets could be attributed to the fact that, unlike HUVECs, MDCKs lack the long-term directional cues provided by the polarized cadherin fingers extending in the direction of motion at cell-cell junctions *(Hayer et al., 2016, Nat Cell Biol; LaChance et al., 2022, PLOS Computational Biology)*. Interestingly, the strength of the chiral bias was independent of the rotation proportion, as doublets with similar bias (CW for HUVECs and MDCKs or CCW for MEF and HeLa cells) displayed different rotation degrees.

Altogether, these results indicate that cell doublets are capable of demonstrating the persistent biased rotation previously described in large cell ensembles and, therefore and can be regarded as minimal biased cell collective systems.

To further study the expression of the chiral phenotype in cells doublets, we decided to use HUVECs as a model because they exhibited a high and persistent rotation in our system. In addition, they we shown to display a strong CW bias in more complex 2D systems and 3D vascular networks, and their chirality was associated with junction strength and endothelium permeability *(Fan et al., 2018, Science Advances; Hang et al., 2022, APL Bioengineering; H. Zhang et al., 2024, Science Advances; Zambuto et al., n.d., Advanced Healthcare Materials)*. Furthermore, the biased chiral alignment of endothelial cells was characterized in the blood vessels in vivo, where it seemed to play an important role in vascular development and physiology *(H. Zhang et al., 2024, Science Advances)*.

2. HUVEC doublets demonstrate a persistent chiral rotation on adhesive disks

To better characterize the chiral phenotype observed among HUVEC doublets, we followed the behavior of these cells shortly after seeding them on 60µm fibronectin-coated disks (Figure 17A). Over the course of 15hrs, we were able to identify three main subpopulations: non-rotating doublets (NR), CW (or rightward)-rotating doublets, and CCW (or leftward)-rotating doublets (Figure 17A-B-C). Doublets reverting their direction of rotation (REV) were excluded from the subsequent analyses. In line with our previous results, rotating HUVEC doublets demonstrated a CW bias (~61% CW versus 39% CCW). To confirm the identified bias, we systematically addressed the underlying statistics. First, we applied dedicated proportion and Chi-Square tests to our individual experiments to check whether the proportions of CW- and CCW-rotating doublets were significantly different from 50:50. Second, we used a classical unpaired t-test to show that the global difference between the percentages of CW and CCW doublets was statistically significant in the ensemble of our experiments. Altogether, these findings validated that HUVEC doublets exhibited a robust and reproducible, rightward chiral bias.

Figure 17: HUVEC doublets demonstrate a persistent chiral rotation on adhesive disks
A: Montage showing the different behaviors of HUVEC doublets on FN-coated, 60µm adhesive disks. The green arrows follow the direction of nuclei displacement. The blue cross, purple arrow, and orange arrow mark non-, CW, and CCW-rotating doublets, respectively. Scale Bar = 15µm
B: Bar graph representing the quantification of the percentage of HUVEC rotating and non-rotating doublets.
C: Bar graph representing the quantification of the percentage of HUVEC CW- and CCW-rotating doublets.
Individual points on the graph represent independent experiments. Statistical significance was assessed using proportion test for individual experiments and Mann Whitney test for all the replicates.
D: Bar graph representing the percentage of HUVEC rotating doublets at two different time points. Statistical significance was assessed using Chi-square (Fischer's exact) test.
E: Bar graph representing the percentage of HUVEC CW-rotating doublets at two different time points. Statistical significance was assessed using Chi-square (Fischer's exact) test.
F: Bar graph representing the evolution of the number of rotating HUVEC doublets over time.
G: Bar graph representing the evolution of the behavior of rotating HUVEC doublets over time.
N is the number of independent experiments performed; *n* is the total number of doublets analyzed.

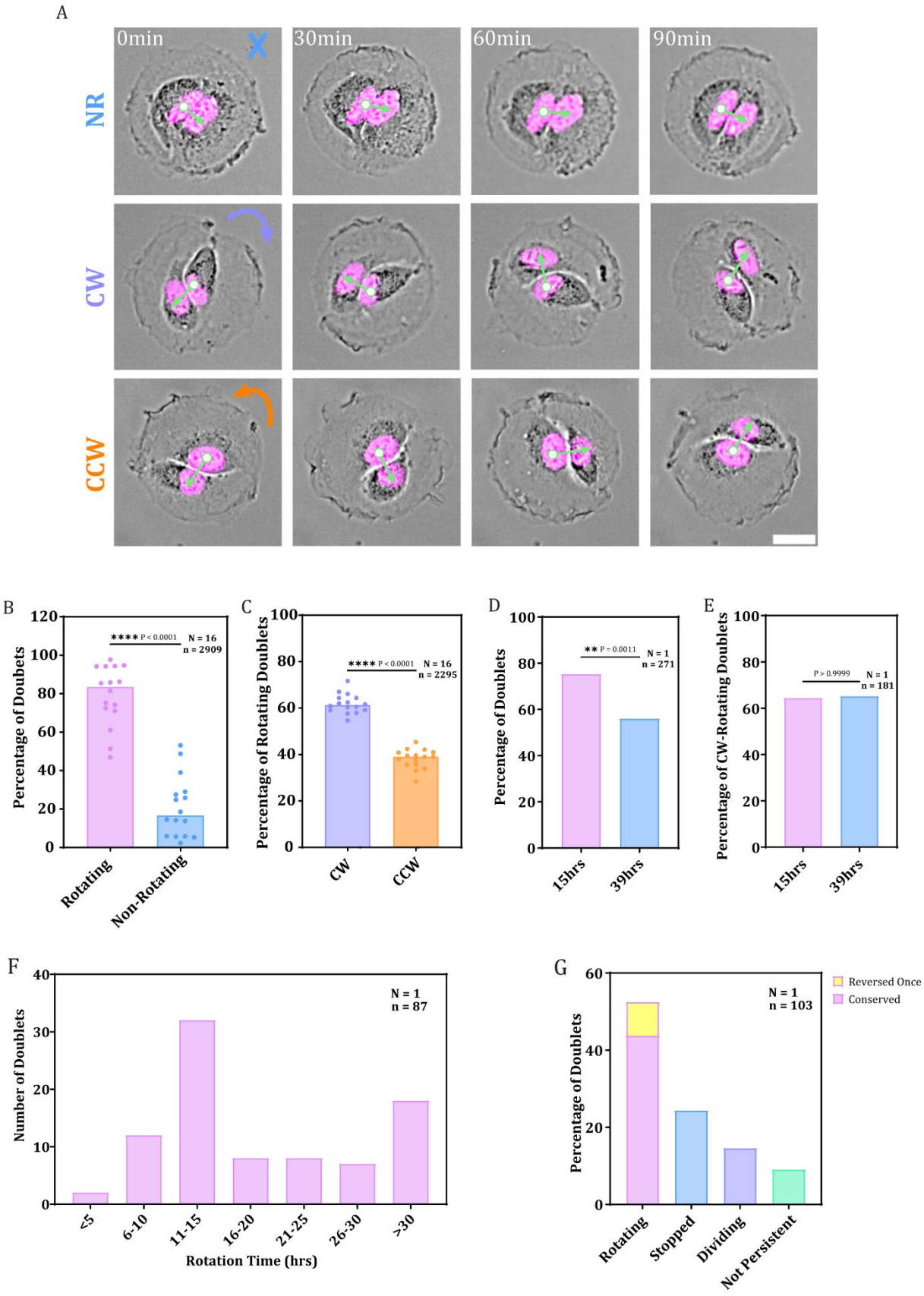
A
0min
30min
60min
90min
NR
CW
CCW
B
Percentage of Doubets
**** P < 0.0001
N = 16
n = 2909
Rotating
Non-Rotating
C
Percentage of Rotating Doublets
**** P < 0.0001
N = 16
n = 2295
CW
CCW
D
Percentage of Doublets
** P = 0.0011
N = 1
n = 271
15hrs
39hrs
E
Percentage of CW-Rotating Doublets
P > 0.9999
N = 1
n = 181
15hrs
39hrs
F
Number of Doublets
N = 1
n = 87
<5
6-10
11-15
16-20
21-25
26-30
>30
Rotation Time (hrs)
G
Percentage of Doublets
N = 1
n = 103
Reversed Once
Conserved
Rotating
Stopped
Dividing
Not Persistent

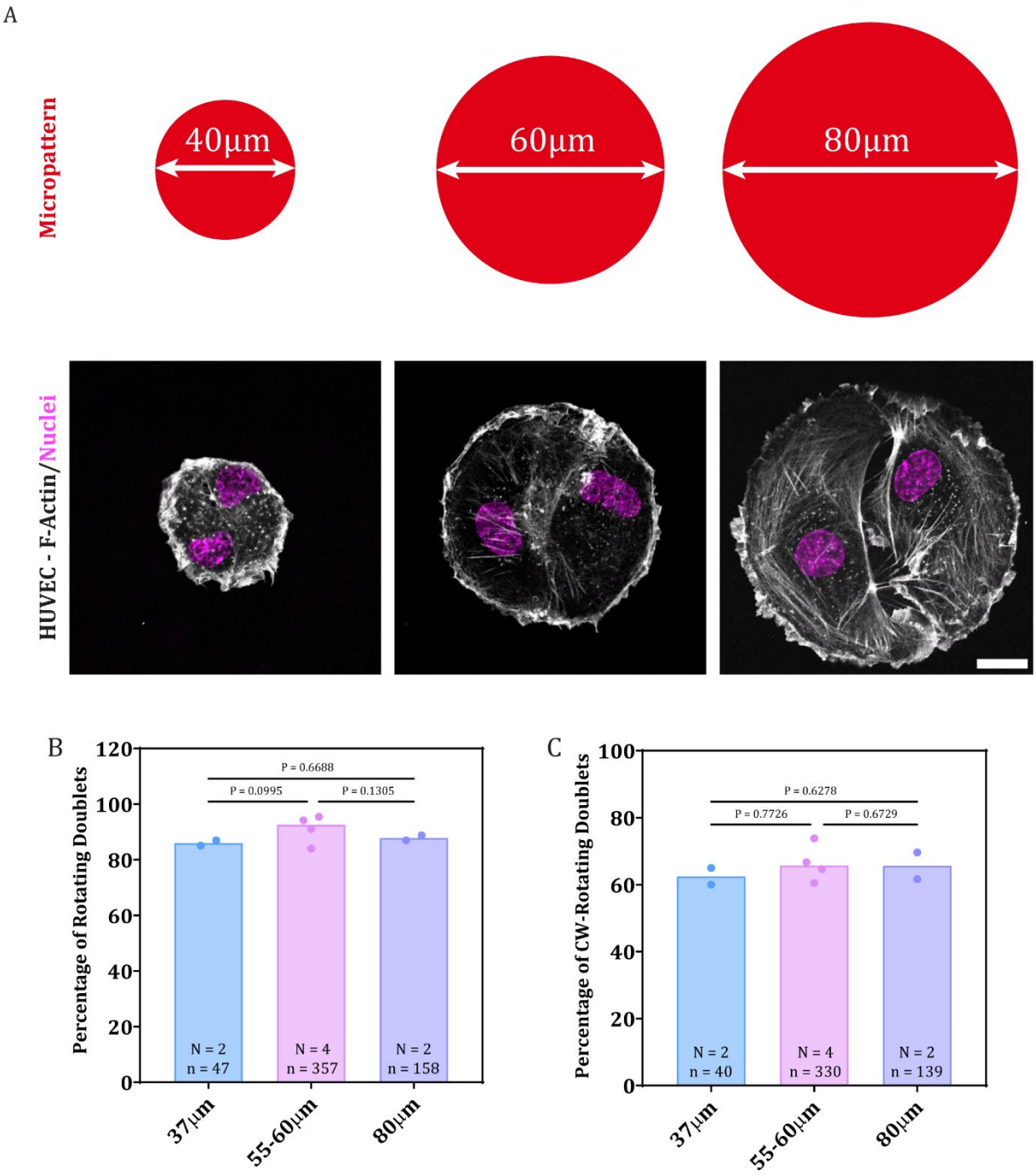

Figure 18: HUVECs biased rotation is independent of the micropattern size.
A: Representative images of HUVEC doublets on disk-shaped micopatterns of different sizes (40 – 60 – 80µm). Doublets were fixed and stained for F-actin and Nuclei. Scale Bar = 15µm.
B: Bar graph representing the quantification of the percentage of rotating HUVEC doublets on the different sizes tested.
C: Bar graph representing the quantification of the percentage of CW-rotating doublets on the different sizes tested.
N is the number of independent experiments performed; *n* is the total number of doublets analyzed. Statistical significance was assessed using Chi-square (Fischer's exact) test.

We then aimed at assessing the persistence of rotation in our system, so we tried to estimate, in a subset of cells, the doublet rotation time, defined as the time interval in which doublets rotated in the same direction. The majority of cells were rotating for 11 to 15hrs, but interestingly the chiral rotation phenomenon could be maintained over extended periods of time that sometimes exceeded 30hrs (Figure 17F). This indicated that the chiral phenotype identified here was more stable and persistent than the transient biased cytoskeletal swirling described in confined single cells *(Tee et al., 2015a, Nat Cell Biol)*. Lastly, we followed the evolution of the chiral phenotype between two different time intervals: 15 and 39hrs (Figure 17D-E). We noticed that although the percentage of rotating doublets dropped at 39hrs – due to certain doublets that stopped rotating, lost persistence, or divided into triplets – the CW bias was maintained over the entire time interval (Figure 17G).

It was previously reported that varying the micropattern size could increase the proportion of single cells displaying chiral swirling *(Jalal et al., 2019a, Journal of Cell Science)*. In addition, several studies demonstrated that this parameter could also affect the dynamics of collective cell rotation *(Lo Vecchio et al., 2024, Nat. Phys.; Glentis et al., 2022, Science Advances; Xi et al., 2017, Nat Commun)*. Thus, we wondered whether the size of the micropattern used and the resulting imposed curvature could influence the expression of chirality in our system. To address this question, we seeded HUVEC doublets on adhesive disks of different sizes (40, 60, and 80μm in diameter), taking into account that the cells were still able to sufficiently spread and initiate rotation, and we followed them over several hours (Figure 18A). Surprisingly, we found no significant differences in both rotation proportion and bias strength among doublets confined on disks of the different sizes tested (Figure 18B).

These findings suggest that HUVEC doublets display a robust chiral phenotype demonstrated by a persistent biased rotation that is independent of the micropattern size and curvature.

3. HUVEC chiral bias is conserved in systems of increased complexity

Given the dynamic biased rotation we described in cell doublets, we wondered how these cells would behave in more complex cellular systems. Therefore, we seeded HUVECs at a higher cell density on 60μm adhesive disks and followed the evolution of the resulting cell collectives for several hours (Figure 19A). We noticed that, similarly to doublets, both HUVEC triplets and quadruplets were able to display persistent rotation (Figure 19B). However, we reported some cell collectives with either a delayed rotational onset or an interrupted rotational course. These events could be related to time needed for the individual cells of a collective to coordinate their polarities and initiate directional motion, as well as the geometrical organization these cells adopt on the micropattern, which could greatly affect their rotational behavior *(Segerer et al., 2015, Phys. Rev. Lett.; B.-C. Wang & Xu, 2022, Biophysical Journal)*. Interestingly, the CW bias was conserved in cell triplets and was even enhanced among quadruplets, suggesting that the chiral phenotype could be

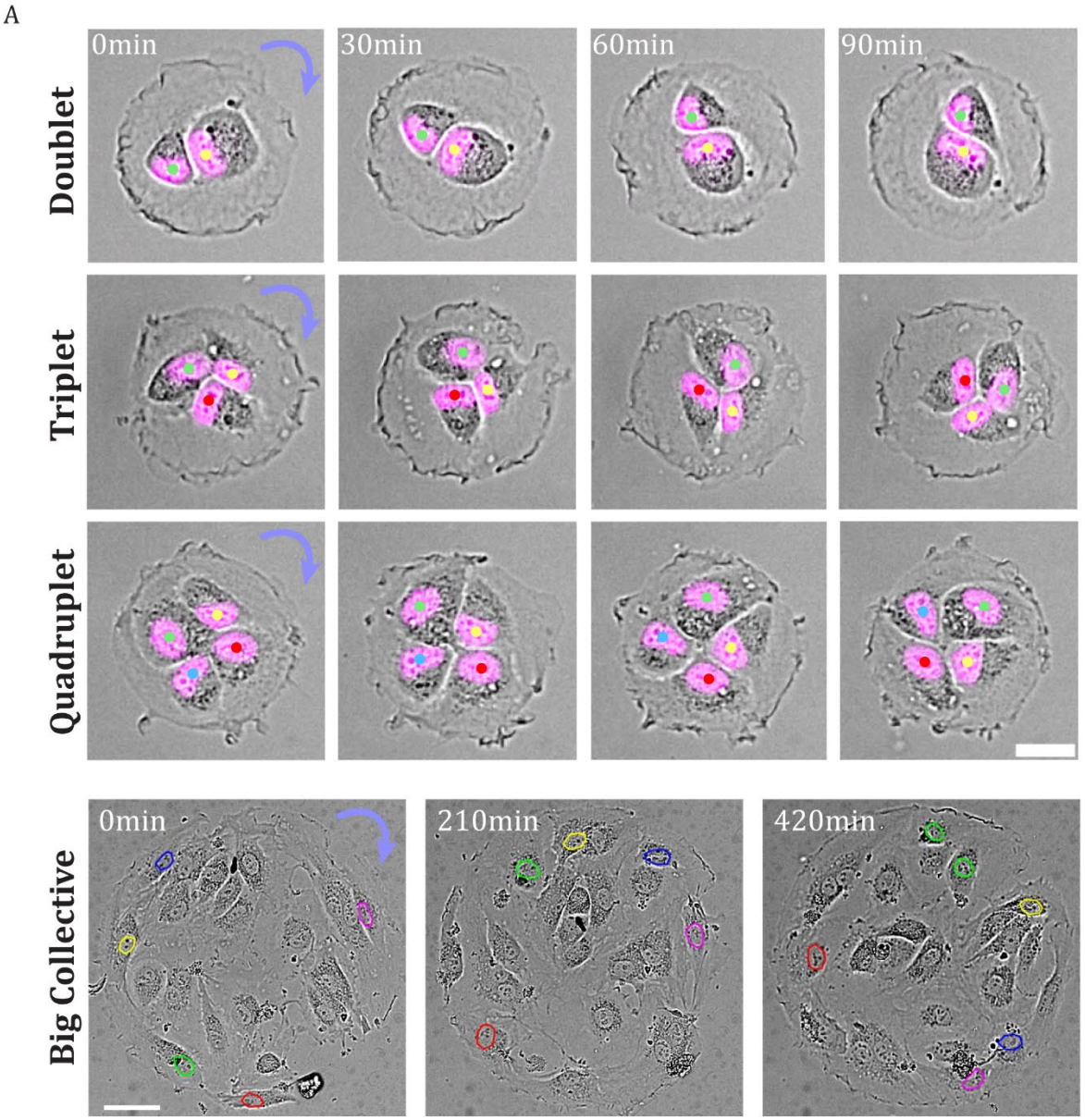
A
Doublet
Triplet
Quadruplet
Big Collective
0min
30min
60min
90min
0min
210min
420min

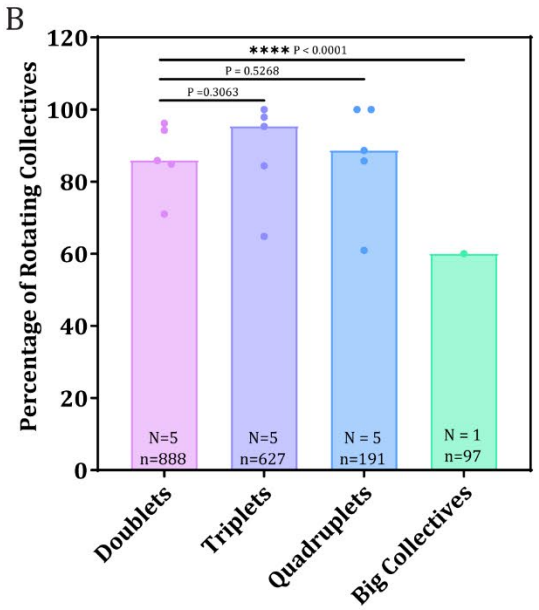
B
Percentage of Rotating Collectives
**** P < 0.0001
P = 0.5268
P =0.3063
N=5 n=888
N=5 n=627
N = 5 n=191
N = 1 n=97
Doublets
Triplets
Quadruplets
Big Collectives

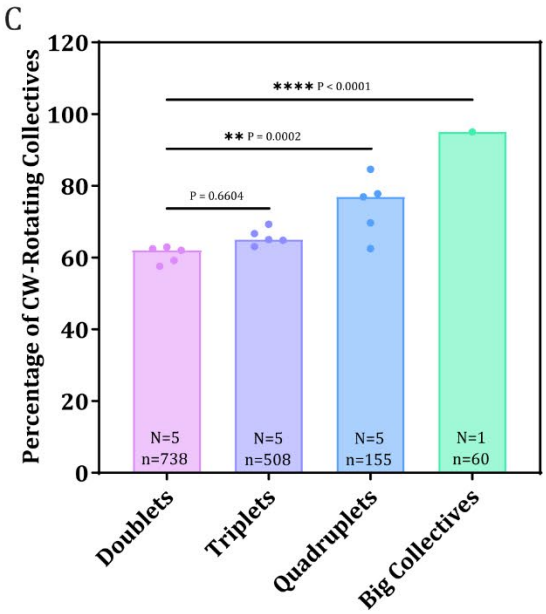
C
Percentage of CW-Rotating Collectives
**** P < 0.0001
** P = 0.0002
P = 0.6604
N=5 n=738
N=5 n=508
N=5 n=155
N=1 n=60
Doublets
Triplets
Quadruplets
Big Collectives

Figure 19: HUVEC chiral bias is conserved in systems of higher complexity.
A: Montage showing the rotation of HUVEC collectives on FN-coated adhesive disks. Micropatterns used for doublets, triplets, and quadruplets are 60µm in diameter; those used for big collectives are 250µm in diameter. The green, yellow, red, and blue dots or ROIs on the images follow the displacement of the nuclei and cells. The direction of rotation of the collectives is indicated by the purple arrow. Scale Bar = 15µm and 50µm for the big collective.
B: Bar graph representing the quantification of the percentage of rotating cell collectives.
C: Bar graph representing the quantification of the percentage of CW-rotating cell collectives.
N is the number of independent experiments performed; *n* is the total number of doublets analyzed. Statistical significance was assessed using Chi-square (Fischer's exact) test.

amplified across increasing levels of complexity (Figure 19C). We further tested this hypothesis by creating even bigger cell ensembles on 250µm disks and assessing their behavior for hours (Figure 19A). Although they required a relatively longer time to collectively polarize and initiate motion, the majority of these ensembles eventually displayed a coherent and persistent rotation. Cell collectives with no apparent motion or directionality were considered non-rotating (Figure 19B). Quantifying the directionality of rotation revealed that the rightward bias was greatly enhanced among big cell ensembles with around 95% CW-rotating collectives, consistent with the previously reported bias of HUVEC collectives on donut-shaped micropatterns (Figure 19C). The amplification of the chiral bias as it propagates to more complex cellular systems might be associated with the greater number of cells generating a chiral torque gradient with a particular handedness to drive the collective biased migration *(Yamamoto et al., 2020, Phys. Rev. Res.)*.

Taken together, these results suggest that HUVEC doublets exhibit a collective biased behavior, reminiscent of that demonstrated at higher complexity levels, thereby further confirming their validity as minimal collective models to investigate the phenomenon of chirality.

4. CW and CCW rotations have different motility signatures

To further characterize HUVEC doublet rotation, we first followed the trajectories of the nuclei over the course of rotation. Based on the resulting profiles, we noticed that some doublets exhibited a symmetric displacement, in which the two nuclei rotated together following similar trajectories. On the contrary, others displayed an asymmetric displacement characterized by a peripheral, more elongated and motile cell turning around a more central one. This asymmetric phenotype resulted in the outer cell covering a larger distance than the inner one (Figure 20A). We thus hypothesized that the motility of individual cells could influence the rotation of the doublets, thereby driving differences in the chiral bias observed at the level of the population. In this context, we wondered whether the symmetric and asymmetric cell doublet populations would demonstrate

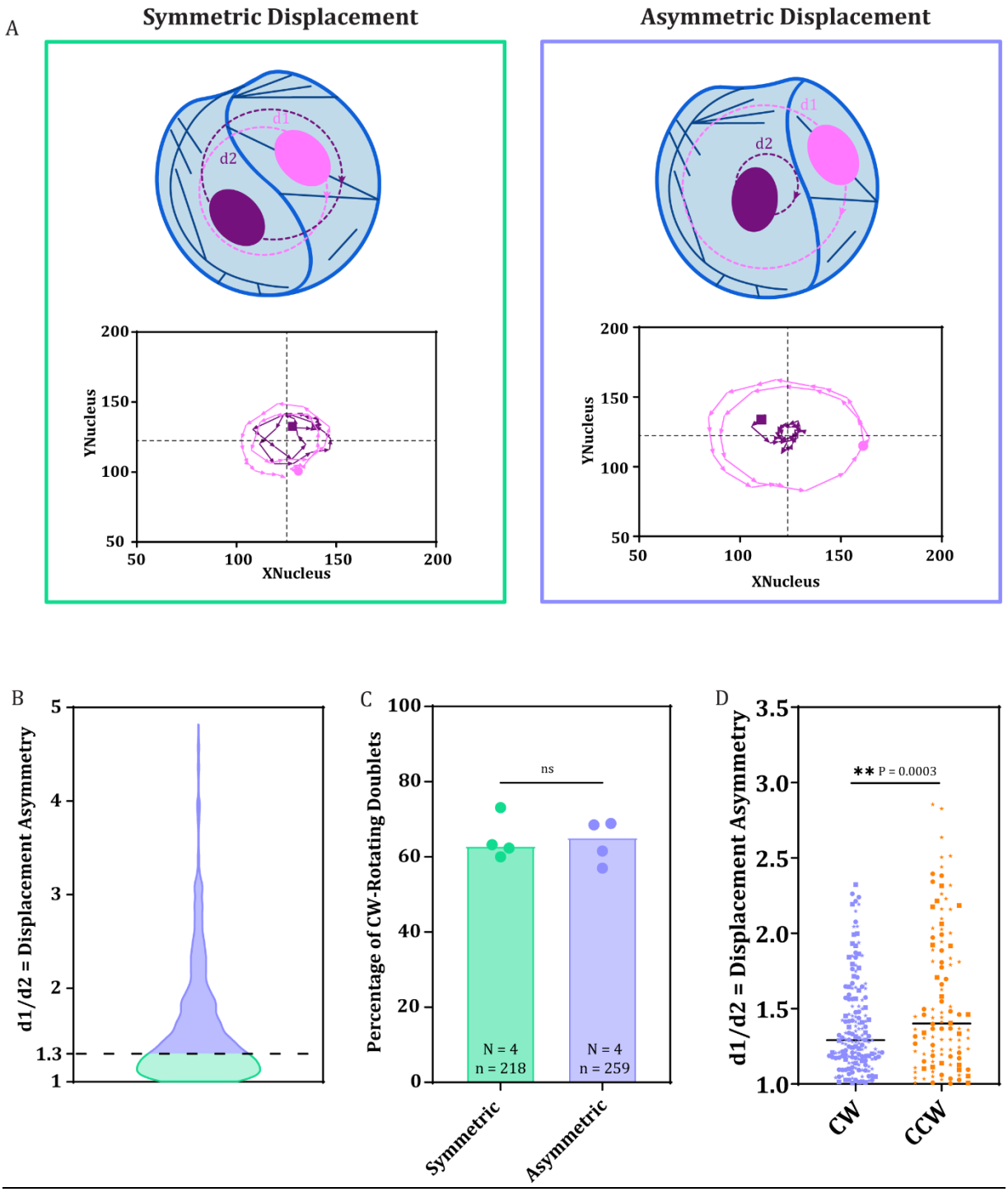

Figure 20: Asymmetry in cell motility has no effect on the chiral bias of doublets.
A: Schemes illustrating the two modes of rotation identified in doublets based on the displacement of the nuclei, symmetric and asymmetric, with a corresponding example of the nuclei trajectories recorded for each. The distance covered by nucleus 1 and 2 are referred to as d1 and d2, respectively.
B: Graph showing the distribution of the displacement asymmetry ratio d1/d2 calculated for all the doublets from four independent experiments. The dashed line marks the threshold defined at 1.3.

C: Bar graph representing the quantification of the percentage of CW-rotating doublets in the symmetric and asymmetric subpopulations. Statistical significance was assessed using Chi-square (Fischer's exact) test.
N is the number of independent experiments performed; *n* is the total number of doublets analyzed.
D: Graph representing the computed displacement asymmetry ratio for CW- and CCW-rotating doublets. Statistical significance was assessed using unpaired t-test.

---

differences in the expression of the chiral phenotype. To address this question, we used the total distance covered by the nuclei to compute the Displacement Asymmetry, defined as the ratio d_1/d_2, where $d_1>d_2$ (Figure 20A). We then sorted the doublets into symmetric (having ratios < 1.3) or asymmetric (having ratios > or = 1.3) and quantified the corresponding bias separately (Figure20B). Both subpopulations demonstrated an equally CW-biased rotation (Figure 20C). The same result was obtained by setting various asymmetry thresholds (lower or higher than 1.3), suggesting that the differences identified in displacement had no effect on the demonstration of chirality among HUVEC doublets. Interestingly however, by comparing the displacement asymmetry between CW- and CCW-rotating doublets, we noticed that the latter showed greater asymmetry in nuclei trajectories (Figure 20D).

Moreover, CCW-rotating doublets were on average characterized with a shorter rotation time that could be associated with a lower persistence of rotation (reversion) or by a shorter delay to initiate rotation compared to CW (Figure 21A). In addition, tracking the junction over the interval of rotation provided a measure for the corresponding angular velocity (ω), which was found to be lower in CCW-rotating doublets (Figure 21B). Knowing that both the speed and persistence of migration were previously associated with cellular contractility levels *(Gupton & Waterman-Storer, 2006, Cell; Mitin et al., 2013, PLOS ONE; Pasapera et al., 2022, Current Biology; Shi et al., 2021, Frontiers in Cell and Developmental Biology)*, these results suggest that CW- and CCW-rotating doublets may have different contractile properties.

Figure 21: CW and CCW rotations have different motility signatures.
A: Schematic representation of the total rotation time (t) estimated for each doublet. Graph representing the total rotation time measure for CW- and CCW-rotating doublets. Statistical significance was assessed using unpaired t-test.
B: Schematic representation of the method used to compute the angular velocity of doublet rotation (ω): an ellipse (dashed yellow) is fitted to the defined junction, and its long axis is used to calculate the angular displacement. Graph representing the computed angular velocity for CW- and CCW-rotating doublets. Statistical significance was assessed using unpaired t-test.
N is the number of independent experiments performed; *n* is the total number of doublets analyzed.

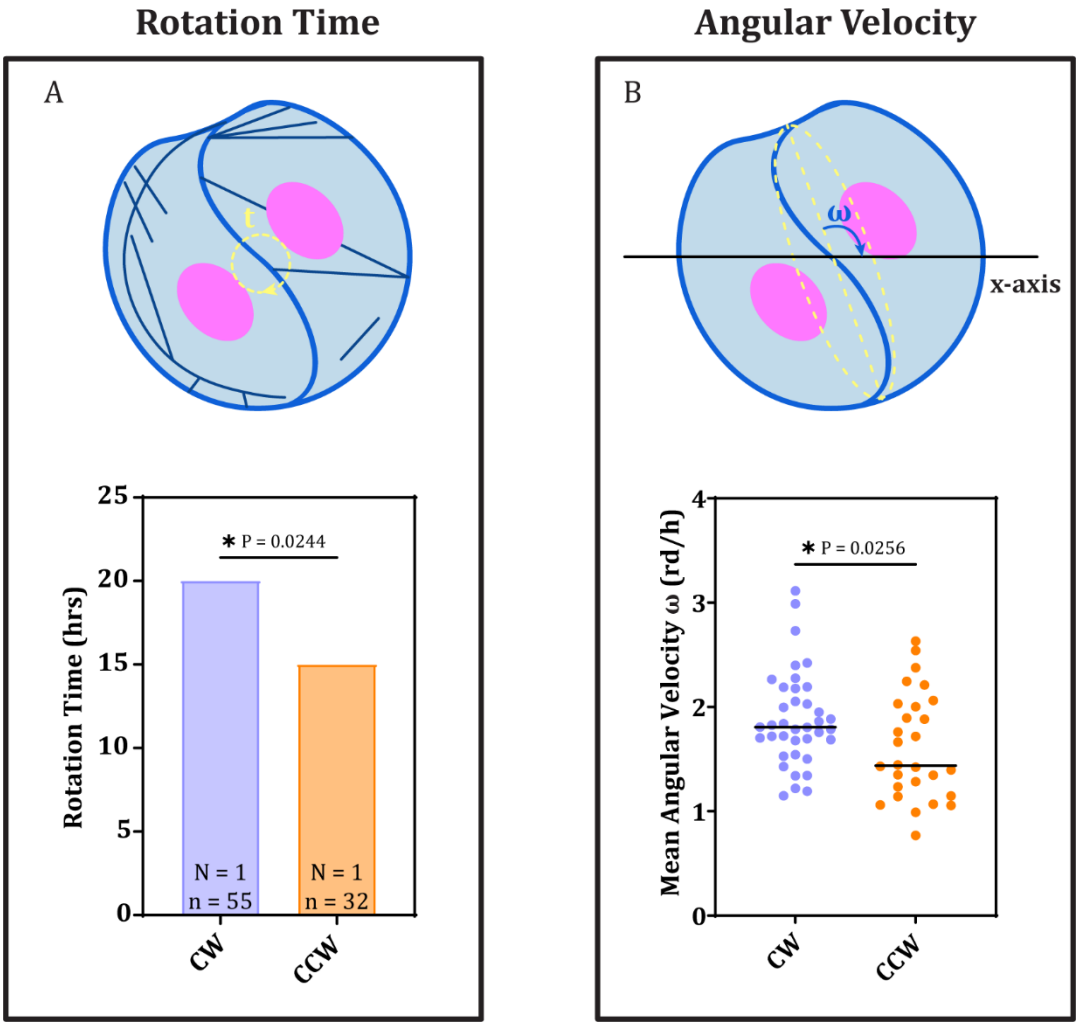

5. CW- and CCW-rotating doublets display different mechanical characteristics

In an attempt to understand the observed differences between the two subpopulations, we decided to study the mechanics associated with the chiral rotation. To this end, we performed Traction Force Microscopy (TFM), in which we seeded HUVEC doublets on polyacrylamide (PAA) gels containing fluorescent beads (Figure 22A). As the doublets rotated, they produced forces that deformed the gels and, thereby, displaced the beads. We used this bead displacement to quantify the magnitude of the cellular forces during rotation *(Martiel et al., 2015, Methods in Cell Biology)*.

The forces identified within a pair of rotating HUVEC cells included the traction forces (TFs) exerted on the extracellular matrix (ECM) ($\vec{f}$), which were centripetal and concentrated at the doublet periphery with a particularly high magnitude at the edges of the junction, where the front of one cell contacted the rear of the other (Figure 22A-1). The localization of the TFs corresponded to the distribution of focal adhesions (FAs) in the doublets, and their magnitude was extracted using conventional TFM analysis. To

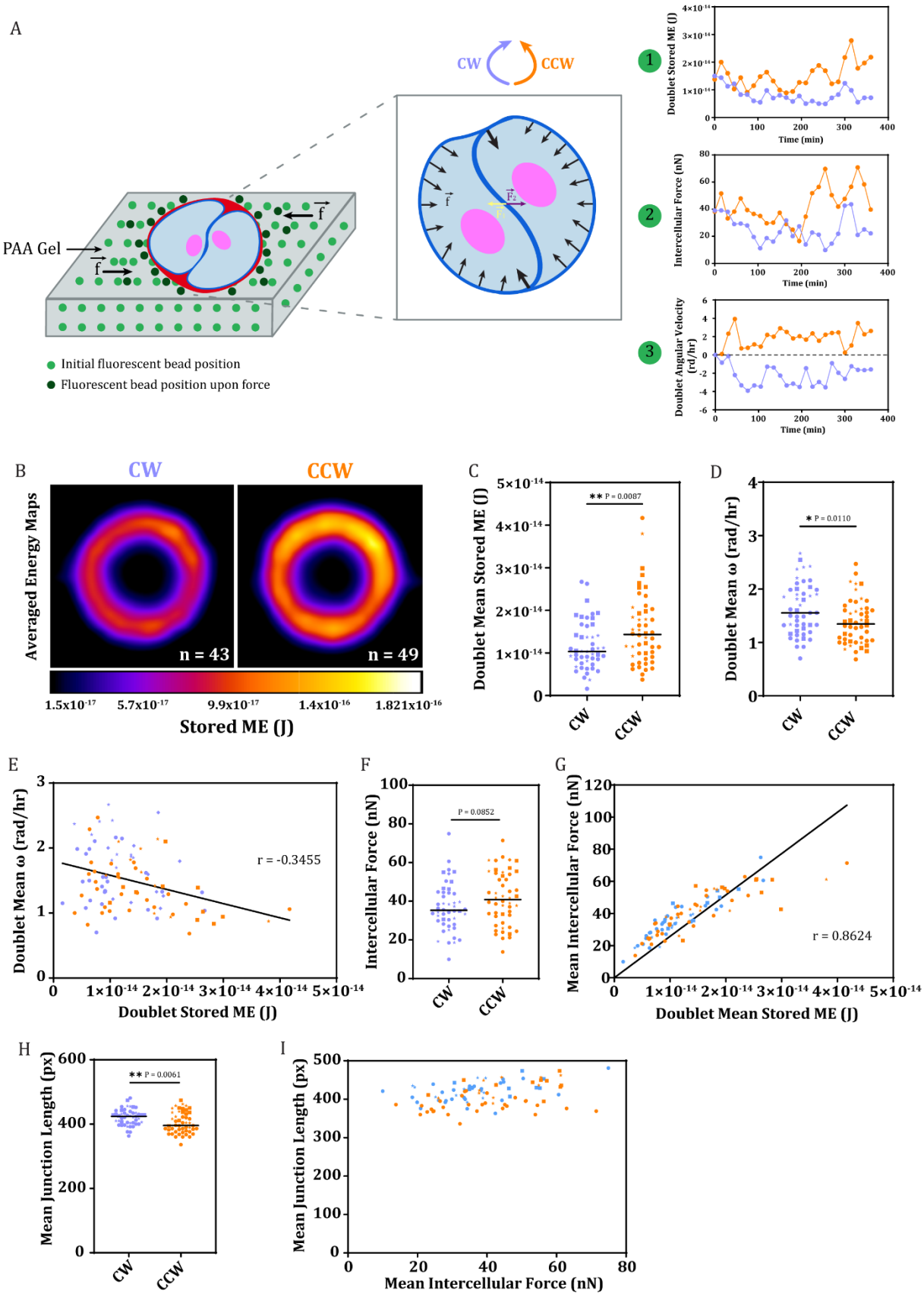
A
CW
CCW
PAA Gel
Initial fluorescent bead position
Fluorescent bead position upon force
Doublet Stored ME (J)
Intercellular Force (nN)
Doublet Angular Velocity (rd/hr)
Time (min)
B
CW
CCW
Averaged Energy Maps
n = 43
n = 49
1.5x10-17
5.7x10-17
9.9x10-17
1.4x10-16
1.821x10-16
Stored ME (J)
C
Doublet Mean Stored ME (J)
** P = 0.0087
D
Doublet Mean ω (rad/hr)
* P = 0.0110
E
Doublet Mean ω (rad/hr)
r = -0.3455
Doublet Stored ME (J)
F
Intercellular Force (nN)
P = 0.0852
G
Mean Intercellular Force (nN)
r = 0.8624
Doublet Mean Stored ME (J)
H
Mean Junction Length (px)
** P = 0.0061
I
Mean Junction Length (px)
Mean Intercellular Force (nN)

Figure 22: CW- and CCW-rotating doublets demonstrate different mechanical characteristics.
A: Schematic representation of the experimental setup used for TFM, as well as the forces exerted within a rotating doublet. $\vec{f}$ represents the TFs exerted by the doublet during rotation to displace the fluorescent beads; $\vec{F}1$ and $\vec{F}2$ are the intercellular forces exerted at the cell-cell junction.
1: An example for the variation profile of the stored mechanical energy (J) during rotation for CW- and CCW- doublets.
2: An example for the variation profile of the intercellular force (nN) during rotation for CW and CCW doublets.
3: An example for the variation profile of the angular velocity (rd/hr) during rotation for CW and CCW- doublets.
B: Average Energy Maps of all the mean energy maps of CW and CCW doublets.
C: Graph representing the mean stored ME for CW- and CCW-rotating doublets. Statistical significance was assessed using unpaired t-test.
D: Graph representing the mean angular velocity ω for CW- and CCW-rotating doublets. Statistical significance was assessed using unpaired t-test.
E: Scatter plot of the mean angular velocity ω as a function of mean stored ME for rotating doublets. The Pearson Coefficient of correlation r is indicated on the graph.
F: Graph representing the mean intercellular force for CW- and CCW-rotating doublets. Statistical significance was assessed using unpaired t-test.
G: Scatter plot of the mean intercellular force as a function of mean stored ME for rotating doublets. The Pearson Coefficient of correlation r is indicated on the graph.
H: Graph representing the junction length measured for CW- and CCW-rotating doublets. Statistical significance was assessed using unpaired t-test.
I: Scatter plot of the mean junction length as a function of mean intercellular force for rotating doublets.
Data was pooled from three independent experiments (N).

better characterize the mechanics of rotating doublets, we used the elastic energy stored in the gel deformation (ME), which was previously defined as a cell mechanical output independent of gel rigidity (Oakes et al., 2014, *Biophysical Journal*). In the light of all the inherent variabilities that could make the reproducibility of TFM procedures particularly challenging, the stored ME provided a more reliable and robust measure than simply the average TFs. In addition, at the intercellular junction, each of the two cells produced a tensile force ($\vec{F}_1$), perpendicular to the cell-cell interface, which was sensed and equally opposed by the other ($\vec{F}_2$) (Figure 22A-2). To quantify the magnitude of these forces, we adapted the Traction Force Imbalance Method (TFIM), previously described in MDCK cell pairs, to our TFM analysis *(Maruthamuthu et al., 2011, Proceedings of the National Academy of Sciences)*. This method relies on the fact that contrary to a cell doublet, where all the forces are well balanced, the force imbalance across an individual cell of a pair is relatively high. As the cell is in mechanical equilibrium, this imbalance reflects the force produced at the cell-cell interface by its neighbor, and suggests that the two cells must

exert equal and opposite forces on each other. Moreover, because TFIM required defining the intercellular junction at every time point, we were able to simultaneously follow the angular velocity (ω) of doublets over the interval of rotation, which led to an interesting observation; the angular velocity varied negatively in CW-rotating doublets and positively in CCW-rotating ones (Figure 22A-3).

We first noticed that CCW-rotating doublets displayed higher levels of average stored ME compared to CW-rotating ones, which were found to rotate faster, consistent with what we previously observed on glass. These results suggested that doublets with higher contractility levels tend to rotate slower (Figure 22B-C-D). Indeed, we could see a tendency for a negative correlation between the magnitude of the stored ME and the angular velocity of rotation (Figure 22E). Like TFs, intercellular forces were also higher among CCW-rotating doublets, although the difference was not statistically significant (Figure 22F). Interestingly however, intercellular forces were scaling with the magnitude of doublet ME, which implied a strong correlation between forces transmitted at cell-cell contacts and those exerted by the cells on the ECM through focal adhesions (Figure 22G). Such a coordination in the mechanics at the cell-cell and cell-ECM contacts could be attributed to a direct physical link mediated by a common actomyosin structural framework. Moreover, as it was previously shown that the size of the cell-cell junction could be associated with the magnitude of the intercellular force, we quantified the junction length in rotating doublets *(Z. Liu et al., 2010, Proceedings of the National Academy of Sciences)*. Although CW doublets appeared to possess longer junctions (Figure 22H), we did not find any correlation between the junction length and the magnitude of the intercellular force (Figure 22I), which could be, in part, due to the dynamic remodeling of the junction during rotation that was not necessarily accompanied by variations in the intercellular force *(Maruthamuthu et al., 2011, Proceedings of the National Academy of Sciences)*.

The implementation of TFIM into our analysis enabled us to isolate the forces and, consequently, the stored ME, of individual cells of doublets along with their variations over time (Figure 23A). We noticed that all rotating doublets exhibited a certain degree of asymmetry in ME that was maintained over the interval of rotation, despite the variations in the magnitude of forces (Figure 23A). We defined ME asymmetry as being the absolute value of the difference between the mean ME of individual cells in a pair. As evident by the energy maps where all doublets were aligned such that the stronger cell is on the right and the weaker one is on the left, CCW-rotating doublets displayed greater ME asymmetry (Figure 23B-C). More interestingly, a positive correlation was found to exist between the magnitude of doublet ME and the asymmetry degree within doublets: a more contractile cell pair was also characterized by higher asymmetry (Figure 23D).

The increasing presence of asymmetry among CCW-rotating doublets, which also displayed higher ME hinted at the existence of a subpopulation of highly contractile cells, which when present in a pair favored the rotation in the CCW direction and enforced a

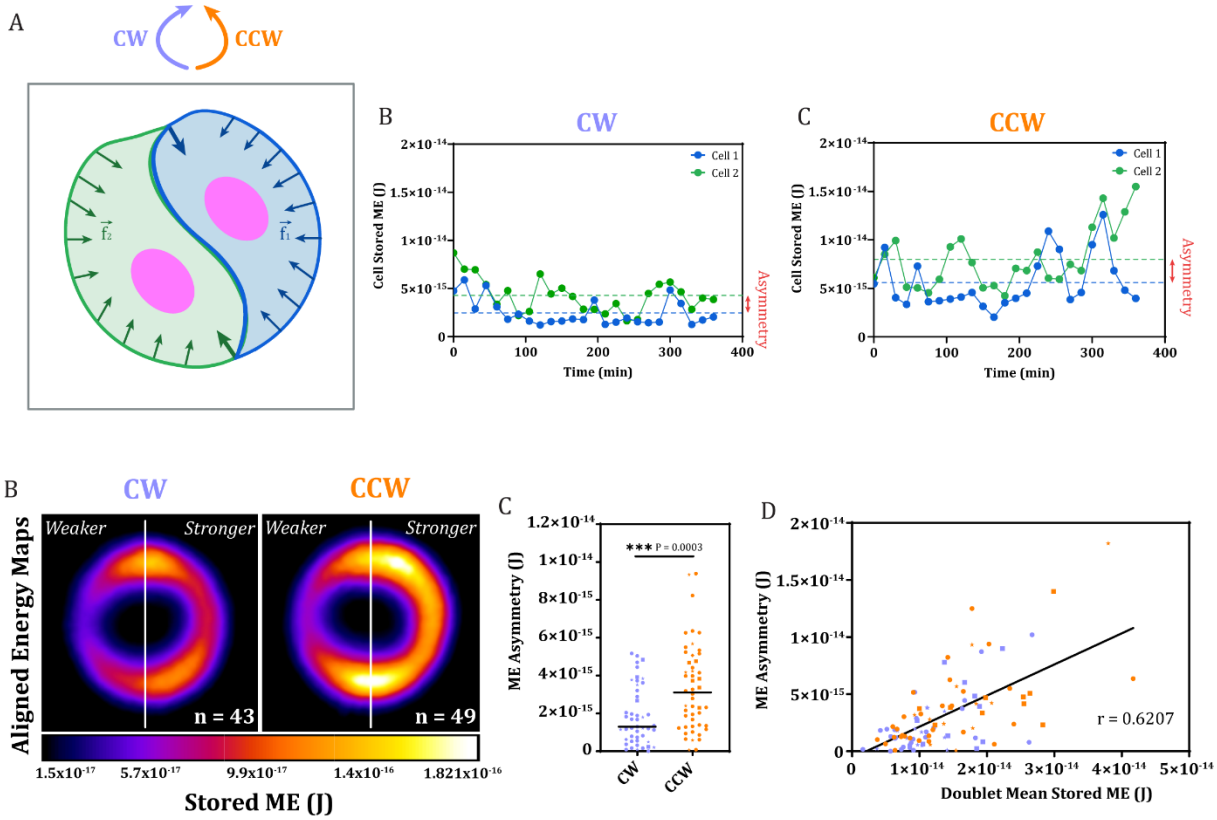

Figure 23: CW- and CCW-rotating doublets demonstrate a persistent ME asymmetry.

A: Schematic representation of the repartition of the traction forces within a doublet: $\overrightarrow{f1}$ and $\overrightarrow{f2}$ are the forces exerted by Cell1 and Cell2, respectively. To the right are graphs of the variation profile of the forces by Cell1 and Cell2 over time, as well as the asymmetry between the two cells computed by calculating the difference of the mean forces in CW- and CCW-rotating doublets.

B: Aligned Average Energy Maps obtained by aligning and averaging all the mean energy maps of CW and CCW doublets such that the cell with higher forces is on the right and that with lower forces is on the left.

C: Graph representing the stored ME asymmetry for CW- and CCW-rotating doublets. Statistical significance was assessed using unpaired t-test.

D: Scatter plot of the stored ME asymmetry as a function of doublet mean stored ME for rotating doublets. The Pearson Coefficient of correlation r is indicated on the graph.

Data was pooled from three independent experiments (N).

greater degree of asymmetry. To test this hypothesis, we first compared the frequency distribution as a function of stored ME of the entire cell population to that of the four existing subpopulations: CW-Weaker, CW-Stronger, CCW-Weaker, and CCW-Stronger (Figure 24B). Individual CW cells exhibited a comparable frequency distribution to that of the entire population consistent with the existent CW bias; the distribution of CW-

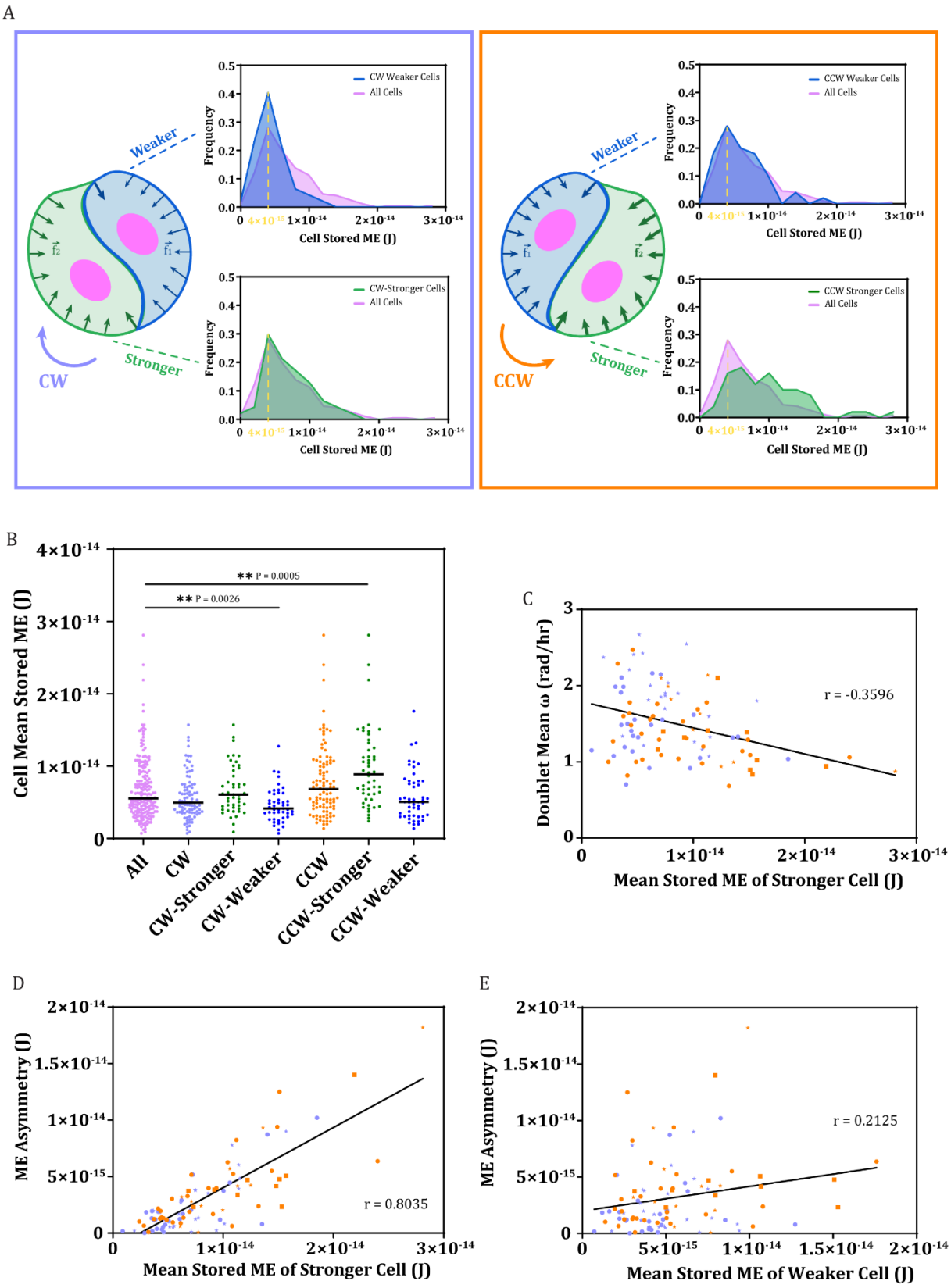

Figure 24: Stronger cells within doublets best describe the rotational phenotype. **A:** Schemes and graphs showing the frequency distribution of stronger and weaker individual cells in CW and CCW doublets relative to that of the entire cell population.

B: Graph showing the mean stored ME of all the cell subpopulations identified. The mean rank of each subpopulation is compared to that of the entire cell population. Statistical significance was assessed using a Kruskal-Wallis test.
C: Scatter plot of the doublet mean angular velocity ω as a function of the mean stored ME of the stronger cell. The Pearson Coefficient of correlation r is indicated on the graph.
D: Scatter plot of the ME asymmetry as a function of the mean stored ME of the stronger cell. The Pearson Coefficient of correlation r is indicated on the graph.
E: Scatter plot of the ME asymmetry as a function of the mean stored ME of the weaker cell. The Pearson Coefficient of correlation r is indicated on the graph.
Data was pooled from three independent experiments (N).

Weaker cells had fewer cells toward higher energy levels, yet it peaked at the same energy value as the entire population. Interestingly, whereas CCW-Weaker cells displayed the same frequency distribution as the entire population, that of CCW-stronger cells exhibited a shift toward higher energy levels. This, in addition to the fact that CCW-Stronger cells exhibited a significantly higher mean ME compared to the rest of the population (Figure 24B), further confirmed that these cells constituted a distinct subpopulation of less frequent, highly contractile cells, which could drive CCW rotation and lead to higher asymmetry within doublets. In the light of these results, we wanted to check whether ME asymmetry could be associated with the contractility levels of stronger cells in the population. Indeed, we noticed that the asymmetry was strongly scaling with the stored ME of stronger cells but not with that of weaker cells population (Figure 24D-E). Furthermore, stronger cells demonstrated the same negative correlation with the angular velocity of rotation as doublets population (Figure 24C).

Finally, as evident by the rotation probability diagram, the bias of doublets seemed to be strongly associated with the contractility levels of stronger cells population (Figure 25). Interestingly, to have the representative 60% CW bias at the level of the population, the stored ME of stronger cells should be around $4x10^{-15}$ J, which was the range at which the total population peaked in the frequency distribution. As the stronger cell ME increased, the probability of CW rotation gradually decreased whereas that of CCW rotation increased until it reached 100% at significantly high ME levels. The probability curves of CW and CCW rotation intersected at ME range around $7x10^{-15}$, where one could expect no bias at the level of the population. Therefore, our data suggests that individual stronger cells not only control the rotation of the doublets by limiting their speed, but also explain the asymmetry in ME and predict the bias at the level of the population.

Figure 25: The ME of stronger cells can predict the bias of the population.
Probability curves for the bias at the level of the population of rotating doublets as a function of the stored ME of the stronger cell, along with representative doublet schemes at the different regions of the curves. Probability for CW and CCW are represented in

purple and orange, respectively. The dashed yellow lines indicate the ME values of particularly interesting probabilities: 60% (cell population bias) and 50% (no bias).

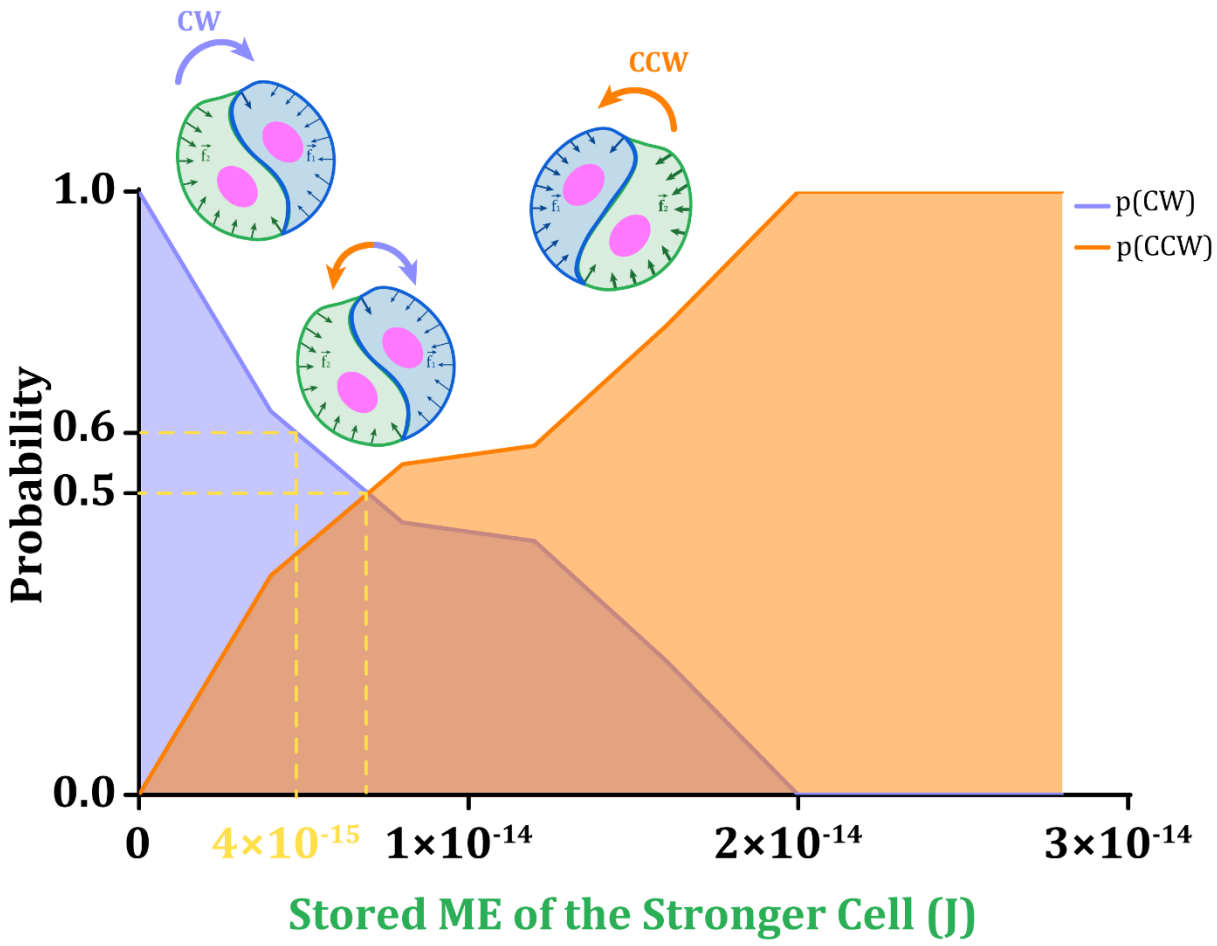

6. Characterization of the contractile machinery composition in swirling doublets

In an attempt to associate the observed differences in the elastic energy with the underlying biochemical composition of the contractile machinery of cells, we quantified, in both CW- and CCW-rotating doublets, the repartition of the main cytoskeletal proteins actively involved in force production and transmission (Figure 26A). We decided to focus our analysis on actomyosin ratio, defined as the ratio of phospho-myosin (p-MLC) to F-actin, as its levels were previously associated with optimum force production, as well as vinculin, a protein increasingly present in mature FAs *(Legerstee et al., 2019, Sci Rep; Kollimada et al., 2021, MBoC)*. At the level of doublets, the actomyosin ratio was slightly higher in the CCW subpopulation, indicating a higher potential for force production among these doublets, consistent with their previously reported higher ME (Figure 26B). Surprisingly however, CW-rotating doublets showed a higher vinculin adhesion intensity and area, which were previously shown to be strongly correlated with the magnitude of

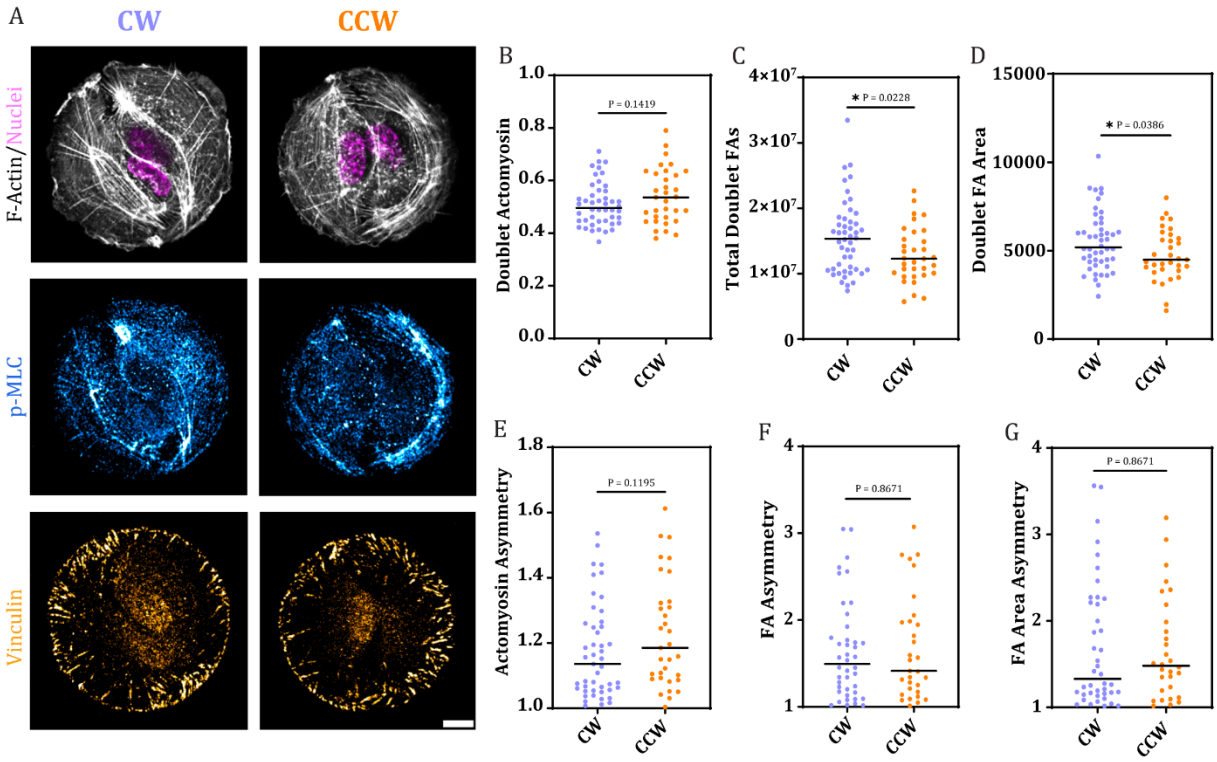

Figure 26: Characterization of the contractile machinery in swirling doublets.
A: Representative images of CW- and CCW-rotating doublets after a six-hour live movie, fixation, and staining for F-actin, Nuclei, p-MLC, and Vinculin. Scale Bar = 15µm.
B – C: Graphs representing the biochemical content (actomyosin ratio and total FA signal) as well as FA area quantified in CW- and CCW-rotating doublets. Statistical significance was assessed using unpaired t-test.
E – F: Graphs representing the asymmetry in biochemical content quantified in CW- and CCW-rotating doublets: actomyosin, FA intensity, and FA area ratio of the individual cells in rotating doublets. Statistical significance was assessed using unpaired t-test.

traction force in stationary cells (Figure 26C-D). As we could not get an accurate measurement of the individual FA size and number in these experiments, we cannot exclude that these differences were due to a higher number of smaller FA in CW-rotating doublets.

To obtain a readout of asymmetry, we computed the ratio of the contractile proteins in question between the individual cells of a pair. For that, the intercellular junction had to be manually defined in order to isolate the biochemical components of individual cells, similar to what was previously done in TFM analysis. Although there were no differences in vinculin intensity asymmetry between CW- and CCW-rotating doublets, we noticed that CCW-rotating doublets tend to have greater asymmetries in their actomyosin content and vinculin adhesion area (Figure 26E-F-G). These preliminary results implied that the differences in the magnitude and the asymmetry of ME previously reported could arise

from underlying variations at the level of contractile components, but further experiments would be required to confirm this outcome.

The lack of significant differences in the biochemical composition associated with force production could arise in part from the fact that the variations in forces recorded with TFM were inherently small in magnitude. On the other hand, our quantification relied mostly on the manual definition of the junction by the user, which might introduce some errors into the measurements. Thus, the immunofluorescence technique we used, along with the imaging resolution and analysis pipeline, might not be sensitive enough to detect and quantify such small differences. Moreover, our biochemical assay was missing certain proteins that might be actively involved in the modulation of doublet strain energy, such as α-actinin for example. Interestingly, a previous study reporting a correlation between protein content (F-Actin and p-MLC, and α-actinin) and the magnitude of traction forces, showed that the cells exhibited a huge deviation from the global fit, indicating the contribution of other, unassessed parameters to the production and transmission of contractile forces *(Kollimada et al., 2021, MBoC)*. In this context, several in vitro studies demonstrated that network contraction is largely dependent on the global architecture of the actin cytoskeleton, whose organization is governed by motors and crosslinkers *(Reymann et al., 2012, Science; Ennomani et al., 2016, Current Biology)*. Therefore, it would be best to directly couple TF measurement in CW- and CCW-rotating doublets and the quantification of the underlying biochemical components in the same doublets using the dedicated technique previously described *(Kollimada et al., 2021, MBoC)*. This would also allow the association of the previously described mechanical properties in the dominant cell with a particular composition of contractile proteins, which might help further explain its role in the emergence of chirality in doublets.

7. Cellular contractility levels can modulate the amount of rotation and the strength of the chiral bias in cell doublets

Our TFM results suggested that cellular contractility levels in the population could predict the rotational bias of HUVEC doublets and pointed at a key, predominant role for stronger cells within the doublets in driving the chiral motion. To challenge this hypothesis, we took advantage of different systems, in which variations in contractility levels were induced or already existent.

7.1. Chemical modulation of contractility

In our first attempt to address this hypothesis, we opted for the modulation of contractility by chemical drugs, which would allow us to assess the chiral bias in response to acute changes in contractility. To induce a low contractility regime within the cell population, we used the Rho-Kinase inhibitor (ROCKI) that was previously shown to block the phosphorylation of myosin light chain (MLC) by ROCKI and decrease the formation of stress fibers and focal adhesions (FAs) involved in force generation and transmission *(Chrzanowska-Wodnicka & Burridge, 1996, Journal of Cell Biology)*. Indeed, compared to the control, HUVEC doublets treated with 7μM of ROCKI demonstrated a decrease in p-

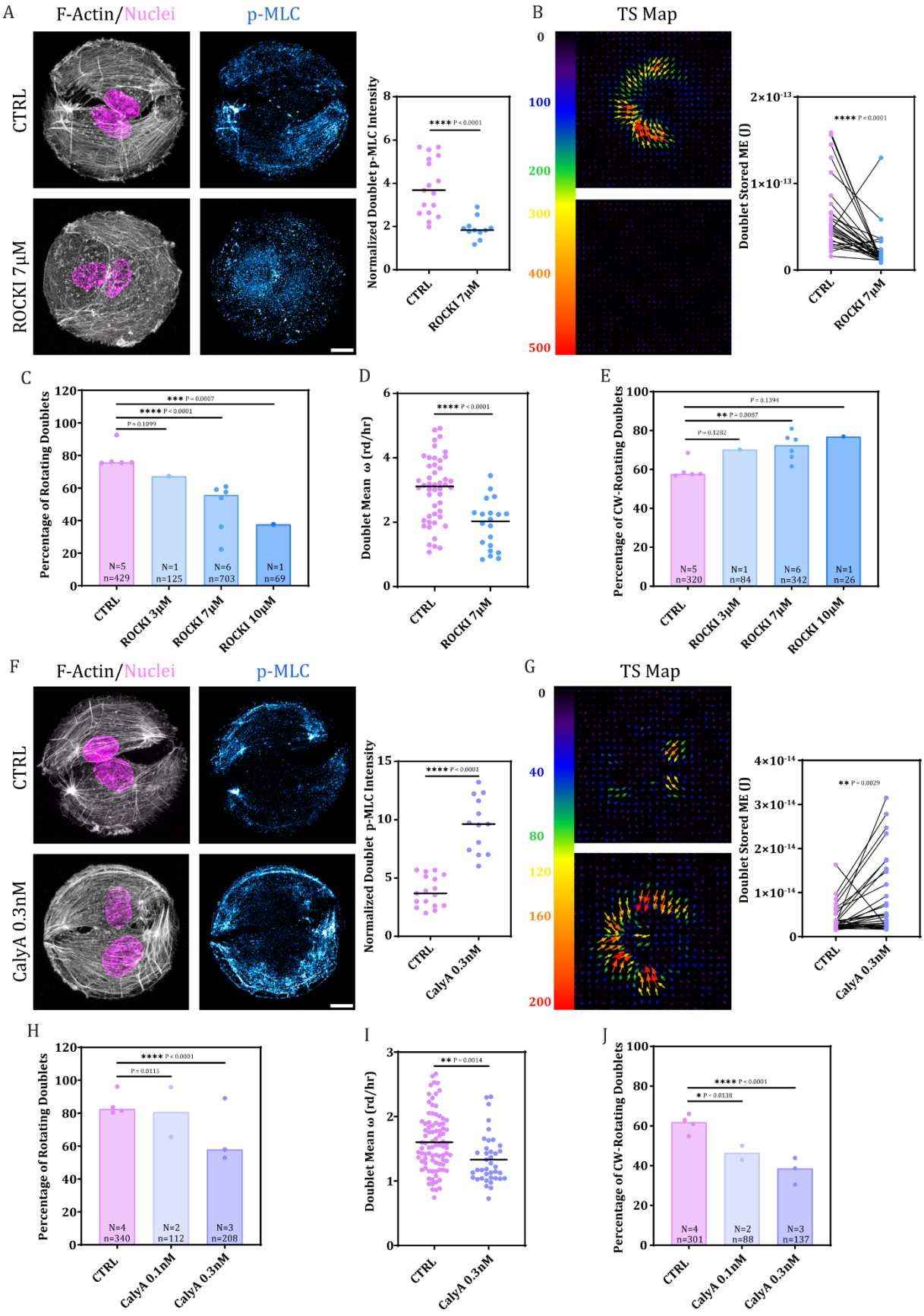
A
F-Actin/Nuclei
p-MLC
CTRL
ROCKI 7µM
Normalized Doublet p-MLC Intensity
**** P < 0.0001
CTRL
ROCKI 7µM
B
TS Map
0
100
200
300
400
500
Doublet Stored ME (J)
2×10-13
1×10-13
0
**** P < 0.0001
CTRL
ROCKI 7µM
C
Percentage of Rotating Doublets
*** P = 0.0007
**** P < 0.0001
P = 0.1099
N=5 n=429
N=1 n=125
N=6 n=703
N=1 n=69
CTRL
ROCKI 3µM
ROCKI 7µM
ROCKI 10µM
D
Doublet Mean ω (rd/hr)
**** P < 0.0001
CTRL
ROCKI 7µM
E
Percentage of CW-Rotating Doublets
P = 0.1394
** P = 0.0087
P = 0.1282
N=5 n=320
N=1 n=84
N=6 n=342
N=1 n=26
CTRL
ROCKI 3µM
ROCKI 7µM
ROCKI 10µM
F
F-Actin/Nuclei
p-MLC
CTRL
CalyA 0.3nM
Normalized Doublet p-MLC Intensity
**** P < 0.0001
CTRL
CalyA 0.3nM
G
TS Map
0
40
80
120
160
200
Doublet Stored ME (J)
4×10-14
3×10-14
2×10-14
1×10-14
0
** P = 0.0029
CTRL
CalyA 0.3nM
H
Percentage of Rotating Doublets
**** P < 0.0001
P = 0.0115
N=4 n=340
N=2 n=112
N=3 n=208
CTRL
CalyA 0.1nM
CalyA 0.3nM
I
Doublet Mean ω (rd/hr)
** P = 0.0014
CTRL
CalyA 0.3nM
J
Percentage of CW-Rotating Doublets
**** P < 0.0001
* P = 0.0138
N=4 n=301
N=2 n=88
N=3 n=137
CTRL
CalyA 0.1nM
CalyA 0.3nM

Figure 27: Chemical modulation of contractility: the chiral rotation of doublets in response to treatment with chemical drugs.
A: Representative images of control doublets and those treated with ROCKI (7µM). Six hours after the addition of the inhibitor, doublets were fixed and stained for F-actin, Nuclei, and p-MLC. To the right is the graph representing the p-MLC intensity, measured and normalized by fluorescent beads, in doublets of the CTRL and ROCKI-treated groups. Statistical significance was assessed using unpaired t-test. Scale Bar = 15µm.
B: To the left, examples of traction stress maps of the same cell before and after the treatment with ROCKI (7µM for 1hr). To the right is the graph representing the evolution of the ME after treating the doublets with ROCKI. Statistical significance was assessed using paired t-test.
C: Bar graph representing the quantification of the percentage of rotating doublets upon treatment with increasing ROCKI concentrations (3 – 7 – 10µM). Individual points on the graph represent independent experiments. Statistical significance was assessed using Chi-square (Fischer's exact) test.
D: Graph representing the measured mean angular velocity of rotating doublets. In the presence or absence of ROCKI (7µM). Statistical significance was assessed using unpaired t-test.
E: Bar graph representing the quantification of the percentage of CW-rotating doublets upon treatment with increasing ROCKI concentrations (3 – 7 – 10µM). Individual points on the graph represent independent experiments. Statistical significance was assessed using Chi-square (Fischer's exact) test.
F: Representative images of control doublets and those treated with CalyA (0.3nM). Six hours after the addition of the inhibitor, doublets were fixed and stained for F-actin, Nuclei, and p-MLC. To the right is the graph representing the p-MLC intensity, measured and normalized by fluorescent beads, in doublets of the CTRL and CalyA-treated groups. Statistical significance was assessed using unpaired t-test. Scale Bar = 15µm.
G: To the left, examples of traction stress maps of the same cell before and after the treatment with CalyA (0.3nM for 1hr). To the right is the graph representing the evolution of the ME after treating the doublets with CalyA. Statistical significance was assessed using paired t-test.
H: Bar graph representing the quantification of the percentage of rotating doublets upon treatment with increasing CalyA concentrations (0.1 – 0.3nM). Individual points on the graph represent independent experiments. Statistical significance was assessed using Chi-square (Fischer's exact) test.
I: Graph representing the measured mean angular velocity of rotating doublets. In the presence or absence of CalyA (0.3nM). Statistical significance was assessed using unpaired t-test.
J: Bar graph representing the quantification of the percentage of CW-rotating doublets upon treatment with increasing CalyA concentrations (0.1 – 0.3nM). Individual points on the graph represent independent experiments. Statistical significance was assessed using Chi-square (Fischer's exact) test.
N is the number of independent experiments performed; *n* is the total number of doublets analyzed.

MLC intensity, accompanied by fewer stress fibers and more prominent lamellipodia (Figure 27A). Moreover, TFM performed in the same doublets before and after the addition of ROCKI showed that treated cells experienced a significant decrease in their stored ME shortly after the administration of the drug, further supporting the efficiency of ROCKI in reducing contractility (Figure 27B). To decipher the effect of reduced contractility on the chiral phenotype, we treated the doublets with increasing ROCKI concentrations (3, 7, and 10μM) shortly after seeding them on micropatterns, and we followed their behavior over at least 8hrs, in the presence of a control. We first noticed a concentration-dependent decrease in the proportion of rotation among ROCKI-treated doublets, which, when rotating, exhibited a lower angular velocity compared to the control (Figure 27C-D). Additionally, the presence of increasing ROCKI concentrations led to a proportional increase in the prevalence of CW-rotating doublets, thereby enhancing the rightward bias existing in the population (Figure 27E).

On the other hand, a high contractility regime within the cell population was achieved through the use of Calyculin A (CalyA), a chemical drug previously shown to inhibit myosin-light-chain phosphatase from dephosphorylating myosin *(W. Y. Wang et al., 2019, Nat Commun)*. Consistently, CalyA triggered an increase in p-MLC intensity among treated doublets, which also exhibited more frequent and bigger stress fibers, as well as prominent contractile transverse arcs at the cell periphery (Figure 27F). In addition, as evident by the TFM data, the stored ME of doublets significantly increased shortly after the introduction of CalyA (Figure 27G). To identify the consequent evolution of the bias upon increasing contractility, HUVEC doublets on micropatterns were treated with two different CalyA concentrations (0.1 and 0.3nM) and followed over the course of several hours, in parallel to a control. Like ROCKI, CalyA treatment resulted in a reduced proportion of rotation among doublets, accompanied by a lower angular velocity among rotating ones (Figure 27H-I). Interestingly, the percentage of CCW-rotating doublets in the population gradually increased with increasing CalyA concentrations, leading to the cancellation of the bias at 0.1nM and its reversion to CCW at 0.3nM (Figure 27J).

Taken together, our results suggest that cellular contractility levels can determine the amount of rotation and the strength of the chiral bias. On one hand, we show that modulating contractility in both directions affects the ability of the cells to rotate, as both the proportion and the velocity of rotation are reduced. This result is consistent with previous studies showing that a biphasic relationship exists between migration speed, adhesion strength, and actin retrograde flow, with the maximal migration speed being achieved at intermediate adhesion strength, which is often associated with a relatively low retrograde flow *(Barnhart et al., 2011, PLOS Biology; Gupton & Waterman-Storer, 2006, Cell; Jurado et al., 2005, MBoC)*. However, we have previously reported, in our TFM data, that the angular velocity of rotation tends to be negatively correlated with the magnitude of TFs, which is tightly linked to adhesion strength. This could be because the PAA gels used for TFM had an intermediate rigidity (16.7kPa): soft enough to support the visualization of bead displacement but at the same time, stiff enough to ensure the maximal possible doublet rotation. Therefore, under such conditions, the cells were still able to exert the sufficient forces required to break symmetry and initiate rotation. In

other words, the magnitude of cellular contractile forces on PAA gels is higher than that achieved upon treating the cells with ROCKI, which effectively reduced the proportion and speed of rotation.

On the other hand, the differential effect of contractility modulation on the chiral bias confirmed our previous results and provided evidence supporting our initial hypothesis. By treating the cells with ROCKI, the entire population would be shifted toward low contractility levels; stronger cells would become less contractile and favor CW rotation of doublets, thereby enhancing the existent rightward bias. Conversely, CalyA treatment would cause the entire cell population to be shifted toward high levels of contractility; stronger cells would become more contractile and preferentially drive rotation in the CCW direction, thereby cancelling the bias and progressively enforcing a leftward bias in the cell population. Further confirmation of these results would require performing the TFM analysis previously described in the presence of the inhibitors (ROCKI and CalyA), which would allow us to identify the extent of the variations in cellular traction forces and assess the resulting changes in the population distribution as well as the accompanying evolution in the chiral bias.

7.2. Modulation of contractility through the cell cycle: Daughter Cell Doublets

It has been previously demonstrated that cells experience variations in TFs throughout the cell cycle, concomitant with changes in their area, volume, and DNA content. After mitosis, cellular TFs progressively increase during G1 to reach a maximum in S-phase and then slightly decrease toward the end of the cell cycle in the late S/G2 phase *(Panagiotakopoulou et al., 2018, MBoC; Vianay et al., 2018, Biology of the Cell)*. Knowing this, we wondered whether the chiral phenotype would be expressed in a population of doublets consisting of daughter cells after division. To address this question, we seeded HUVEC single cells on 60µm, FN-coated adhesive disks, allowed them to divide, and followed the behavior of the resulting daughter cells doublets over extended periods of time (Figure 28A-B). We noticed that these doublets broke symmetry very rapidly after division and initiated rotation that could persist for hours. Compared to a control of heterogeneous doublets, daughter cell doublets demonstrated a higher proportion of rotation that was statistically significant (Figure 28C). This can be attributed to the fact that in cells exiting mitosis, the Golgi adopts a compact configuration around the centrosome, reflecting a high degree of polarization, which is frequently associated with greater migration capacities, including higher migration speed and directional persistence *(Frye et al., 2020, Cells)*. Surprisingly however, unlike heterogeneous doublets, which were CW biased, daughter cell doublets did not display any directional bias at the level of the population (Figure 28D). Considering that the mitotic exit is marked by a gradual increase in cellular TFs that persists through G1 and S phase, the population of daughter cells is expected be shift toward higher contractility levels, where CCW rotation would be favored, thereby cancelling the bias. Confirmation of this hypothesis requires carrying out the previously described TFM analysis on daughter cells after cell division to validate the extent of increase in TFs and the associated changes in distribution and bias. Moreover, it would be interesting to treat the doublets resulting from cell division with

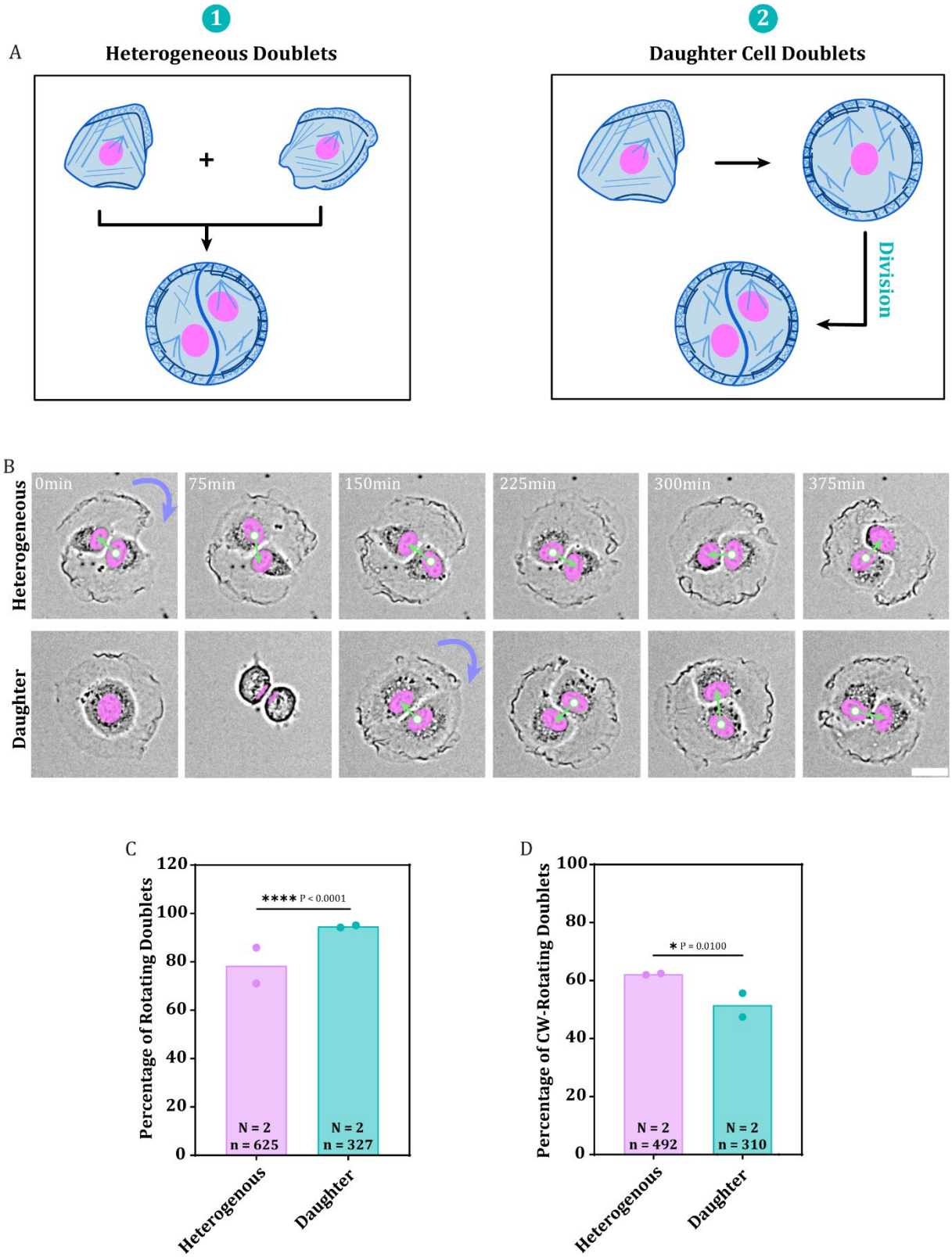

Figure 28: Modulation of contractility through the cell cycle: the chiral rotation in daughter cell doublets.

A: Schematic representation of the two compared doublet populations. In A-1, heterogeneous doublets are obtained by randomly seeding two cells on the same pattern. In A-2, daughter cell doublets result from the division of single cells already seeded on the

micropatterns. After cell seeding, the cells were imaged for extended periods of time (>48hrs).
B: On top, montage showing the rotation of a heterogeneous doublet. Below, is a montage of a single cells that divided, resulting in a rotating daughter cells doublet. The green arrows follow the direction of the nuclei displacement. The purple arrows indicate the direction of doublet rotation. Scale Bar = 15µm.
C: Bar graph representing the quantification of the percentage of rotating doublets composed of heterogeneous and daughter cells.
D: Bar graph representing the quantification of the percentage of CW-rotating doublets of rotating doublets composed of heterogeneous and daughter cells.
Individual points on the graph represent independent experiments.
Statistical significance was assessed using Chi-square (Fischer's exact) test.
N is the number of independent experiments performed; *n* is the total number of doublets analyzed.

---

both ROCKI and CalyA to see if decreasing or increasing contractility would recover a bias in the system in the CW or CCW direction, respectively.

7.3. Modulation of contractility within the doublet using different cell types: Heterotypic Doublets

Our results suggest that cells with higher contractility levels tend to rotate in the CCW direction, and contractility levels of stronger cells within the doublets can drive the rotation in one direction or the other, thereby determining the bias at the level of the population. To further challenge this hypothesis, we tried to introduce other cell types having different levels of contractility. Given their reported magnitudes of TFs, fibroblasts are believed to be more contractile than epithelial and endothelial cells *(Schwingel & Bastmeyer, 2013, PLoS One)*. Therefore, MEFs appeared as good candidates to test in our system. To confirm the differences in contractility levels, we started by simultaneously measuring the magnitude of TFs in HUVECs and MEFs. Subsequent TFM analysis revealed that the latter are indeed more contractile, with significantly higher stored ME as evident by the average energy maps (Figure 29A). Then, we independently seeded HUVECs and MEFs as doublets on 60µm, FN-coated disk-shaped micropatterns and followed their rotation over several hours (Figure 29B1-2-C). Compared to HUVECs, not only did MEF doublets exhibit a decreased proportion and speed of rotation, but also they were biased in the CCW direction, consistent with the fact that they were more contractile (Figure 29D-E-F). These encouraging results gave rise to the idea of creating a heterotypic system, in which doublets would be hybrids consisting of one HUVEC and one MEF cell. The fact that HUVECs and MEFs were biased in opposite directions would enable us to identify whose bias would predominate in the heterotypic system. We mixed the two cell populations at dilutions that would result in equal proportions of the two cell types in the final cell mixture used to seed the micropatterns (Figure 29B-3). To facilitate the identification of heterotypic doublets, we pre-labelled MEFs with Calcein-AM, which resulted in an initially bright and homogenous green signal in the cytoplasm progressively resolving into

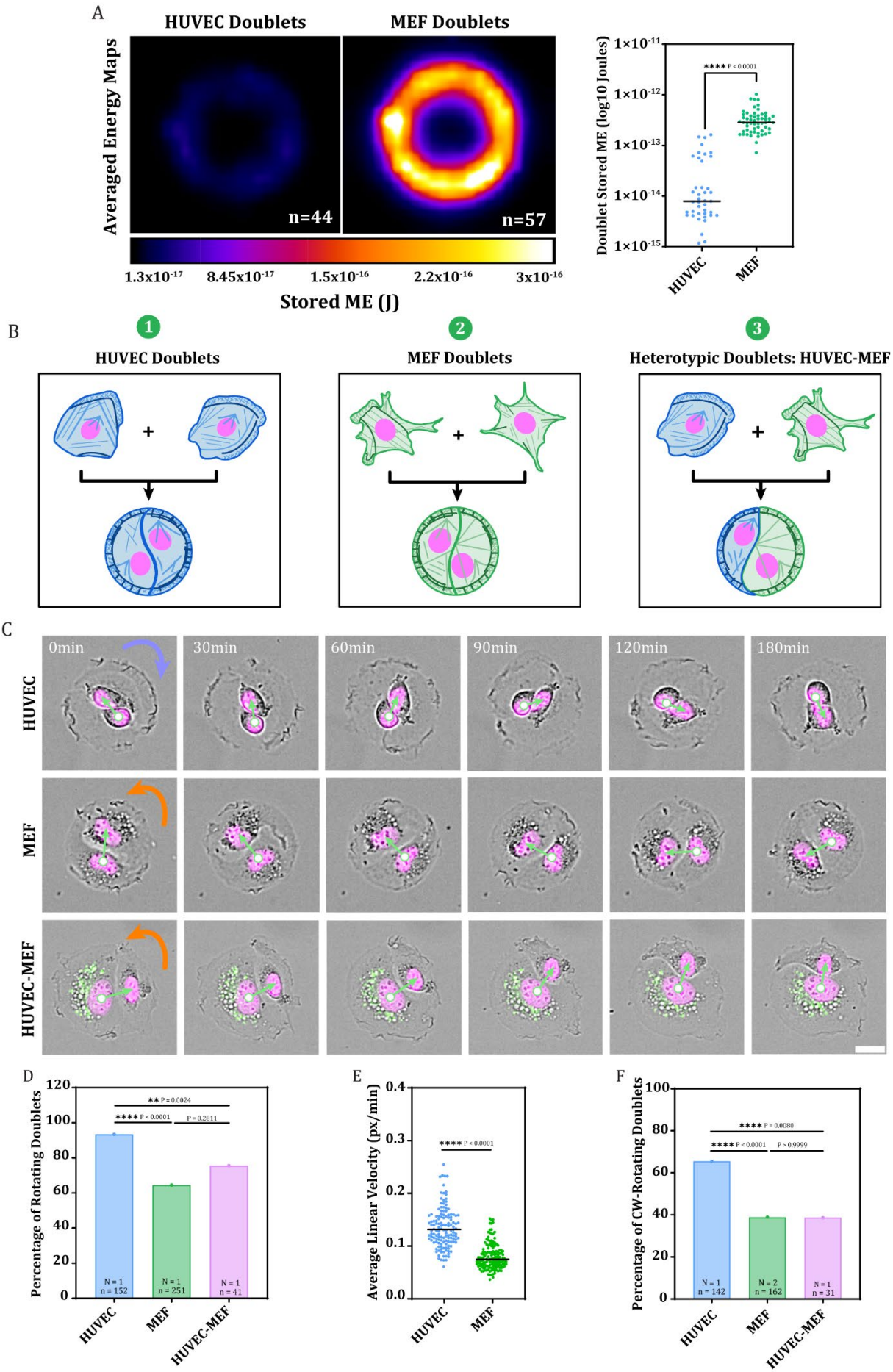
A
HUVEC Doublets
MEF Doublets
Averaged Energy Maps
n=44
n=57
1.3x10-17
8.45x10-17
1.5x10-16
2.2x10-16
3x10-16
Stored ME (J)
Doublet Stored ME (log10 Joules)
**** P < 0.0001
HUVEC
MEF
B
1
2
3
HUVEC Doublets
MEF Doublets
Heterotypic Doublets: HUVEC-MEF
C
0min
30min
60min
90min
120min
180min
HUVEC
MEF
HUVEC-MEF
D
Percentage of Rotating Doublets
** P = 0.0024
**** P < 0.0001
P = 0.2811
N = 1
n = 152
N = 1
n = 251
N = 1
n = 41
HUVEC
MEF
HUVEC-MEF
E
Average Linear Velocity (px/min)
**** P < 0.0001
HUVEC
MEF
F
Percentage of CW-Rotating Doublets
**** P = 0.0080
**** P < 0.0001
P > 0.9999
N = 1
n = 142
N = 2
n = 162
N = 1
n = 31
HUVEC
MEF
HUVEC-MEF

Figure 29: Modulation of contractility through the cell cycle: the chiral rotation in heterotypic doublets.
A: Average Energy Maps obtained by averaging all the energy maps of HUVEC and MEF doublets obtained after TFM analysis. To the right is a graph showing the quantification of the stored ME in HUVEC and MEF doublets in log10 scale. Statistical significance was assessed using unpaired t-test.
B: Schematic representation of the three compared doublet populations. In A-1, HUVEC cells are seeded on micropatterns to yield doublets. In A-2, MEF cells are seeded on micropatterns to yield doublets. In A-3, a HUVEC and MEF cells are mixed to yield a heterogeneous cell population that is then seeded on micropatterns resulting in heterotypic doublets.
C: Montage showing examples of rotating doublets from the three different populations (HUVEC doublets – MEF doublets – HUVEC-MEF doublets). In the heterotypic cell population, MEF cells were pre-labeled with Calcein-AM, which resulted in a green signal inside the MEF cells, thereby allowing their distinction within doublets. The cell nuclei were labelled with Hoechst shortly after seeding. The green arrows follow the direction of the nuclei displacement. Purple arrows indicate CW rotation; orange arrows indicate CCW rotation. Scale Bar = 15µm.
D: Bar graph representing the quantification of the percentage of rotating doublets in the three different populations. Individual points on the graph represent independent experiments. Statistical significance was assessed using Chi-square (Fischer's exact) test.
E: Graph showing the mean linear velocity (µm/min) measured for rotating HUVEC and MEF doublets. Statistical significance was assessed using unpaired t-test.
F: Bar graph representing the quantification of the percentage of CW-rotating doublets in the three different populations. Individual points on the graph represent independent experiments. Statistical significance was assessed using Chi-square (Fischer's exact) test.
N is the number of independent experiments performed; *n* is the total number of doublets analyzed.

dispersed granules in the cells *(Giaime et al., 2012, Mol Neurodegener)*. By monitoring the heterotypic doublets over several hours, we noticed that, contrary to HUVECs and MEFs, where the individual cells of doublets often occupied a comparable space on the micropattern, these doublets displayed a unique phenotype, in which MEFs occupied most of the space on the disk, whereas HUVECs were pushed to the periphery. The latter were also characterized by a greater motility degree, as in the majority of the cases, this system was characterized by a smaller HUVEC rotating around a larger, less motile MEF (Figure 29C). In comparison to HUVECs, heterotypic doublets exhibited reduced rotation that was CCW biased in line with the fact that the more contractile MEFs driving the motion were less prone to rotation and displayed a CCW chiral bias (Figure 29D-F). These results validate our initial hypothesis indicating that it is the more contractile cells within the doublets that govern the chiral rotation and, therefore, dictate the prevailing bias in the population.

Further challenging the validity and generality of our hypothesis would require testing the effect of contractility-modulating drugs on the bias of different cells types that could

be less or more contractile than HUVECs, as well as assessing the chirality in diverse combinations of heterotypic doublets.

VII.2. Chirality in the building blocks of a tissue: Individual Cells

We have described a chiral phenotype in a minimal tissue of a cell doublet demonstrated by a persistent biased rotation that is modulated and maintained by contractility. Our results point out that the chiral behavior of a doublet is dictated by a dominant cell, whose contractility levels set the rotational speed and bias. This supports the idea that individual cells are intrinsically chiral, despite the existing controversy about the way in which they display their chirality. In this context, we wondered about the possibility of identifying a chiral phenotype, comparable to that described in doublets, among single cells, as well as determining the minimal requirements associated with the expression of this phenotype.

1. Single HUVEC cells on disks only exhibit a transient, chiral nucleus swirling

We started our attempt of investigating the nature of the chiral phenotype among individual cells by seeding HUVECs as single cells on 60µm, FN-coated adhesive disks (Figure 30A). Monitoring their behavior over 12hrs or more, we first noticed that, unlike doublets, HUVEC singlets did not display a physical rotation on these micropatterns. However, a closer examination of the cell population led to the identification of a small proportion of individual cells (in average 30%) exhibiting nucleus swirling that was quantified to be CW-biased (Figure 30B-C). In fact, such a phenotype was previously described in fibroblasts and LatA-treated keratinocytes, and was shown to be associated with an underlying cytoskeletal swirling, particularly resulting from actin polymerization and crosslinking driven by certain actin-binding proteins, like formins and α-actinin *(Jalal et al., 2019a, Journal of Cell Science; Tee et al., 2015a, Nat Cell Biol; 2023, Nat Commun)*. Despite being chiral, this nucleus-actin swirling phenomenon was devoid of any aspect of cell migration, persisted for a short period of time, and eventually disappeared. It was therefore distinct from the chiral phenotype identified among HUVEC doublets, suggesting that the latter might be driven by a different mechanism.

We next tested the behavior of single cells on different sizes of micropatterns. Consequently, we seeded individual HUVEC cells on disk-shaped micropatterns of 37, 60, and 80µm diameters and assessed the consequences on the evolution of the chiral behavior. However, HUVEC singlets did not demonstrate a persistent, rotational phenomenon on either smaller (37µm) or larger (80µm) adhesive disks. Furthermore, the percentage of cells demonstrating nucleus swirling remained low on the three micropattern sizes, and, surprisingly, no changes in the CW bias were reported (Figure 30D-E).

Altogether, these results indicate that the chiral phenotype arising among single cells on adhesive disks is a static one, demonstrated by a transient nucleus-actin swirling.

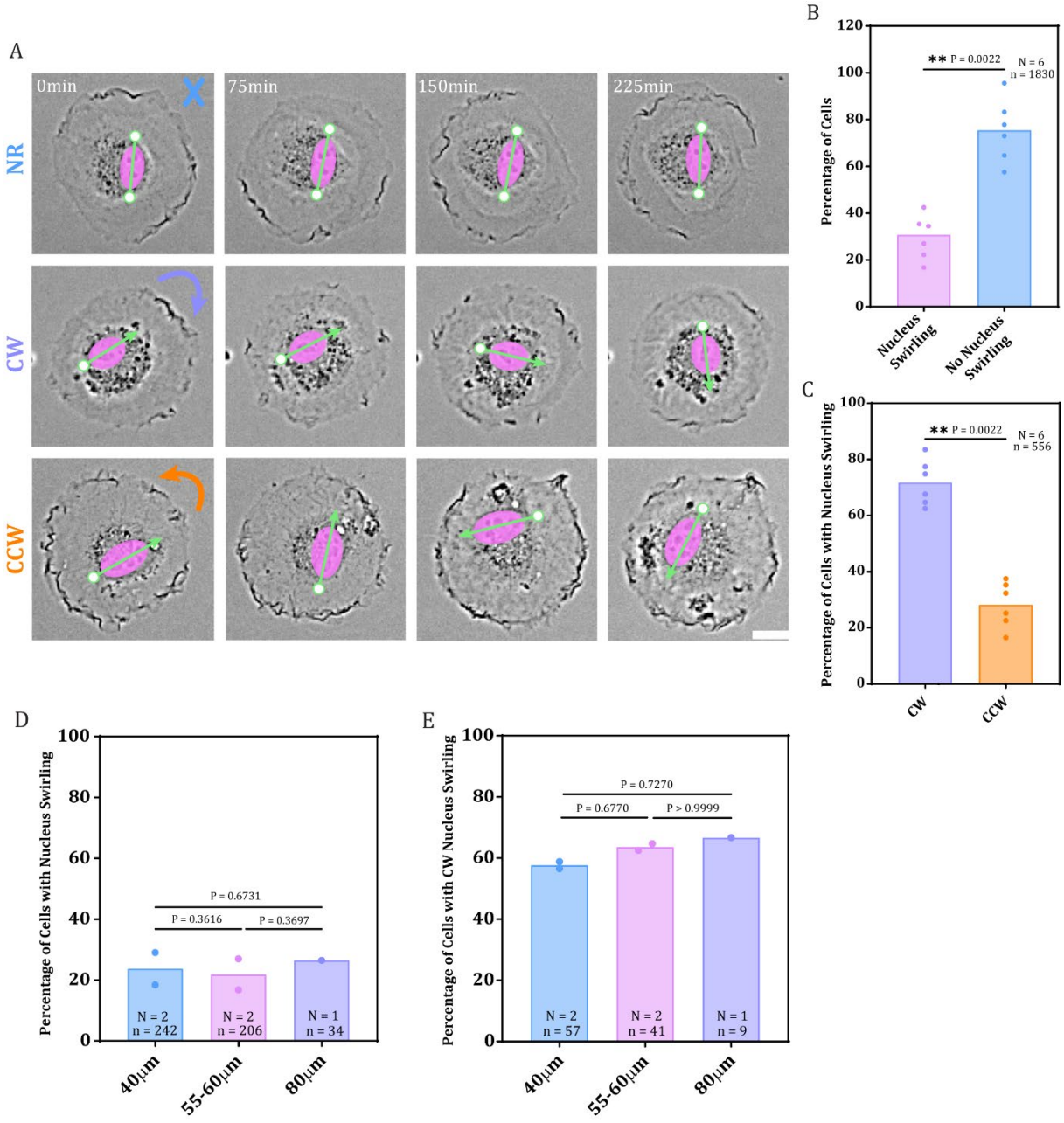

Figure 30: Single HUVEC cells on disks only exhibit a transient, chiral nucleus swirling.

A: Montage showing the different behaviors of HUVEC single cells on FN-coated, 60µm adhesive disks. The green lines with white circles at both edges indicate the absence of motion. The green lines with arrowheads at one edge follow the direction of nuclei displacement. The blue cross, purple arrow, and orange arrow mark non-, CW, and CCW-rotating doublets, respectively. Scale Bar = 15µm.

B: Bar graph representing the quantification of the percentage of single cells demonstrating nucleus swirling.

C: Bar graph representing the quantification of the percentage of single cells demonstrating CW and CCW nucleus swirling.

Individual points on the graphs represent independent experiments. Statistical significance was assessed using a Mann Whitney test for all the replicates.

D: Bar graph representing the quantification of the percentage of single cells demonstrating nucleus swirling on the different micropattern sizes tested (40 – 60 – 80μm).
E: Bar graph representing the quantification of the percentage of single cells demonstrating CW nucleus swirling on the different micropattern sizes tested (40 – 60 – 80μm).
N is the number of independent experiments performed; *n* is the total number of single cells analyzed. Individual points on the graph represent independent experiments. Statistical significance was assessed using Chi-square (Fischer's exact) test.

---

2. A modulation of the adhesive area geometry can trigger persistent rotation of individual HUVEC cells

We next tried different micropattern geometries that preserved the size and the curvature of the initial disk, two of which were of particular interest: a 60μm-diameter ring with a 5μm thickness and a 15μm diameter dot in its center (hereon referred to as a Ring+Dot) and a conventional 60μm-diameter ring with a 6μm thickness. In the former, the dot was intended to attract and fix the cell body with the nucleus, thereby facilitating cell spreading. On the other hand, the latter was equivalent to a 1D line, which represented a system in which cells were shown to display increasingly persistent and stable migration *(Pouthas et al., 2008, Journal of Cell Science; J. Zhang et al., 2014, Proceedings of the National Academy of Sciences)*. We believed that these two micropatterns could help the cells stably polarize and, thereby, facilitate their rotation initiation. Indeed, by seeding HUVEC single cells on these micropatterns and globally looking at their actin cytoskeleton, we could see a clear front-rear polarization, demonstrated by differential actin structural organizations: extended, ruffled lamellipodia at the cell front and a bright aster marking the cell rear, both of which could be regarded as characteristic features of migrating cells (Figure 31A-B). However, cells on the Ring+Dot tend to have a larger spread area compared to those on the Ring, where cell spreading was mostly restricted to the micropattern border. We then wondered whether such changes in cell polarization triggered by different geometries would be translated into distinct dynamic behaviors. To address this question, we plated single cells on the Ring+Dot and the Ring and monitored them over several hours (Figure 31A-B). We noticed that on these two micropatterns, more than 50% of the cells were able to initiate rotation that persisted for long periods of time (Figure 31C). In particular, a single cell rotating on the Ring+Dot adopted a configuration resembling that of an individual cell within a rotating doublet on the disk, whereas a cell rotating on the Ring mostly followed the border of the pattern. After that, we quantified the directionality of the rotational behavior on both micropatterns, and interestingly, the cells on the Ring+Dot demonstrated a rightward bias, similar to doublets on disks, with around 60% CW-rotating cells (Figure 31D). On the other hand, the bias among individual cells on rings was less clear, as the difference in the proportions of CW- and CCW-rotating cells was less significant, indicating that the cells tend to have no bias

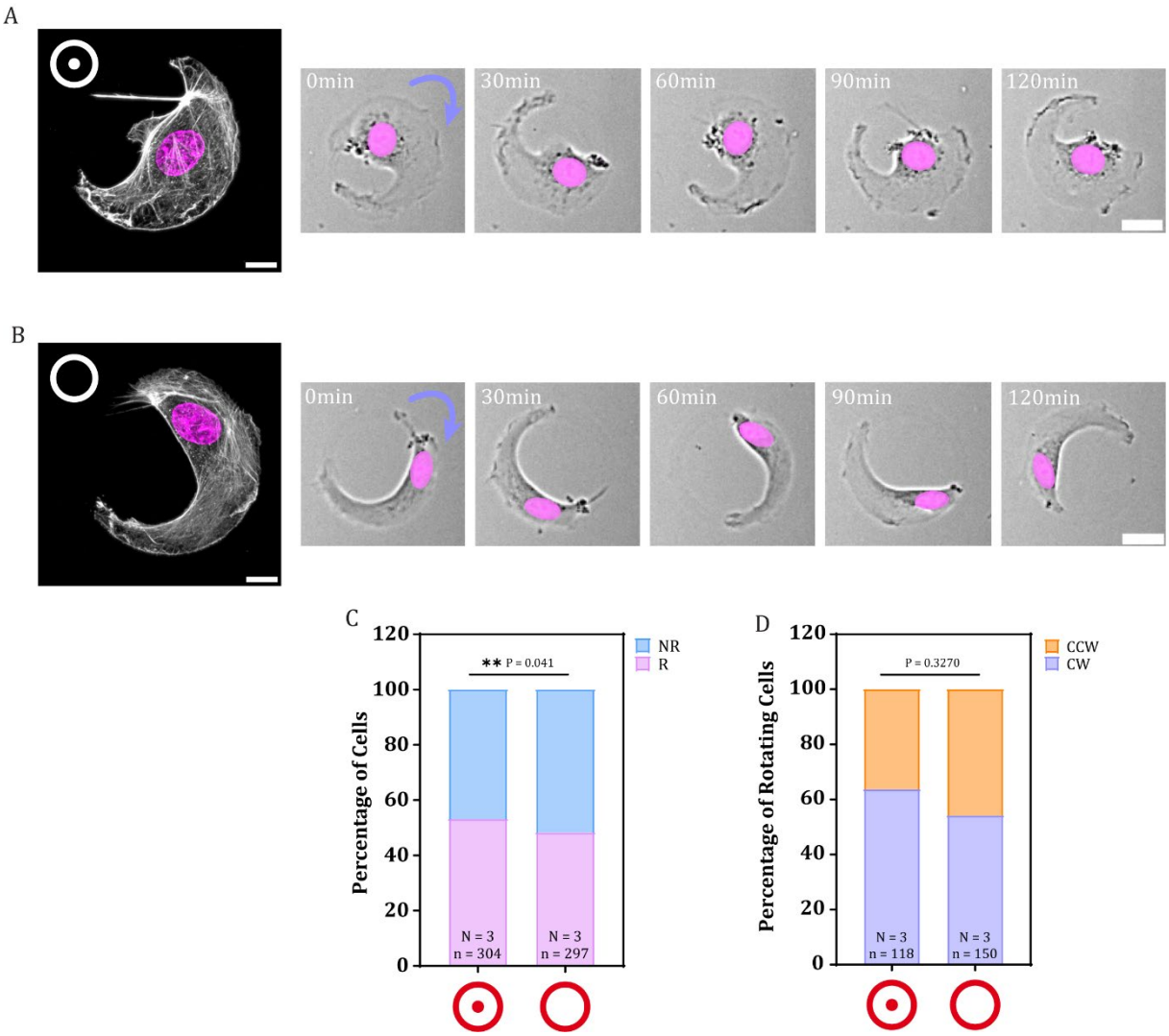

Figure 31: A modulation of the adhesive area geometry can trigger persistent rotation of individual HUVEC cells.
A – B: On the left, representative images of a single cells on Ring+Dot (A) and Ring (B). Cells were fixed and stained for F-actin and Nuclei six hours after seeding. Scale Bar = 10µm. To the right, a montage showing the rotation of single cells on Ring+Dot (A) and Ring (B). The purple arrow indicates the direction of rotation. Scale Bar = 15µm.
C: Bar graph representing the quantification of the percentage of rotating and non-rotating single cells on Ring+Dot and Ring.
D: Bar graph representing the quantification of the percentage of CW- and CCW-rotating single cells on Ring+Dot and Ring.
N is the number of independent experiments performed; *n* is the total number of single cells analyzed. Statistical significance was assessed using Chi-square (Fischer's exact) test.

on this micropattern (Figure 31D).

3. The chiral rotation of HUVEC singlets may be associated with a bias in polarity

As mentioned previously, cell rotation is a form of migration that is initiated after a symmetry break in the actin network, which gives rise to a protrusive leading edge represented by a lamellipodium and a contractile trailing edge enriched in stress fibers. The subsequent polarization of the microtubule network maintains the stability of the established polarity, thereby ensuring a higher persistence in migration. Overall, this will bias the vesicular transport machinery toward the cell front through the reorientation of the Nucleus – Centrosome – Golgi axis toward the direction of migration *(R. Li & Gundersen, 2008, Nat Rev Mol Cell Biol)*. In this context, we sought to characterize the polarization in HUVEC single cells and correlate it with the described biased rotation, using the Nucleus – Centrosome and Nucleus – Golgi axes, which were also frequently utilized to describe chirality in previous studies *(Fan et al., 2018, Science Advances; Wan et al., 2011, PNAS; H. Zhang et al., 2024, Science Advances)*. For this, we fixed single cells, on Ring+Dot and Ring, and labelled them for F-actin, nucleus, centrosome, and Golgi. As these cells were motile, their shapes as well as their positions on the micropattern were random, which made the comparison of the polarity between the cells, even those spread on the same micropattern, very difficult. To overcome this limitation, each cell was fit to a circle whose diameter represented the symmetry axis of the corresponding actin signal. Then, all the cells were rotated, in a way that their symmetry axes were aligned with the horizontal (Figure 32A-B). After that, the angles between the horizontal and the axes joining the centroid of the nucleus to that of either the centrosome or the Golgi were computed, such that angles lying to the right of the symmetry axis were negative, and those lying to the left were positive. Thus, cells were identified to be CW or CCW based on whether the angles of their axes with the horizontal were negative or positive, respectively (Figure 32A-B). We then used the computed angles to construct heat maps of the contours of all the cells aligned on the actin centroid, showing the distribution of the positions of the nucleus, centrosome, and the Golgi. In addition, by aligning all the cells on the nucleus centroid, we were able to obtain vector plots, in which all the vectors corresponding to the angles were represented together with the average polarity vector.

Figure 32: Schematic representation of the method used to quantify the polarity of rotating single cells on Ring+Dot and Ring.
A – B: Each cell (A – B to the left) was fit to a circle, whose diameter represented the symmetry axis of the F-actin signal. All the cells analyzed were rotated so that their symmetry axes (dashed line) were aligned with the horizontal (A – B to the right). The angles of the vectors joining the Nucleus – Centrosome and the Nucleus – Golgi with the horizontal (symmetry axis) were quantified, such that the angles lying to the right of the symmetry axis were negative (-180 > 0) indicative of CW chirality (polarity), whereas those lying to the left were positive (0 > 180), indicative of CCW chirality (polarity).

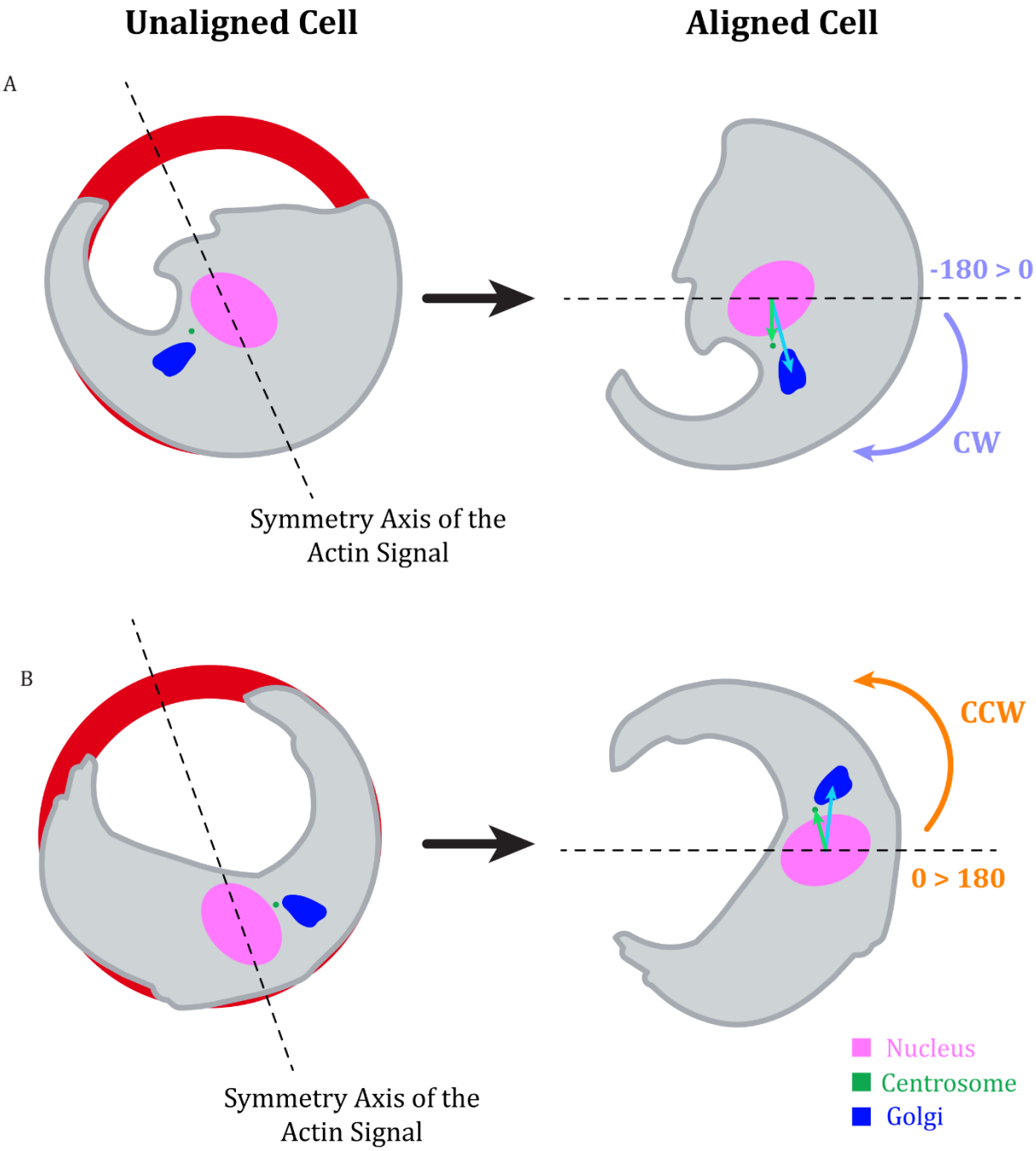

Finally, we tried to eliminate all the cells that were occupying more than half of the micropatterns, as well as those with no clear front-rear actin polarization, which most likely represented the non-rotating subpopulation of cells.

By looking at the heat maps and the vector plots of the cells on Ring+Dot and Ring (Figure 33A-B), we first noticed that although these cells were mostly displaying the expected front-back polarity, their polarity axes were not uniformly oriented toward the same direction. In addition, we could not see a clear LR bias among the cells. These observations could be attributed to several factors. First, despite eliminating all non-polarized cells that

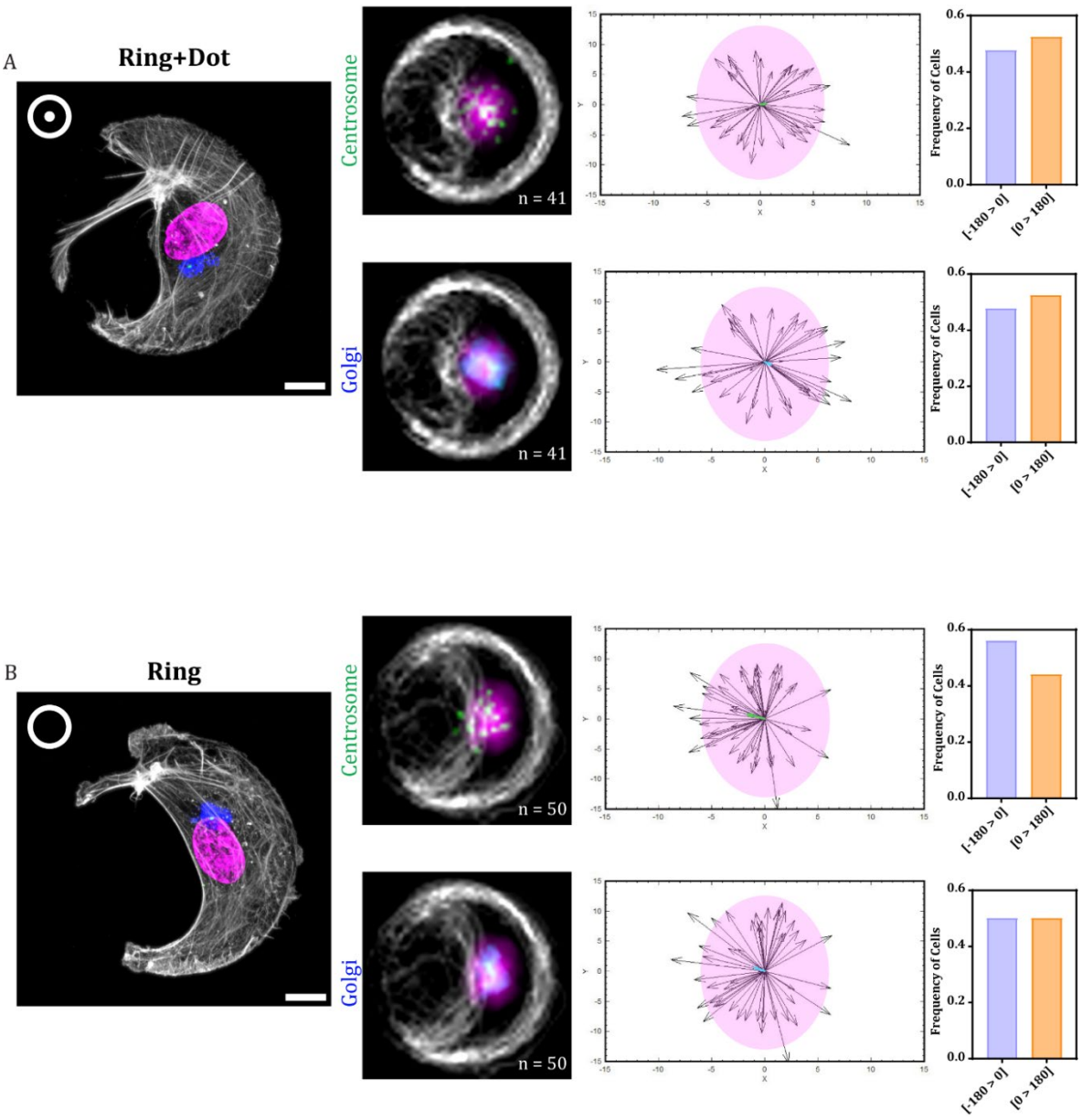

Figure 33: HUVEC singlets chiral rotation may be associated with a biased polarity.
A – B: Single cells on Ring+Dot and Ring were fixed and stained for F-actin, Nuclei, Centrosome, and Golgi six hours after seeding. From left to right:
Representative images of a single cells on Ring+Dot (A) and Ring (B). Scale Bar = 10µm. Heatmaps of the cells aligned on the centroid of the actin signal showing the distribution of the nuclei, centrosomes, and Golgi in the aligned contours of the cells on the corresponding micropattern.
Vector plots representing Nucleus – Centrosome and the Nucleus – Golgi vectors after aligning all the cells on the nucleus centroid; the green and blue vectors on the plots depict the average polarity vector (direction and magnitude) of the Nucleus – Centrosome and the Nucleus – Golgi vectors extracted for all the analyzed cells on the micropattern. Graphs representing the frequency of cells with negative (-180 > 0; CW) and positive (0 > 180; CCW) angles quantified using the Nucleus – Centrosome and the Nucleus – Golgi vectors – *Polarity Bias*. *n* is the total number of single cells analyzed.

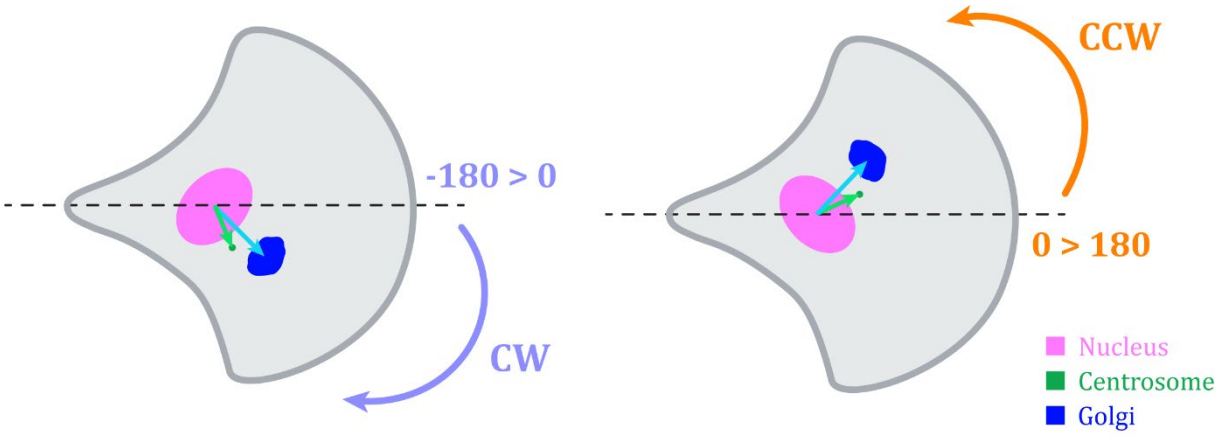

Figure 34: Schematic representation of the method used to quantify the polarity of static single cells on Crossbow, Ring+Dot, Half Ring+Dot, and Arc+Dot.
If needed, some of the cells analyzed were rotated so that their symmetry axes (dashed black line) were aligned with the horizontal (A – B to the right). The angles of the vectors joining the Nucleus – Centrosome and the Nucleus – Golgi with the horizontal (symmetry axis) were quantified, such that the angles lying to the right of the symmetry axis were negative (-180 > 0) indicative of CW chirality (polarity), whereas those lying to the left were positive (0 > 180), indicative of CCW chirality (polarity).

were assumed non-rotating, we could not be certain that all the cells included in the analysis were indeed rotating. Second, as the cells on these micropatterns were moving, they underwent dynamic shape changes associated with cell migration, which made their alignment and normalization more challenging. Third, it was previously demonstrated that the positioning of the Centrosome – Golgi to the front or the rear of migrating cells was strongly influenced by geometrical constraints, single cells persistently migrating on rings were characterized by a predominantly posterior Golgi position *(Pouthas et al., 2008, Journal of Cell Science)*. Indeed, we could see that in some cases the Nucleus – Centrosome and Nucleus – Golgi axes were oriented in a direction opposite to that of the actin polarization, which could bias our analysis. Therefore, it would be crucial to try to associate the direction of rotation and the orientation of the polarity vector in a more dynamic context, which would make possible the identification of the existing correlation between the two parameters in the cell populations on both the Ring+Dot and Ring and adjust the analysis accordingly.

4. Static, individual HUVECs do not display a chiral bias

The fact that a persistent chiral phenotype among single cells emerged only upon triggering rotation made us question the minimal requirements needed for the expression of chirality. Can a persistent chiral phenotype arise solely from the inherent chirality of cells? Alternatively, is motility a prerequisite for the manifestation of chirality?

The best way to address these questions would be by investigating the chirality of individual HUVEC cells on micropatterns with comparable geometries but different outcomes. To this end, we tested anisotropic static micropatterns on which the confined cells could polarize in the absence of motion. These micropatterns included the crossbow, serving as a control, as well as the Half-Ring+Dot, and Arc+Dot, designed so that the cells could adopt the same overall shape as those rotating on Ring+Dot.

As a readout for chirality among single static cells, we decided to check the bias in the orientation of the polarity axes (Nucleus – Centrosome and Nucleus – Golgi). Thus, we seeded single HUVECs on the designed micropatterns and waited for several hours to allow spreading and polarization, and then we fixed and labelled the cells for F-actin, nucleus, centrosome, and Golgi. The orientation of the axes was extracted in the same way previously described for the cells on rings (Figure 34). However, the static confinement of the cells, as well as the alignment of their symmetry axis with the horizontal, overrode the need for their rotation and facilitated their analysis including the computation and comparison of the angles and the associated vectors, as well as their representation. Similarly, cells were identified to be CW or CCW based on whether the angles of their axes with the horizontal were negative or positive, respectively. In the cells on crossbow, the anisotropy in the ECM induced the polarization of actin architecture into a polymerizing network at the adhesive edges and contractile stress fibers over non-adhesive edges. Consequently, the nuclei were off-centered toward non-adhesive edges, and the Nucleus – Centrosome and Nucleus – Golgi axes were oriented toward the adhesive area, showing no particular LR bias consistent with what was previously shown in RPE1 cells on crossbow (Figure 35A) *(Théry et al., 2006, Proceedings of the National Academy of Sciences)*. On the Half-Ring+Dot, and Arc+Dot, the cells indeed adopted the overall shape of rotating cells on Ring+Dot, but they could not move. Although the actin network polarization was similar to that described in cells on crossbow, with contractile stress fibers mostly enriched over non-adhesive edges, the internal polarization was different. In cells on Half-Ring+Dot, the nucleus was localized to or very close to the dot, and the Nucleus – Centrosome and Nucleus – Golgi axes were randomly oriented toward the adhesive area (Figure 35AB). On the other hand, the nucleus of the cells on the Arc+Dot was surprisingly off-centered away from the dot, toward the adhesive edges, and the Nucleus – Centrosome and Nucleus – Golgi axes were robustly polarized toward the dot (Figure 35C). Such a polarization phenotype was previously reported in MEFs confined on comparable U-shaped micropatterns *(Jimenez et al., 2021, Current Biology)*. These differences in polarization can be associated with the actin retrograde flow, which is often directed from the sites of adhesion toward non-adhesive edges with dense stress fibers. On distinct micropatterns, the associated confinement geometries, including the relative size of adhesive and non-adhesive areas, can often induce differences in actomyosin contractility, thereby modulating the retrograde flow direction and, consequently, the positioning of the nucleus, centrosome, and the Golgi *(T. Chen et al., 2019, Nat. Phys.; Théry et al., 2006, Cell Motility)*. Despite the existing differences in polarization, we could not

report an evident LR bias in the polarity axes on either of the micropatterns (Figure 35A-B-C).

Altogether, these results question the intrinsic nature of chirality in individual cells as manifested by their biased, transient nucleus – actin swirling and suggest that motility may be a pre-requisite for the emergence and the stable expression of chirality.

Figure 35: Static, individual HUVECs do not display a chiral bias.
A – C: Single cells on Crossbow, Half Ring+Dot, and Arc+Dot were fixed and stained for F-actin, Nuclei, Centrosome, and Golgi six hours after seeding. From left to right:
Representative images of a single cells on Crossbow (A), Half Ring+Dot (B), and Arc+Dot (C). Scale Bar = 10μm.
Heatmaps of the cells aligned on the centroid of the actin signal showing the distribution of the nuclei, centrosomes, and Golgi in the aligned contours of the cells on the corresponding micropattern.
Vector plots representing Nucleus – Centrosome and the Nucleus – Golgi vectors after aligning all the cells on the nucleus centroid; the green and blue vectors on the plots depict the average polarity vector (direction and magnitude) of the Nucleus – Centrosome and the Nucleus – Golgi vectors extracted for all the analyzed cells on the micropattern.
Graphs representing the frequency of cells with negative (-180 > 0; CW) and positive (0 > 180; CCW) angles quantified using the Nucleus – Centrosome and the Nucleus – Golgi vectors – *Polarity Bias*.
n is the total number of single cells analyzed.

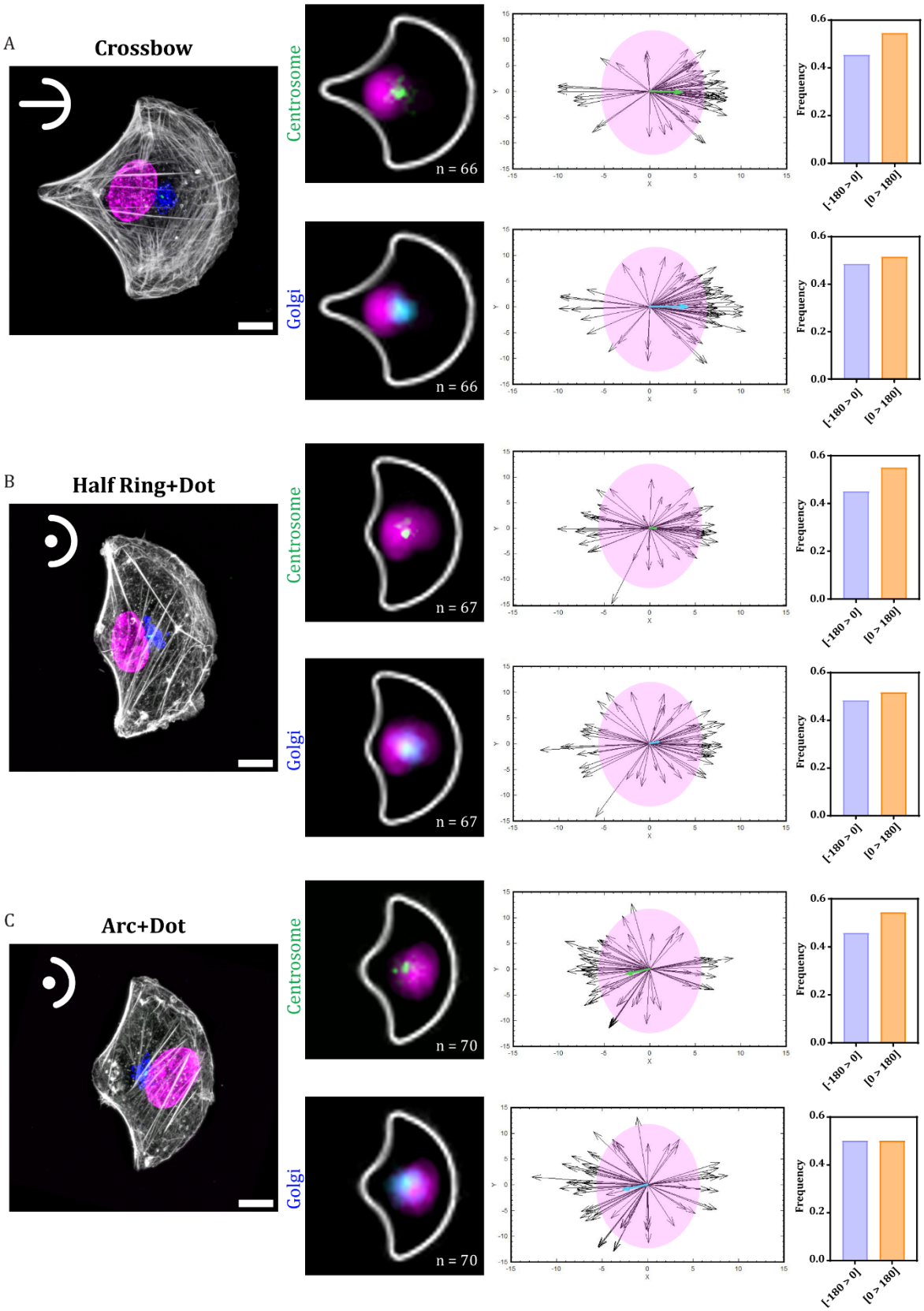
A
Crossbow
Centrosome
n = 66
Golgi
n = 66
B
Half Ring+Dot
Centrosome
n = 67
Golgi
n = 67
C
Arc+Dot
Centrosome
n = 70
Golgi
n = 70
Frequency
[-180 > 0]
[0 > 180]

VIII. CONCLUSION

Upon confinement on adhesive disks, cells of a pair spontaneously break symmetry and engage in a persistent chiral rotation characterized by a robust rightward bias, which is propagated and even amplified across increasing cellular complexity levels. Therefore, cell doublets constitute a simplified, yet powerful and reliable model for studying the mechanisms underlying the emergence, maintenance, and regulation of collective chiral behaviors.

The ability of the cells to polarize and initiate rotation is strongly dependent on the magnitude of their traction forces. Varying cellular contractility levels within the doublets in both directions is accompanied by a reduced rotation proportion and speed. This suggests the existence of a biphasic relationship, in which the maximum amount of rotation is mediated by an intermediate level of contractile forces designated as a force optimum (Figure 36A). The rotational behavior is best described by the more contractile cells of the pairs, which not only tend to limit the speed of motion, but also explain the existing force asymmetry within the doublets. In addition to being strongly correlated to the magnitude of the imposed asymmetry, the contractility levels of these dominant cells modulate the expression of the chiral phenotype of doublets, thereby predicting the directional bias prevailing at the level of the cell population (Figure 36B).

Single endothelial cells can also undergo a dynamic and persistent rotation on anisotropic micropatterns adapted to facilitate their front-rear polarization, which is required to initiate their directional motility. Consequently, the emergence of a rotational bias may be accompanied by a bias in the polarity axes that underlie initial symmetry breaking and migratory persistence (Figure 36C). Despite being largely polarized, individual cells confined on micropatterns that suppress their motion seem to lack a left-right preference (Figure 36D). We postulate that the stable expression of chirality potentially requires a motile background, which thereby challenges the intrinsic nature of cellular chirality.

Overall, our findings demonstrate that the balance of contractile forces within doublets plays a key role in driving the expression of a persistent, biased chiral phenotype. Furthermore, they point at a potential feedback between polarity and chirality emergence, in which motility appears to be a prerequisite.

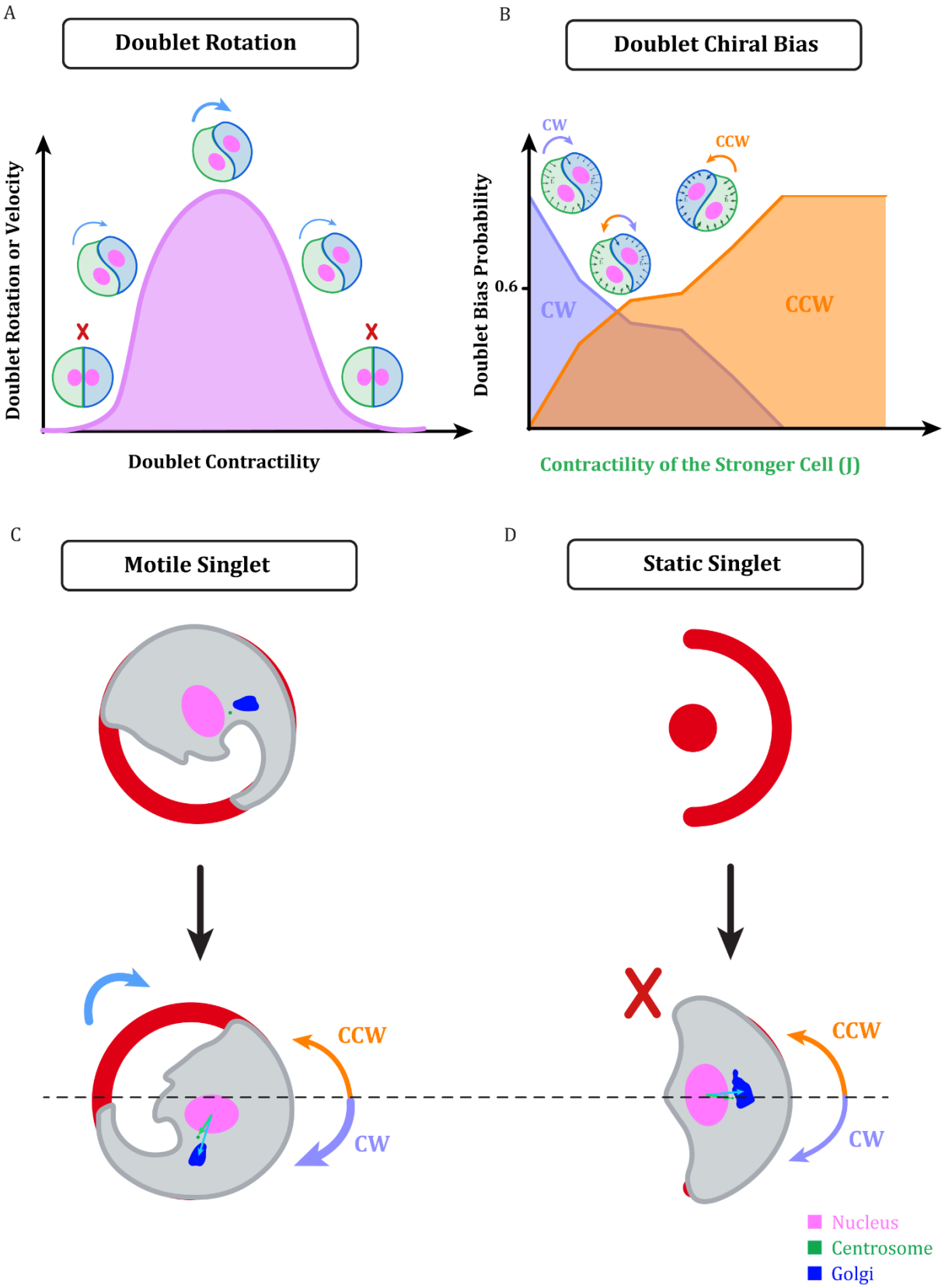
A
Doublet Rotation
Doublet Rotation or Velocity
Doublet Contractility
B
Doublet Chiral Bias
CW
CCW
Doublet Bias Probability
0.6
CW
CCW
Contractility of the Stronger Cell (J)
C
Motile Singlet
CCW
CW
D
Static Singlet
CCW
CW
Nucleus
Centrosome
Golgi

Figure 36: Conclusions about the characterized chiral phenotypes in HUVEC doublets and singlets.
A: Schematic representation of the variation in the percentage of doublets rotation and velocity as a function of increasing doublets contractility levels. The red cross indicates the absence of rotation at the corresponding regions on the curve. The variation in the thickness of the blue arrows reflects the amount of doublet rotation at the different regions of the curve.
B: Schematic representation of the evolution of the chiral bias in rotating doublets at the level of the cell population as a function of increasing contractility levels of the stronger cell. The schemes of the doublets on top of the graph reflect the magnitude of forces in the stronger and weaker cells within the doublets, as well as the directional bias of the population at the different regions of the curve. The red cross indicates the absence of rotation at the corresponding regions on the curve. The probability curves for CW and CCW rotation are represented in purple and orange, respectively. Purple arrows indicate CW rotation; orange arrows indicate CCW rotation.
C – D: Schematic representation of the expected polarity and chirality in motile (C) and static (D) single cells. The micropattern geometry appears in red. The expected organization of F-actin, as well as the positions of the nucleus, centrosome, and Golgi in the single cells spread on the motile and static micropatterns are represented, along with the corresponding directions of the Nucleus – Centrosome and the Nucleus – Golgi axes. The dashed balck line defines the symmetry axes of the cells. . The blue arrow defines the direction of rotation; the red cross reflects the absence of rotation. Purple arrows indicate CW rotation; orange arrows indicate CCW rotation. The bias of the cell population, defined by the rotation direction and polarity in (C) and by the orientation of polarity axes in (D), is reflected by the thickness of the purple and orange arrows in either case.

IX. LIMITATIONS

This section will be dedicated to describe and discuss some of the experimental and methodological limitations we encountered during our study.

1. Our model for the study of cellular chirality

Chirality is defined as a particular case of LR asymmetry, in which an object cannot be superimposed on its mirror image. Despite this universal definition, chirality has various demonstrations in different biological systems across scales. Our study focused, in part, on a minimal system of endothelial cell doublets, where chirality was manifested as a persistent biased rotation. The choice of this model was associated with several challenges.

First, to achieve this phenotype, cell doublets were plated on adhesive disk-shaped micropatterns, which not only provided a geometrical confinement equivalent to that described in tissues in vivo, but also normalized the initial cell adhesion state required to promote the reproducibility of LR symmetry break and chirality emergence. Such micropatterns also conferred a certain degree of curvature that could have influenced the organization of the cytoskeletal structures involved in this phenomenon, thereby biasing the outcome. However, when increasing the size of the micropatterns used, spread doublets exhibited not only a larger spread area but also a decreased curvature, and yet they demonstrated the same degree of rotation with the same chiral bias. This suggested that micropattern curvature was not significantly influencing the expression of the chiral phenotype in our system.

Second, in our analysis, the major readout for chirality relied on the manual identification of the rotation direction by the user, which in some cases could be subjective. We systematically tried to decrease the influence of inherent user bias on our outcomes through the analysis (blind or not) of the data generated from different experiments by two, three, or four independent users. In addition, tracking the displacement of the nuclei in some experiments provided a semi-automated quantification of doublet rotation and bias that confirmed our previous manual findings. Moreover, to avoid inconsistencies in the analysis and the interpretation of the results, we verified that the microscopes used for imaging throughout the study were not introducing variability in the definition of left and right.

Third, as symmetry breaking resulted in a rightward or leftward rotation, the bias identified here, like in all the other cell chirality studies, was based mainly on a difference in probability. Thus, the validation of the chiral bias was largely dependent on the statistical methods used to compare the proportions of the two co-existing chiral subpopulations. In our study, we identified a 60% CW bias among rotating endothelial cell doublets. Our statistical approach to validate this chiral bias relied on the use of proportion tests that could determine whether the reported percentages of CW and CCW were statistically significantly different from 50:50 (proportion (hypothesis) tests or Chi-

Square test). The reliable application of these tests required the use of relatively large cell populations consisting of at least 100 cells per experiment or condition. Individual control experiments were all subjected to these tests to confirm the reproducibility of the identified bias. In addition, the Chi-Square test was also used to compare the differences at the level of the chiral bias between two or more cell populations (control versus inhibitor-treated conditions for example). The fact that independent experiments performed and analyzed by different users, at different time intervals using different cell batches generated the same, statistically significant difference in proportions proved that the chiral bias detected in rotating endothelial doublets is robust and reliable.

A major parameter limiting chirality studies is the dependence of the chiral bias on the cell type: fibroblasts, myoblasts, and some cancer cell lines display a CCW bias, whereas most endothelial and epithelial cells possess a CW bias. This poses a great challenge for the identification of a general and universal mechanism for the emergence of chirality at the cellular level.

Finally, our study demonstrated a role for contractility in the emergence and the modulation of chirality in cell doublets. However, as the latter only constituted minimal systems of cell collectives, we could not exclude that the mechanisms highlighted here may be distinct from those driving the chiral phenotype in big ensembles or tissue monolayers.

2. The use of chemical inhibitors

Challenging the role of contractility in rotating doublets relied in part on the use of chemical drugs, which allowed us to assess the effect of rapid changes in contractility on doublet chirality. However, these drugs target certain kinases or phosphatases in particular signaling pathways and lead to a global decrease or increase in cellular contractility levels, whose efficiency may vary among the treated cells. Thus, despite showing that contractility levels can modulate the chiral bias in doublets, the implicated players and the interactions mediating the observed effect on the expression of the chiral phenotype remain to be elucidated. Further investigation may necessitate the use of more specific inhibitors or the development of knockouts or knock-ins targeting specific players in force generation and transmission. The latter can allow addressing the long-term effects of contractility modulation on the chiral bias. On the other hand, stable knockouts can favor certain compensatory mechanisms that can interfere with the outcomes. Finally, it is worth mentioning that depending on the concentration used, many of the chemical drugs may show off-target effects that can interfere with the results. For example, high concentrations of ROCKI can also inhibit myosin light chain kinase (MLCK) in addition to Rho kinase, which can lead to a more drastic decrease in contractility that may be associated with different effects on doublet rotation and chiral bias.

3. The TFM method and analysis pipeline

The mechanical characterization of doublet rotation mainly relied on the previously described TFM method, in which the bead displacement produced as rotating doublets

deform the underlying gel was used to quantify the associated forces *(Martiel et al., 2015, Methods in Cell Biology)*. Several sources of variability attributed to this method might affect its reproducibility, including the PAA gel. Despite using the same ratios of acrylamide and bis-acrylamide and the same bead dilution to prepare the TFM gels, certain parameters during the procedure could affect the resulting PAA gel rigidity and homogeneity, as well as the integrity and density of beads inside the gel. We partly addressed these limitations by using the stored ME, previously shown to be independent of gel rigidity, as our main mechanical output *(Oakes et al., 2014, Biophysical Journal)*.

In our TFM analysis, junction detection, which was later used for the quantification of the intercellular force and the isolation of the forces exerted by the individual cells in doublets, required manually defining the cell-cell interface by a line using the movies acquired in phase contrast. This manual detection could sometimes be challenging especially at the edges of the junction, where the front of one cell and the rear of the other overlapped and accounted for the highest magnitude of forces. We tried to facilitate junction detection by creating a heterogeneous cell population, composed of a 1:1 ratio of unlabeled and labeled (using Calcein-AM or cell Tracker) cells. We also considered using VE-Cadherin to identify the interface between the two cells, but HUVEC transfection was difficult and associated with relatively higher toxicity compared to other cell lines. Moreover, our immunofluorescence staining did not show a particular enrichment of VE-Cadherin all along the junction in our system of doublets, and thus, it might not have been of great help. Errors in junction definition would result in attributing forces to the wrong cell, which could give rise to errors in the associated force measurements. One control used to assess the quality of junction detection was the imbalance ratio of individual cells; because the doublet is in force equilibrium, the forces applied by each cell at the junction must be equal in magnitude and opposite in direction. Therefore, the imbalance ratios for individual cells of a doublet must be approximately equal. In addition, errors in the assignment of forces may also occur when one cell in a pair is much stronger than its partner. In this case, bead displacements originating from the stronger cell may be seen under the weaker one, and the resulting forces will be attributed to the wrong cell.

To quantify the magnitude of the intercellular forces, we used the TFIM, which was previously described for doublets of different cells types in different contexts (confined or not) *(Z. Liu et al., 2010, Proceedings of the National Academy of Sciences; Maruthamuthu et al., 2011, Proceedings of the National Academy of Sciences; Tseng et al., 2012, Proc. Natl. Acad. Sci. U.S.A.)*. In our system, similarly to Maruthamuthu et al., the junction was regarded as a line. Thus, all variations in area (2D) and height (3D) within the cell pair were neglected in the estimation of the forces at the intercellular junction, unlike previous studies where the junction domain represented the area of overlap between the two cells *(Heuzé et al., 2019, ELife; Z. Liu et al., 2010, Proceedings of the National Academy of Sciences)*.

X. DISCUSSION AND FUTURE PERSPECTIVES

1. The biased chiral phenotype in cell doublets

Our results demonstrated that, following symmetry breaking, endothelial cell doublets underwent a biased persistent chiral rotation, with about 60% CW-rotating cells. Despite being relatively small, this bias was robust and reproducible. Interestingly, none of the other cell types tested under the same conditions displayed an absolute bias in either direction, consistent with previous studies, which also reported the chiral bias among individual cells and collectives as a difference in probability between two co-existing subpopulations. Thus, what could be the advantage of such a non-uniform directional bias? Given that the expression of cellular chirality was shown to be in part dependent on external factors, having a non-absolute bias might permit the cells to adapt their chirality more easily in response to changes in the extracellular environment in order to maintain their proper functioning, thereby providing them with an overall fitness advantage. In the case of endothelial cells, changes in blood flow intensity or directionality may be potential triggers for chirality switches, although the actual contribution of blood flow to chirality development in blood vessels is still unclear *(George & Korolev, 2018, PLOS Computational Biology; H. Zhang et al., 2024, Science Advances)*.

2. Challenging the mechanism underlying contractility-driven modulation of cell chirality

2.1. An imbalance between two competing actin networks

In this study, we showed that, within a population of endothelial cells confined on adhesive disks, doublets rotating rightward and leftward exhibited different mechanics; CCW rotation was characterized by a higher ME as well as a lower angular velocity compared to CW. We also demonstrated that shifting the contractility levels using chemical inhibitors modulated the chiral bias of the doublet population: ROCKI enhanced the CW bias, whereas CalyA caused its reversion to CCW. Moreover, varying contractility in both directions was also accompanied by a reduction in the proportion and the speed of rotating doublets, suggesting that an intermediate magnitude of contractile forces was required to support persistent rotation: doublets with too low or too high TFs failed to break symmetry and initiate rotation. This can be attributed in part to the biphasic relationship existing between migration speed, adhesion strength, and actin retrograde flow, which suggests that the maximal migration velocity is associated with a force optimum characterized by an intermediate adhesion strength and a relatively low retrograde flow *(Barnhart et al., 2011, PLOS Biology; Gupton & Waterman-Storer, 2006, Cell; Jurado et al., 2005, MBoC)*. Given that, in our system, variations in rotation were coupled to changes at the level of the chiral bias suggested that the two mechanisms might be linked. In fact, the initiation of doublet rotation seems to be critical for the demonstration of the chiral phenotype, which indicated that the front-rear polarization established by the cells at rotation onset might bias the expression of chirality. One way to assess better the existence of a relationship between rotation and bias emergence or

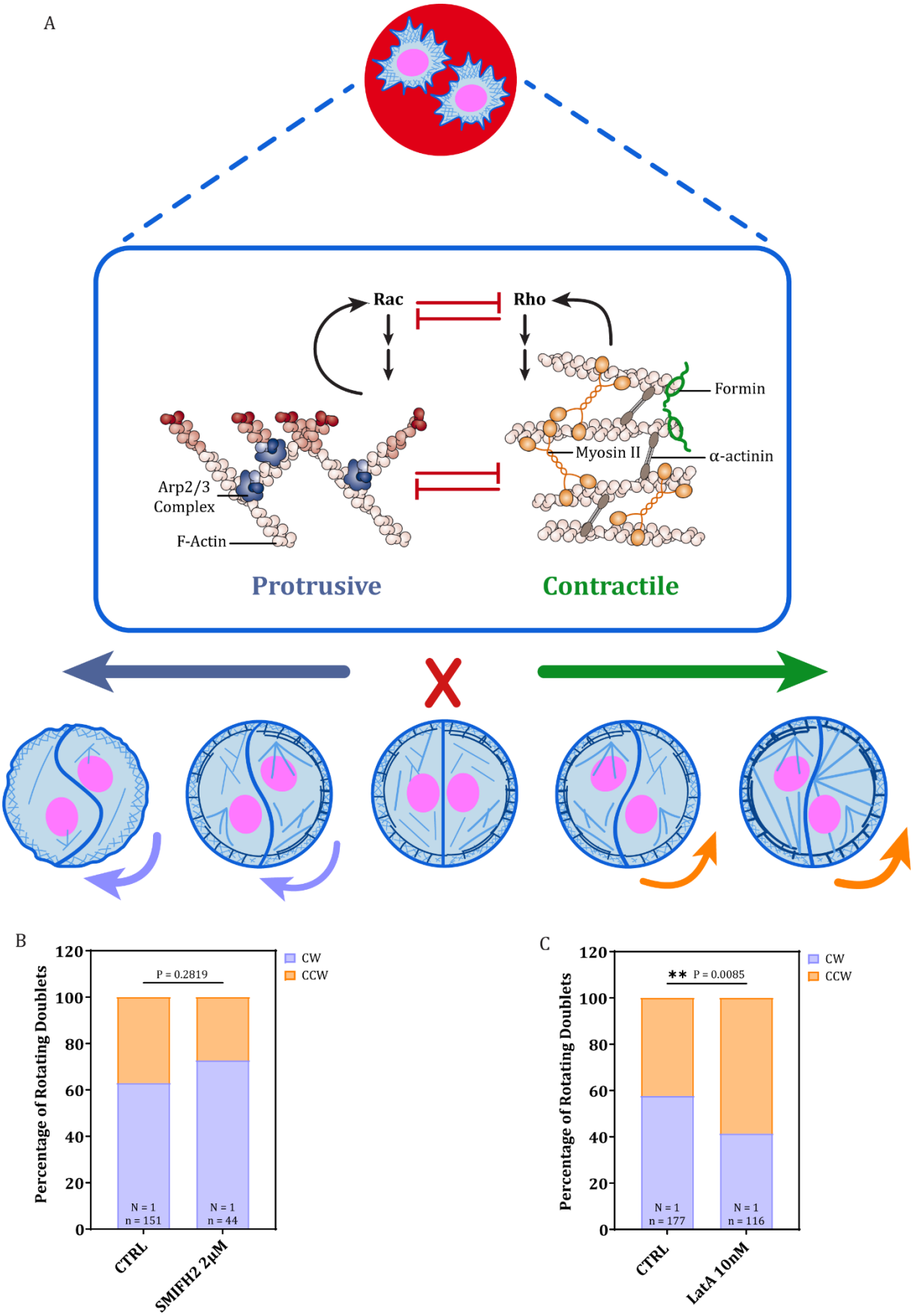
A
Rac
Rho
Formin
Myosin II
α-actinin
Arp2/3
Complex
F-Actin
Protrusive
Contractile
B
Percentage of Rotating Doublets
P = 0.2819
CW
CCW
N = 1
n = 151
N = 1
n = 44
CTRL
SMIFH2 2μM
C
Percentage of Rotating Doublets
** P = 0.0085
CW
CCW
N = 1
n = 177
N = 1
n = 116
CTRL
LatA 10nM

Figure 37: An imbalance between two competing actin networks breaks symmetry and initiate chiral rotation.
A: Schematic representation suggesting the dependence of the rotation and the chiral bias on the early events of cell spreading and actin organization. On top, two cells attaching and spreading on the micropattern. In the middle, an illustration of the mutual inhibitory interactions between protrusive and contractile actin structures regulated by the upstream signaling of Rac and Rho, respectively (Adapted from *(R. Li & Gundersen, 2008, Nat Rev Mol Cell Biol)*). On the bottom, the chiral phenotype may be governed by the dominating actin networks at the time of symmetry break and rotation initiation. The purple and green arrows depict the dominance of protrusive and contractile networks, respectively. The red cross indicates the absence of rotation. The purple and orange arrows indicate CW and CCW rotation, respectively. The thickness of the arrows reflects the prevalent bias.
B: Bar graph representing the quantification of the percentage of CW- and CCW-rotating doublets in the absence or presence of SMIFH2 2µM.
C: Bar graph representing the quantification of the percentage of CW- and CCW-rotating doublets in the absence or presence of LatA 10nM.
N is the number of independent experiments performed; *n* is the total number of doublets analyzed. Statistical significance was assessed using Chi-square (Fischer's exact) test.

modulation would be to quantify the evolution of the latter in response to fine variations in contractility. Treating doublets with ranges of ROCKI and CalyA concentrations would not only gradually modulate rotation amount and/or speed, but also help closely follow the shifts in the chiral bias arising from these variations.

In addition to the variations observed at the level of TFs, doublets treated with the aforementioned inhibitors displayed distinct actin network organizations in response to the prevalent contractility regime. Doublets with reduced contractility demonstrated prominent protrusions, which could be associated with the ability of ROCKI to inhibit formin-driven actin incorporation into stress fibers *(Nishimura et al., 2021, Cells & Development)*. By contrast, CalyA-treated doublets predominantly displayed intense, contractile stress fibers, along with the absence of prominent lamellipodia, an effect that could be attributed to the mechanosensitive nature of formin, which was shown to potentiate its activity in response to increased myosin-pulling forces *(Jégou et al., 2013, Nat Commun; Yu et al., 2017, Nat Commun; Vavylonis & Horan, 2017, Curr Biol; Zimmermann & Kovar, 2019, Current Opinion in Cell Biology; Alieva et al., 2019, Nat Commun)*. It seems that two distinct actin networks dominate doublet phenotype depending on the contractility regime: a dendritic network nucleated by Arp2/3 in case of ROCKI and a network based on MyoII-rich contractile structures polymerized by formin in case of CalyA. Interestingly, it is has been shown that these two networks are mutually exclusive at the structural level and compete for the same pool of actin monomers in yeasts and certain animal cells *(Burke et al., 2014, Current Biology; Henson et al., 2015, MBoC; Rotty et al., 2015, Developmental Cell; Suarez et al., 2015, Developmental Cell)*. In addition, they are regulated by two upstream Rho-GTPases that inhibit each other and

play critical roles in cell polarization: Rac induces Arp2/3-dependent actin polymerization and RhoA activates formin *(Sander et al., 1999, Journal of Cell Biology; Nimnual et al., 2003, Nat Cell Biol; Ridley, 2006, Trends in Cell Biology)*. Therefore, can contractility levels shift the balance between these two competing networks, so that one dominates, breaks symmetry and, subsequently, determines the chiral bias?

Along this line, it was demonstrated that treating predominantly immotile, circular epithelial cells with Blebbistatin could trigger front-rear polarization and the initiation of directional migration *(Lomakin et al., 2015, Nat Cell Biol)*. This was attributed to a potentiated Arp2/3 activity supported by the increased availability of actin monomers, previously sequestered by myosin in contractile, circumferential bundles, as well as the decreased actin polymerization by formin caused by reduced contractility. Therefore, within intermediate ranges of myosin activity, a protrusion emerged resulting from activated polymerization of branched actin networks that pushed the membrane forward, while the remaining actomyosin bundles accumulated in the cell rear. This suggests that shifting the balance to favor one of the two competing actin networks, in this case through contractility reduction, can induce symmetry break and front-rear polarization, leading to the initiation of directional rotation. Furthermore, it was shown that the imbalance between two classes of actin fibers could underlie the reversal of chiral actin swirling and nucleus rotation in cells confined on disk-shaped micropatterns *(Kwong et al., 2023, ELife)*.

In the light of all of these findings, it would be interesting to verify whether distinct dominating actin networks could lead to differences in the expression of the chiral phenotype at the level of rotating doublets (Figure 37A). Our preliminary results show that decreasing formin activity using SMIFH2, small molecule inhibitor of formin homology 2 domain *(Kim et al., 2015, PLOS ONE)*, at concentrations that do not interfere with myosin activity *(Nishimura et al., 2021, Journal of Cell Science)*, can enhance the CW bias among rotating doublets (Figure 37B). On the other hand, treating doublets with small doses of LatA, which favors actin depolymerization leading to increased availability of free G-actin monomers that can stimulate the activity of formins *(Fujiwara et al., 2018, Current Biology; Jalal et al., 2019b, Journal of Cell Science; Yarmola et al., 2000, Journal of Biological Chemistry)*, reverses the bias to CCW (Figure 37C). Thus, it appears that a polarized actin network dominated by formins during symmetry break favors CCW rotation; the absence of formins potentially increases the activity of Arp2/3, which takes over during initial symmetry breaking and polarization, leading to CW rotation (Figure 37A). Further confirmation would require the identification of the chiral bias in doublets upon reducing Arp2/3 activity (using CK-666 for example). In addition, it would be necessary to validate that the mechanism described here underlies contractility-driven modulation of the chiral bias. One way to do that is to vary the contractility levels while blocking one of the two actin nucleators, using drug combinations for example (CK-666 in parallel to ROCKI or SMIFH2 in parallel to CalyA) and check if the effect on the bias is preserved. Another possible, yet challenging, way is to demonstrate the dominance of one

network over the other in response to changes in contractility by closely assessing the corresponding repartition of the two competing networks using immunofluorescence.

2.2. The interplay between network connectivity and contraction

An interesting study investigating the crosstalk between MyoII and formin in TF generation and transmission in fibroblasts revealed that SMIFH2-induced formin inhibition not only blocked actin incorporation into stress fibers, but also decreased TFs in a MyoII-independent manner *(Nishimura et al., 2021, Cells & Development)*. The rescue of this drop by the overexpression of α-actinin suggested that SMIFH2-driven decrease in TFs was probably due to reduced network connectivity, thereby pointing at a key role for formins in force transmission by acting as actin cross-linkers *(Esue et al., 2008, Journal of Molecular Biology; Jaiswal et al., 2013, Current Biology; Nishimura et al., 2021, Cells & Development)*. In fact, it has been previously shown that the contractile ability of different actomyosin structures in vitro is governed by two interrelated parameters: the degree of network connectivity determined by the amount of connectors present, as well as actin network organization that affects the spatial distribution of the available cross-linkers. This results in a biphasic response as a function of connectivity, where optimal force production is achieved at an intermediate level of connectivity for different actin architectures *(Bendix et al., 2008, Biophysical Journal; Alvarado et al., 2013, Nature Phys; Ennomani et al., 2016, Current Biology)*. Accordingly, the major actin cross-linker α-actinin has been reported to play a key role in the regulation of TFs, as well as in the ability of cells to translate spatial cues and anisotropies provided by the extracellular environment into an integrated cellular response, represented by the establishment of internal symmetry and the initiation of directional migration *(Oakes et al., 2012, Journal of Cell Biology; Senger et al., 2019, Journal of Cell Science)*. Interestingly, in addition to the effect its movement along growing actin filaments has on the chiral swirling *(X. Li & Chen, 2021, Journal of Applied Mechanics)*, the overexpression of α-actinin has been associated with the reversal of biased actin cytoskeletal swirling in single cells *(Tee et al., 2015b, Nat Cell Biol; 2023, Nat Commun)*, alignment of cell collectives on rectangles in 2D *(Tee et al., 2023, Nat Commun)*, and collective rotation in 3D *(Chin et al., 2018, Proc. Natl. Acad. Sci. U.S.A.)*. Knowing that the knockdown of α-actinin is often associated with higher TFs and its overexpression with increased frictional constraints that limit filament rotation leading to a more rigid network and reduced overall force transmission, it would be interesting and relevant to assess the implication of α-actinin in the biased rotation of doublets in our system.

Consequently, applying the previously described technique to couple TFM and biochemical content measurements in cells would enable the quantification of the repartition of interesting proteins (F-actin, p-MLC, vinculin, Arp2/3, α-actinin) in parallel to the recorded TFs in CW, CCW-, and non-rotating doublets (Figure 38) *(Kollimada et al., 2021, MBoC)*.

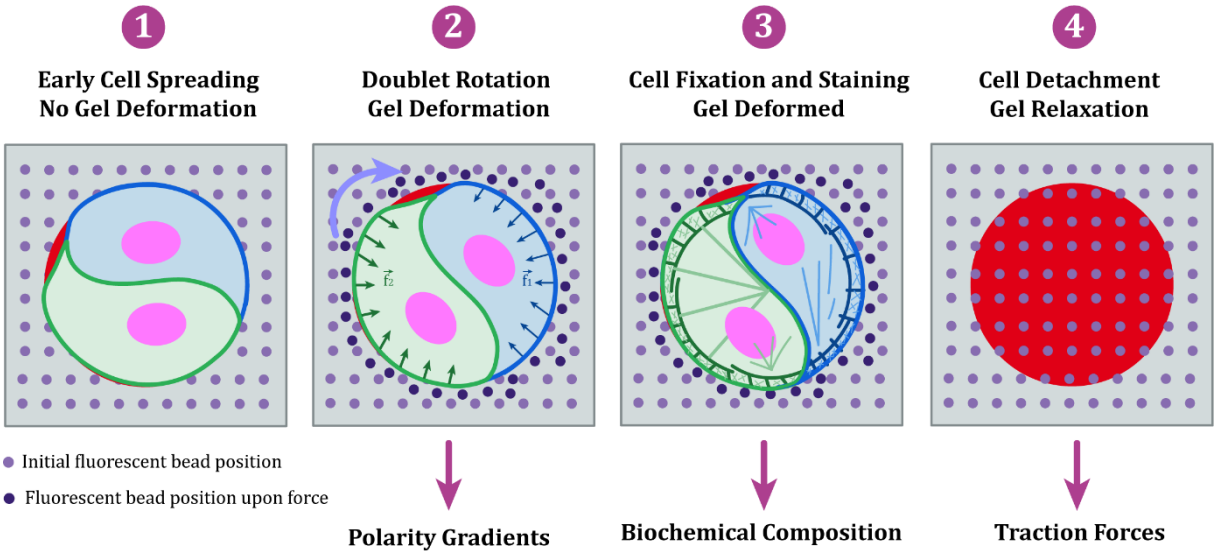

Figure 38: Coupling the measurements of contractile forces to the biochemical composition and organization of the actomyosin cytoskeleton.
Scheme illustrating the sequential steps of the modified TFM assay that enables coupling force measurements to the evolution of polarity gradients and/or the quantification of the biochemical content of the doublets. Within the doublet, the cell in green is the stronger, dominant cell; the weaker cell is in blue.

2.3. In vitro reconstituted systems: Towards a better understanding of chirality emergence at the molecular level

A better understanding of the mechanisms underlying the emergence of chirality in cellular systems, including ours, as well as its molecular origin nictitates the simplification of the involved parameters. In this context, in vitro reconstituted systems, which use controlled mixtures of defined proteins, seem to be the most promising approach, especially with the recent technological advances that have introduced the concept of lipid micropatterning, in which actin structures are grown from and interact with membrane-like systems, and cell-sized microwells *(Reymann et al., 2010, Nature Mater; 2012, Science; Ennomani et al., 2016, Current Biology)*. Using these reconstituted systems would help impose 2D or 3D boundaries to the experimental setups, thereby providing a more "physiological" context to assess closely the mechanisms driving different cellular phenomena, including chirality.

Both formins and myosins have been shown to trigger the chiral motion of single actin filaments in vitro *(Mizuno et al., 2011, Science; Pyrpassopoulos et al., 2012, Current Biology; Mizuno et al., 2018, Proceedings of the National Academy of Sciences; Lebreton et al., 2018, Science; Y. Sato et al., 2023, Sci Rep)*. However, whether their individual and/or combined activities can actually drive the emergence of the "macroscopic" chiral actin self-organization or motility described by the different numerical simulations remains unknown and undemonstrated experimentally. To address this question, we could take

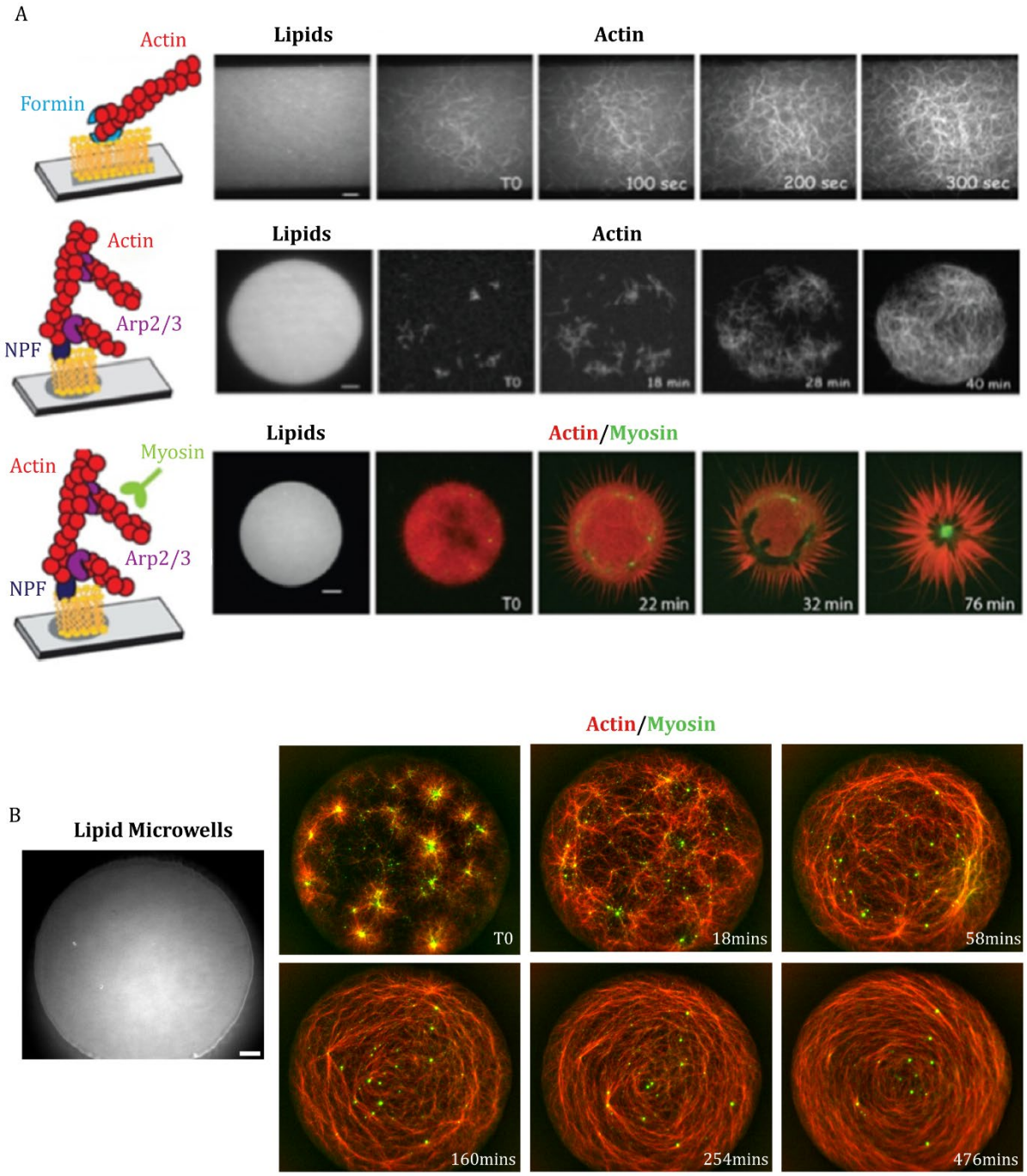

Figure 39: Reconstituted systems can be used to investigate the molecular origin of chirality.
A: Myosin-induced self-organization of actin network generated by formin or the Arp2/3 complex grafted on supported lipid bilayers. Data adapted from *Christophe Guerin*.
B: Myosin-induced contraction of Arp2/3-generated actin network inside lipid microwells (Scale Bar = 10µm). Data adapted from *Alfredo Sciortino*.

advantage of some previously established actin-based reconstituted systems that can effectively reproduce a variety of actin structures and associated phenomena.

It has been demonstrated that actin network architecture and connectivity largely govern myosin motor activity and global network contraction in vitro *(Reymann et al., 2012, Science; Ennomani et al., 2016, Current Biology)*. Therefore, it would be interesting to determine if the action of myosin on different actin architectures generates distinct chiral behaviors. By growing geometrically constrained branched and unbranched (parallel or anti-parallel) actin networks, whose assembly is triggered by either Nucleating Promoter Factors (NPFs) or Formin grafted on cell-sized lipid micropatterns or microwells, we would be able to observe whether their interaction with myosin (MyoII or others) could generate distinct chiral actin self-organization or network contraction (Figure 39A-B). Then, adding crosslinkers, like α-actinin, to these systems would allow us to assess the effect of network connectivity on the observed chiral phenotype. Although technically and biochemically challenging, it is also possible to develop reconstituted systems with competing actin networks: an Arp2/3-nucleated lamellipodium-like branched network and formin-nucleated bundles. In this case, it would be interesting to determine whether and how the competition and/or the interaction between these two distinct networks could trigger the emergence of a chiral self-organization, as well as how the presence of myosin could influence balance between the two networks and consequently their global architecture.

2.4. Polarization cues by the dominant cell to propagate the LR bias

Our TFM results suggest the existence of stronger, more contractile cells within doublets, whose ME levels can predict the bias and, thereby, dominate the expression of the chiral phenotype. This raises a number of relevant questions. First, how can one justify the emergence of such stronger within the doublets? One possibility is that dominant cells are inherently more contractile since the beginning, due to their cell cycle stage, for example. Alternatively, during the early stages of spreading, these cells become stronger because of specific interactions with their surrounding environment and their partners on the micropattern. Second, how can these stronger, dominant cells drive the biased rotation of the entire system? In fact, these cells appear to have some shared characteristics with the well-known leader cells guiding directional motion of cell collectives; they are more contractile compared to the follower cells and possibly have the ability to sense and respond more rapidly to polarizing, directional cues provided by the surrounding environment *(Ladoux et al., 2016, Trends in Cell Biology; Ladoux & Mège, 2017, Nat Rev Mol Cell Biol)*. As such, one hypothesis can be that the dominant cells of the doublets first establish a stable front-rear polarization with a particular bias based on their contractility levels, which is then propagated to their partners either through intercellular junctions (discussed below) or through front-front inhibition, previously shown to drive symmetry break in simulated confined doublets *(Camley et al., 2014, Proceedings of the National Academy of Sciences)*. In this context, Jain et al. demonstrated that after the initial collision between the two cells leading oppositely migrating trains, the cell with the more spread lamellipodium at the site of contact induced the repolarization of the other cell, which, consequently, triggered the onset of a collective persistent and coherent rotation. This

was accompanied by the development of a polarization gradient that extended to the single cell level, and whose perturbation arrested the entire system *(Jain et al., 2020, Nat. Phys.)*. Therefore, following the evolution TFs in parallel to the establishment of polarization (using Rac or RhoA fluorescent probes in association to force dipoles) during the early process of symmetry break in doublets would help identify the events leading to rotation initiation, as well as the contribution of each individual cell to the overall polarization and symmetry break of the system (Figure 38).

It was previously shown that the persistent rotation of doublets in 3D was largely dependent on the polarization of the constituting cells that was marked by the localized accumulation of myosin at the edges of the cell-cell junctions. This resulted in the establishment of an active tension gradient within the doublets, whose perturbation at any time point abolished rotation *(Lu et al., 2022)*. Consequently, attempts to interfere with the polarization in one or the two cells of a pair during rotation would provide greater insights into the contribution of individual cells to the chiral phenotype of doublets as well as the mechanism underlying its emergence. In this context, we noticed that rotating doublets were characterized by the localization of myosin clusters at the rear of individual cells. Laser ablation of these clusters during rotation would possibly abolish the established polarization, causing a temporary arrest that might be followed by a repolarization event to restart rotation (Figure 40A). In addition, cells within doublets appeared to share certain structures, of which the most prominent were actin fibers extending from the edge of one cell to that of the other in a way that was reminiscent of the supracellular actin cables characterized in migrating cell collectives *(Ladoux & Mège, 2017, Nat Rev Mol Cell Biol)*. As these actin structures tend to be particularly stable, they might be essential for the maintenance of the established polarization and the persistence of rotation. Laser ablation of these shared actin fibers would help determine their role in the emergence of the chiral phenotype in doublets. On the other hand, targeted local activation of particular proteins like RhoA or Rac, using optogenetics for example, might give rise to interesting results *(Jain et al., 2020, Nat. Phys.; Lu et al., 2022; Ruppel et al., 2023, ELife)*. Following a brief rotation arrest, the local activation of either of the two proteins in one of the two cells might induce a repolarization event within the doublet and, accordingly, drive rotation in the same or opposite direction (Figure 40B).

To challenge further the validity of our hypothesis regarding bias determination by more contractile cells, we can take advantage of several interesting systems (Figure 41A). The first one consists of using enucleated HUVECs, commonly referred to as cytoplasts, which have been previously shown to exert less TFs on the underlying substrate while preserving polarization and migratory abilities for hours *(Graham et al., 2018, Journal of Cell Biology)*. In addition, single cytoplasts are also capable of demonstrating a chiral actin swirling when confined on adhesive disks *(Jalal et al., 2019b, Journal of Cell Science; Tee et al., 2023, Nat Commun)*. By using a homogenous population of cytoplasts, the ME values are supposed to shift toward lower contractility levels (leftward), thereby enhancing the CW bias. Quantifying the bias of heterogeneous cell-cytoplast doublets (CytoCells) can be informative as well. The second system is based on using the inherent variation of forces

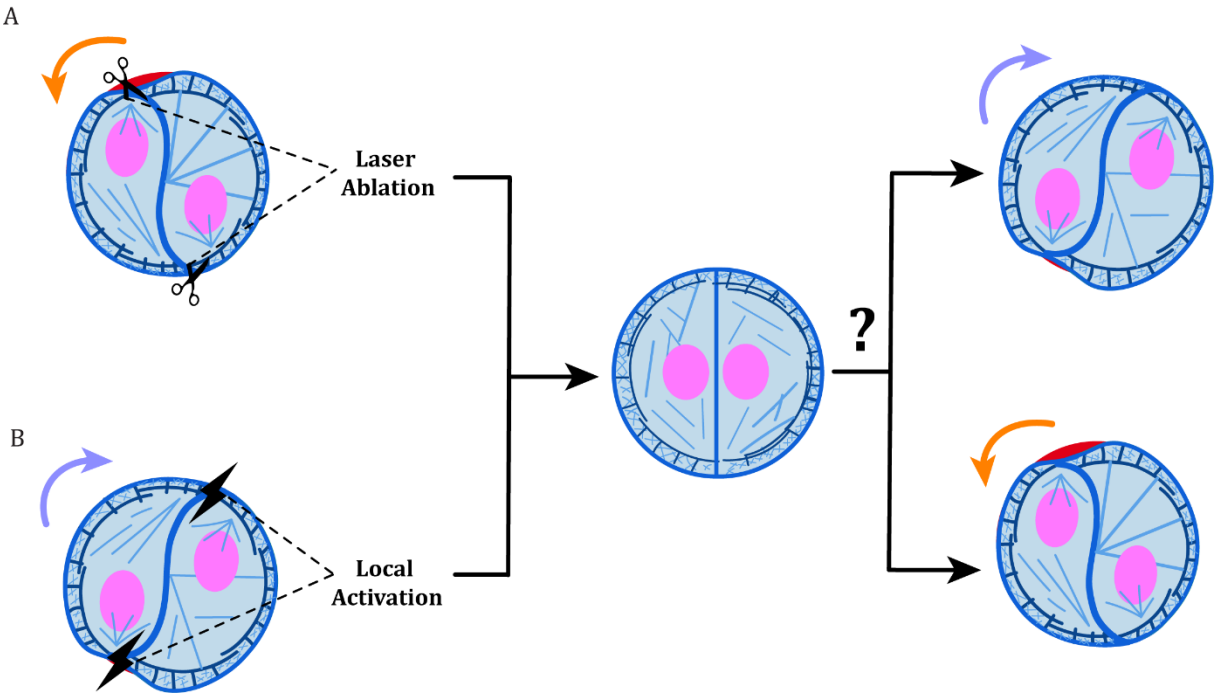

Figure 40: Proposed ways to perturb the polarization within the doublets and their possible outcomes.
A: Laser ablation of myosin clusters in the cells rears or the shared actin structures between the two cells.
B: Local activation of Rho, Rac, or others by optogenetics.
The purple and orange arrows indicate CW and CCW rotation, respectively

throughout the cell cycle *(Vianay et al., 2018, Biology of the Cell; Panagiotakopoulou et al., 2018, MBoC)*. As the maximal TFs have been recorded over the S-phase, synchronizing the cells at the G1/S transition provides a population of cells, whose ME values are expected to shift toward higher contractility levels, thereby increasing the proportion of CCW-biased doublets. On the other hand, quiescent cells are known to be less contractile than cycling cells and, therefore, may display an increased CW bias *(Pitaval et al., 2010, Journal of Cell Biology)*. Moreover, assessing the bias of a doublet population created by mixing S-phase synchronized cells or quiescent cells with cells from other cell cycle stages would help confirm the dominance of more contractile cells. In addition, as doublets composed of daughter cells after division are supposed to be symmetric in terms of traction forces, selectively increasing contractility in one of the two cells (using optogenetics) may drive the emergence of a dominant cell that can adjust the chiral behavior of the doublet (rotation speed or direction) based on its contractility levels (Figure 41B-1). The same method can be used to try modulating the dominance in the previously described heterotypic system consisting of HUVEC and MEF by selectively increasing the

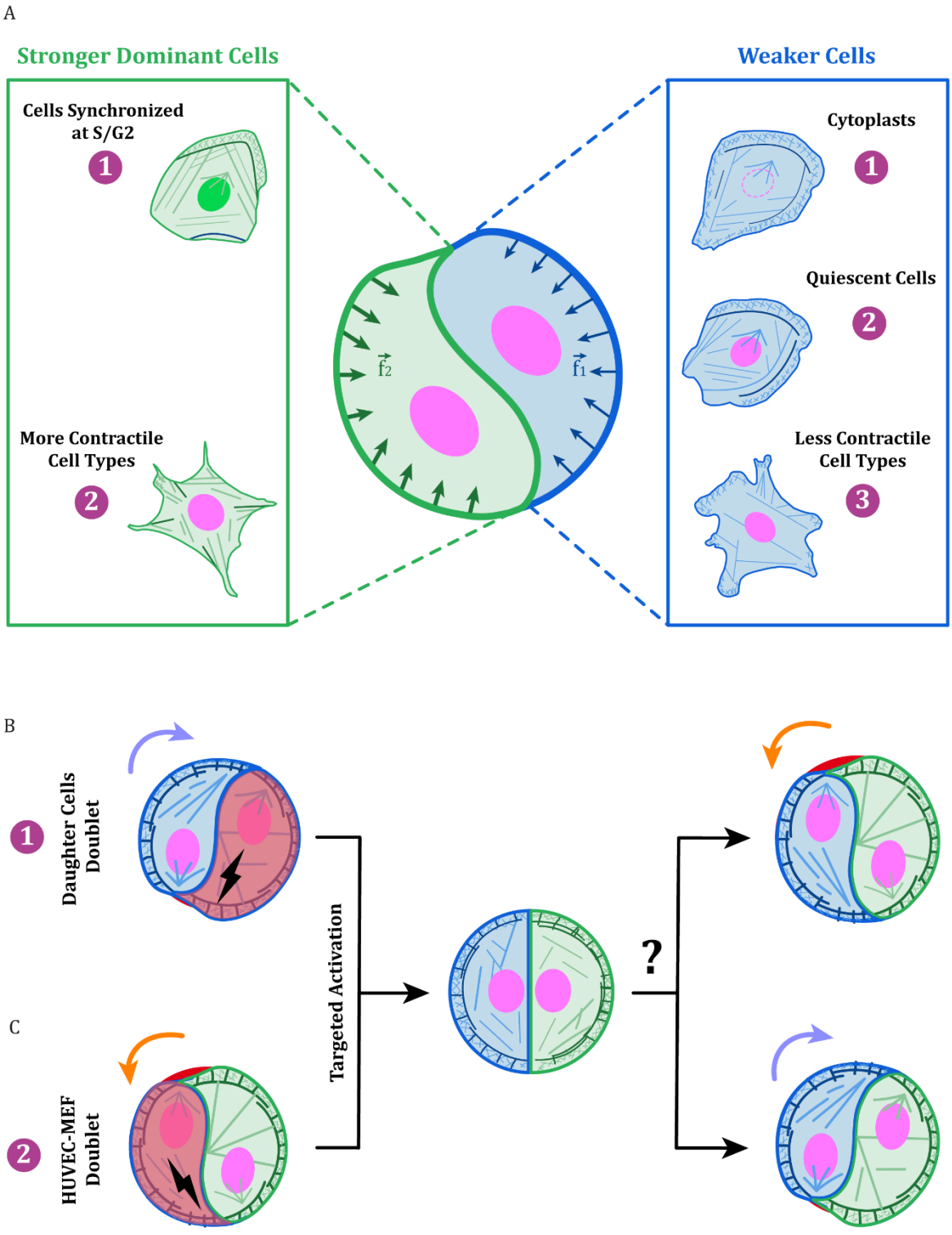

Figure 41: The different approaches proposed to challenge the dominance of the stronger cell.
A: Relevant cellular models that can be used as the stronger or weaker cells within the doublets and can be associated with different outcomes.
B: Targeted activation of one of the two cells in a symmetric, daughter cells doublet (top) without a clear dominance or a heterotypic doublet (bottom) with a dominant, more

contractile cell, along with its potential outcomes on the dominance and consequently, rotation and bias.
Within the doublet, the cell in green is the stronger, dominant cell; the weaker cell is in blue. The purple and orange arrows indicate CW and CCW rotation, respectively.

---

contractility levels of the HUVEC partners (Figure 41B-2). Both of these systems would provide great insights into the mechanism by which stronger, dominant cells govern the chiral behavior of doublets and, consequently, predict the bias at the level of the population.

Finally, it would be interesting to challenge our hypothesis in other cell types. For example, we have used MEFs in our study because they are more contractile than HUVECs, and thus their population is shifted toward the right, where the bias is CCW. According to our hypothesis, treating MEFs with ROCKI would shift their contractility levels to the left, thereby causing the reversion of the chiral bias to CW. In addition, it would be interesting to test whether cell types with lower contractility levels compared to HUVEC demonstrate an enhanced CW bias (Figure 41A).

3. PKCs: possible molecular effectors in the pathway underlying cellular LR asymmetry

PKC isoforms are crucial cellular components that regulate a variety of cellular processes, including cell polarity and migration, through their ability to reshape the global architecture of the actin cytoskeleton *(Larsson, 2006, Cellular Signalling)*. Recent reports revealed a possible implication of PKC isoforms in cellular chirality. In this context, it was demonstrated that mouse fibroblasts display a reversed biased alignment in response to PKC activation. As a direct PKC substrate, involved in the regulation of cell migration and FA remodeling, fascin appeared to be the potential mediator of this effect *(Anilkumar et al., 2003, The EMBO Journal; H. Zhang et al., 2023, Advanced Biology)*. In a similar manner, chemically induced PKC activation caused a dose-dependent reversion of the biased alignment of HUVEC collectives on 2D donut-shaped micropatterns as well as the chiral helical asymmetry of engineered vessels in 3D. This effect of PKC activation on endothelial cell chirality particularly required the conventional PKC-α isoform *(Fan et al., 2018, Science Advances; H. Zhang et al., 2024, Science Advances)*. Interestingly, it has been shown that upon activation, PKC-α phosphorylates a particular RhoGEF (p115RhoGEF), which stimulates Rho signaling leading to the excessive formation of actin stress fibers and the disruption of the integrity of the endothelial barrier *(Holinstat et al., 2003, Journal of Biological Chemistry)*. This suggests that the activity of PKC-α can induce an increase in contractility, which biases the overall actin organization, giving rise to an opposing chiral phenotype.

Nevertheless, given their essential roles in cell polarization and directional migration, atypical PKCs (aPKCs) may also be implicated in the emergence of LR asymmetry. In particular, through their characteristic interactions with Rho GTPases, (RhoA, Rac, Cdc42) as well as their close association with certain PAR proteins, aPKCs drive the

reorganization of the actin cytoskeleton that mediates the front-rear polarization of mammalian cells during directional migration and the polarity establishment of the C. elegans zygote during early development *(Hong, 2018, F1000Res; Xiao & Liu, 2013, Cell. Mol. Life Sci.)*.

Therefore, assessing the effect of PKC activation on the biased rotation of HUVEC doublets would help further validate our hypothesis.

4. The contribution of the intercellular junction to the chiral phenotype

One of the earliest hallmarks of symmetry break and rotation initiation among cell doublets is the emergence of an S-shaped, curvilinear cell-cell interface that gives rotating doublets an overall morphology of a Yin-Yang, whose orientation reflects the direction of rotation *(Huang et al., 2005, Cell Motil. Cytoskeleton; Leong, 2013, Biophysical Journal; Chin et al., 2018, Proc. Natl. Acad. Sci. U.S.A.; Lu et al., 2022)*. Indeed, we saw that the front-rear polarization of the cells constituting the doublets was accompanied by the emergence of a dynamic Yin-Yang junction at the onset of rotation. Interestingly, when quantifying the length of the junction in rotating doublets, we noticed that it was shorter for CCW-rotating doublets, indicating that the latter are characterized by straighter intercellular junctions in addition to elevated stored ME levels. Moreover, doublets treated with the contractility-modulating drugs displayed differences at the level of the junction morphology as well. Whereas more deformed cell-cell junctions were observed among ROCKI-treated doublets, CalyA treatment was predominantly associated with straighter junctions. In this context, using a particle-based model, Leong suggested that actomyosin forcing and cortical tension governed the extent of junction deflection. He showed that low or high levels of actomyosin forces leading to the loss of doublet rotation were associated with excessively deformed or straight junctions, respectively *(Leong, 2013, Biophysical Journal)*. Recently, it was demonstrated that cells confined on different micropattern geometries displayed distinct junctional morphologies that could be associated with the cellular mechanical properties on the respective micropatterns *(Sri-Ranjan et al., 2022, Nat Commun)*. In particular, doublets on disks were characterized by sigmoidal, immature, and dynamic cell-cell contacts, whereas stiffer doublets on triangles displayed straight, mature, and more stable junctions. Interestingly, seeding doublets on disks of higher stiffness or treating doublets on triangles with ROCKI induced the transition between the two interfacial morphologies. This, together with the previously reported implication of the ECM in junction positioning and stability *(Tseng et al., 2012, Proc. Natl. Acad. Sci. U.S.A.)*, highlights the existence of a feedback between cell-ECM traction forces underlying cell migration and intercellular forces maintaining cell-cell contact in mediating junction deformation that often accompanies symmetry break in doublets.

By using cadherin knockdown cells or EGTA treatment, it has been shown that intercellular junctions are important for biased collective behaviors, particularly through their implication in the transmission of chiral cues across the cells *(Luo et al., 2023, Genes to Cells; Worley et al., 2015, Integrative Biology)*. However, an interesting study suggested that cell-cell contacts were required only for the initial establishment of directional collective rotation but not for its maintenance. The latter appeared to be completely dependent on the emergence of a stable, coordinated front-rear polarization at the level

of individual cells through the extension of cryptic lamellipodia *(Jain et al., 2020, Nat. Phys.)*. Treating HUVEC doublets with EGTA at different time points will help indicate whether the intercellular junction is a limiting factor throughout the entire process of symmetry break and rotation, or whether it is required only for the initial establishment of a polarized single cell behavior characterized by active RhoA-Rac gradients, which then maintain the persistence and coherence of biased rotation (Figure 42A-B). Our preliminary results show that treating doublets with EGTA during early spreading drastically decreases the proportion of rotating cells (Figure 42C). Interestingly, the few cells able to initiate rotation in the absence of the intercellular junction still demonstrate a CW bias (Figure 42D). This may indicate that, in our system of doublets, cell-cell adhesions are involved in the early events of symmetry break underlying rotation initiation. Further confirmation of the results requires washing out EGTA and monitoring whether the doublets can initiate rotation, as well as adding the compound at delayed time point to report its effect at the later stages of rotation. Despite being widely used to disrupt cell-cell junctions, the calcium chelator EGTA could have certain underlying side effects that would bias the interpretation of the results. Therefore, identifying the exact contribution of the intercellular junction to the chiral phenotype in doublets might require the development of VE-cadherin knockouts to ensure a more specific disruption of the junctions.

However, given the interdependence between cadherin-based cell-cell adhesion and integrin-based cell-ECM adhesion in the coordination of the mechanical forces underlying collective behaviors, it is most likely that the inhibition of intercellular junctions by any means would cause the upregulation of cell-ECM adhesion that would favor the emergence of highly uncoordinated motion at the single cell level *(Goodwin et al., 2017, MBoC; Ladoux & Mège, 2017, Nat Rev Mol Cell Biol; Tixi et al., 2023, ELife)*. This suggests that the effect of junction disruption on the expression of chirality in cell doublets could be always attributed at least in part to the overall increase in contractility levels and its accompanying effects on cell polarity.

In our system where one of the two cells of the doublet seems to govern the chiral phenotype, how can the dominant cell propagate its emergent bias following symmetry break to its partner so that a persistent chiral phenotype arises at the level of the doublet? It has been reported that junctions between collectively migrating endothelial cells comprise polarized VE-cadherin fingers that extend from the p-MLC-rich rear of leader cells and are engulfed by the followers, where p-MLC is inhibited. Interestingly, increased contractility, marked by RhoA activation, in the leader cell can initiate the extension of cadherin fingers from its rear. The engulfment of the incoming fingers by the follower cells is often accompanied by increased protrusive activity characteristic of Rac-induced dendritic actin polymerization. The resulting asymmetric recruitment of curvature-sensitive BAR domain-containing proteins (like PKC) to the opposing curvatures generated in the two cells can help regulate and maintain the emerging RhoA-Rac activity gradients *(Hayer et al., 2016, Nat Cell Biol)*. This suggests that engulfed VE-cadherin fingers can provide polarization and guidance cues to direct collective cell migration.

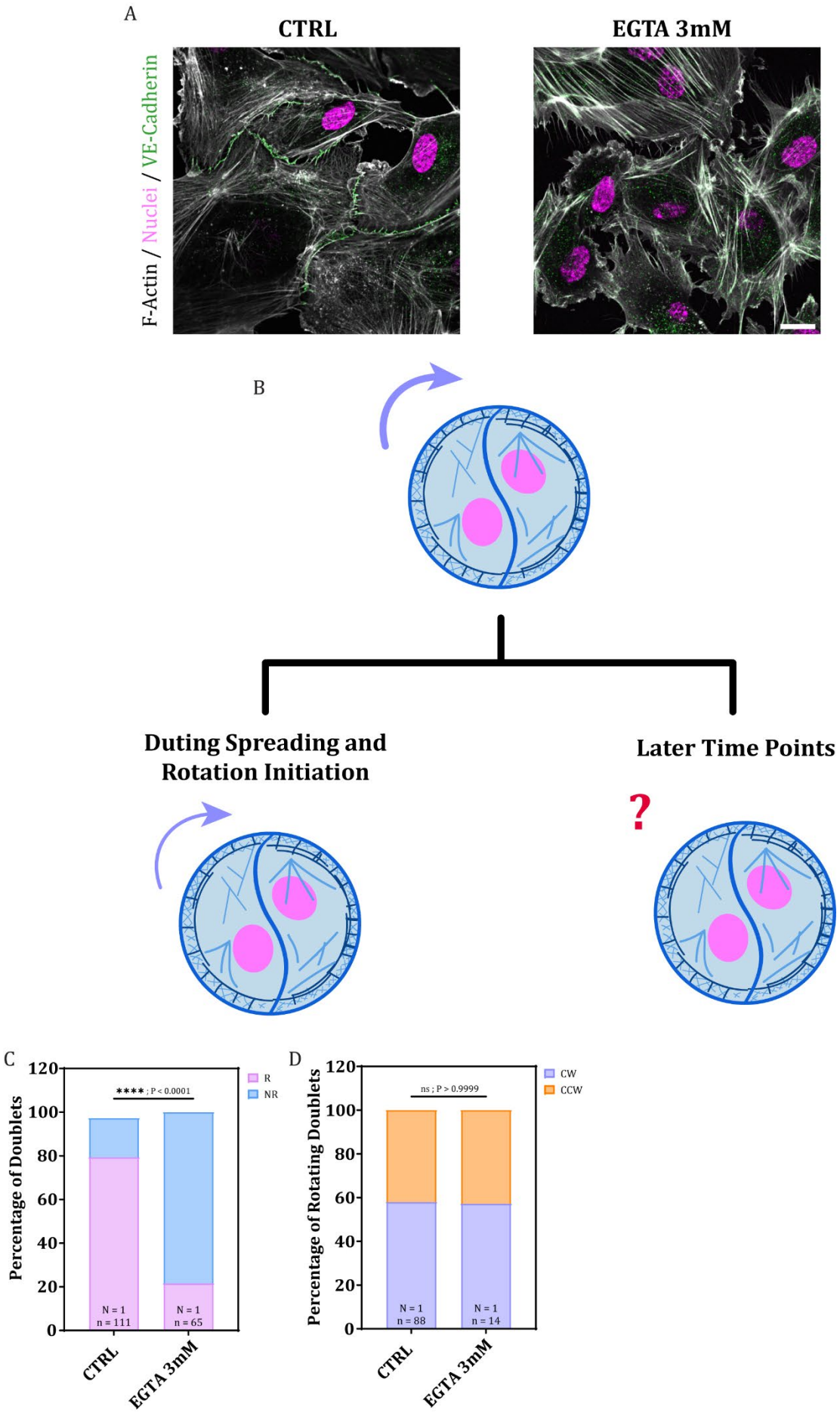
A
CTRL
EGTA 3mM
F-Actin / Nuclei / VE-Cadherin
B
Duting Spreading and
Rotation Initiation
Later Time Points
?
C
Percentage of Doublets
120
100
80
60
40
20
0
****; P < 0.0001
R
NR
N = 1
n = 111
N = 1
n = 65
CTRL
EGTA 3mM
D
Percentage of Rotating Doublets
ns; P > 0.9999
CW
CCW
N = 1
n = 88
N = 1
n = 14
CTRL
EGTA 3mM

Figure 42: The contribution of the intercellular junction to the chiral phenotype.
A: Representative images of immunofluorescence of HUVECs in the absence or presence of EGTA 3mM stained for F-actin, VE-cadherin, and Nuclei. Scale Bar = 10µm.
B: Schematic representation illustrating the proposed experiment to identify the contribution of the intercellular junction in the chiral phenotype of doublets. Adding EGTA at different time points can be associated with different outcomes. The purple arrows indicate CW rotation. The thickness of the arrows reflect the amount of rotation.
B: Bar graph representing the quantification of the percentage of rotating and non-rotating doublets in the absence or presence of EGTA 3mM.
C: Bar graph representing the quantification of the percentage of CW- and CCW-rotating doublets in the absence or presence of EGTA 3mM.
N is the number of independent experiments performed; *n* is the total number of doublets analyzed. Statistical significance was assessed using Chi-square (Fischer's exact) test.

Therefore, characterizing such force-sensitive polarized cadherin fingers in our system of doublets could be key to understanding how the dominant cell biases the polarization of its partner and enforces its asymmetry at the level of the doublet (Figure 42A).

5. A potential additional layer of regulation by unconventional MyoI isoforms

MyoI isoforms constitute a family of unconventional, monomeric, single-headed motors that are widely expressed in the cells of vertebrates, where they mediate diverse cellular functions including structural organization, endocytosis, membrane trafficking, and motility *(McIntosh & Ostap, 2016, Journal of Cell Science)*. Among these isoforms, two were identified (MyoID and MyoIC) to be essential for chirality development in Drosophila organs, tissues, and cells *(Hozumi et al., 2006, Nature; Juan et al., 2018, Nat Commun; Lebreton et al., 2018, Science)*. Such a role was associated with the ability of MyoIC and MyoID to produce molecular torques that can twist and rotate gliding actin filaments in vitro *(Pyrpassopoulos et al., 2012, Current Biology; Lebreton et al., 2018, Science; Y. Sato et al., 2023, Sci Rep; Pernier & Schauer, 2022, Biology)*. Consequently, it has been widely believed that MyoI isoforms and their interactions with the actin cytoskeleton can drive the emergence of chirality at the molecular level and its propagation to higher scales. Intriguingly, a recent study reported certain discrepancies concerning the role of these MyoI isoforms in the expression of chirality in human fibroblasts *(Tee et al., 2023, Nat Commun)*. Whereas the knockdown of either MyoIC or MyoID had no effect on the chiral actin swirling in single fibroblasts, collectives composed of MyoIC knockdown cells displayed a more pronounced biased alignment. These results question the conserved requirement of MyoI isoforms for the development of cell chirality and suggest that their effect on the emergence of LR asymmetry may be largely dependent on the cellular context and the interaction with the other implicated effectors.

Interestingly, the wide spectrum of functions regulated by MyoI isoforms in different cell types highlights their ability to remodel the architecture of the actin cytoskeleton. Because their motor domains demonstrate a preference for different actin filament

populations, MyoI isoforms can modulate the balance between actin bundles and branched networks *(Pernier & Schauer, 2022, Biology)*. Indeed, genetic screening in Drosophila has revealed that MyoID interacts with the formin DAAM, FAs, and adherens junctions *(Chougule et al., 2020, PLOS Genetics)*. Conversely, other MyoI isoforms, including MyoIC and MyoIB, prefer the interaction with dendritic actin networks, as their loss alters the activity of Arp2/3 and the associated distribution of the nucleated branched actin networks *(Pernier et al., 2020, Journal of Cell Science; Pernier & Schauer, 2022, Biology; Schauer et al., 2010, Nat Methods)*. In addition, MyoI isoforms actively participate in exocytosis, endocytosis, and intracellular membrane trafficking, indicating that they can be implicated in the stabilization and the maintenance of cell polarity that may affect the expression of LR asymmetry *(McIntosh & Ostap, 2016, Journal of Cell Science; Vaidžiulytė et al., 2019, Journal of Cell Science)*. Overall, this suggests that the modulation of chirality by MyoI isoforms may be mediated through their interactions with actin and its binding partners, which govern the global organization of the actin cytoskeleton and, consequently, the symmetry-breaking event. Future attempts to uncover how MyoI isoforms interact with F-actin and MyoII to bias the overall actin architecture in cellular systems including ours may help better understand its implication in the development of LR asymmetry across scales.

6. The involvement of microtubules in chirality

6.1. Microtubules can also break LR asymmetry

As mentioned previously, motor proteins of the microtubule network (certain kinesins and dyneins) are also capable of generating rotational forces or torques that can contribute to LR symmetry break. This has been clearly demonstrated, in vitro, through the right-handed helical rotation of anti-parallel cross-linked microtubules mediated by kinesin-14 *(Mitra et al., 2020, Nat Commun)*, and, in vivo, through the chirality of the mitotic spindle, reflected by the left-handed twist of microtubule bundles created by the movement of the associated motors *(Trupinić et al., 2022, Current Biology)*. However, the role of microtubules in LR symmetry break and chirality emergence in cells is still debatable. It was shown that the treatment of dHL60 neutrophils, normally displaying a leftward biased migration, with Nocodazole resulted in random cell polarization and migration *(Xu et al., 2007, PNAS)*. On the other hand, the depolymerization of microtubules had no effect on the chiral actin cytoskeleton swirling or nucleus rotation in other cell types *(Tee et al., 2015a, Nat Cell Biol; Yamanaka & Kondo, 2015, Genes to Cells)*. Such controversial findings raise serious questions regarding the importance of microtubules in the development and maintenance of cellular chirality.

The emergence of LR asymmetry is associated with the early events of cell polarity establishment, in which the initial symmetry of the system is broken by the actin network independently of microtubules. Thus, it seems less likely that the latter actively participate in the emergence of cellular chirality. Nonetheless, the subsequent polarization of microtubules, guided by the actin cytoskeleton, is essential for the maintenance of the emergent cell polarity *(R. Li & Gundersen, 2008, Nat Rev Mol Cell Biol)*. Therefore, microtubules may have long-term consequences on the expression and the stability of the chiral phenotype. Assessing the biased rotation of cells treated with Nocodazole, in the presence of ROCKI to compensate for the contractility increase

resulting from the depolymerization of microtubules, over long intervals of time may enable us to evaluate the importance of microtubules in our system.

6.2. The polarity axis in relation to chirality

The acquisition of a polarized state by cells after an initial symmetry-breaking event is often characterized by the repositioning of the microtubule-organizing center (MTOC) or the centrosome, which acts to reinforce the established polarity and ensure its persistence. Such is the case for directional cell migration, whose long-term persistence relies on the maintenance of the previously established front-rear polarity by the actin cytoskeleton through the subsequent polarization of microtubule network that is marked by the reorientation of the Nucleus – Centrosome – Golgi axis depending on the cell type and geometrical constraints *(Gundersen & Bulinski, 1988, Proceedings of the National Academy of Sciences; R. Li & Gundersen, 2008, Nat Rev Mol Cell Biol; Palazzo et al., 2001, Nat Cell Biol; Wittmann & Waterman-Storer, 2001, Journal of Cell Science)*.

Given its importance in cell polarity, the Nucleus – Centrosome – Golgi axis has been extensively used as a readout for intracellular chirality, in both individual cells and collectives *(Fan et al., 2018, Science Advances; T.-H. Chen et al., 2012, Circulation Research; Wan et al., 2011, PNAS; Xu et al., 2007, PNAS; Hachem et al., 2024, APL Bioeng.)*. In our study, we have described a dynamic chiral phenotype among doublets and single cells, in which directional migration constitutes an important parameter, suggesting that the expression of the identified chiral bias in the cell population may be dependent on the front-rear polarity established by the cells during symmetry break. Therefore, it would be interesting to characterize the polarity axes in rotating doublets and single cells on rings. Identifying the how the Nucleus – Centrosome – Golgi axis is oriented relative to the direction of rotation and the associated actin polarization would help better understand the correlation between cell chirality and polarity and, in the case of doublets, would provide more insight into the coupling between individual cells.

Furthermore, it has been shown that in adherent cells, the centrosome occupies the center of an area largely devoid of actin structures, known as the actin inner zone, whose position is determined by the actomyosin architecture *(Jimenez et al., 2021, Current Biology; Schaeffer, 2023)*. Consequently, changes in the organization of the actomyosin network elicited by the extracellular environment can displace the actin inner zone, thereby biasing the positioning of the centrosome independently of the microtubules. Interestingly, it was demonstrated that in response to the increase in cellular contractility triggered by microtubule depolymerization *(Chang et al., 2008, MBoC; Krendel et al., 2002, Nat Cell Biol)*, enucleated fibroblasts confined on micropatterns readily broke symmetry as marked by their off-centered centrosomes (Figure 43A) *(Jimenez et al., 2021, Current Biology; Schaeffer, 2023)*. In addition, epithelial-to-mesenchymal transition (EMT) in doublets on H-shaped micropatterns, whose centrosomes are normally oriented toward the intercellular junction, induces selective microtubule disassembly that may be accompanied by local increases in contractility, which lead to the repositioning of the centrosomes toward cell-ECM adhesions and, thus, promote the scattering of the cells upon their release (Figure 43B) *(Burute et al., 2017, Developmental Cell)*. The polarity of the cells in this system was shown to be strongly dependent on contractility, as varying the stiffness of the matrix triggered an equivalent reversal of centrosome orientation.

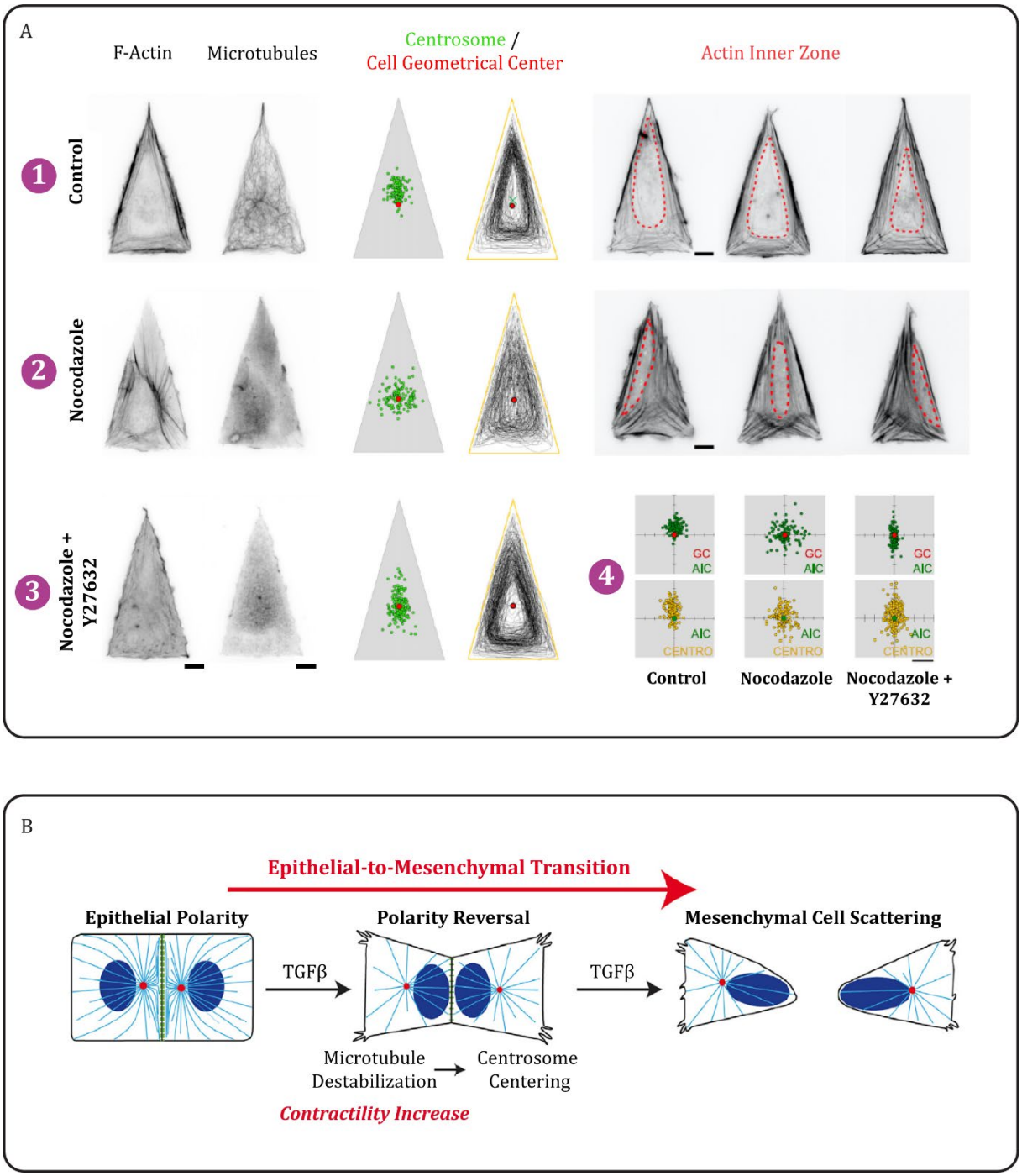

Figure 43: Centrosome positioning is strongly influenced by cellular contractility levels and the associated actomyosin network organization.

A: MEF-vimentin knockout cytoplasts expressing EGFP-centrin plated on 2000µm² isosceles triangles to assess centrosome positioning under different conditions. After fixation, cytoplasts were stained for actin and microtubules (Scale Bar = 10µm). Adapted from *(Jimenez et al., 2021, Current Biology; Schaeffer, 2023)*.

(1) Control Condition (n = 121 cells). To the left, representative images of the actin and microtubule networks. In the middle, distribution of the centrosome with respect to the geometrical center (GC) of the cytoplasts and distribution of the actin inner zone

(AIZ) boundaries inside the isosceles triangle shape. To the right, representative images of AIZs on the isosceles triangle patterns.
(2) Nocodazole Condition (n = 120 cells). To the left, representative images of the actin and microtubule networks. In the middle, distribution of the centrosome with respect to the geometrical center (GC) of the cytoplasts and distribution of the actin inner zone (AIZ) boundaries inside the isosceles triangle shape. To the right, representative images of AIZs on the isosceles triangle patterns.
(3) Nocodazole + Y-27632 Condition (n = 170 cells). To the left, representative images of the actin and microtubule networks. To the right, distribution of the centrosome with respect to the geometrical center (GC) of the cytoplasts and distribution of the actin inner zone (AIZ) boundaries inside the isosceles triangle shape.
(4) From left to right: Control Condition, Nocodazole Condition, Nocodazole + Y-27632 Condition. On top, graphs depicting the actin inner zone center (AIC) distribution around the GC of the isosceles triangle. On the bottom, graphs depicting the distribution of the centrosome with respect to the AIC.

B: Scheme illustrating microtubules and centrosome repositioning that causes polarity reversal and finally cell separation during epithelial-to-mesenchymal transition (EMT). Adapted from *(Burute et al., 2017, Developmental Cell)*.

These findings suggest that the orientation of the Nucleus – Centrosome axis, which serves as a major readout for both polarity and chirality, is strongly influenced by cellular contractility levels and the associated actomyosin network organization. Therefore, it would be interesting to assess how the variations in contractility, previously shown to modulate the chiral bias among rotating cells, affect the orientation of the Nucleus – Centrosome axis and, consequently, the polarity of the cells. This can also be relevant in the context of single cells on static micropatterns, which due to the geometry of the adhesive area, may experience elevated levels of contractility that can induce polarity reversal. Moreover, the cellular model employed by Burute et al. could serve to further investigate the feedback between polarity and chirality. By using epithelial cells, such as MDCKs, in our system, we might be able to determine how polarity reversion, induced by triggering EMT, could affect the chiral bias in the cell population.

7. Motility: a key factor for chirality emergence?

Most of the existing studies investigating biased cell behaviors, including ours, have relied on systems in which motility is actively contributing to the phenotype; even biased collective alignment is driven by the flow generated by the migration of individual cells on opposing boundaries *(Wan et al., 2011, PNAS; T.-H. Chen et al., 2012, Circulation Research; Tee et al., 2023, Nat Commun)*. Chiral demonstrations in static contexts are limited to transient actin swirling and nucleus rotation that resolve after a certain duration of time *(Tee et al., 2015b, Nat Cell Biol; Jalal et al., 2019b, Journal of Cell Science; Kwong et al., 2023, ELife)*. However, by triggering motility, we have identified a system in which single HUVEC cells display a persistent biased rotation, comparable to that described among doublets. This raises interesting questions regarding the inherent nature of cell chirality and the contribution of motility to the establishment of a persistent chiral phenotype.

We have tried to address this question by assessing the behavior of cells on static, anisotropic micropatterns comparable to rings, on which they can break symmetry but cannot move. Using the orientation of the Nucleus – Centrosome – Golgi axis, we have not seen a particular LR bias, suggesting that motility may be required for the manifestation of chirality in our system. These findings oppose the leftward bias reported in C2C12 cells seeded on T-shaped micropatterns, which appears to mirror the CCW-biased alignment of C2C12 collectives. However, the authors of this work did not directly use the orientation of the Nucleus – Centrosome axis as a readout; instead, they assessed the LR positioning of certain organelles associated with the cellular metabolic activity and contraction (Golgi, lysosomes, mitochondria, actomyosin) relative to the Nucleus – Centrosome axis. They claimed that the bias of these organelles to the left of the axis reflected an increased cellular activity on that side, which favored a CCW migration, opposite to the orientation of the polarity axis, of the cells along the boundaries of the donut-shaped micropatterns and, eventually, drove the collective leftward alignment of these cells *(Hachem et al., 2024, APL Bioeng.)*. On the other hand, it was previously demonstrated that upon the stimulation of unbiased dHL60, these cells could initiate a leftward biased migration as evident by the orientation of their Nucleus – Centrosome axis *(Xu et al., 2007, PNAS)*.

Two approaches come to mind and can be employed to address this controversy. The orientation of the Nucleus – Centrosome – Golgi axis can be quantified among single cells on rings in relation to rotation, which will enable the identification of the relative positioning of the centrosome and the Golgi and the subsequent confirmation of whether the bias in rotation direction is translated into a biased orientation of the polarity axis. Alternatively, the single cells on static patterns can be freed to allow their migration using the previously described technique of dynamic micropatterning *(Isomursu et al., 2024, Small Methods; Vaidžiulytė et al., 2022, ELife)*. The subsequent monitoring of the LR decision making and the initiation of migration, in parallel to the orientation of the Nucleus – Centrosome – Golgi axis would enable the quantification of the emergent bias (Figure 44). Based on what has been previously reported in the same context and what has been established regarding the mechanism driving the positioning of the Centrosome – Golgi, the initial orientation of the polarity axis, in the majority of cases, does not appear to provide good prediction regarding the future direction of migration. However, it would be interesting to see how the initial polarization in the actin network, caused by the anisotropy in cell adhesions enforced by the micropatterns, would bias the emergence of protrusions upon the removal of confinement, which in turn will reorient the polarity axis to initiate directional, persistent migration.

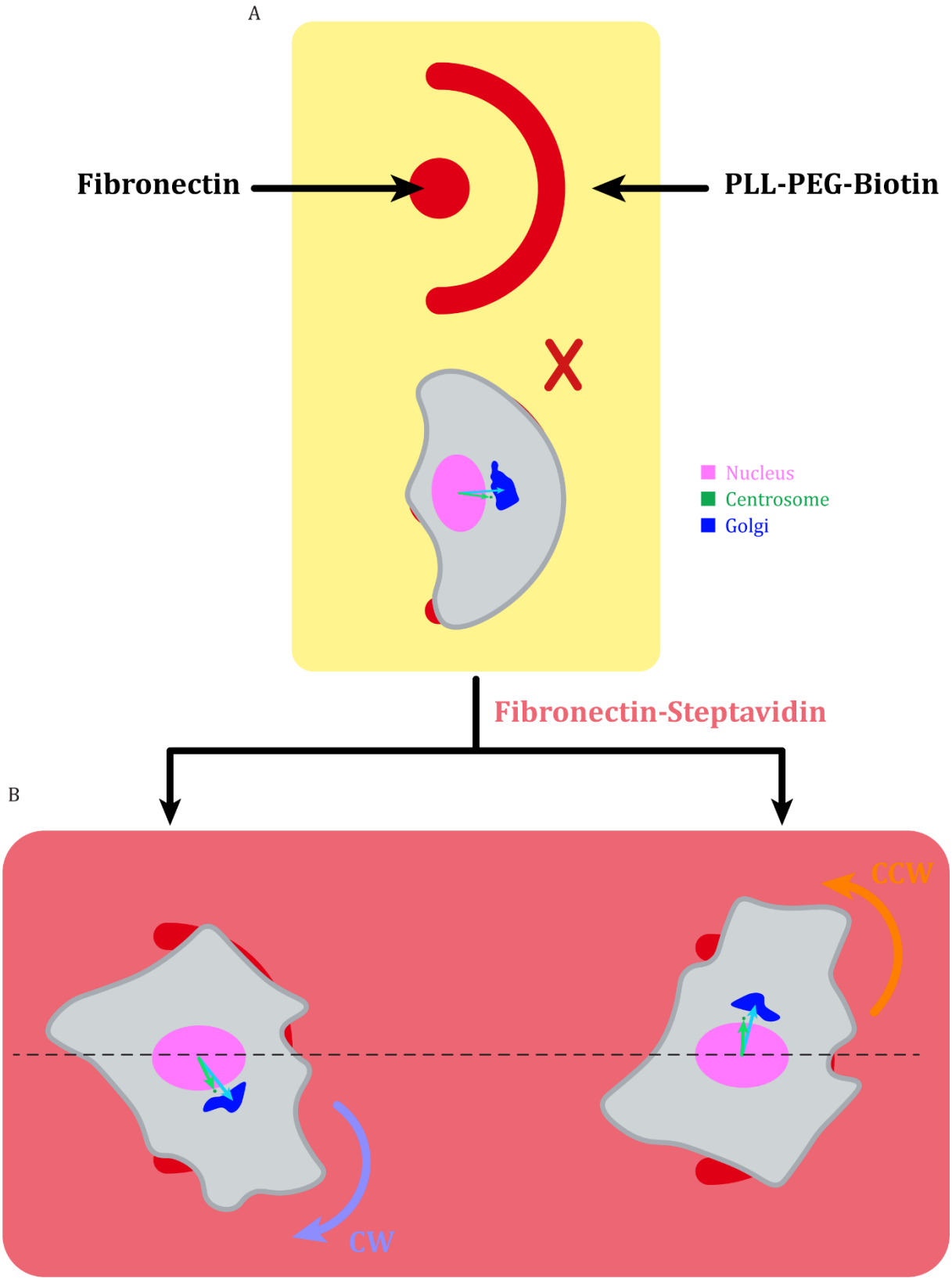
A
Fibronectin
PLL-PEG-Biotin
Nucleus
Centrosome
Golgi
Fibronectin-Steptavidin
B
CCW
CW

Figure 44: The possible outcomes of dynamic micropatterning in our system.
A: On top, the geometry of the static micropattern used (Half-Ring+Dot). On the bottom, the organization of F-actin and the orientation of the polarity axes, Nucleus – Centrosome and the Nucleus – Golgi, of the cell spread on the micropattern. The red cross indicates the absence of rotation. The yellow region represents the PLL-PEG-Biotin surrounding the cell.
B: The addition of FN-Streptavidin is expected to free the cells from the boundaries of the micropattern, which will stimulate the emergence of protrusions and the consequent reorientation of the Nucleus – Centrosome and the Nucleus – Golgi axes. The purple and orange arrows indicate CW and CCW turning, respectively. The dashed black line represents the symmetry axis.

8. Cellular chirality across scales

In this study, we have explored the phenomenon of cell chirality at different complexity levels, where the characterization of distinct biased behaviors have raised important questions regarding the origin of chirality and the minimal requirements for its stable expression, as well as its conservation and propagation across scales.

Similar to previous reports, cells of a big collective exhibited a coherent, directional rotation that was largely biased in the CW direction and was often coupled to the emergence of a distinctive, rightward-biased collective cell alignment. Although we characterized an equivalent persistent chiral behavior among minimal cell collectives consisting of doublets, the directional bias of the latter was significantly lower than that characterized in big cell ensembles. This suggests that the chiral bias may be amplified as it is propagates to higher complexity levels. What could be the mechanism underlying such an effect? Could it be related to the number of cells in a collective?

Focusing on the chiral behavior in cell doublets, we have identified contractility as a key parameter in the emergence and the modulation of the chiral bias. However, given that cell doublets are only minimal models of cell collectives, the mechanisms underlying the coordination and the persistence of the collective behavior, including those driving the propagation and the maintenance of polarity and contractile forces, may not be exactly similar to those described in the context of tissue monolayers. Therefore, the generalization of our findings regarding the role of contractility and the mechanism driving chirality emergence to the level of larger cell ensembles requires further investigation.

In the light of our results suggesting that the chiral behavior of cell doublets is governed by dominant cells, whose contractility levels can set the bias, we have characterized the chiral phenotype demonstrated at the level of single cells. On isotropic disk-shaped micropatterns, individual cells demonstrated a transient, CW-biased nucleus swirling, similar to that previously described among fibroblasts. This cytoskeletal/nucleus swirling is characterized by its transient nature, as it resolves after a certain duration of time. In addition, such a chiral behavior tends to be rare; it is demonstrated in only 30% of the

entire cell population in our system, and it does not appear among keratinocytes and other epithelial cells under the same conditions. How can this identified chiral phenotype among single cells account for the persistent and biased rotation in cell collectives? Using computational models, it has been shown that the cytoskeletal swirling in single cells is associated with the generation of a chiral torque by the actomyosin cytoskeleton exclusively at the apical surface of the single cells since the basal side is fixed by friction arising from the substrate. Interestingly, these models predict that such a dynamic chiral property reported at the single cell level can induce collective cell migration. Furthermore, the introduction of polarization cues favoring the initiation of motility among single cells in our system has triggered the emergence of a biased phenotype that is equivalent to the one described in collectives in terms of proportion and persistence. These findings suggest that the cells can modulate their manifestation of chirality in response to changes in their surrounding environment (boundary conditions). Intriguingly, both cell-cell interactions and motility initiation (which is largely dependent on the cells interaction with the ECM) comprise large-scale actin cytoskeleton reorganization driven by the activity of diverse ABPs that modulate the dynamics and the architecture of the actin network to best accommodate the changes in the surrounding environment and support the desired functions.

Altogether, this suggests that although the chiral information is intrinsic as to being stored in the actin filaments and their binding partners, the extent to which it is expressed as well as the way it manifests in cells is largely dependent on their microenvironment.

XI. GENERAL CONCLUSION

Asymmetry is a universal feature in nature, with crucial roles in cosmology, mathematics, physics, chemistry, and biology. Understanding how asymmetry emerges from an initially symmetric condition has always represented a major scientific challenge.

The development of living organisms on earth is fundamentally based on repeated symmetry-breaking events, of which the one driving the emergence of LR asymmetry is essential for the proper positioning, morphogenesis, and function of vital organs. The conserved nature of LR asymmetry among organisms of diverse complexity questions the existence of a unifying mechanism, stemming from their homochiral building blocks. One attractive hypothesis is that the intrinsic chirality of cytoskeletal elements, particularly actin filaments and their binding partners can be at the origin of LR asymmetry. However, the mechanisms by which such intrinsic molecular chirality impacts the macroscopic asymmetry found in organisms remain poorly understood.

Bridging the gap between these two extreme scales of asymmetry has relied on studies performed at an intermediate level consisting of cells and their collectives. The ability of the latter to distinguish between left and right, commonly referred to as chirality, gives rise to a variety of asymmetric behaviors, including biased cytoskeletal swirling, rotation, and alignment.

Our study has targeted this particular area and aimed at uncovering certain parameters associated with the emergence and the regulation of chirality in minimal cellular systems. First, we show that cell doublets confined on adhesive disks display their chirality by spontaneously initiating a persistent, rightward biased rotation, which is strongly modulated by the magnitude of the mechanical forces produced by the actin cytoskeleton. Interestingly, our results reveal that this chiral behavior is dominated by the more contractile cells within the pairs, which not only govern the speed and the direction of doublet rotation, but also predict the bias exiting at the level of the cell population.

Second, we demonstrate that single cells can adopt an equivalent chiral rotation in response to changes in the geometry of the adhesive area. Based on this system, we propose that the emergence of chirality may be dependent on the establishment of polarity, with a possible requirement for motility in the expression of a persistent chiral phenotype. This suggests that although the origin of chirality resides within the actin cytoskeleton, its expression by the cells is strongly influenced by their surrounding environment (cell-ECM and cell-cell adhesion), which can significantly alter actin network architecture and dynamics.

Altogether, our findings point at the existence of an interplay between contractility and polarity in the emergence of cellular chirality, yet the associated feedback mechanisms remain to be elucidated. Moreover, they provide preliminary insights that challenge the absolute intrinsic nature of chirality and shed the light on the implication of certain parameters that may be key for its stable expression and propagation to higher scales.

XII. MATERIALS AND METHODS

1. Cell Culture (Cell Lines and Culture Conditions)

1.1. Human Umbilical Vein Endothelial Cells (HUVEC-h-TERT2)

HUVEC-h-TERT2 (Evercyte CHT-006-0008) cells were cultured in Endothelial Cell Growth Medium (Lonza EGM BulletKit CC- 3121 & CC-4133) supplemented with the growth factors provided in the kit, 2% fetal bovine serum, and 1% antibiotic-antimycotic solution (Gibco 15240062). The culture flasks were coated with Gelatin (Sigma G1890) 0.1% in Dulbecco's phosphate-buffered saline (DPBS Gibco 14200075) for 30 minutes before use.

1.2. Mouse Embryonic Fibroblasts (MEF)

MEF fibroblasts were cultured in Dulbecco's Modified Eagle Medium high glucose, (DMEM GlutaMAX Gibco 10566016) supplemented with 10% fetal bovine serum (Gibco A5256701) and 1% antibiotic-antimycotic solution (Gibco 15240062).

1.3. Madin-Darby Canine Kidney Cells (MDCK)

MDCK cells were cultured in Dulbecco's Modified Eagle Medium high glucose, (DMEM GlutaMAX Gibco 10566016) supplemented with 10% fetal bovine serum (Gibco A5256701) and 1% antibiotic-antimycotic solution (Gibco 15240062).

1.4. HeLa Cells

HeLa cells were cultured in Dulbecco's Modified Eagle Medium high glucose, (DMEM GlutaMAX Gibco 10566016) supplemented with 10% fetal bovine serum (Gibco A5256701) and 1% antibiotic-antimycotic solution (Gibco 15240062).

All cells were grown at 37°C and 5% CO2 and tested regularly for Mycoplasma using VenorGeM Advance (11-7024) PCR kit. When passaging, the cells were washed once with DPBS (Gibco 14200075) and detached using TrypLE Express Enzyme (Gibco 12605010).

2. Glass Coverslips Preparation

2.1. Cleaning

Coverslips (EPREDIA) 20x20 mm #1.5 (CS) were submitted to three rounds of washing: sonication in acetone (Carlo Erba 528203) for 30mins, sonication in isopropanol (Sigma 34863) for 30mins, and sonication in MilliQ water for 30mins. CS were then air-dried.

2.2. Polystyrene Coating

To promote cellular adhesion, the CS were coated with a thin layer of polystyrene on top of an adhesion promoter. Clean CS were activated by an air plasma treatment (Diener electronic GmbH & Co KG - Plasma-Surface-Technology) then placed inside a semi-closed recipient heated at 75°C in the presence of a few drops of Hexamethyldisilazane (HMDS Sigma 440191) for a least 6hrs. Alternatively, a layer of Ti-Prime was spin-coated on the CS. The CS were then placed in the spin coater (Laurell Technologies), covered with a solution of Polystyrene (PS) 1% (Acros Organics AC404720250) in toluene (108325), and

spun for 30secs at 1500rpm. Polystyrene-coated CS stored in a dry place and protected from light, are stable for several weeks.

2.3. PLL-PEG Coating

PLL-PEG 1mg/mL solution (stable for 10 days) was prepared by dissolving poly(L-Lysine)-poly(ethylene-glycol) (PLL-PEG JenKemTechnology ZL187P072) in HEPES (H3375) 10mM, pH 7.4 in MilliQ water.

The PS-coated slides CS were activated by air plasma treatment (Diener electronic), then flipped on 120µL drops of the prepared PLL-PEG solution for at least 30mins at room temperature. After incubation, the CS were lifted using 500µL of HEPES 10mM and rapidly dewetted. The PLL-PEG CS were then stored at 4°C for at least 1 hour (overnight is best) before use.

2.4. Deep UV Micropatterning

PLL-PEG-coated CS were placed on a vacuum holder and put in tight contact with a quartz-chrome printed photomask (Toppan Photomask) previously cleaned with MilliQ water and soap, acetone, and isopropanol in this order. The sandwich was then placed in a pre-warmed UVO cleaner (Model No. 342A-220, Jelight), at a distance of 1cm from the UV lamp with a power of 6mW/cm^2, for 5 min, during which the PLL-PEG layer was burned with deep UV (190nm) through the non-chrome windows of the photomask. After exposure, the patterned CS were gently detached from the mask by vacuum.

2.5. Protein Coating

The protein solution, composed of fibronectin (FN Sigma F1141) 20µg/mL ± Fibrinogen from Human Plasma, Alexa Fluor 546 or 647 Conjugate (FNG Invitrogen F13192 or F35200) 10µg/mL in sodium bicarbonate ($NaHCO_3$ Sigma S6297) 100mM in MilliQ water was prepared. The patterned CS (from the previous step) were flipped on 120µL drops of the prepared protein solution and incubated for 30mins protected from light. After incubation, the patterned CS were lifted using 500µL $NaHCO_3$, washed 3 times with the same buffer, and dewetted. The CS were then washed in sterile DPBS and used directly for seeding cells. Alternatively, they could be stored at 4^{o}C protected from light for several days.

3. TFM Gels Preparation

3.1. Coverslip Silanization

To ensure the attachment of the PAA gels to the CS, the latter were silanized. To do so, the 20x20mm #1.5 CS were first activated by air plasma treatment. Then, they were submerged in a solution of 3-(Trimethoxysilyl)propyl methacrylate (Sigma 440159) 2% (v/v) in absolute ethanol (Carlo Erba 4127022), containing acetic acid (Honeywell 33209) 1% (v/v) for 20mins. After that, the CS were rinsed twice with ethanol to remove residual silane, dried with compressed air, and baked in a pre-warmed oven at 100^{o}C for 1hr. The CS were stored at 4^{o}C and used in gel fabrication for at least 4 months.

3.2. Passivation of Fluorescent Beads

FluoSpheres Carboxylate-Modified 200nm Polystyrene Microspheres (Invitrogen F8810 – 580/605nm or F8807 – 660/680 nm) were passivated by covalent linkage of PLL-PEG as follows.

The stock was first vortexed to disperse the beads. Then, the following solutions, always kept on ice, were prepared:

- Solution 1: 20µL of the bead suspension diluted in 80µL of MES (ROTH Art. No. 4256.4) buffer (10mM, pH = 5.5 in MilliQ water)
- Solution 2: 500µL of PLL-PEG 1mg/mL in HEPES 10mM, pH = 8.5
- Solution 3: 200µL of 1-ethyl-3-(3-dimethylaminopropyl)carbodiimide hydrochloride (EDC Sigma E6383) 8mg/mL in MES 10mM, pH = 5.5
- Solution 4 : 200µL of 16mg/mL of N-Hydroxysuccinimide (NHS Sigma 130672) 16mg/mL in MES 10mM, pH = 5.5

Solutions 1 and 2 were mixed, and beads were sonicated for 30secs. Then, Solutions 3 and 4 were mixed and immediately added to the mix containing the beads and PLL-PEG. This final mixture was vortexed for 30secs, covered in aluminum foil, and allowed to agitate on a rotatory mixer for 1hr at room temperature to complete the covalent linking. After the incubation, the beads were recovered by spinning down the suspension at 13000 rpm (Eppendorf Centrifuge 5420) for 15mins. The supernatant was discarded, and the beads were re-suspended in 2mL of HEPES buffer 10mM, pH = 7.4. This centrifugation step was repeated again to ensure the elimination of all the EDC/NHS and PLL-PEG. After the final spin, the supernatant was discarded, and the beads were re-suspended in 50µL of HEPES buffer 10mM, pH = 7.4 and stored at 4^{o}C until use (stable for 2 weeks).

3.3. Polyacrylaminde Gel Micropatterning

Patterned hydrogels were prepared according to the "Glass Method" previously described in *(Vignaud et al., 2014, Methods in Cell Biology)*. Briefly, 22x22 mm #1.5 glass CS were passivated with PLL-PEG, deep UV-patterned, and coated with adhesive proteins (FN 20µg/mL or a mixture of FN and Col (Collagen I, rat tail Gibco A1048301) 10:10µg/mL) as previously described. A mixture of 40% Acrylamide (Sigma A4058) and 2% Bis-acrylamide (Sigma M1533) in MilliQ water corresponding to an experimental Young modulus of 16.7kPa was prepared, degassed in a vacuum bell during protein incubation, mixed with the passivated 200nm fluorescent beads, sonicated for homogenization, and kept on ice. Ammonium persulfate (APS Sigma A3678) and N,N,N′,N′-Tetramethylethylenediamine (TEMED T9281) were added to the PAA mix. 25µL of the later solution was added on each of the 22x22 mm patterned CS. Silanized 20x20 mm CS were rapidly flipped on top of the PAA drops, and the gel was allowed to polymerize for 40 to 60mins under controlled conditions of temperature and humidity. At the end of the incubation, the sandwiched gels were submerged with $NaHCO_3$ for a few minutes before they were gently detached from the patterned CS using a scalpel. Micropatterned PAA gels were then stored in 35mm Petri plates submerged in $NaHCO_3$ at 4^{0}C until use. Before seeding the cells, the gels were washed twice with sterile DPBS and once with warm medium.

4. PRIMO Micropatterning

New micropattern geometries were designed on Adobe Illustrator and tested using a Nikon eclipse inverted microscope equipped with the Primo Digital Micromirror Device (DMD) (Alveole). The CS to be used underwent the same preparation procedure described previously with some variations. Instead of PLL-PEG, the CS were passivated after plasma activation in 2 steps: Polylysine (PLL Sigma P8920) 0.01% in Milli-Q water for 30mins, followed by PEG-SVA (mPEG-SVA Laysan bio M-SVA-5K) 100mg/mL in HEPES 100mM, pH = 8.5 for 1hr. At the end of the incubation, the CS were rinsed profusely with Milli-Q water and gently air-dried. The CS were then completely covered with a mixture of 3µL of PLPP gel and 0.5µL of surfactant (Alveole) in 30µL of absolute ethanol and left for some time until the ethanol evaporated and a gel was formed. After that, the CS were patterned by the UV laser following the template loaded in Leonardo and the defined parameters of exposure and power. Finally, the CS were repeatedly rinsed with Milli-Q water to fully remove the PLPP gel, coated with adhesive proteins as previously described for shorter time intervals (5 to 15mins), and used for cell seeding.

5. Cytoskeletal Drug Treatments

When used, all the drugs were added to the cells shortly after seeding (30mins) and kept in the medium during the entire time of observation.

Chemical inhibitors used:

- Rho Kinase Inhibitor (Calbiochem 555550) at 3, 7, and 10µM
- Calyculin A (Sigma 208851) at 0.1 and 0.3nM
- Cytochalasin D (Sigma C8273) at 1µg/mL
- Latrunculin A (Sigma L5163) at 10nM
- Formin FH2 Domain Inhibitor, SMIFH2 (Calbiochem 344092) at 2µM

6. Immunoflurescence

Cells were fixed for 10 to 15mins at room temperature in cytoskeleton buffer (CB = MES 10mM, KCl (ROTH Art. No. 6781.1) 138mM, MgCl (ROTH Art. No. KK36.1) 3mM, EGTA (Sigma E0396) 2mM in Milli-Q water) supplemented with Sucrose (ROTH Art. No. 4661.2) 10%, Triton-X100 (EUROMEDEX 3617818) 0.1%, Glutaraldehyde (Polysciences 00216) 0.1%, and Paraformaldehyde 4% (Electron Microscopy Sciences 15710). When staining for p-MLC, fixation was preceded by a brief prepermeabilization step using Triton-X100 0.05% in CB supplemented with Glycerol (Carlo Erba 453742) 10%. The CS were rinsed 3 times with PBS. Aldehyde functions were then reduced using sodium borohydride ($NaBH_4$ Sigma 452882) 1mg/ml in PBS for 10mins at room temperature and washed 3 times with PBS. The blocking solution (Bovine Serum Albumin (BSA A7030) 3% - Tween-20 (Sigma P2287) 0.1% - PBS) was then added for 45 min at room temperature. After that, the CS were successively incubated with the primary and secondary antibodies diluted in the blocking solution for 1hr each at room temperature. After both incubations, the CS were rinsed 3 times using PBS-Tween 0.1%. Then, the CS were labelled with a mixture containing Phalloidin Alexa Fluor 488 (Invitrogen A12379) and Hoechst (Invitrogen

H3570) diluted in the blocking solution. Finally, the slides were rinsed 3 times in PBS-Tween 0.1%, once in PBS, and once in Milli-Q water and were then mounted in Mowiol 4-88.

Primary Antibodies used:

- Rabbit Anti- Phospho-Myosin Light Chain 2 (Ser19) Antibody (Cell Signaling 3671) at 1/100
- Rabbit Anti-Giantin Antibody - Golgi Marker (Abcam ab80864) at 1/500
- Mouse Anti-γ-Tubulin Antibody (Sigma T6557) at 1/500
- Mouse Anti-Vinculin Antibody (Sigma V9131) at 1/500

Secondary Antibodies used:

- Goat anti-Rabbit IgG Alexa Fluor 546 (Invitrogen A11035) at 1/500
- Goat anti-Rabbit IgG Alexa Fluor 647 (Invitrogen A21245) at 1/500
- Goat anti-Mouse IgG Alexa Fluor 546 (Invitrogen A11030) at 1/500
- Goat anti-Mouse IgG Alexa Fluor 546 (Invitrogen A21236) at 1/500

Adapted from Alexandre Schaeffer

7. Cell Enucleation

HUVECs cells were seeded on RINZL slides (DELTA Microscopies) coated with fibronectin and collagen (both at 10µg/mL) and incubated for at least 24hrs until reaching 90% confluence. Prior to enucleation, cells were incubated for 20mins at 37°C in the enucleation buffer (Cytochalasin-D at 1µg/mL in culture medium). Cells were then enucleated inside the enucleation buffer using high-speed centrifugation (13000 RPM) for 25 min at 37°C, performed in Avanti J-26 XP, Beckman Coulter centrifuge equipped with a swinging rotor (JS-13.1, Beckman Coulter). After enucleation, the slides were rinsed with fresh medium every 3mins for 12mins and then placed in the incubator for at least 4hrs to allow the cytoplasts to recover. After that, the cytoplasts were detached and seeded on micropatterns for further experiments.

8. Image Acquisition

Traction force mapping and some of the live experiments were performed on a Nikon confocal spinning-disk system (Eclipse Ti-E) equipped with a CSUX1-A1 Yokogawa confocal head, an Evolve EMCCD camera from Gataca Systems, and a top stage incubator for controlled temperature 37^{O}C and CO_2 5% (TOKAI). The microscope was operated using MetaMorph software. A Phase Contrast 40X (air) or 40X oil objectives were used for the acquisition of images and movies.

Most of the live acquisitions were carried out on an epifluorescence system consisting of a Ti2 Nikon inverted microscope equipped with a Prime BSI Express Camera (Photometrics), a CoolLED pE-4000 Fluo lamp, and a top stage incubator for controlled temperature 37^{O}C and CO_2 5% (Okolab). The following objectives were used: 4X Phase Contrast, 20X DIC, and 40X DIC. Time-lapse courses were followed using the NIS elements software.

Images of the different immunofluorescence stainings were acquired on a Zeiss LSM900 Airyscan 2 confocal microscope (Axio Observer) using 63X objective (Plan-Apochromat 63X/1.4 oil).

In all the cases, only cells that were well fully spread on the micropatterns were selected for imaging.

9. TFM Analysis

Following the method previously described by *(Martiel et al., 2015, Methods in Cell Biology)*, TFM data was analyzed in Fiji ImageJ using a homemade macro that takes advantage of a set of plugins (PIV and FTTC) *(ImageJ plugins by Qingzong TSENG)*. Displacement fields were obtained from fluorescent bead images before and after the detachment of the cells by trypsin treatment. Bead images were paired and realigned with a macro that had a subpixel accuracy (template matching). Displacement fields were calculated by particle imaging velocimetry, which used a normalized cross correlation–based method with an iterative scheme. Final vector-grid size was 4.6μm × 4.6μm.

The TFM analysis was performed in two steps. First, Fourier-transform traction cytometry was used to compute the traction force field, with a regularization parameter of 5×10^{-10}, Poisson coefficient of 0.5, and a Young Modulus of 16.7kPa. A circular region of interest was defined around the doublets, such that its area was larger than that of the micropattern (ROI ∼93μm in diameter). Force vectors located outside this ROI were discarded during the calculation of the doublets stored mechanical energy.

The second step consisted of extracting the magnitude of forces exerted by individual cells as well as the intercellular force, using another homemade macro that repossessed the previously generated traction force files and energy maps based on the manual definition of the cell-cell junction at every time point *(Maruthamuthu et al., 2011, Proceedings of the National Academy of Sciences)*. Briefly, the defined force region was split at the junction into two areas, and then the corresponding forces were assessed. The sum of the TF vectors under each area represented the imbalance or the intercellular force. As the sum of TFs in a doublet was zero (mechanical equilibrium), the imbalance across both cells was the equal in magnitude and opposite in direction.

In the process, the junction was fitted into an ellipse, whose long axis was rescaled to the size of the pattern and used to compute the instantaneous angular displacement that provided both the direction and magnitude of doublet angular velocity.

10. Image Analysis

Analyses were performed using Fiji ImageJ software.

10.1. Nuclei Tracking

A threshold was first applied to the two detected nuclei and a binary mask was created. The nuclei were then tracked during the rotation of the doublets by minimal distance between two time points. The tracking process was semi-automatized, as the user had to interfere in certain cases to refine the detection of the nuclei (if less or more than two nuclei were detected by the macro).

10.2. Biochemical Composition of Doublets

For each set of z-stacks, the focal plane was first defined by the user. A sum-intensity projection of six z-slices (~3µm) starting from the focal plane was done for the F-actin and p-MLC signals. On the other hand, a maximum-intensity projection of only two z-slices starting from the focal plane was done for vinculin signal. The actin signal was thresholded and used to create a mask for each doublet. After that, a threshold was set for the vinculin signal, and the detected FAs were subjected to a second selection based on size; all FAs that were less than 4 pixels in size were eliminated. To isolate the signal of the proteins for each individual cell, a polyline was drawn by the user to outline the junction between the two cells of each doublet. Finally, the background signal arising from the auto-fluorescence of the pattern was eliminated by normalizing the detected signals in all the wavelengths using a reference micropattern generated by superimposing at least 10 empty patterns with no cell attached.

10.3. Polarity Axes in Single Cells

The actin signal of each cell was used to create a mask and define the cell's symmetry axis. For motile cells, the actin signals were fit to circles whose diameters represented the corresponding symmetry axes. Subsequently, the resulting symmetry axes of all the cells were aligned with the horizontal. Then, the coordinates of the centroids of the actin, nucleus, centrosome, and Golgi were retrieved. After that, the angles between the horizontal and the axes joining the centroid of the nucleus to that of either the centrosome or the Golgi were computed. The computed angles were used to construct heat maps of the contours of all the cells aligned on the actin centroid, showing the distribution of the positions of the nucleus, centrosome, and the Golgi. In addition, vector plots were created by aligning all the cells on the nucleus centroid.

11. Data representation and Statistical Analysis

Energy maps, heat maps, and vector plots were created in Fiji ImageJ.

Data plotting, graph design, frequency distributions, and probability distributions were done on Graphpad Prism 8 (www.graphpad.com).

Statistical analysis for individual control experiments were performed in R or MATLAB, in which the proportions of CW and CCW doublets were tested to determine if they were significantly different from 50:50.

The other statistical tests used throughout the study (t-test, Mann-Whitney, Chi-square (Fisher exact) test…) were done on Graphpad Prism 8.

XIII. BIBLIOGRAPHY

Abe, M., & Kuroda, R. (2019). The development of CRISPR for a mollusc establishes the formin Lsdia1 as the long-sought gene for snail dextral/sinistral coiling. *Development*, *146*(9), dev175976. https://doi.org/10.1242/dev.175976

Abu Shah, E., & Keren, K. (2014). Symmetry breaking in reconstituted actin cortices. *ELife*, *3*, e01433. https://doi.org/10.7554/eLife.01433

Alberts, B. (2017). *Molecular Biology of the Cell*. Garland Science.

Ali, M. Y., Uemura, S., Adachi, K., Itoh, H., Kinosita, K., & Ishiwata, S. (2002). Myosin V is a left-handed spiral motor on the right-handed actin helix. *Nature Structural Biology*, *9*(6), 464–467. https://doi.org/10.1038/nsb803

Alieva, N. O., Efremov, A. K., Hu, S., Oh, D., Chen, Z., Natarajan, M., Ong, H. T., Jégou, A., Romet-Lemonne, G., Groves, J. T., Sheetz, M. P., Yan, J., & Bershadsky, A. D. (2019). Myosin IIA and formin dependent mechanosensitivity of filopodia adhesion. *Nature Communications*, *10*(1), 3593. https://doi.org/10.1038/s41467-019-10964-w

Alvarado, J., Sheinman, M., Sharma, A., MacKintosh, F. C., & Koenderink, G. H. (2013). Molecular motors robustly drive active gels to a critically connected state. *Nature Physics*, *9*(9), 591–597. https://doi.org/10.1038/nphys2715

Anilkumar, N., Parsons, M., Monk, R., Ng, T., & Adams, J. C. (2003). Interaction of fascin and protein kinase Cα: A novel intersection in cell adhesion and motility. *The EMBO Journal*, *22*(20), 5390–5402. https://doi.org/10.1093/emboj/cdg521

Aumeier, C., Schaedel, L., Gaillard, J., John, K., Blanchoin, L., & Théry, M. (2016). Self-repair promotes microtubule rescue. *Nature Cell Biology*, *18*(10), 1054–1064. https://doi.org/10.1038/ncb3406

Azpeitia, E., Tichtinsky, G., Le Masson, M., Serrano-Mislata, A., Lucas, J., Gregis, V., Gimenez, C., Prunet, N., Farcot, E., Kater, M. M., Bradley, D., Madueño, F., Godin, C., & Parcy, F. (2021). Cauliflower fractal forms arise from perturbations of floral gene networks. *Science*, *373*(6551), 192–197. https://doi.org/10.1126/science.abg5999

Balan, A., Lazoura, O., Padley, S. P., Rubens, M., & Nicol, E. D. (2012). Atrial isomerism: A pictorial review. *Journal of Cardiovascular Computed Tomography*, *6*(2), 127–136. https://doi.org/10.1016/j.jcct.2011.10.019

Bamburg, J. r., Harris, H. e., & Weeds, A. g. (1980). Partial purification and characterization of an actin depolymerizing factor from brain. *FEBS Letters*, *121*(1), 178–182. https://doi.org/10.1016/0014-5793(80)81292-0

Bao, Y., Wu, S., Chu, L. T., Kwong, H. K., Hartanto, H., Huang, Y., Lam, M. L., Lam, R. H. W., & Chen, T.-H. (2020). Early Committed Clockwise Cell Chirality Upregulates Adipogenic Differentiation of Mesenchymal Stem Cells. *Advanced Biosystems*, *4*(10), 2000161. https://doi.org/10.1002/adbi.202000161

Barnhart, E. L., Lee, K.-C., Keren, K., Mogilner, A., & Theriot, J. A. (2011). An Adhesion-Dependent Switch between Mechanisms That Determine Motile Cell Shape. *PLOS Biology*, *9*(5), e1001059. https://doi.org/10.1371/journal.pbio.1001059

Bazellières, E., Conte, V., Elosegui-Artola, A., Serra-Picamal, X., Bintanel-Morcillo, M., Roca-Cusachs, P., Muñoz, J. J., Sales-Pardo, M., Guimerà, R., & Trepat, X. (2015). Control of cell–cell forces and collective cell dynamics by the intercellular adhesome. *Nature Cell Biology*, *17*(4), 409–420. https://doi.org/10.1038/ncb3135

Begnaud, S., Chen, T., Delacour, D., Mège, R.-M., & Ladoux, B. (2016). Mechanics of epithelial tissues during gap closure. *Current Opinion in Cell Biology*, *42*, 52–62. https://doi.org/10.1016/j.ceb.2016.04.006

Bendix, P. M., Koenderink, G. H., Cuvelier, D., Dogic, Z., Koeleman, B. N., Brieher, W. M., Field, C. M., Mahadevan, L., & Weitz, D. A. (2008). A Quantitative Analysis of Contractility in Active Cytoskeletal Protein Networks. *Biophysical Journal*, *94*(8), 3126–3136. https://doi.org/10.1529/biophysj.107.117960

Bernstein, B. W., & Bamburg, J. R. (2010). ADF/Cofilin: A functional node in cell biology. *Trends in Cell Biology*, *20*(4), 187–195. https://doi.org/10.1016/j.tcb.2010.01.001

Blanchoin, L., Boujemaa-Paterski, R., Sykes, C., & Plastino, J. (2014). Actin Dynamics, Architecture, and Mechanics in Cell Motility. *Physiological Reviews*, *94*(1), 235–263. https://doi.org/10.1152/physrev.00018.2013

Blanchoin, L., & Pollard, T. D. (2002). Hydrolysis of ATP by Polymerized Actin Depends on the Bound Divalent Cation but Not Profilin. *Biochemistry*, *41*(2), 597–602. https://doi.org/10.1021/bi011214b

Brown, N. A., & Wolpert, L. (1990). The development of handedness in left/right asymmetry. *Development*, *109*(1), 1–9. https://doi.org/10.1242/dev.109.1.1

Brücker, L., Kretschmer, V., & May-Simera, H. L. (2020). The entangled relationship between cilia and actin. *The International Journal of Biochemistry & Cell Biology*, *129*, 105877. https://doi.org/10.1016/j.biocel.2020.105877

Brueckner, M. (2007). Heterotaxia, Congenital Heart Disease, and Primary Ciliary Dyskinesia. *Circulation*, *115*(22), 2793–2795. https://doi.org/10.1161/CIRCULATIONAHA.107.699256

Burke, T. A., Christensen, J. R., Barone, E., Suarez, C., Sirotkin, V., & Kovar, D. R. (2014). Homeostatic Actin Cytoskeleton Networks Are Regulated by Assembly Factor Competition for Monomers. *Current Biology*, *24*(5), 579–585. https://doi.org/10.1016/j.cub.2014.01.072

Burute, M., Prioux, M., Blin, G., Truchet, S., Letort, G., Tseng, Q., Bessy, T., Lowell, S., Young, J., Filhol, O., & Théry, M. (2017). Polarity Reversal by Centrosome Repositioning Primes Cell Scattering during Epithelial-to-Mesenchymal Transition. *Developmental Cell*, *40*(2), 168–184. https://doi.org/10.1016/j.devcel.2016.12.004

Cai, D., Chen, S.-C., Prasad, M., He, L., Wang, X., Choesmel-Cadamuro, V., Sawyer, J. K., Danuser, G., & Montell, D. J. (2014). Mechanical Feedback through E-Cadherin Promotes Direction Sensing during Collective Cell Migration. *Cell*, *157*(5), 1146–1159. https://doi.org/10.1016/j.cell.2014.03.045

Camley, B. A., Zhang, Y., Zhao, Y., Li, B., Ben-Jacob, E., Levine, H., & Rappel, W.-J. (2014). Polarity mechanisms such as contact inhibition of locomotion regulate persistent rotational motion of mammalian cells on micropatterns. *Proceedings of the National Academy of Sciences*, *111*(41), 14770–14775. https://doi.org/10.1073/pnas.1414498111

Can, S., Dewitt, M. A., & Yildiz, A. (2014). Bidirectional helical motility of cytoplasmic dynein around microtubules. *ELife*, *3*, e03205. https://doi.org/10.7554/eLife.03205

Chang, Y.-C., Nalbant, P., Birkenfeld, J., Chang, Z.-F., & Bokoch, G. M. (2008). GEF-H1 Couples Nocodazole-induced Microtubule Disassembly to Cell Contractility via RhoA. *Molecular Biology of the Cell*, *19*(5), 2147–2153. https://doi.org/10.1091/mbc.e07-12-1269

Chen, T., Callan-Jones, A., Fedorov, E., Ravasio, A., Brugués, A., Ong, H. T., Toyama, Y., Low, B. C., Trepat, X., Shemesh, T., Voituriez, R., & Ladoux, B. (2019). Large-scale curvature sensing by directional actin flow drives cellular migration mode switching. *Nature Physics*, *15*(4), 393–402. https://doi.org/10.1038/s41567-018-0383-6

Chen, T.-H., Hsu, J. J., Zhao, X., Guo, C., Wong, M. N., Huang, Y., Li, Z., Garfinkel, A., Ho, C.-M., Tintut, Y., & Demer, L. L. (2012). Left-Right Symmetry Breaking in Tissue Morphogenesis via Cytoskeletal Mechanics. *Circulation Research*, *110*(4), 551–559. https://doi.org/10.1161/CIRCRESAHA.111.255927

Cheney, R. E., O'Shea, M. K., Heuser, J. E., Coelho, M. V., Wolenski, J. S., Espreafico, E. M., Forscher, P., Larson, R. E., & Mooseker, M. S. (1993). Brain myosin-V is a two-headed unconventional myosin with motor activity. *Cell*, *75*(1), 13–23. https://doi.org/10.1016/S0092-8674(05)80080-7

Cheng, H., & Leblond, C. P. (1974). Origin, differentiation and renewal of the four main epithelial cell types in the mouse small intestine. I. Columnar cell. *The American Journal of Anatomy*, *141*(4), 461–479. https://doi.org/10.1002/aja.1001410403

Chin, A. S., Worley, K. E., Ray, P., Kaur, G., Fan, J., & Wan, L. Q. (2018). Epithelial Cell Chirality Revealed by Three-Dimensional Spontaneous Rotation. *Proceedings of the National Academy of Sciences*, *115*(48), 12188–12193. https://doi.org/10.1073/pnas.1805932115

Chou, S. Z., & Pollard, T. D. (2019). Mechanism of actin polymerization revealed by cryo-EM structures of actin filaments with three different bound nucleotides. *Proceedings of the National Academy of Sciences*, *116*(10), 4265–4274. https://doi.org/10.1073/pnas.1807028115

Chougule, A., Lapraz, F., Földi, I., Cerezo, D., Mihály, J., & Noselli, S. (2020). The Drosophila actin nucleator DAAM is essential for left-right asymmetry. *PLOS Genetics*, *16*(4), e1008758. https://doi.org/10.1371/journal.pgen.1008758

Chrzanowska-Wodnicka, M., & Burridge, K. (1996). Rho-stimulated contractility drives the formation of stress fibers and focal adhesions. *Journal of Cell Biology*, *133*(6), 1403–1415. https://doi.org/10.1083/jcb.133.6.1403

Claessens, M. M. A. E., Semmrich, C., Ramos, L., & Bausch, A. R. (2008). Helical twist controls the thickness of F-actin bundles. *Proceedings of the National Academy of Sciences*, *105*(26), 8819–8822. https://doi.org/10.1073/pnas.0711149105

Clothilde Utzschneider, Bhagyanath Suresh, Alfredo Sciortino, Jeremie Gaillard, Alexandre Schaeffer, Sudipta Pattanayak, Jean-Francois Joanny, Laurent Blanchoin, & Manuel Thery. (n.d.). Force balance of opposing diffusive motors generates polarity-sorted microtubule patterns. *Under Revision*.

Colin, A., Kotila, T., Guérin, C., Orhant-Prioux, M., Vianay, B., Mogilner, A., Lappalainen, P., Théry, M., & Blanchoin, L. (2023). Recycling of the actin monomer pool limits the lifetime of network turnover. *The EMBO Journal*, *42*(9), e112717. https://doi.org/10.15252/embj.2022112717

Cowan, C. R., & Hyman, A. A. (2004). Asymmetric cell division in C. elegans: Cortical polarity and spindle positioning. *Annual Review of Cell and Developmental Biology*, *20*, 427–453. https://doi.org/10.1146/annurev.cellbio.19.111301.113823

Crevenna, A. H., Naredi-Rainer, N., Schönichen, A., Dzubiella, J., Barber, D. L., Lamb, D. C., & Wedlich-Söldner, R. (2013). Electrostatics Control Actin Filament Nucleation and Elongation Kinetics*. *Journal of Biological Chemistry*, *288*(17), 12102–12113. https://doi.org/10.1074/jbc.M113.456327

Cuenca, A. A., Schetter, A., Aceto, D., Kemphues, K., & Seydoux, G. (2003). Polarization of the C. elegans zygote proceeds via distinct establishment and maintenance phases. *Development*, *130*(7), 1255–1265. https://doi.org/10.1242/dev.00284

Danilchik, M. V., Brown, E. E., & Riegert, K. (2006). Intrinsic chiral properties of the Xenopus egg cortex: An early indicator of left-right asymmetry? *Development*, *133*(22), 4517–4526. https://doi.org/10.1242/dev.02642

Davison, A., McDowell, G. S., Holden, J. M., Johnson, H. F., Koutsovoulos, G. D., Liu, M. M., Hulpiau, P., Van Roy, F., Wade, C. M., Banerjee, R., Yang, F., Chiba, S., Davey, J. W., Jackson, D. J., Levin, M., & Blaxter, M. L. (2016). Formin Is Associated with Left-Right Asymmetry in the Pond Snail and the Frog. *Current Biology*, *26*(5), 654–660. https://doi.org/10.1016/j.cub.2015.12.071

Desai, R. A., Gao, L., Raghavan, S., Liu, W. F., & Chen, C. S. (2009). Cell polarity triggered by cell-cell adhesion via E-cadherin. *Journal of Cell Science*, *122*(7), 905–911. https://doi.org/10.1242/jcs.028183

du Roure, O., Saez, A., Buguin, A., Austin, R. H., Chavrier, P., Siberzan, P., & Ladoux, B. (2005). Force mapping in epithelial cell migration. *Proceedings of the National Academy of Sciences*, *102*(7), 2390–2395. https://doi.org/10.1073/pnas.0408482102

Ennomani, H., Letort, G., Guérin, C., Martiel, J.-L., Cao, W., Nédélec, F., De La Cruz, E. M., Théry, M., & Blanchoin, L. (2016). Architecture and Connectivity Govern Actin Network

Contractility. *Current Biology*, *26*(5), 616–626. https://doi.org/10.1016/j.cub.2015.12.069

Esue, O., Harris, E. S., Higgs, H. N., & Wirtz, D. (2008). The Filamentous Actin Cross-Linking/Bundling Activity of Mammalian Formins. *Journal of Molecular Biology*, *384*(2), 324–334. https://doi.org/10.1016/j.jmb.2008.09.043

Fan, J., Ray, P., Lu, Y. W., Kaur, G., Schwarz, J. J., & Wan, L. Q. (2018). Cell chirality regulates intercellular junctions and endothelial permeability. *Science Advances*, *4*(10), eaat2111. https://doi.org/10.1126/sciadv.aat2111

Farooqui, R., & Fenteany, G. (2005). Multiple rows of cells behind an epithelial wound edge extend cryptic lamellipodia to collectively drive cell-sheet movement. *Journal of Cell Science*, *118*(1), 51–63. https://doi.org/10.1242/jcs.01577

Fernández-Muñoz, B., Yurrita, M. M., Martín-Villar, E., Carrasco-Ramírez, P., Megías, D., Renart, J., & Quintanilla, M. (2011). The transmembrane domain of podoplanin is required for its association with lipid rafts and the induction of epithelial-mesenchymal transition. *The International Journal of Biochemistry & Cell Biology*, *43*(6), 886–896. https://doi.org/10.1016/j.biocel.2011.02.010

Finer, J. T., Simmons, R. M., & Spudich, J. A. (1994). Single myosin molecule mechanics: Piconewton forces and nanometre steps. *Nature*, *368*(6467), 113–119. https://doi.org/10.1038/368113a0

Frye, K., Renda, F., Fomicheva, M., Zhu, X., Gong, L., Khodjakov, A., & Kaverina, I. (2020). Cell Cycle-Dependent Dynamics of the Golgi-Centrosome Association in Motile Cells. *Cells*, *9*(5), 1069. https://doi.org/10.3390/cells9051069

Fujii, T., Iwane, A. H., Yanagida, T., & Namba, K. (2010). Direct visualization of secondary structures of F-actin by electron cryomicroscopy. *Nature*, *467*(7316), 724–728. https://doi.org/10.1038/nature09372

Fujiwara, I., Zweifel, M. E., Courtemanche, N., & Pollard, T. D. (2018). Latrunculin A Accelerates Actin Filament Depolymerization in Addition to Sequestering Actin Monomers. *Current Biology*, *28*(19), 3183-3192.e2. https://doi.org/10.1016/j.cub.2018.07.082

Galkin, V. E., Orlova, A., Kudryashov, D. S., Solodukhin, A., Reisler, E., Schröder, G. F., & Egelman, E. H. (2011). Remodeling of actin filaments by ADF/cofilin proteins. *Proceedings of the National Academy of Sciences*, *108*(51), 20568–20572. https://doi.org/10.1073/pnas.1110109108

Gardner, M. K., Zanic, M., & Howard, J. (2013). Microtubule Catastrophe and Rescue. *Current Opinion in Cell Biology*, *25*(1), 14–22. https://doi.org/10.1016/j.ceb.2012.09.006

George, A. B., & Korolev, K. S. (2018). Chirality provides a direct fitness advantage and facilitates intermixing in cellular aggregates. *PLOS Computational Biology*, *14*(12), e1006645. https://doi.org/10.1371/journal.pcbi.1006645

Giaime, E., Caballero, E., Núñez, L., Song, Z., Chan, D., Villalobos, C., & Shen, J. (2012). Regulation of mitochondrial permeability transition pore by PINK1. *Molecular Neurodegeneration*, *7*, 22. https://doi.org/10.1186/1750-1326-7-22

Glentis, A., Blanch-Mercader, C., Balasubramaniam, L., Saw, T. B., d'Alessandro, J., Janel, S., Douanier, A., Delaval, B., Lafont, F., Lim, C. T., Delacour, D., Prost, J., Xi, W., & Ladoux, B. (2022). The emergence of spontaneous coordinated epithelial rotation on cylindrical curved surfaces. *Science Advances*, *8*(37), eabn5406. https://doi.org/10.1126/sciadv.abn5406

Gönczy, P. (2008). Mechanisms of asymmetric cell division: Flies and worms pave the way. *Nature Reviews Molecular Cell Biology*, *9*(5), 355–366. https://doi.org/10.1038/nrm2388

Goodwin, K., Lostchuck, E. E., Cramb, K. M. L., Zulueta-Coarasa, T., Fernandez-Gonzalez, R., & Tanentzapf, G. (2017). Cell–cell and cell–extracellular matrix adhesions cooperate to organize actomyosin networks and maintain force transmission during dorsal closure. *Molecular Biology of the Cell*, *28*(10), 1301–1310. https://doi.org/10.1091/mbc.e17-01-0033

Graham, D. M., Andersen, T., Sharek, L., Uzer, G., Rothenberg, K., Hoffman, B. D., Rubin, J., Balland, M., Bear, J. E., & Burridge, K. (2018). Enucleated cells reveal differential roles of the nucleus in cell migration, polarity, and mechanotransduction. *Journal of Cell Biology*, *217*(3), 895–914. https://doi.org/10.1083/jcb.201706097

Gros, J., Feistel, K., Viebahn, C., Blum, M., & Tabin, C. J. (2009). Cell Movements at Hensen's Node Establish Left/Right Asymmetric Gene Expression in the Chick. *Science*, *324*(5929), 941–944. https://doi.org/10.1126/science.1172478

Gros, O. J., Damstra, H. G. J., Kapitein, L. C., Akhmanova, A., & Berger, F. (2021). Dynein self-organizes while translocating the centrosome in T-cells. *Molecular Biology of the Cell*, *32*(9), 855–868. https://doi.org/10.1091/mbc.E20-10-0668

Gundersen, G. G., & Bulinski, J. C. (1988). Selective stabilization of microtubules oriented toward the direction of cell migration. *Proceedings of the National Academy of Sciences*, *85*(16), 5946–5950. https://doi.org/10.1073/pnas.85.16.5946

Gupton, S. L., & Waterman-Storer, C. M. (2006). Spatiotemporal Feedback between Actomyosin and Focal-Adhesion Systems Optimizes Rapid Cell Migration. *Cell*, *125*(7), 1361–1374. https://doi.org/10.1016/j.cell.2006.05.029

Hachem, Z., Hadrian, C., Aldbaisi, L., Alkaabi, M., Wan, L. Q., & Fan, J. (2024). Asymmetrical positioning of cell organelles reflects the cell chirality of mouse myoblast cells. *APL Bioengineering*, *8*(1). https://doi.org/10.1063/5.0189401

Hang, B., Jassem, E., Mohammed, H., Wan, L. Q., Herschkowitz, J. I., & Fan, J. (2022). Interacting with tumor cells weakens the intrinsic clockwise chirality of endothelial cells. *APL Bioengineering*, *6*(4), 046107. https://doi.org/10.1063/5.0115827

Hao, Y., Boyd, L., & Seydoux, G. (2006). Stabilization of Cell Polarity by the *C. elegans* RING Protein PAR-2. *Developmental Cell*, *10*(2), 199–208. https://doi.org/10.1016/j.devcel.2005.12.015

Hartman, M. A., & Spudich, J. A. (2012). The myosin superfamily at a glance. *Journal of Cell Science*, *125*(7), 1627–1632. https://doi.org/10.1242/jcs.094300

Hatori, R., Ando, T., Sasamura, T., Nakazawa, N., Nakamura, M., Taniguchi, K., Hozumi, S., Kikuta, J., Ishii, M., & Matsuno, K. (2014). Left–right asymmetry is formed in individual cells by intrinsic cell chirality. *Mechanisms of Development*, *133*, 146–162. https://doi.org/10.1016/j.mod.2014.04.002

Hayer, A., Shao, L., Chung, M., Joubert, L.-M., Yang, H. W., Tsai, F.-C., Bisaria, A., Betzig, E., & Meyer, T. (2016). Engulfed cadherin fingers are polarized junctional structures between collectively migrating endothelial cells. *Nature Cell Biology*, *18*(12), 1311–1323. https://doi.org/10.1038/ncb3438

Henson, J. H., Yeterian, M., Weeks, R. M., Medrano, A. E., Brown, B. L., Geist, H. L., Pais, M. D., Oldenbourg, R., & Shuster, C. B. (2015). Arp2/3 complex inhibition radically alters lamellipodial actin architecture, suspended cell shape, and the cell spreading process. *Molecular Biology of the Cell*, *26*(5), 887–900. https://doi.org/10.1091/mbc.E14-07-1244

Hernández, A. M. P., Tenje, M., & Antfolk, M. (2022). Cell chirality exhibition of brain microvascular endothelial cells is dependent on micropattern width. *RSC Advances*, *12*(46), 30135–30144. https://doi.org/10.1039/D2RA05434E

Heussinger, C., & Grason, G. M. (2011). Theory of crosslinked bundles of helical filaments: Intrinsic torques in self-limiting biopolymer assemblies. *The Journal of Chemical Physics*, *135*(3), 035104. https://doi.org/10.1063/1.3610431

Heuzé, M. L., Sankara Narayana, G. H. N., D'Alessandro, J., Cellerin, V., Dang, T., Williams, D. S., Van Hest, J. C., Marcq, P., Mège, R.-M., & Ladoux, B. (2019). Myosin II isoforms play distinct roles in adherens junction biogenesis. *ELife*, *8*, e46599. https://doi.org/10.7554/eLife.46599

Higashida, C., Miyoshi, T., Fujita, A., Oceguera-Yanez, F., Monypenny, J., Andou, Y., Narumiya, S., & Watanabe, N. (2004). Actin Polymerization-Driven Molecular Movement of mDia1 in Living Cells. *Science*, *303*(5666), 2007–2010. https://doi.org/10.1126/science.1093923

Holinstat, M., Mehta, D., Kozasa, T., Minshall, R. D., & Malik, A. B. (2003). Protein Kinase Cα-Induced p115RhoGEF Phosphorylation Signals Endothelial Cytoskeletal Rearrangement*. *Journal of Biological Chemistry*, *278*(31), 28793–28798. https://doi.org/10.1074/jbc.M303900200

Holmes, K. C., Popp, D., Gebhard, W., & Kabsch, W. (1990). Atomic model of the actin filament. *Nature*, *347*(6288), 44–49. https://doi.org/10.1038/347044a0

Hong, Y. (2018). aPKC: The Kinase that Phosphorylates Cell Polarity. *F1000Research*, *7*, F1000 Faculty Rev-903. https://doi.org/10.12688/f1000research.14427.1

Howard, J. (1997). Molecular motors: Structural adaptations to cellular functions. *Nature*, *389*(6651), 561–567. https://doi.org/10.1038/39247

Hozumi, S., Maeda, R., Taniguchi, K., Kanai, M., Shirakabe, S., Sasamura, T., Spéder, P., Noselli, S., Aigaki, T., Murakami, R., & Matsuno, K. (2006). An unconventional myosin in Drosophila reverses the default handedness in visceral organs. *Nature*, *440*(7085), 798–802. https://doi.org/10.1038/nature04625

Huang, S., Brangwynne, C. P., Parker, K. K., & Ingber, D. E. (2005). Symmetry-breaking in mammalian cell cohort migration during tissue pattern formation: Role of random-walk persistence. *Cell Motility and the Cytoskeleton*, *61*(4), 201–213. https://doi.org/10.1002/cm.20077

Ierushalmi, N., & Keren, K. (2021). Cytoskeletal symmetry breaking in animal cells. *Current Opinion in Cell Biology*, *72*, 91–99. https://doi.org/10.1016/j.ceb.2021.07.003

ImageJ plugins by Qingzong TSENG. (n.d.). Retrieved May 10, 2024, from https://sites.google.com/site/qingzongtseng/imagejplugins

Ingerman, E., Hsiao, J. Y., & Mullins, R. D. (2013). Arp2/3 complex ATP hydrolysis promotes lamellipodial actin network disassembly but is dispensable for assembly. *Journal of Cell Biology*, *200*(5), 619–633. https://doi.org/10.1083/jcb.201211069

Isomursu, A., Alanko, J., Hernández-Pérez, S., Saukkonen, K., Saari, M., Mattila, P. K., & Ivaska, J. (2024). Dynamic Micropatterning Reveals Substrate-Dependent Differences in the Geometric Control of Cell Polarization and Migration. *Small Methods*, *8*(1), 2300719. https://doi.org/10.1002/smtd.202300719

Jain, S., Cachoux, V. M. L., Narayana, G. H. N. S., de Beco, S., D'Alessandro, J., Cellerin, V., Chen, T., Heuzé, M. L., Marcq, P., Mège, R.-M., Kabla, A. J., Lim, C. T., & Ladoux, B. (2020). The role of single-cell mechanical behaviour and polarity in driving collective cell migration. *Nature Physics*, *16*(7), 802–809. https://doi.org/10.1038/s41567-020-0875-z

Jaiswal, R., Breitsprecher, D., Collins, A., Corrêa, I. R., Xu, M.-Q., & Goode, B. L. (2013). The Formin Daam1 and Fascin Directly Collaborate to Promote Filopodia Formation. *Current Biology*, *23*(14), 1373–1379. https://doi.org/10.1016/j.cub.2013.06.013

Jalal, S., Shi, S., Acharya, V., Huang, R. Y.-J., Viasnoff, V., Bershadsky, A. D., & Tee, Y. H. (2019a). Actin cytoskeleton self-organization in single epithelial cells and fibroblasts under isotropic confinement. *Journal of Cell Science*, *132*(5). https://doi.org/10.1242/jcs.220780

Jalal, S., Shi, S., Acharya, V., Huang, R. Y.-J., Viasnoff, V., Bershadsky, A. D., & Tee, Y. H. (2019b). Actin cytoskeleton self-organization in single epithelial cells and fibroblasts under isotropic confinement. *Journal of Cell Science*, *132*(5), jcs220780. https://doi.org/10.1242/jcs.220780

Jégou, A., Carlier, M.-F., & Romet-Lemonne, G. (2013). Formin mDia1 senses and generates mechanical forces on actin filaments. *Nature Communications*, *4*(1), 1883. https://doi.org/10.1038/ncomms2888

Jegou, A., & Romet-Lemonne, G. (2020). The many implications of actin filament helicity. *Seminars in Cell & Developmental Biology*, *102*, 65–72. https://doi.org/10.1016/j.semcdb.2019.10.018

Jenkins, N., Saam, J. R., & Mango, S. E. (2006). CYK-4/GAP Provides a Localized Cue to Initiate Anteroposterior Polarity upon Fertilization. *Science*, *313*(5791), 1298–1301. https://doi.org/10.1126/science.1130291

Jimenez, A. J., Schaeffer, A., De Pascalis, C., Letort, G., Vianay, B., Bornens, M., Piel, M., Blanchoin, L., & Théry, M. (2021). Acto-myosin network geometry defines centrosome position. *Current Biology*, *31*(6), 1206-1220.e5. https://doi.org/10.1016/j.cub.2021.01.002

Juan, T., Géminard, C., Coutelis, J.-B., Cerezo, D., Polès, S., Noselli, S., & Fürthauer, M. (2018). Myosin1D is an evolutionarily conserved regulator of animal left–right asymmetry. *Nature Communications*, *9*(1), 1942. https://doi.org/10.1038/s41467-018-04284-8

Jurado, C., Haserick, J. R., & Lee, J. (2005). Slipping or Gripping? Fluorescent Speckle Microscopy in Fish Keratocytes Reveals Two Different Mechanisms for Generating a Retrograde Flow of Actin. *Molecular Biology of the Cell*, *16*(2), 507–518. https://doi.org/10.1091/mbc.e04-10-0860

Kabsch, W., Mannherz, H. G., Suck, D., Pai, E. F., & Holmes, K. C. (1990). Atomic structure of the actin: DNase I complex. *Nature*, *347*(6288), 37–44. https://doi.org/10.1038/347037a0

Kaur, P., & Potten, C. S. (1986). Cell migration velocities in the crypts of the small intestine after cytotoxic insult are not dependent on mitotic activity. *Cell and Tissue Kinetics*, *19*(6), 601–610. https://doi.org/10.1111/j.1365-2184.1986.tb00761.x

Kim, H.-C., Jo, Y.-J., Kim, N.-H., & Namgoong, S. (2015). Small Molecule Inhibitor of Formin Homology 2 Domains (SMIFH2) Reveals the Roles of the Formin Family of Proteins in Spindle Assembly and Asymmetric Division in Mouse Oocytes. *PLOS ONE*, *10*(4), e0123438. https://doi.org/10.1371/journal.pone.0123438

Kirschner, M., & Mitchison, T. (1986). Beyond self-assembly: From microtubules to morphogenesis. *Cell*, *45*(3), 329–342. https://doi.org/10.1016/0092-8674(86)90318-1

Kollimada, S., Senger, F., Vignaud, T., Théry, M., Blanchoin, L., & Kurzawa, L. (2021). The biochemical composition of the actomyosin network sets the magnitude of cellular traction forces. *Molecular Biology of the Cell*, *32*(18), 1737–1748. https://doi.org/10.1091/mbc.E21-03-0109

Kovar, D. R., & Pollard, T. D. (2004). Insertional assembly of actin filament barbed ends in association with formins produces piconewton forces. *Proceedings of the National Academy of Sciences*, *101*(41), 14725–14730. https://doi.org/10.1073/pnas.0405902101

Krendel, M., Zenke, F. T., & Bokoch, G. M. (2002). Nucleotide exchange factor GEF-H1 mediates cross-talk between microtubules and the actin cytoskeleton. *Nature Cell Biology*, *4*(4), 294–301. https://doi.org/10.1038/ncb773

Krndija, D., El Marjou, F., Guirao, B., Richon, S., Leroy, O., Bellaiche, Y., Hannezo, E., & Matic Vignjevic, D. (2019). Active cell migration is critical for steady-state epithelial turnover in the gut. *Science*, *365*(6454), 705–710. https://doi.org/10.1126/science.aau3429

Kuroda, R., Fujikura, K., Abe, M., Hosoiri, Y., Asakawa, S., Shimizu, M., Umeda, S., Ichikawa, F., & Takahashi, H. (2016). Diaphanous gene mutation affects spiral cleavage and chirality in snails. *Scientific Reports*, *6*(1), 34809. https://doi.org/10.1038/srep34809

Kwong, H. K., Lam, M. L., Wu, S., Chung, C. F., Wu, J., Chu, L. T., Lim, K. H., Chow, H. L., Hartanto, H., Liu, W., Chow, K. T., & Chen, T.-H. (2023). Cell chirality reversal through tilted balance between polymerization of radial fibers and clockwise-swirling of transverse arcs. *ELife*, *12*. https://doi.org/10.7554/eLife.92632.1

LaChance, J., Suh, K., Clausen, J., & Cohen, D. J. (2022). Learning the rules of collective cell migration using deep attention networks. *PLOS Computational Biology*, *18*(4), e1009293. https://doi.org/10.1371/journal.pcbi.1009293

Ladoux, B., & Mège, R.-M. (2017). Mechanobiology of collective cell behaviours. *Nature Reviews Molecular Cell Biology*, *18*(12), 743–757. https://doi.org/10.1038/nrm.2017.98

Ladoux, B., Mège, R.-M., & Trepat, X. (2016). Front–Rear Polarization by Mechanical Cues: From Single Cells to Tissues. *Trends in Cell Biology*, *26*(6), 420–433. https://doi.org/10.1016/j.tcb.2016.02.002

Laporte, D., Ojkic, N., Vavylonis, D., & Wu, J.-Q. (2012). α-Actinin and fimbrin cooperate with myosin II to organize actomyosin bundles during contractile-ring assembly. *Molecular Biology of the Cell*, *23*(16), 3094–3110. https://doi.org/10.1091/mbc.e12-02-0123

Larsson, C. (2006). Protein kinase C and the regulation of the actin cytoskeleton. *Cellular Signalling*, *18*(3), 276–284. https://doi.org/10.1016/j.cellsig.2005.07.010

Lawson, C. D., & Burridge, K. (2014). The on-off relationship of Rho and Rac during integrin-mediated adhesion and cell migration. *Small GTPases*, *5*(1), e27958. https://doi.org/10.4161/sgtp.27958

Lebreton, G., Géminard, C., Lapraz, F., Pyrpassopoulos, S., Cerezo, D., Spéder, P., Ostap, E. M., & Noselli, S. (2018). Molecular to organismal chirality is induced by the conserved myosin 1D. *Science*, *362*(6417), 949–952. https://doi.org/10.1126/science.aat8642

Lecuit, T., & Yap, A. S. (2015). E-cadherin junctions as active mechanical integrators in tissue dynamics. *Nature Cell Biology*, *17*(5), 533–539. https://doi.org/10.1038/ncb3136

Legerstee, K., Geverts, B., Slotman, J. A., & Houtsmuller, A. B. (2019). Dynamics and distribution of paxillin, vinculin, zyxin and VASP depend on focal adhesion location and orientation. *Scientific Reports*, *9*(1), 10460. https://doi.org/10.1038/s41598-019-46905-2

Leong, F. Y. (2013). Physical Explanation of Coupled Cell-Cell Rotational Behavior and Interfacial Morphology: A Particle Dynamics Model. *Biophysical Journal*, *105*(10), 2301–2311. https://doi.org/10.1016/j.bpj.2013.09.051

Levayer, R., & Lecuit, T. (2012). Biomechanical regulation of contractility: Spatial control and dynamics. *Trends in Cell Biology*, *22*(2), 61–81. https://doi.org/10.1016/j.tcb.2011.10.001

Levin, M. (2005). Left–right asymmetry in embryonic development: A comprehensive review. *Mechanisms of Development*, *122*(1), 3–25. https://doi.org/10.1016/j.mod.2004.08.006

Li, R., & Gundersen, G. G. (2008). Beyond polymer polarity: How the cytoskeleton builds a polarized cell. *Nature Reviews Molecular Cell Biology*, *9*(11), 860–873. https://doi.org/10.1038/nrm2522

Li, X., & Chen, B. (2021). Mobility of Alpha-Actinin Along Growing Actin Filaments Might Affect the Cellular Chirality. *Journal of Applied Mechanics*, *88*(071002). https://doi.org/10.1115/1.4050476

Li, X., & Chen, B. (2022). How torque on formins is relaxed strongly affects cellular swirling. *Biophysical Journal*, *121*(15), 2952–2961. https://doi.org/10.1016/j.bpj.2022.06.027

Liu, X., Kapoor, T. M., Chen, J. K., & Huse, M. (2013). Diacylglycerol promotes centrosome polarization in T cells via reciprocal localization of dynein and myosin II. *Proceedings of the National Academy of Sciences*, *110*(29), 11976–11981. https://doi.org/10.1073/pnas.1306180110

Liu, Z., Tan, J. L., Cohen, D. M., Yang, M. T., Sniadecki, N. J., Ruiz, S. A., Nelson, C. M., & Chen, C. S. (2010). Mechanical tugging force regulates the size of cell–cell junctions. *Proceedings of the National Academy of Sciences*, *107*(22), 9944–9949. https://doi.org/10.1073/pnas.0914547107

Lo Vecchio, S., Pertz, O., Szopos, M., Navoret, L., & Riveline, D. (2024). Spontaneous rotations in epithelia as an interplay between cell polarity and boundaries. *Nature Physics*, 1–10. https://doi.org/10.1038/s41567-023-02295-x

Lomakin, A. J., Lee, K.-C., Han, S. J., Bui, D. A., Davidson, M., Mogilner, A., & Danuser, G. (2015). Competition for actin between two distinct F-actin networks defines a bistable switch for cell polarization. *Nature Cell Biology*, *17*(11), 1435–1445. https://doi.org/10.1038/ncb3246

Lu, L., Guyomar, T., Vagne, Q., Berthoz, R., Torres-Sánchez, A., Lieb, M., Martin-Lemaitre, C., van Unen, K., Honigmann, A., Pertz, O., Salbreux, G., & Riveline, D. (2022). *Polarity-driven three-dimensional spontaneous rotation of a cell doublet* [Preprint]. Biophysics. https://doi.org/10.1101/2022.12.21.521355

Luo, S., Furuya, K., Matsuda, K., Tsukasa, Y., Usui, T., & Uemura, T. (2023). E-cadherin-dependent coordinated epithelial rotation on a two-dimensional discoidal pattern. *Genes to Cells*, *28*(3), 175–187. https://doi.org/10.1111/gtc.13001

Martiel, J.-L., Leal, A., Kurzawa, L., Balland, M., Wang, I., Vignaud, T., Tseng, Q., & Théry, M. (2015). Chapter 15—Measurement of cell traction forces with ImageJ. In E. K. Paluch (Ed.), *Methods in Cell Biology* (Vol. 125, pp. 269–287). Academic Press. https://doi.org/10.1016/bs.mcb.2014.10.008

Maruthamuthu, V., Sabass, B., Schwarz, U. S., & Gardel, M. L. (2011). Cell-ECM traction force modulates endogenous tension at cell–cell contacts. *Proceedings of the National Academy of Sciences*, *108*(12), 4708–4713. https://doi.org/10.1073/pnas.1011123108

Maxian, O., & Mogilner, A. (2024). Helical motors and formins synergize to compact chiral filopodial bundles: A theoretical perspective. *European Journal of Cell Biology*, *103*(1), 151383. https://doi.org/10.1016/j.ejcb.2023.151383

Mayor, R., & Etienne-Manneville, S. (2016). The front and rear of collective cell migration. *Nature Reviews Molecular Cell Biology*, *17*(2), 97–109. https://doi.org/10.1038/nrm.2015.14

McGough, A., Pope, B., Chiu, W., & Weeds, A. (1997). Cofilin Changes the Twist of F-Actin: Implications for Actin Filament Dynamics and Cellular Function. *Journal of Cell Biology*, *138*(4), 771–781. https://doi.org/10.1083/jcb.138.4.771

McIntosh, B. B., & Ostap, E. M. (2016). Myosin-I molecular motors at a glance. *Journal of Cell Science*, *129*(14), 2689–2695. https://doi.org/10.1242/jcs.186403

Melki, R., Fievez, S., & Carlier, M. F. (1996). Continuous monitoring of Pi release following nucleotide hydrolysis in actin or tubulin assembly using 2-amino-6-mercapto-7-methylpurine ribonucleoside and purine-nucleoside phosphorylase as an enzyme-linked assay. *Biochemistry*, *35*(37), 12038–12045. https://doi.org/10.1021/bi961325o

Merino, F., Pospich, S., Funk, J., Wagner, T., Küllmer, F., Arndt, H.-D., Bieling, P., & Raunser, S. (2018). Structural transitions of F-actin upon ATP hydrolysis at near-atomic resolution revealed by cryo-EM. *Nature Structural & Molecular Biology*, *25*(6), 528–537. https://doi.org/10.1038/s41594-018-0074-0

Mertz, A. F., Che, Y., Banerjee, S., Goldstein, J. M., Rosowski, K. A., Revilla, S. F., Niessen, C. M., Marchetti, M. C., Dufresne, E. R., & Horsley, V. (2013). Cadherin-based intercellular adhesions organize epithelial cell–matrix traction forces. *Proceedings of the National Academy of Sciences*, *110*(3), 842–847. https://doi.org/10.1073/pnas.1217279110

Middelkoop, T. C., Garcia-Baucells, J., Quintero-Cadena, P., Pimpale, L. G., Yazdi, S., Sternberg, P. W., Gross, P., & Grill, S. W. (2021). CYK-1/Formin activation in cortical RhoA signaling centers promotes organismal left–right symmetry breaking. *Proceedings of the National Academy of Sciences*, *118*(20), e2021814118. https://doi.org/10.1073/pnas.2021814118

Mitchison, T., & Kirschner, M. (1984a). Dynamic instability of microtubule growth. *Nature*, *312*(5991), 237–242. https://doi.org/10.1038/312237a0

Mitchison, T., & Kirschner, M. (1984b). Microtubule assembly nucleated by isolated centrosomes. *Nature*, *312*(5991), 232–237. https://doi.org/10.1038/312232a0

Mitin, N., Rossman, K. L., Currin, R., Anne, S., Marshall, T. W., Bear, J. E., Bautch, V. L., & Der, C. J. (2013). The RhoGEF TEM4 Regulates Endothelial Cell Migration by Suppressing Actomyosin Contractility. *PLOS ONE*, *8*(6), e66260. https://doi.org/10.1371/journal.pone.0066260

Mitra, A., Meißner, L., Gandhimathi, R., Renger, R., Ruhnow, F., & Diez, S. (2020). Kinesin-14 motors drive a right-handed helical motion of antiparallel microtubules around each other. *Nature Communications*, *11*(1), 2565. https://doi.org/10.1038/s41467-020-16328-z

Mizuno, H., Higashida, C., Yuan, Y., Ishizaki, T., Narumiya, S., & Watanabe, N. (2011). Rotational Movement of the Formin mDia1 Along the Double Helical Strand of an Actin Filament. *Science*, *331*(6013), 80–83. https://doi.org/10.1126/science.1197692

Mizuno, H., Tanaka, K., Yamashiro, S., Narita, A., & Watanabe, N. (2018). Helical rotation of the diaphanous-related formin mDia1 generates actin filaments resistant to cofilin. *Proceedings of the National Academy of Sciences*, *115*(22), E5000–E5007. https://doi.org/10.1073/pnas.1803415115

Moseley, J. B., Sagot, I., Manning, A. L., Xu, Y., Eck, M. J., Pellman, D., & Goode, B. L. (2004). A Conserved Mechanism for Bni1- and mDia1-induced Actin Assembly and Dual Regulation of Bni1 by Bud6 and Profilin. *Molecular Biology of the Cell*, *15*(2), 896–907. https://doi.org/10.1091/mbc.e03-08-0621

Motegi, F., & Sugimoto, A. (2006). Sequential functioning of the ECT-2 RhoGEF, RHO-1 and CDC-42 establishes cell polarity in Caenorhabditis elegans embryos. *Nature Cell Biology*, *8*(9), 978–985. https://doi.org/10.1038/ncb1459

Munro, E., Nance, J., & Priess, J. R. (2004). Cortical Flows Powered by Asymmetrical Contraction Transport PAR Proteins to Establish and Maintain Anterior-Posterior Polarity in the Early *C. elegans* Embryo. *Developmental Cell*, *7*(3), 413–424. https://doi.org/10.1016/j.devcel.2004.08.001

Naganathan, S. R., Fürthauer, S., Nishikawa, M., Jülicher, F., & Grill, S. W. (2014). Active torque generation by the actomyosin cell cortex drives left–right symmetry breaking. *ELife*, *3*, e04165. https://doi.org/10.7554/eLife.04165

Naganathan, S. R., Middelkoop, T. C., Fürthauer, S., & Grill, S. W. (2016). Actomyosin-driven left-right asymmetry: From molecular torques to chiral self organization. *Current Opinion in Cell Biology*, *38*, 24–30. https://doi.org/10.1016/j.ceb.2016.01.004

Ng, M. R., Besser, A., Danuser, G., & Brugge, J. S. (2012). Substrate stiffness regulates cadherin-dependent collective migration through myosin-II contractility. *Journal of Cell Biology*, *199*(3), 545–563. https://doi.org/10.1083/jcb.201207148

Niederman, R., & Pollard, T. D. (1975). Human platelet myosin. II. In vitro assembly and structure of myosin filaments. *Journal of Cell Biology*, *67*(1), 72–92. https://doi.org/10.1083/jcb.67.1.72

Nimnual, A. S., Taylor, L. J., & Bar-Sagi, D. (2003). Redox-dependent downregulation of Rho by Rac. *Nature Cell Biology*, *5*(3), 236–241. https://doi.org/10.1038/ncb938

Nishimura, Y., Shi, S., Li, Q., Bershadsky, A. D., & Viasnoff, V. (2021). Crosstalk between myosin II and formin functions in the regulation of force generation and actomyosin dynamics in stress fibers. *Cells & Development*, *168*, 203736. https://doi.org/10.1016/j.cdev.2021.203736

Nishimura, Y., Shi, S., Zhang, F., Liu, R., Takagi, Y., Bershadsky, A. D., Viasnoff, V., & Sellers, J. R. (2021). The formin inhibitor SMIFH2 inhibits members of the myosin superfamily. *Journal of Cell Science*, *134*(8), jcs253708. https://doi.org/10.1242/jcs.253708

Nishizaka, T., Yagi, T., Tanaka, Y., & Ishiwata, S. (1993). Right-handed rotation of an actin filament in an in vitro motile system. *Nature*, *361*(6409), 269–271. https://doi.org/10.1038/361269a0

Noël, E. S., Verhoeven, M., Lagendijk, A. K., Tessadori, F., Smith, K., Choorapoikayil, S., den Hertog, J., & Bakkers, J. (2013). A Nodal-independent and tissue-intrinsic mechanism controls heart-looping chirality. *Nature Communications*, *4*(1), 2754. https://doi.org/10.1038/ncomms3754

Oakes, P. W., Banerjee, S., Marchetti, M. C., & Gardel, M. L. (2014). Geometry Regulates Traction Stresses in Adherent Cells. *Biophysical Journal*, *107*(4), 825–833. https://doi.org/10.1016/j.bpj.2014.06.045

Oakes, P. W., Beckham, Y., Stricker, J., & Gardel, M. L. (2012). Tension is required but not sufficient for focal adhesion maturation without a stress fiber template. *Journal of Cell Biology*, *196*(3), 363–374. https://doi.org/10.1083/jcb.201107042

Oda, T., Iwasa, M., Aihara, T., Maéda, Y., & Narita, A. (2009). The nature of the globular- to fibrous-actin transition. *Nature*, *457*(7228), 441–445. https://doi.org/10.1038/nature07685

Oosterheert, W., Boiero Sanders, M., Funk, J., Prumbaum, D., Raunser, S., & Bieling, P. (2024). Molecular mechanism of actin filament elongation by formins. *Science*, *384*(6692), eadn9560. https://doi.org/10.1126/science.adn9560

Ouyang, M., Lu, S., Kim, T., Chen, C.-E., Seong, J., Leckband, D. E., Wang, F., Reynolds, A. B., Schwartz, M. A., & Wang, Y. (2013). N-cadherin regulates spatially polarized signals through distinct p120ctn and β-catenin-dependent signalling pathways. *Nature Communications*, *4*(1), 1589. https://doi.org/10.1038/ncomms2560

Ozawa, M., Hiver, S., Yamamoto, T., Shibata, T., Upadhyayula, S., Mimori-Kiyosue, Y., & Takeichi, M. (2020). Adherens junction regulates cryptic lamellipodia formation for epithelial cell migration. *Journal of Cell Biology*, *219*(10), e202006196. https://doi.org/10.1083/jcb.202006196

Padinhateeri, R., Kolomeisky, A. B., & Lacoste, D. (2012). Random Hydrolysis Controls the Dynamic Instability of Microtubules. *Biophysical Journal*, *102*(6), 1274–1283. https://doi.org/10.1016/j.bpj.2011.12.059

Palazzo, A. F., Cook, T. A., Alberts, A. S., & Gundersen, G. G. (2001). MDia mediates Rho-regulated formation and orientation of stable microtubules. *Nature Cell Biology*, *3*(8), 723–729. https://doi.org/10.1038/35087035

Panagiotakopoulou, M., Lendenmann, T., Pramotton, F. M., Giampietro, C., Stefopoulos, G., Poulikakos, D., & Ferrari, A. (2018). Cell cycle–dependent force transmission in cancer cells. *Molecular Biology of the Cell*, *29*(21), 2528–2539. https://doi.org/10.1091/mbc.E17-12-0726

Parker, A., Maclaren, O. J., Fletcher, A. G., Muraro, D., Kreuzaler, P. A., Byrne, H. M., Maini, P. K., Watson, A. J. M., & Pin, C. (2017). Cell proliferation within small intestinal crypts is the principal driving force for cell migration on villi. *FASEB Journal: Official Publication of the Federation of American Societies for Experimental Biology*, *31*(2), 636–649. https://doi.org/10.1096/fj.201601002

Pasapera, A. M., Heissler, S. M., Eto, M., Nishimura, Y., Fischer, R. S., Thiam, H. R., & Waterman, C. M. (2022). MARK2 regulates directed cell migration through modulation of myosin II contractility and focal adhesion organization. *Current Biology*, *32*(12), 2704-2718.e6. https://doi.org/10.1016/j.cub.2022.04.088

Pavin, N., & Tolić, I. M. (2016). Self-Organization and Forces in the Mitotic Spindle. *Annual Review of Biophysics*, *45*, 279–298. https://doi.org/10.1146/annurev-biophys-062215-010934

Pernier, J., Morchain, A., Caorsi, V., Bertin, A., Bousquet, H., Bassereau, P., & Coudrier, E. (2020). Myosin 1b flattens and prunes branched actin filaments. *Journal of Cell Science*, *133*(18), jcs247403. https://doi.org/10.1242/jcs.247403

Pernier, J., & Schauer, K. (2022). Does the Actin Network Architecture Leverage Myosin-I Functions? *Biology*, *11*(7), 989. https://doi.org/10.3390/biology11070989

Petry, S. (2016). Mechanisms of Mitotic Spindle Assembly. *Annual Review of Biochemistry*, *85*, 659–683. https://doi.org/10.1146/annurev-biochem-060815-014528

Petzoldt, A. G., Coutelis, J.-B., Géminard, C., Spéder, P., Suzanne, M., Cerezo, D., & Noselli, S. (2012). DE-Cadherin regulates unconventional Myosin ID and Myosin IC in Drosophila left-right asymmetry establishment. *Development*, *139*(10), 1874–1884. https://doi.org/10.1242/dev.047589

Pimpale, L. G., Middelkoop, T. C., Mietke, A., & Grill, S. W. (2020). Cell lineage-dependent chiral actomyosin flows drive cellular rearrangements in early Caenorhabditis elegans development. *ELife*, *9*, e54930. https://doi.org/10.7554/eLife.54930

Pitaval, A., Senger, F., Letort, G., Gidrol, X., Guyon, L., Sillibourne, J., & Théry, M. (2017). Microtubule stabilization drives 3D centrosome migration to initiate primary ciliogenesis. *Journal of Cell Biology*, *216*(11), 3713–3728. https://doi.org/10.1083/jcb.201610039

Pitaval, A., Tseng, Q., Bornens, M., & Théry, M. (2010). Cell shape and contractility regulate ciliogenesis in cell cycle–arrested cells. *Journal of Cell Biology*, *191*(2), 303–312. https://doi.org/10.1083/jcb.201004003

Pohl, C. (2015). Cytoskeletal Symmetry Breaking and Chirality: From Reconstituted Systems to Animal Development. *Symmetry*, *7*(4), 2062–2107. https://doi.org/10.3390/sym7042062

Pollard, T D. (1986). Rate constants for the reactions of ATP- and ADP-actin with the ends of actin filaments. *Journal of Cell Biology*, *103*(6), 2747–2754. https://doi.org/10.1083/jcb.103.6.2747

Pollard, Thomas D, & Borisy, G. G. (2003). Cellular Motility Driven by Assembly and Disassembly of Actin Filaments. *Cell*, *112*(4), 453–465. https://doi.org/10.1016/S0092-8674(03)00120-X

Pollard, Thomas Dean, & Goldman, R. D. (2017). *The Cytoskeleton*. Cold Spring Harbor Laboratory Press.

Ponti, A., Machacek, M., Gupton, S. L., Waterman-Storer, C. M., & Danuser, G. (2004). Two Distinct Actin Networks Drive the Protrusion of Migrating Cells. *Science*, *305*(5691), 1782–1786. https://doi.org/10.1126/science.1100533

Poujade, M., Grasland-Mongrain, E., Hertzog, A., Jouanneau, J., Chavrier, P., Ladoux, B., Buguin, A., & Silberzan, P. (2007). Collective migration of an epithelial monolayer in response to a model wound. *Proceedings of the National Academy of Sciences*, *104*(41), 15988–15993. https://doi.org/10.1073/pnas.0705062104

Pouthas, F., Girard, P., Lecaudey, V., Ly, T. B. N., Gilmour, D., Boulin, C., Pepperkok, R., & Reynaud, E. G. (2008). In migrating cells, the Golgi complex and the position of the centrosome depend on geometrical constraints of the substratum. *Journal of Cell Science*, *121*(14), 2406–2414. https://doi.org/10.1242/jcs.026849

Pyrpassopoulos, S., Feeser, E. A., Mazerik, J. N., Tyska, M. J., & Ostap, E. M. (2012). Membrane-Bound Myo1c Powers Asymmetric Motility of Actin Filaments. *Current Biology*, *22*(18), 1688–1692. https://doi.org/10.1016/j.cub.2012.06.069

Qiu, D., Cheng, S.-M., Wozniak, L., McSweeney, M., Perrone, E., & Levin, M. (2005). Localization and loss-of-function implicates ciliary proteins in early, cytoplasmic roles in left-right asymmetry. *Developmental Dynamics*, *234*(1), 176–189. https://doi.org/10.1002/dvdy.20509

Rahman, T., Peters, F., & Wan, L. (2024). Biomechanical modeling of cell chirality and symmetry breaking of biological systems ☆. *Mechanobiology in Medicine*, *2*, 100038. https://doi.org/10.1016/j.mbm.2024.100038

Ray, P., Chin, A. S., Worley, K. E., Fan, J., Kaur, G., Wu, M., & Wan, L. Q. (2018). Intrinsic cellular chirality regulates left–right symmetry breaking during cardiac looping. *Proceedings of the National Academy of Sciences*, *115*(50), E11568–E11577. https://doi.org/10.1073/pnas.1808052115

Reffay, M., Parrini, M. C., Cochet-Escartin, O., Ladoux, B., Buguin, A., Coscoy, S., Amblard, F., Camonis, J., & Silberzan, P. (2014). Interplay of RhoA and mechanical forces in collective cell migration driven by leader cells. *Nature Cell Biology*, *16*(3), 217–223. https://doi.org/10.1038/ncb2917

Reffay, M., Petitjean, L., Coscoy, S., Grasland-Mongrain, E., Amblard, F., Buguin, A., & Silberzan, P. (2011). Orientation and Polarity in Collectively Migrating Cell Structures: Statics and Dynamics. *Biophysical Journal*, *100*(11), 2566–2575. https://doi.org/10.1016/j.bpj.2011.04.047

Reymann, A.-C., Boujemaa-Paterski, R., Martiel, J.-L., Guérin, C., Cao, W., Chin, H. F., De La Cruz, E. M., Théry, M., & Blanchoin, L. (2012). Actin Network Architecture Can Determine

Myosin Motor Activity. *Science*, *336*(6086), 1310–1314. https://doi.org/10.1126/science.1221708

Reymann, A.-C., Martiel, J.-L., Cambier, T., Blanchoin, L., Boujemaa-Paterski, R., & Théry, M. (2010). Nucleation geometry governs ordered actin networks structures. *Nature Materials*, *9*(10), 827–832. https://doi.org/10.1038/nmat2855

Reymann, A.-C., Suarez, C., Guérin, C., Martiel, J.-L., Staiger, C. J., Blanchoin, L., & Boujemaa-Paterski, R. (2011). Turnover of branched actin filament networks by stochastic fragmentation with ADF/cofilin. *Molecular Biology of the Cell*, *22*(14), 2541–2550. https://doi.org/10.1091/mbc.e11-01-0052

Ridley, A. J. (2006). Rho GTPases and actin dynamics in membrane protrusions and vesicle trafficking. *Trends in Cell Biology*, *16*(10), 522–529. https://doi.org/10.1016/j.tcb.2006.08.006

Ritter, A. T., Asano, Y., Stinchcombe, J. C., Dieckmann, N. M. G., Chen, B.-C., Gawden-Bone, C., van Engelenburg, S., Legant, W., Gao, L., Davidson, M. W., Betzig, E., Lippincott-Schwartz, J., & Griffiths, G. M. (2015). Actin Depletion Initiates Events Leading to Granule Secretion at the Immunological Synapse. *Immunity*, *42*(5), 864–876. https://doi.org/10.1016/j.immuni.2015.04.013

Romero, S., Le Clainche, C., Didry, D., Egile, C., Pantaloni, D., & Carlier, M.-F. (2004). Formin Is a Processive Motor that Requires Profilin to Accelerate Actin Assembly and Associated ATP Hydrolysis. *Cell*, *119*(3), 419–429. https://doi.org/10.1016/j.cell.2004.09.039

Rottner, K., Faix, J., Bogdan, S., Linder, S., & Kerkhoff, E. (2017). Actin assembly mechanisms at a glance. *Journal of Cell Science*, *130*(20), 3427–3435. https://doi.org/10.1242/jcs.206433

Rotty, J. D., Wu, C., Haynes, E. M., Suarez, C., Winkelman, J. D., Johnson, H. E., Haugh, J. M., Kovar, D. R., & Bear, J. E. (2015). Profilin-1 Serves as a Gatekeeper for Actin Assembly by Arp2/3-Dependent and -Independent Pathways. *Developmental Cell*, *32*(1), 54–67. https://doi.org/10.1016/j.devcel.2014.10.026

Ruppel, A., Wörthmüller, D., Misiak, V., Kelkar, M., Wang, I., Moreau, P., Méry, A., Révilloud, J., Charras, G., Cappello, G., Boudou, T., Schwarz, U. S., & Balland, M. (2023). Force propagation between epithelial cells depends on active coupling and mechano-structural polarization. *ELife*, *12*, e83588. https://doi.org/10.7554/eLife.83588

Sanchez, T., Chen, D. T. N., DeCamp, S. J., Heymann, M., & Dogic, Z. (2012). Spontaneous motion in hierarchically assembled active matter. *Nature*, *491*(7424), 431–434. https://doi.org/10.1038/nature11591

Sander, E. E., ten Klooster, J. P., van Delft, S., van der Kammen, R. A., & Collard, J. G. (1999). Rac Downregulates Rho Activity: Reciprocal Balance between Both Gtpases Determines Cellular Morphology and Migratory Behavior. *Journal of Cell Biology*, *147*(5), 1009–1022. https://doi.org/10.1083/jcb.147.5.1009

Sato, K., Hiraiwa, T., Maekawa, E., Isomura, A., Shibata, T., & Kuranaga, E. (2015a). Left–right asymmetric cell intercalation drives directional collective cell movement in

epithelial morphogenesis. *Nature Communications*, *6*(1), 10074. https://doi.org/10.1038/ncomms10074

Sato, K., Hiraiwa, T., Maekawa, E., Isomura, A., Shibata, T., & Kuranaga, E. (2015b). Left–right asymmetric cell intercalation drives directional collective cell movement in epithelial morphogenesis. *Nature Communications*, *6*(1), 10074. https://doi.org/10.1038/ncomms10074

Sato, K., Hiraiwa, T., & Shibata, T. (2015). Cell Chirality Induces Collective Cell Migration in Epithelial Sheets. *Physical Review Letters*, *115*(18), 188102. https://doi.org/10.1103/PhysRevLett.115.188102

Sato, Y., Yoshimura, K., Matsuda, K., Haraguchi, T., Marumo, A., Yamagishi, M., Sato, S., Ito, K., & Yajima, J. (2023). Membrane-bound myosin IC drives the chiral rotation of the gliding actin filament around its longitudinal axis. *Scientific Reports*, *13*(1), 19908. https://doi.org/10.1038/s41598-023-47125-5

Schaeffer, A. (2023). *Dynamique, mécanique et architecture des microtubules* [These de doctorat, Université Grenoble Alpes]. https://theses.fr/2023GRALY078

Schauer, K., Duong, T., Bleakley, K., Bardin, S., Bornens, M., & Goud, B. (2010). Probabilistic density maps to study global endomembrane organization. *Nature Methods*, *7*(7), 560–566. https://doi.org/10.1038/nmeth.1462

Schliwa, M., & Woehlke, G. (2001). Switching on kinesin. *Nature*, *411*(6836), 424–425. https://doi.org/10.1038/35078167

Schwingel, M., & Bastmeyer, M. (2013). Force Mapping during the Formation and Maturation of Cell Adhesion Sites with Multiple Optical Tweezers. *PLoS ONE*, *8*(1), e54850. https://doi.org/10.1371/journal.pone.0054850

Segerer, F. J., Thüroff, F., Piera Alberola, A., Frey, E., & Rädler, J. O. (2015). Emergence and Persistence of Collective Cell Migration on Small Circular Micropatterns. *Physical Review Letters*, *114*(22), 228102. https://doi.org/10.1103/PhysRevLett.114.228102

Senger, F., Pitaval, A., Ennomani, H., Kurzawa, L., Blanchoin, L., & Théry, M. (2019). Spatial integration of mechanical forces by α-actinin establishes actin network symmetry. *Journal of Cell Science*, *132*(22), jcs236604. https://doi.org/10.1242/jcs.236604

Sept, D., Elcock, A. H., & McCammon, J. A. (1999). Computer simulations of actin polymerization can explain the barbed-pointed end asymmetry1. *Journal of Molecular Biology*, *294*(5), 1181–1189. https://doi.org/10.1006/jmbi.1999.3332

Severson, A. F., & Bowerman, B. (2003). Myosin and the PAR proteins polarize microfilament-dependent forces that shape and position mitotic spindles in Caenorhabditis elegans. *Journal of Cell Biology*, *161*(1), 21–26. https://doi.org/10.1083/jcb.200210171

Shemesh, T., Otomo, T., Rosen, M. K., Bershadsky, A. D., & Kozlov, M. M. (2005). A novel mechanism of actin filament processive capping by formin: Solution of the rotation

paradox. *Journal of Cell Biology*, *170*(6), 889–893. https://doi.org/10.1083/jcb.200504156

Shi, X., Wen, Z., Wang, Y., Liu, Y.-J., Shi, K., & Jiu, Y. (2021). Feedback-Driven Mechanisms Between Phosphorylated Caveolin-1 and Contractile Actin Assemblies Instruct Persistent Cell Migration. *Frontiers in Cell and Developmental Biology*, *9*. https://www.frontiersin.org/articles/10.3389/fcell.2021.665919

Shibazaki, Y., Shimizu, M., & Kuroda, R. (2004). Body Handedness Is Directed by Genetically Determined Cytoskeletal Dynamics in the Early Embryo. *Current Biology*, *14*(16), 1462–1467. https://doi.org/10.1016/j.cub.2004.08.018

Shin, H., Drew, K. R. P., Bartles, J. R., Wong, G. C. L., & Grason, G. M. (2009). Cooperativity and Frustration in Protein-Mediated Parallel Actin Bundles. *Physical Review Letters*, *103*(23), 238102. https://doi.org/10.1103/PhysRevLett.103.238102

Shin, J. H., Gardel, M. L., Mahadevan, L., Matsudaira, P., & Weitz, D. A. (2004). Relating microstructure to rheology of a bundled and cross-linked F-actin network in vitro. *Proceedings of the National Academy of Sciences*, *101*(26), 9636–9641. https://doi.org/10.1073/pnas.0308733101

Sri-Ranjan, K., Sanchez-Alonso, J. L., Swiatlowska, P., Rothery, S., Novak, P., Gerlach, S., Koeninger, D., Hoffmann, B., Merkel, R., Stevens, M. M., Sun, S. X., Gorelik, J., & Braga, V. M. M. (2022). Intrinsic cell rheology drives junction maturation. *Nature Communications*, *13*(1), 4832. https://doi.org/10.1038/s41467-022-32102-9

Suarez, C., Carroll, R. T., Burke, T. A., Christensen, J. R., Bestul, A. J., Sees, J. A., James, M. L., Sirotkin, V., & Kovar, D. R. (2015). Profilin Regulates F-Actin Network Homeostasis by Favoring Formin over Arp2/3 Complex. *Developmental Cell*, *32*(1), 43–53. https://doi.org/10.1016/j.devcel.2014.10.027

Sun, Y., Sato, O., Ruhnow, F., Arsenault, M. E., Ikebe, M., & Goldman, Y. E. (2010). Single-molecule stepping and structural dynamics of myosin X. *Nature Structural & Molecular Biology*, *17*(4), 485–491. https://doi.org/10.1038/nsmb.1785

Suzuki, E. L., Chikireddy, J., Dmitrieff, S., Guichard, B., Romet-Lemonne, G., & Jégou, A. (2020). Geometrical Constraints Greatly Hinder Formin mDia1 Activity. *Nano Letters*, *20*(1), 22–32. https://doi.org/10.1021/acs.nanolett.9b02241

Takaki Yamamoto, Tomoki Ishibashi, Yuko Mimori-Kiyosue, Sylvain Hiver, Naoko Tokushige, Mitsusuke Tarama, Masatoshi Takeichi, & Tatsuo Shibata. (2023). Epithelial cell chirality emerges through the dynamic concentric pattern of actomyosin cytoskeleton. *BioRxiv*.

Tanaka, K., Takeda, S., Mitsuoka, K., Oda, T., Kimura-Sakiyama, C., Maéda, Y., & Narita, A. (2018). Structural basis for cofilin binding and actin filament disassembly. *Nature Communications*, *9*(1), 1860. https://doi.org/10.1038/s41467-018-04290-w

Taniguchi, K., Maeda, R., Ando, T., Okumura, T., Nakazawa, N., Hatori, R., Nakamura, M., Hozumi, S., Fujiwara, H., & Matsuno, K. (2011). Chirality in Planar Cell Shape Contributes

to Left-Right Asymmetric Epithelial Morphogenesis. *Science*, *333*(6040), 339–341. https://doi.org/10.1126/science.1200940

Tee, Y. H., Goh, W. J., Yong, X., Ong, H. T., Hu, J., Tay, I. Y. Y., Shi, S., Jalal, S., Barnett, S. F. H., Kanchanawong, P., Huang, W., Yan, J., Lim, Y. A. B., Thiagarajan, V., Mogilner, A., & Bershadsky, A. D. (2023). Actin polymerisation and crosslinking drive left-right asymmetry in single cell and cell collectives. *Nature Communications*, *14*(1), 776. https://doi.org/10.1038/s41467-023-35918-1

Tee, Y. H., Shemesh, T., Thiagarajan, V., Hariadi, R. F., Anderson, K. L., Page, C., Volkmann, N., Hanein, D., Sivaramakrishnan, S., Kozlov, M. M., & Bershadsky, A. D. (2015a). Cellular chirality arising from the self-organization of the actin cytoskeleton. *Nature Cell Biology*, *17*(4), 445–457. https://doi.org/10.1038/ncb3137

Tee, Y. H., Shemesh, T., Thiagarajan, V., Hariadi, R. F., Anderson, K. L., Page, C., Volkmann, N., Hanein, D., Sivaramakrishnan, S., Kozlov, M. M., & Bershadsky, A. D. (2015b). Cellular chirality arising from the self-organization of the actin cytoskeleton. *Nature Cell Biology*, *17*(4), 445–457. https://doi.org/10.1038/ncb3137

Théry, M. (2010). Micropatterning as a tool to decipher cell morphogenesis and functions. *Journal of Cell Science*, *123*(24), 4201–4213. https://doi.org/10.1242/jcs.075150

Théry, M., & Blanchoin, L. (2021). Microtubule self-repair. *Current Opinion in Cell Biology*, *68*, 144–154. https://doi.org/10.1016/j.ceb.2020.10.012

Théry, M., Pépin, A., Dressaire, E., Chen, Y., & Bornens, M. (2006). Cell distribution of stress fibres in response to the geometry of the adhesive environment. *Cell Motility*, *63*(6), 341–355. https://doi.org/10.1002/cm.20126

Théry, M., Racine, V., Piel, M., Pépin, A., Dimitrov, A., Chen, Y., Sibarita, J.-B., & Bornens, M. (2006). Anisotropy of cell adhesive microenvironment governs cell internal organization and orientation of polarity. *Proceedings of the National Academy of Sciences*, *103*(52), 19771–19776. https://doi.org/10.1073/pnas.0609267103

Thompson, R. F., & Langford, G. M. (2002). Myosin superfamily evolutionary history. *The Anatomical Record*, *268*(3), 276–289. https://doi.org/10.1002/ar.10160

Tixi, W., Maldonado, M., Chang, Y.-T., Chiu, A., Yeung, W., Parveen, N., Nelson, M. S., Hart, R., Wang, S., Hsu, W. J., Fueger, P., Kopp, J. L., Huising, M. O., Dhawan, S., & Shih, H. P. (2023). Coordination between ECM and cell-cell adhesion regulates the development of islet aggregation, architecture, and functional maturation. *ELife*, *12*, e90006. https://doi.org/10.7554/eLife.90006

Trepat, X., Wasserman, M. R., Angelini, T. E., Millet, E., Weitz, D. A., Butler, J. P., & Fredberg, J. J. (2009). Physical forces during collective cell migration. *Nature Physics*, *5*(6), 426–430. https://doi.org/10.1038/nphys1269

Trupinić, M., Kokanović, B., Ponjavić, I., Barišić, I., Šegvić, S., Ivec, A., & Tolić, I. M. (2022). The chirality of the mitotic spindle provides a mechanical response to forces and depends on microtubule motors and augmin. *Current Biology*, *32*(11), 2480-2493.e6. https://doi.org/10.1016/j.cub.2022.04.035

Tsai, F.-C., Seki, A., Yang, H. W., Hayer, A., Carrasco, S., Malmersjö, S., & Meyer, T. (2014). A polarized Ca2+, diacylglycerol and STIM1 signalling system regulates directed cell migration. *Nature Cell Biology*, *16*(2), 133–144. https://doi.org/10.1038/ncb2906

Tseng, Q., Duchemin-Pelletier, E., Deshiere, A., Balland, M., Guillou, H., Filhol, O., & Théry, M. (2012). Spatial organization of the extracellular matrix regulates cell–cell junction positioning. *Proceedings of the National Academy of Sciences*, *109*(5), 1506–1511. https://doi.org/10.1073/pnas.1106377109

Uyeda, T. Q. P., Iwadate, Y., Umeki, N., Nagasaki, A., & Yumura, S. (2011). Stretching Actin Filaments within Cells Enhances their Affinity for the Myosin II Motor Domain. *PLOS ONE*, *6*(10), e26200. https://doi.org/10.1371/journal.pone.0026200

Vaidžiulytė, K., Coppey, M., & Schauer, K. (2019). Intracellular organization in cell polarity – placing organelles into the polarity loop. *Journal of Cell Science*, *132*(24), jcs230995. https://doi.org/10.1242/jcs.230995

Vaidžiulytė, K., Macé, A.-S., Battistella, A., Beng, W., Schauer, K., & Coppey, M. (2022). Persistent cell migration emerges from a coupling between protrusion dynamics and polarized trafficking. *ELife*, *11*, e69229. https://doi.org/10.7554/eLife.69229

Vallotton, P., Gupton, S. L., Waterman-Storer, C. M., & Danuser, G. (2004). Simultaneous mapping of filamentous actin flow and turnover in migrating cells by quantitative fluorescent speckle microscopy. *Proceedings of the National Academy of Sciences*, *101*(26), 9660–9665. https://doi.org/10.1073/pnas.0300552101

van der Flier, L. G., & Clevers, H. (2009). Stem cells, self-renewal, and differentiation in the intestinal epithelium. *Annual Review of Physiology*, *71*, 241–260. https://doi.org/10.1146/annurev.physiol.010908.163145

van der Gucht, J., Paluch, E., Plastino, J., & Sykes, C. (2005). Stress release drives symmetry breaking for actin-based movement. *Proceedings of the National Academy of Sciences*, *102*(22), 7847–7852. https://doi.org/10.1073/pnas.0502121102

van Oudenaarden, A., & Theriot, J. A. (1999). Cooperative symmetry-breaking by actin polymerization in a model for cell motility. *Nature Cell Biology*, *1*(8), 493–499. https://doi.org/10.1038/70281

Vavylonis, D., & Horan, B. G. (2017). Cell Biology: Capturing Formin's Mechano-Inhibition. *Current Biology : CB*, *27*(19), R1078–R1080. https://doi.org/10.1016/j.cub.2017.08.020

Verkhovsky, A. B., Svitkina, T. M., & Borisy, G. G. (1999). Self-polarization and directional motility of cytoplasm. *Current Biology*, *9*(1), 11-S1. https://doi.org/10.1016/S0960-9822(99)80042-6

Vianay, B., Senger, F., Alamos, S., Anjur-Dietrich, M., Bearce, E., Cheeseman, B., Lee, L., & Théry, M. (2018). Variation in traction forces during cell cycle progression. *Biology of the Cell*, *110*(4), 91–96. https://doi.org/10.1111/boc.201800006

Vicente-Manzanares, M., Ma, X., Adelstein, R. S., & Horwitz, A. R. (2009). Non-muscle myosin II takes centre stage in cell adhesion and migration. *Nature Reviews Molecular Cell Biology*, *10*(11), 778–790. https://doi.org/10.1038/nrm2786

Vignaud, T., Ennomani, H., & Théry, M. (2014). Chapter 6—Polyacrylamide Hydrogel Micropatterning. In M. Piel & M. Théry (Eds.), *Methods in Cell Biology* (Vol. 120, pp. 93–116). Academic Press. https://doi.org/10.1016/B978-0-12-417136-7.00006-9

Vilfan, A. (2009). Twirling Motion of Actin Filaments in Gliding Assays with Nonprocessive Myosin Motors. *Biophysical Journal*, *97*(4), 1130–1137. https://doi.org/10.1016/j.bpj.2009.06.008

Wan, L. Q., Ronaldson, K., Park, M., Taylor, G., Zhang, Y., Gimble, J. M., & Vunjak-Novakovic, G. (2011). Micropatterned mammalian cells exhibit phenotype-specific left-right asymmetry. *Proceedings of the National Academy of Sciences*, *108*(30), 12295–12300. https://doi.org/10.1073/pnas.1103834108

Wang, B.-C., & Xu, G.-K. (2022). Cell chirality regulates coherent angular motion on small circular substrates. *Biophysical Journal*, *121*(10), 1931–1939. https://doi.org/10.1016/j.bpj.2022.04.011

Wang, W. Y., Davidson, C. D., Lin, D., & Baker, B. M. (2019). Actomyosin contractility-dependent matrix stretch and recoil induces rapid cell migration. *Nature Communications*, *10*(1), 1186. https://doi.org/10.1038/s41467-019-09121-0

Watts, J. L., Etemad-Moghadam, B., Guo, S., Boyd, L., Draper, B. W., Mello, C. C., Priess, J. R., & Kemphues, K. J. (1996). Par-6, a gene involved in the establishment of asymmetry in early C. elegans embryos, mediates the asymmetric localization of PAR-3. *Development*, *122*(10), 3133–3140. https://doi.org/10.1242/dev.122.10.3133

Wegner, A., & Engel, J. (1975). Kinetics of the cooperative association of actin to actin filament. *Biophysical Chemistry*, *3*(3), 215–225. https://doi.org/10.1016/0301-4622(75)80013-5

Wioland, H., Jegou, A., & Romet-Lemonne, G. (2019). Torsional stress generated by ADF/cofilin on cross-linked actin filaments boosts their severing. *Proceedings of the National Academy of Sciences*, *116*(7), 2595–2602. https://doi.org/10.1073/pnas.1812053116

Wittmann, T., & Waterman-Storer, C. M. (2001). Cell motility: Can Rho GTPases and microtubules point the way? *Journal of Cell Science*, *114*(21), 3795–3803. https://doi.org/10.1242/jcs.114.21.3795

Worley, K. E., Shieh, D., & Wan, L. Q. (2015). Inhibition of cell–cell adhesion impairs directional epithelial migration on micropatterned surfaces. *Integrative Biology*, *7*(5), 580–590. https://doi.org/10.1039/c5ib00073d

Xi, W., Sonam, S., Beng Saw, T., Ladoux, B., & Teck Lim, C. (2017). Emergent patterns of collective cell migration under tubular confinement. *Nature Communications*, *8*(1), 1517. https://doi.org/10.1038/s41467-017-01390-x

Xiao, H., & Liu, M. (2013). Atypical protein kinase C in cell motility. *Cellular and Molecular Life Sciences*, *70*(17), 3057–3066. https://doi.org/10.1007/s00018-012-1192-1

Xu, J., Keymeulen, A. V., Wakida, N. M., Carlton, P., Berns, M. W., & Bourne, H. R. (2007). Polarity reveals intrinsic cell chirality. *Proceedings of the National Academy of Sciences*, *104*(22), 9296–9300. https://doi.org/10.1073/pnas.0703153104

Yam, P. T., Wilson, C. A., Ji, L., Hebert, B., Barnhart, E. L., Dye, N. A., Wiseman, P. W., Danuser, G., & Theriot, J. A. (2007). Actin–myosin network reorganization breaks symmetry at the cell rear to spontaneously initiate polarized cell motility. *Journal of Cell Biology*, *178*(7), 1207–1221. https://doi.org/10.1083/jcb.200706012

Yamahira, S., Yamaguchi, S., Kawahara, M., & Nagamune, T. (2014). Collagen Surfaces Modified with Photo-Cleavable Polyethylene Glycol-Lipid Support Versatile Single-Cell Arrays of Both Non-adherent and Adherent Cells. *Macromolecular Bioscience*, *14*(12), 1670–1676. https://doi.org/10.1002/mabi.201400312

Yamamoto, T., Hiraiwa, T., & Shibata, T. (2020). Collective cell migration of epithelial cells driven by chiral torque generation. *Physical Review Research*, *2*(4), 043326. https://doi.org/10.1103/PhysRevResearch.2.043326

Yamanaka, H., & Kondo, S. (2015). Rotating pigment cells exhibit an intrinsic chirality. *Genes to Cells*, *20*(1), 29–35. https://doi.org/10.1111/gtc.12194

Yarmola, E. G., Somasundaram, T., Boring, T. A., Spector, I., & Bubb, M. R. (2000). Actin-Latrunculin A Structure and Function: DIFFERENTIAL MODULATION OF ACTIN-BINDING PROTEIN FUNCTION BY LATRUNCULIN A*. *Journal of Biological Chemistry*, *275*(36), 28120–28127. https://doi.org/10.1074/jbc.M004253200

Yu, M., Le, S., Efremov, A. K., Zeng, X., Bershadsky, A., & Yan, J. (2018). Effects of Mechanical Stimuli on Profilin- and Formin-Mediated Actin Polymerization. *Nano Letters*, *18*(8), 5239–5247. https://doi.org/10.1021/acs.nanolett.8b02211

Yu, M., Yuan, X., Lu, C., Le, S., Kawamura, R., Efremov, A. K., Zhao, Z., Kozlov, M. M., Sheetz, M., Bershadsky, A., & Yan, J. (2017). MDia1 senses both force and torque during F-actin filament polymerization. *Nature Communications*, *8*(1), 1650. https://doi.org/10.1038/s41467-017-01745-4

Zagórska-Marek, B. (2021). Mirror Symmetry of Life. In *Current Topics in Chirality—From Chemistry to Biology*. IntechOpen. https://doi.org/10.5772/intechopen.96507

Zambuto, S. G., Jain, I., Theriault, H. S., Underhill, G. H., & Harley, B. A. C. (n.d.). Cell Chirality of Micropatterned Endometrial Microvascular Endothelial Cells. *Advanced Healthcare Materials*, *n/a*(n/a), 2303928. https://doi.org/10.1002/adhm.202303928

Zhang, H., Fan, J., Maclin, J. M. A., & Wan, L. Q. (n.d.). The Actin Crosslinker Fascin Regulates Cell Chirality. *Advanced Biology*, *n/a*(n/a), 2200240. https://doi.org/10.1002/adbi.202200240

Zhang, H., Rahman, T., Lu, S., Adam, A. P., & Wan, L. Q. (2024). Helical vasculogenesis driven by cell chirality. *Science Advances*, *10*(8), eadj3582. https://doi.org/10.1126/sciadv.adj3582

Zhang, J., Guo, W.-H., & Wang, Y.-L. (2014). Microtubules stabilize cell polarity by localizing rear signals. *Proceedings of the National Academy of Sciences*, *111*(46), 16383–16388. https://doi.org/10.1073/pnas.1410533111

Zhang, J., & Wang, Y. (2017). Centrosome defines the rear of cells during mesenchymal migration. *Molecular Biology of the Cell*, *28*(23), 3240–3251. https://doi.org/10.1091/mbc.e17-06-0366

Zhong, J., Baquiran, J. B., Bonakdar, N., Lees, J., Ching, Y. W., Pugacheva, E., Fabry, B., & O'Neill, G. M. (2012). NEDD9 Stabilizes Focal Adhesions, Increases Binding to the Extra-Cellular Matrix and Differentially Effects 2D versus 3D Cell Migration. *PLOS ONE*, *7*(4), e35058. https://doi.org/10.1371/journal.pone.0035058

Zhu, N., Kwong, H. K., Bao, Y., & Chen, T.-H. (2017a). Chiral Orientation of Skeletal Muscle Cells Requires Rigid Substrate. *Micromachines*, *8*(6), 181. https://doi.org/10.3390/mi8060181

Zhu, N., Kwong, H. K., Bao, Y., & Chen, T.-H. (2017b). Chiral Orientation of Skeletal Muscle Cells Requires Rigid Substrate. *Micromachines*, *8*(6), 181. https://doi.org/10.3390/mi8060181

Zimmermann, D., & Kovar, D. R. (2019). Feeling the force: Formin's role in mechanotransduction. *Current Opinion in Cell Biology*, *56*, 130–140. https://doi.org/10.1016/j.ceb.2018.12.008